IDO-16930
April 1964

SUMMARY DATA REPORT FOR SPERT TRANSIENT PRESSURE MEASUREMENTS IN THE INTERVAL 1955 TO 1961

G. F. Brockett and E. Feinauer

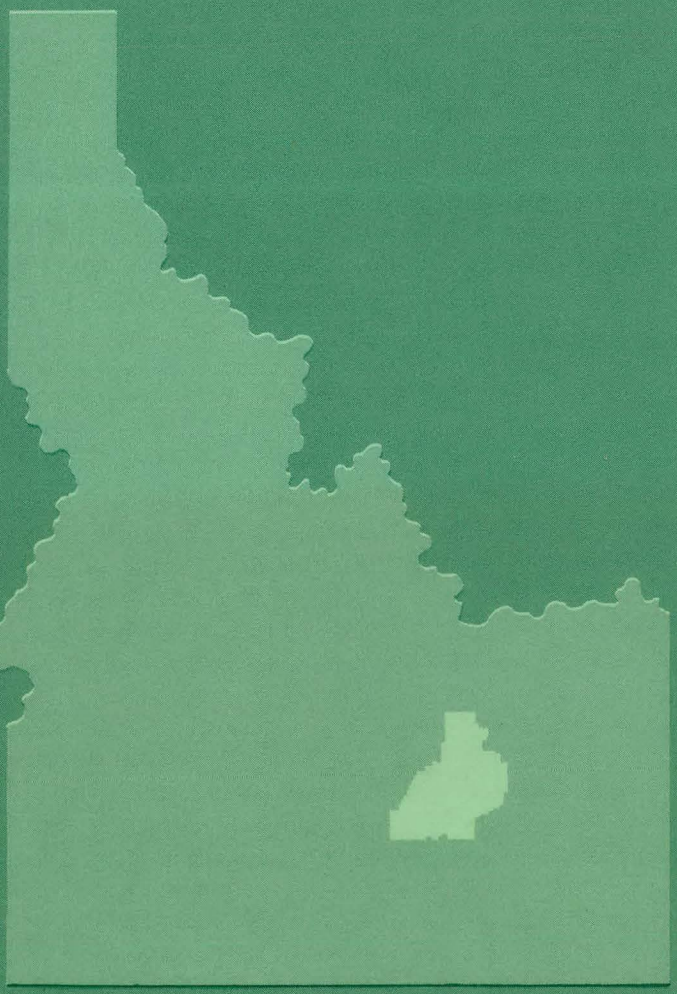

PHILLIPS PETROLEUM COMPANY

ATOMIC ENERGY DIVISION

NATIONAL REACTOR TESTING STATION
US ATOMIC ENERGY COMMISSION

DISCLAIMER

PRICE $2.50

AVAILABLE FROM THE
OFFICE OF TECHNICAL SERVICES
U. S. DEPARTMENT OF COMMERCE
WASHINGTON 25, D. C.

PRINTED IN USA

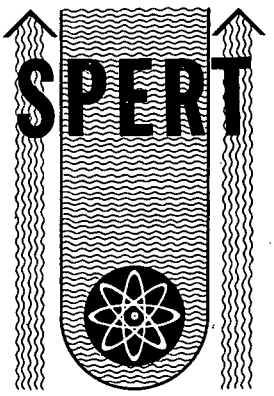

IDO-16930
AEC Research and Development Report
Reactor Technology
TID-4500 (27th Ed.)
Issued: April 15, 1964

SUMMARY DATA REPORT FOR SPERT TRANSIENT PRESSURE MEASUREMENTS IN THE INTERVAL 1955 TO 1961

by

G. F. Brockett

E. Feinauer

PHILLIPS
PETROLEUM
COMPANY

Atomic Energy Division
Contract AT(10-1)-205
Idaho Operations Office
U. S. ATOMIC ENERGY COMMISSION

ACKNOWLEDGEMENT

The authors wish to acknowledge their appreciation to Messrs. W. E. Driskell and C. E. Hardy for their painstaking effort in selection and preparation of data; to the personnel of the Spert data processing group for their efforts in preparing analog reproductions of more than a thousand time histories; and to the personnel of the Spert staff for their many helpful suggestions during the course of preparing this report.

ABSTRACT

The primary pressure data obtained from Spert nuclear reactor power excursion tests in the interval 1955 to 1961 are presented in this report. The data were obtained during testing of seven plate-type reactor cores of either aluminum or stainless steel construction. The data presentation consists of an extensive display of the pressure-time histories with a limited discussion of pertinent features, a tabulation of peak pressures, and illustrative cross plots of peak pressure as a function of a few appropriate variables, including initial system conditions and reciprocal reactor period. Where appropriate, composite plots showing the simultaneous behavior of pressure, energy, power, temperature, and flow have been included to facilitate investigation of the interrelationships between these primary variables. Data for both the open vessel Spert I configuration and the closed vessel, pressurized Spert III configuration are included.

SUMMARY DATA REPORT FOR SPERT TRANSIENT PRESSURE MEASUREMENTS IN THE INTERVAL 1955 TO 1961

CONTENTS

FIGURES

TABLES

SUMMARY DATA REPORT FOR SPERT TRANSIENT PRESSURE MEASUREMENTS IN THE INTERVAL 1955 TO 1961

I. INTRODUCTION

Since the inception of the Spert experimental program in 1955, the dynamic response of plate-type, water-moderated reactors has been investigated in considerable detail. A number of reports treating the appropriate data obtained for such variables as reactor power, energy, temperature, and reactivity feedback have been published during the interim. Although these reports have presented some limited data pertaining to the generation of transient pressures during power excursions, no systematic study of transient pressure behavior has been presented. The existence of a considerable volume of pressure data has made it desirable to provide a single reference which summarizes the information obtained from power excursion tests of a number of different reactor cores in different configurations and under various system conditions.

In this report the primary pressure data obtained in the testing of seven reactor cores are presented. The presentation consists of an extensive display of the pressure-time histories, a tabulation of the peak pressures, and a few illustrative cross plots of the peak pressure as a function of such variables as reciprocal reactor period, initial system pressure, initial system temperature, etc. The primary emphasis is placed on presentation of the pressure data; the discussion of the time-histories of other variables is intended only to serve as an aid to interpretation of the pressure data.

Two basic reactor configurations have been utilized in the Spert tests for which data are reported here: the open-vessel Spert I configuration, and the closed-vessel pressurized Spert III configuration. Data obtained during testing with typical plate-type cores are considered individually in Section III of this report. The only core tested in Spert III to date is a core having stainless steel cladding (designated the C-core). To facilitate comparison of the response of open-vessel and closed-vessel systems, the Spert I data presented in Section III are those obtained from tests of a stainless steel core (designated the P-Core) which is very similar to the core tested in Spert III. In both instances, the data were obtained after considerable experience pertaining to the use of pressure measuring equipment had been gained. These data are more reproducible than those obtained during earlier tests. Only brief descriptions of facilities and details of core design have been included in this report since detailed treatments are available in other reports which are referenced as appropriate.

Some of the data obtained in Spert I with four aluminum clad cores, and one additional stainless-clad core also are discussed briefly in Section III. These data are presented in more detail in Appendix 1. In general, these data are similar to those reported for the P-Core and display the same general pattern of behavior. However, there were a few special tests conducted with these cores which provided information not previously considered.

The instrumentation used in obtaining the data reported is described in Section II of this report. The treatment covers both the measuring and recording systems. System characteristics important to interpretation of the data are

discussed in some detail with emphasis on environmental sensitivities, system bandpass, and calibration techniques.

Throughout the report, discussion of the data has been limited primarily to that required to assure proper interpretation of the format of presentation. In some instances attention is directed to correlations between pressure and other related variables. However, no attempt has been made in this report to establish in detail the reasons for such correlations. Thus, the report does not represent an analysis of the data, but is primarily an analog presentation of the pressure behavior observed during transient testing of plate-type cores at Spert in the time interval from 1955 to 1961.

II. INSTRUMENTATION

1. ELEMENTS OF THE DATA ACQUISITION SYSTEM

The data acquisition system consists of three basic elements. The first of these elements is the detecting element, or transducer, which converts some basic form of energy (eg, pressure) into a more adaptable form (eg, an electrical signal) that may be more readily transmitted, amplified, or modified. The two remaining elements are the signal conditioning equipment, used to modify, amplify, or decode the transducer output, and the readout equipment, which reduces the electronic signal to a form amenable to interpretation or analysis. The conditioning and recording equipment used for obtaining the information presented in this report was more than adequate for the needs. Since the components used are standard units, they need not be described in detail in this report. However, although the transducing element was adequate in most respects, its performance was marginal in some aspects and the transducer represents the weakest link in the data acquisition system. In order to facilitate proper interpretation of the measurements reported, the transducer characteristics will be discussed in some detail.

A functional block diagram of a typical instrument channel of the type utilized in these tests is shown in Figure 1. The blocks contained in the sections labeled by the headings "signal conditioning" and "readout" represent components common to most standard, multi-channel, flexible broad-band data systems. However, those blocks contained in the section labeled "detection" are representative of the equipment used and some of the major problem areas common to most measuring systems, but particularly important in systems used to monitor transient behavior of nuclear reactors. Two of these blocks, "environmental sensitivities" and "field effects", are of particular significance here.

With regard to environmental sensitivities, the physical limitations of available materials and the state of the art in fabricating techniques result in transducing mechanisms that are sensitive to phenomena other than those which they were specifically designed to measure. In particular, most pressure transducers also have some response to

(1) absorption of neutron and gamma radiation, which results in changes in electrical properties of the system and/or heating of the transducer components;

(2) transient temperature changes, which result in differential heating of transducer components, the Peltier effect, etc;

(3) acceleration, which induces microphonics; and

(4) electrostatic and magnetic fields, which generate spurious currents not representative of pressure generation.

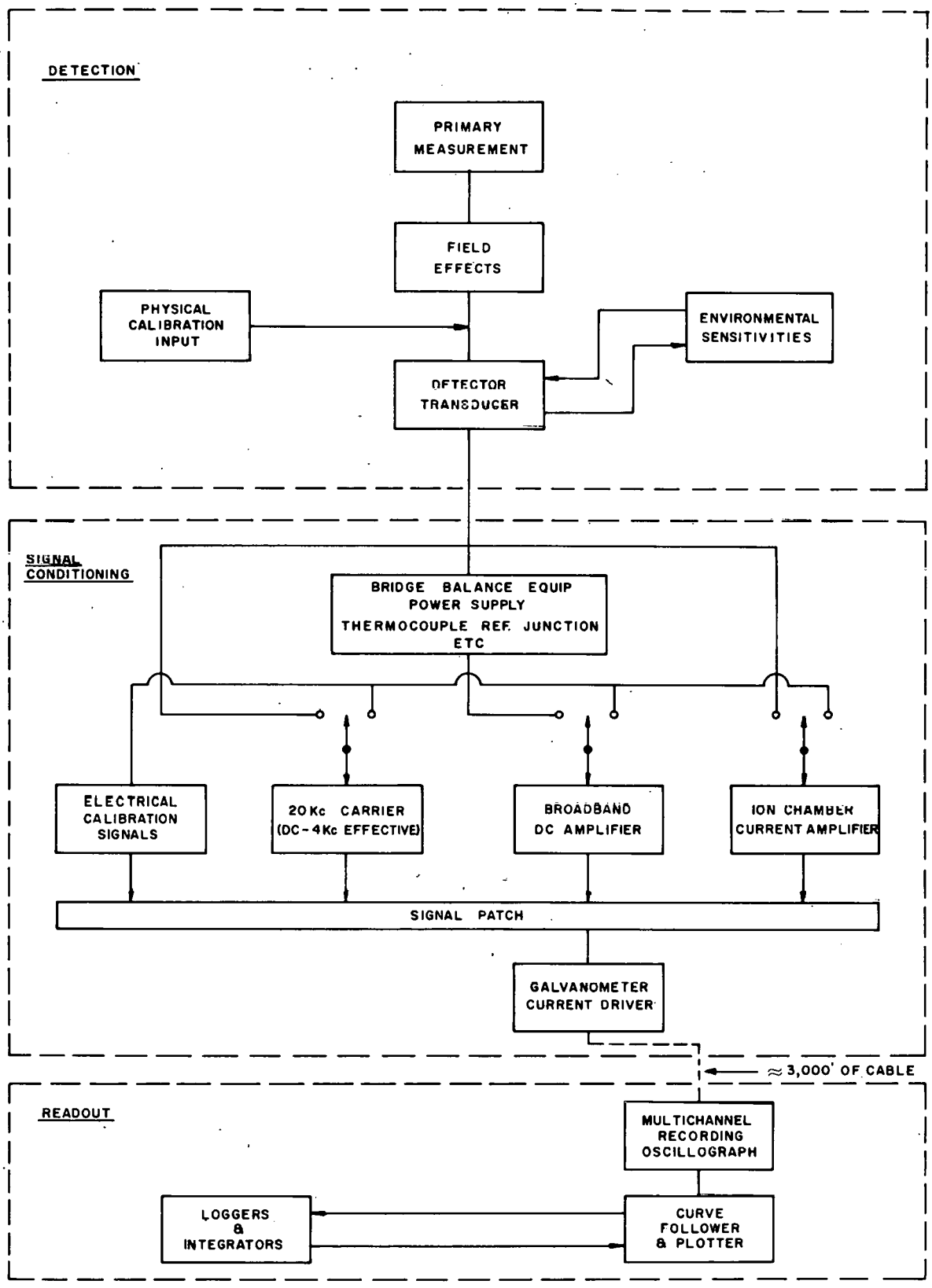

Fig. 1 Schematic representation of the pressure measuring-recording system showing system components and typical problem areas.

The nature of the spurious responses induced from these sources will be discussed briefly in item 3.

In connection with field effects, some clarification of terminology is in order. For present purposes, measurements may be divided into two categories: direct measurements, which are obtained within a source or at the source surface; and field measurements which are obtained at a distance from the source in the radiated field of transmission. Direct measurements, such as those of the fuel-plate surface temperatures, displacements, or strains are limited primarily by uncertainties associated with the response of the transducing mechanism and perturbations of the phenomena monitored due to the presence of the detector. For field measurements, additional uncertainties are introduced due to considerations involving propagation behavior of the radiated field, perturbations incident to the presence of boundaries, and directivity effects of both source and detector. The propagation of pressure, like that of nuclear radiation, light, heat and other wave phenomena, must be treated as a field measurement with the attendant complexity of interpretation. Although a detailed description of the above aspects of field measurements is beyond the scope of this report, a few of the particularly significant aspects of environmental and field effects will be noted as required to aid interpretation of the observed pressure behavior.

Most of the information provided in this report is concerned with measurement of pressure. However, some temperature, power, and flow data are presented for use in comparison, and a brief description of the equipment used is given under Section 2 below. The primary objective, however, is to present those data appropriate to an understanding of the response of a pressure transducer in the nuclear radiation environment.

2. POWER, TEMPERATURE, AND FLOW INSTRUMENTATION

2.1 Power Monitors

Power measurements for these tests employed uncompensated, boron-lined, neutron-sensitive ion chambers. The response is well known and will not be commented on further. The chambers were checked for linearity of response about twice a year in the MTR thermal column. The frequency response (collection time) was such that the expected uncertainty from this source in the measurement of reactor power for a 1-msec period excursion was 5% or less.

2.2 Temperature Monitors

The temperature measurements reported were obtained with chromel-alumel thermocouples. The wire used was 10 mils in diameter; the thermocouples were of two types, welded [1] and peened [2].

All tests involving stainless steel plates, ie, the P-Core, BSR-II Core, and the Spert III C-Core, utilized welded thermocouples. For these cores, each thermocouple wire was spot welded to the stainless steel cladding at the center of the fuel plate and at the selected longitudinal position. The thermocouple consisted of a chromel-stainless junction in close proximity to a stainless-alumel junction, thus completing the chromel-alumel pair.

Tests involving aluminum-clad cores, however, utilized peened thermocouples[a]. These thermocouples were prepared by slitting the surface of the fuel plate with a sharp tool, embedding the thermocouple in the slit at a depth of about 10 mils, and then peening the surface to close the opening and secure the wires. For this type of thermocouple, the last point of contact between the thermocouple wire and the cladding represents the junction location. Thus, the junction may be at the plate surface or at some point beneath the surface depending upon the microscopic structure of each thermocouple. As the temperature of the fuel plate increases during a reactor transient, the clad and thermocouple wires may expand at differing rates, resulting in a change in location of the effective junction within the clad, or momentary loss of contact between clad and thermocouple. The output of the thermocouple might be expected to contain a spurious response associated with these changes. The data presented in Figure 2 show an anomalous behavior observed only with peened thermocouples. The numerous instantaneous discontinuities present in the thermocouple output are probably a composite of the output resulting from real temperature changes due to variations in heat transfer rates, and spurious indications of temperature change resulting from the differential expansion noted. Thus, although these discontinuities may represent real temperature behavior, until the magnitude of the spurious output postulated can be determined, they are subject to question.

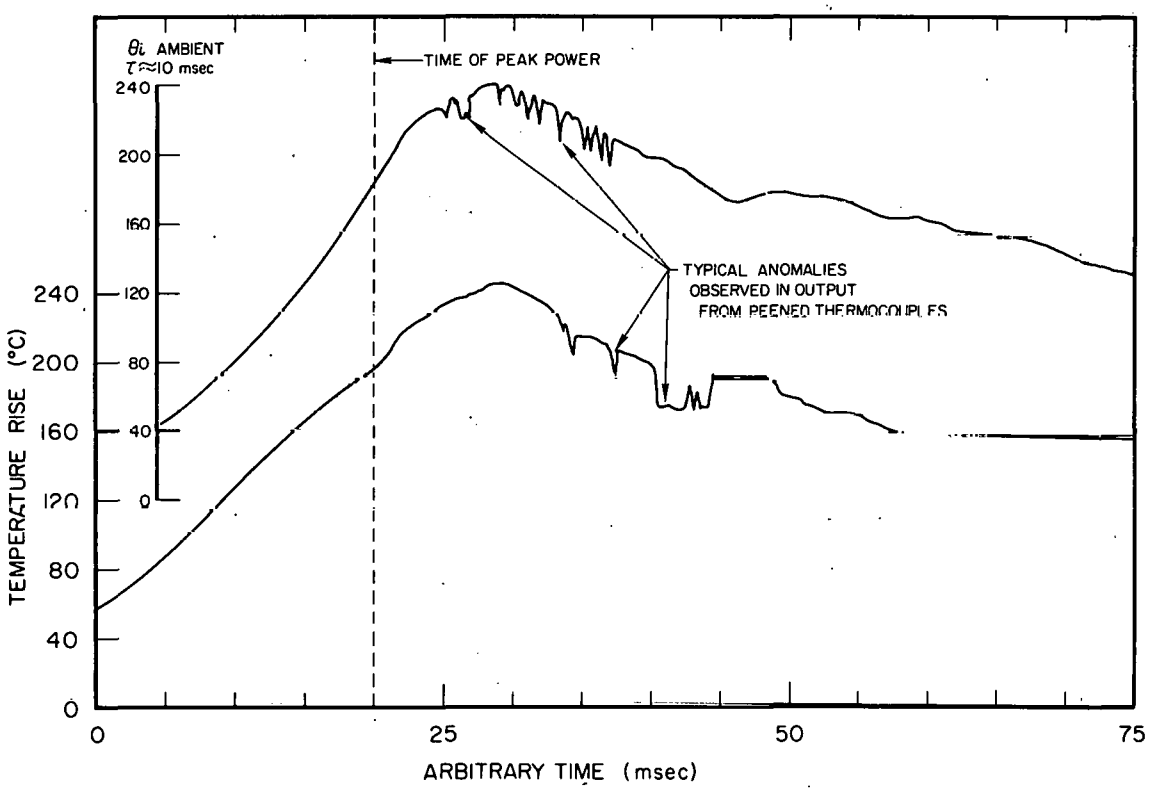

Fig. 2 Anomalous temperature behavior observed with peened thermocouples used in Spert I transient testing.

[a] Development of aluminum welding techniques has permitted use of some welded thermocouples with aluminum fuel plates in recent tests. The data reported, however, were obtained using peened thermocouples.

The question of response time for both peened and welded thermocouples is not yet completely resolved[3, 4]. For the range of reactor periods pertinent to these tests, the time delay between generation of heat within the plate and the indication of this generation as an increase in output of the thermocouple is of the order of 1 to 3 msec. Such a delay represents a second order effect for the comparisons drawn here, but would have to be considered in a quantitative analysis of the data.

2.3 Flow Monitors

The flow devices used are of two types, the impeller flowmeter which is sensitive primarily to flow velocity and the drag flowmeter which is sensitive primarily to mass flow. These flowmeters, shown schematically in Figure 3,

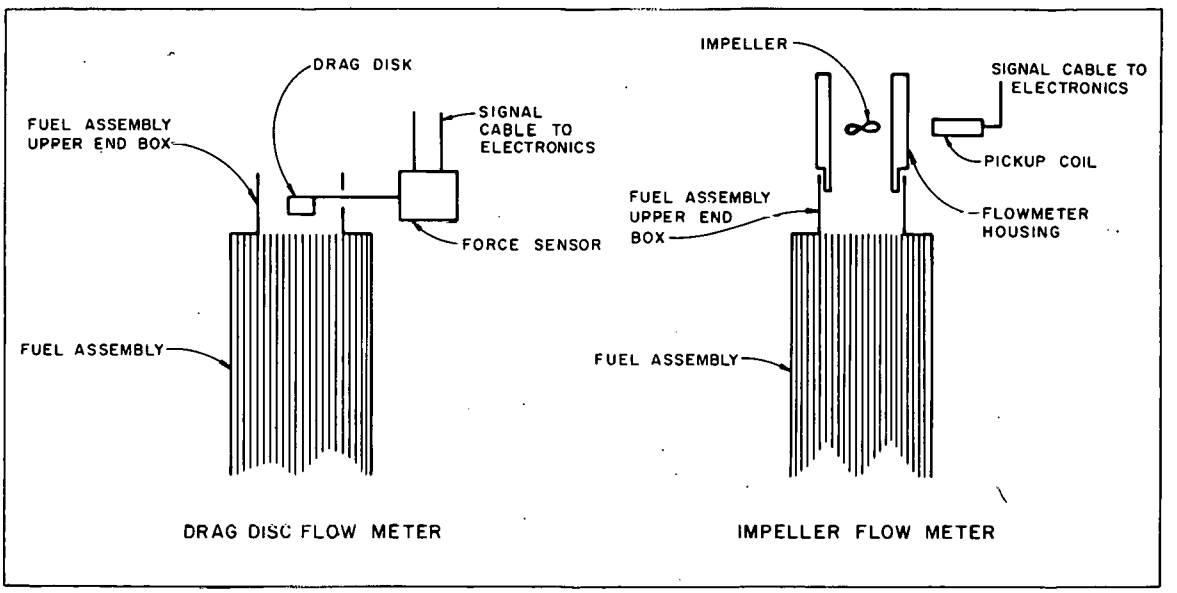

Fig. 3 Schematic representation of impeller and drag disc flowmeters used in Spert transient testing.

were mounted in or directly above the fuel assembly upper end boxes for all tests reported here. For the drag-type flowmeters used in obtaining the P-Core and Spert III data, flow velocity is proportional to the square root of the displacement of the drag disk. Positive deflection of the oscillographic trace indicates flow out of the assembly and negative deflection indicates flow into the assembly. The impeller flowmeters generate an alternating current of a frequency proportional to the flow velocity. The output of these flowmeters does not distinguish between flow out of the assembly and flow into the assembly. Flowmeters of the impeller type were used in conjunction with all testing utilizing the A- and B-Cores. Representative responses for both types of flowmeters are shown in Figure 4. The output of the drag-type flowmeter exhibits a low frequency ($\approx$ 100 cps) component which is especially prominent for tests having low flow rates and which results from vibratory motion of the core (see also the P-Core and Spert III core data presentations).

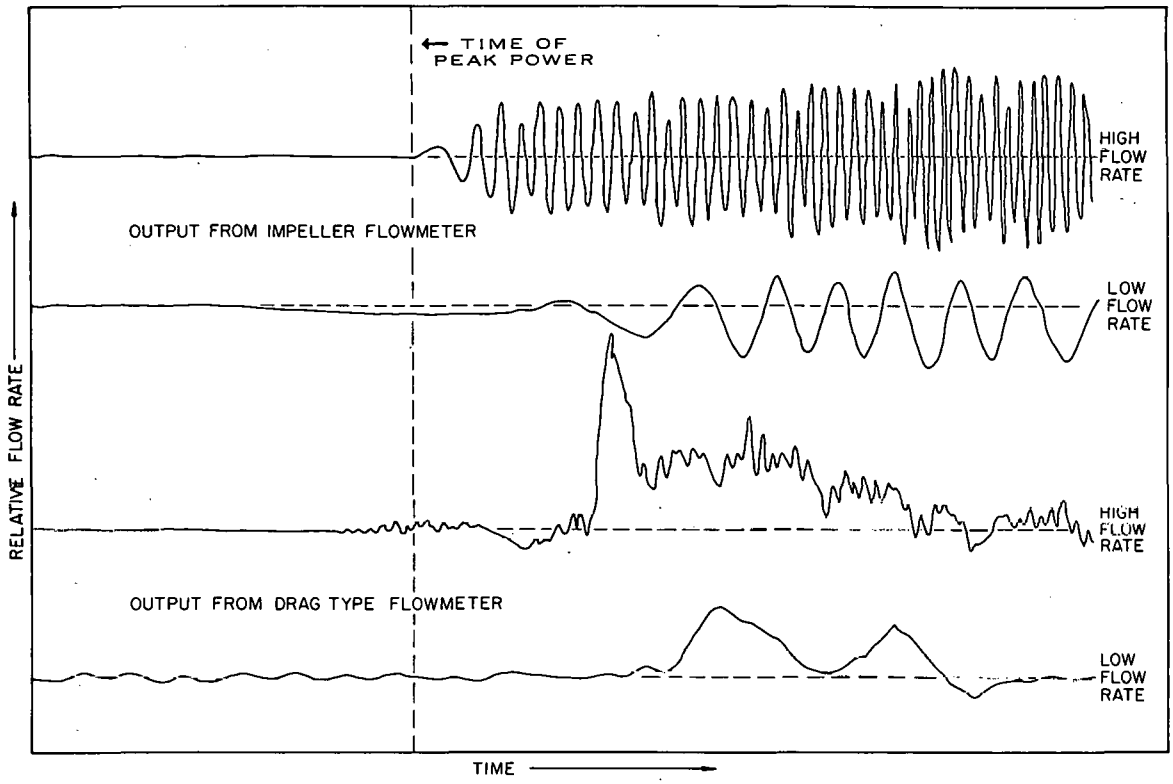

Fig. 4 Typical outputs from impeller and drag-type flowmeters for high and low flow rates.

3. PRESSURE TRANSDUCERS

3.1 Transducer Designations

The data reported were obtained by transducers utilizing two basic transducing mechanisms, a resistance strain bridge and a variable reluctance modulator for high frequency (≈5-20 kc) carrier signals. The transducers used are listed in Table I where the transducer designation (manufacturer) is specified followed by an abbreviation in parentheses which indicates the notation used to identify the transducer in presenting the data.

3.2 Environmental Sensitivities

The Northam, Ultradyne, Wianko, and Standard Controls transducers were of such design that reentrant cavities existed within the transducer mechanism, as shown schematically in Figure 5. Considerable difficulty was experienced in eliminating air pockets from these assemblies during installation and preventing accumulation of radiolytic gas produced during operation. The presence of gas bubbles in the system derated the transducer by lowering its frequency response and decreasing the indicated pressure magnitude for a given pressure input. The Statham and CEC transducers are so constructed that their diaphragms are exposed, thus eliminating the problem of gas entrapment (Figure 5).

TABLE I

SUMMARY OF PRESSURE TRANSDUCER DESIGNATIONS AND SPECIFICATIONS

Transducer Manufacturer	Transducer Type	Range (psi)	resonant frequency (cps) *
Ultradyne Corp. (ULT)	Magnetic Reluctance	0 - 100	500-1000
		0 - 200	500-1000
Wianko Corp. (WIA)	Magnetic Reluctance	0 - 25	800
	(Bourdon Tube)	0 - 3000	3500
Northam Corp. (NOR)	Magnetic Reluctance	0 - 100	3000-4000
Standard Controls Corp. (STD)	Strain Bridge	0 - 100	500
Consolidated Electro Dynamics Corp. (CEC)	Strain Bridge	0 - 100	13,500
		0 - 200	15,000
Statham Instrument Corp. (STA)	Strain Bridge	0 - 100	14,000
		0 - 200	18,000

* The resonant frequency given is the approximate resonant frequency of the diaphragm in water, ie, of the water-diaphragm system.

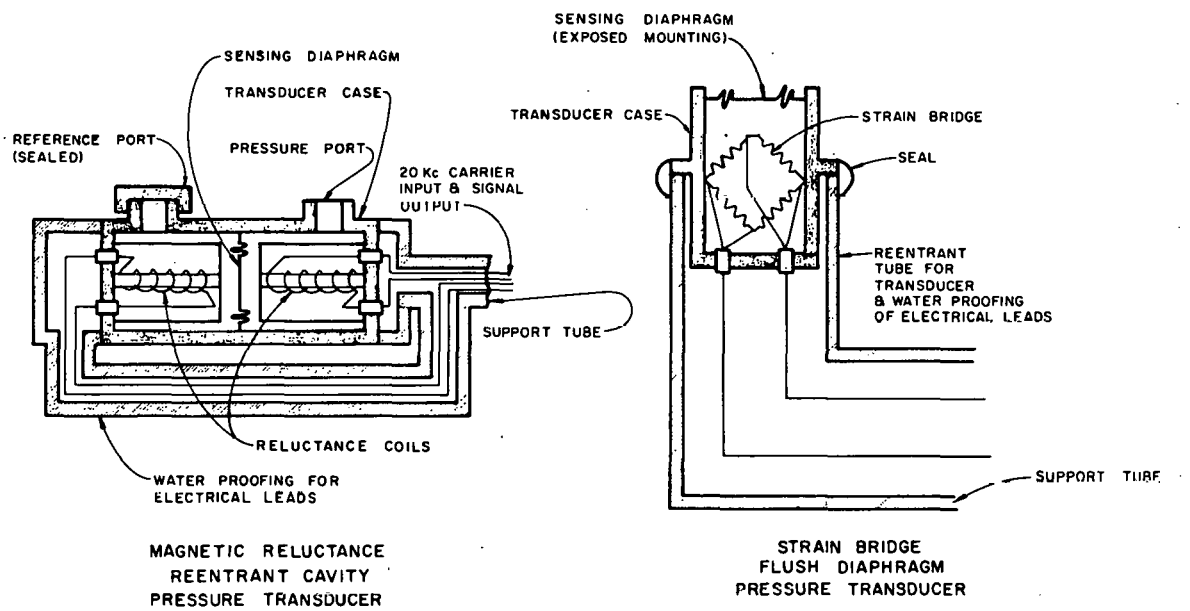

Fig. 5 Schematic representation of pressure transducers showing the flush diaphragm and reentrant cavity designs.

The magnetic reluctance transducers were quite free of radiation sensitivity, but problems arose in conjunction with the high frequency carrier used. Basically, these problems were a result of capacitive shunting of the high frequency carrier component in the detector leads by the water environment. The degree of such shunting varied with changes in environment, as for example between calibration of the assembly in air and normal operation in water. The problem was alleviated (but not eliminated) by utilizing copper sheathed cabling to maintain more uniform cable capacity throughout the calibration-measurement cycle.

The strain gage transducers were dc devices and, hence, were free of the capacitive shunting problem. They were, in general, more sensitive to radiation than were the reluctance transducers. Two types of spurious response have been observed. One occurs during the power burst and is a consequence of changes in the electrical properties of the transducer and its electrical system, due to the effects of the nuclear radiation. A second or integrated effect has been observed which may persist for hundreds of msec, as shown in Figure 6. This effect results from heating of the transducer components due to the absorption of gamma radiation and is similar to that for heating from other sources (Figure 7). It is separately considered here only because the source of heating occurs coincidently with the power burst and is a prompt rather than a delayed effect.

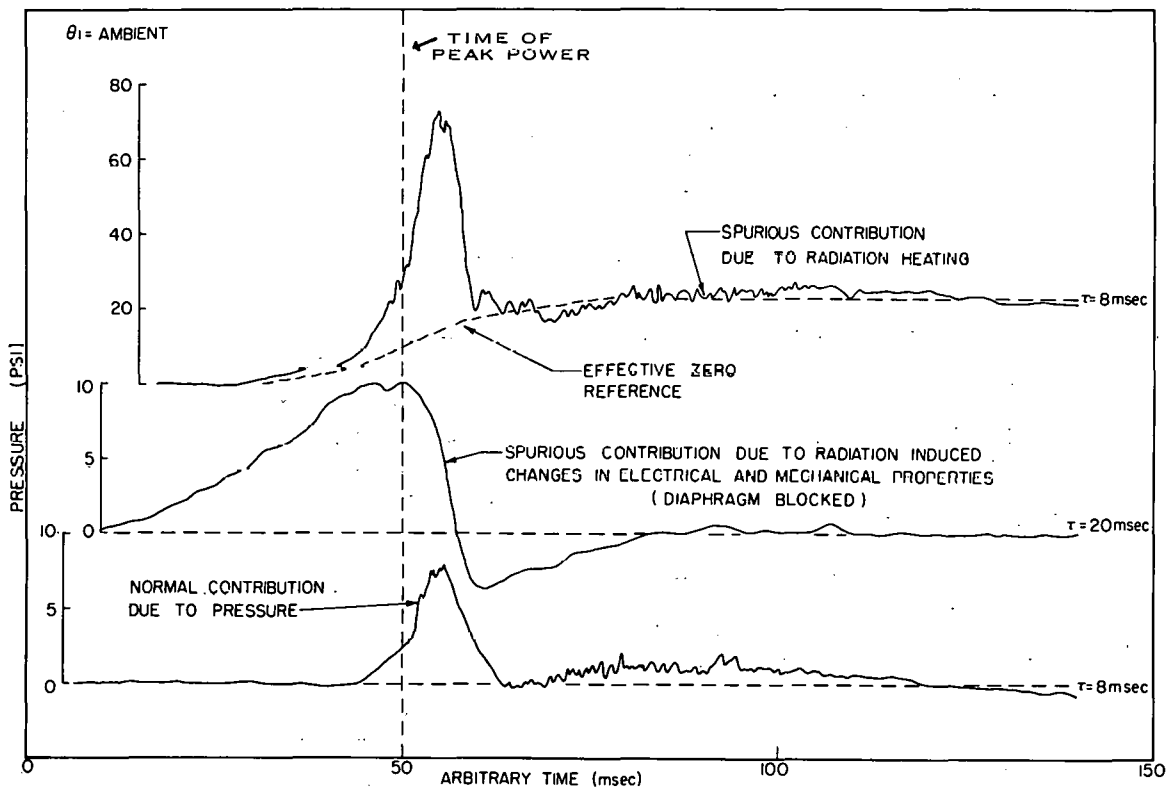

Fig. 6 Spurious output from a pressure transducer indicating the nature of transient and integrated radiation effects.

Because of the loose coupling between elements of the magnetic reluctance transducing mechanism, these transducers are quite sensitive to acceleration. That is, when the assembly is subjected to acceleration, spurious response is engendered in the transducer output. While all transducers are sensitive to acceleration in some degree, the extent of this sensitivity varies considerably with the mode of construction and mounting technique. For the strain bridge transducers used in the tests reported, the spurious response due to acceleration was small and did not significantly affect the data.

All transducers show some spurious response to differential heating of the transducer mechanism, such as occurs when hot liquids expelled from the core come in contact with the transducers. A typical response indicating a component of the recorded pressure profile due to temperature sensitivity is indicated in Figure 7. This effect is normally a delayed effect resulting from heat-transfer and fluid-flow considerations. Gamma heating represents an exception to this rule.

When the transducer was placed in a flow field, an additional spurious output was observed. This component was of two parts, a background error in pressure level due to the stagnation pressure resulting from the flow velocity, and a higher frequency noise component caused by turbulence which excited the resonant frequency of the diaphragm. For most measurements, this effect was of minor importance.

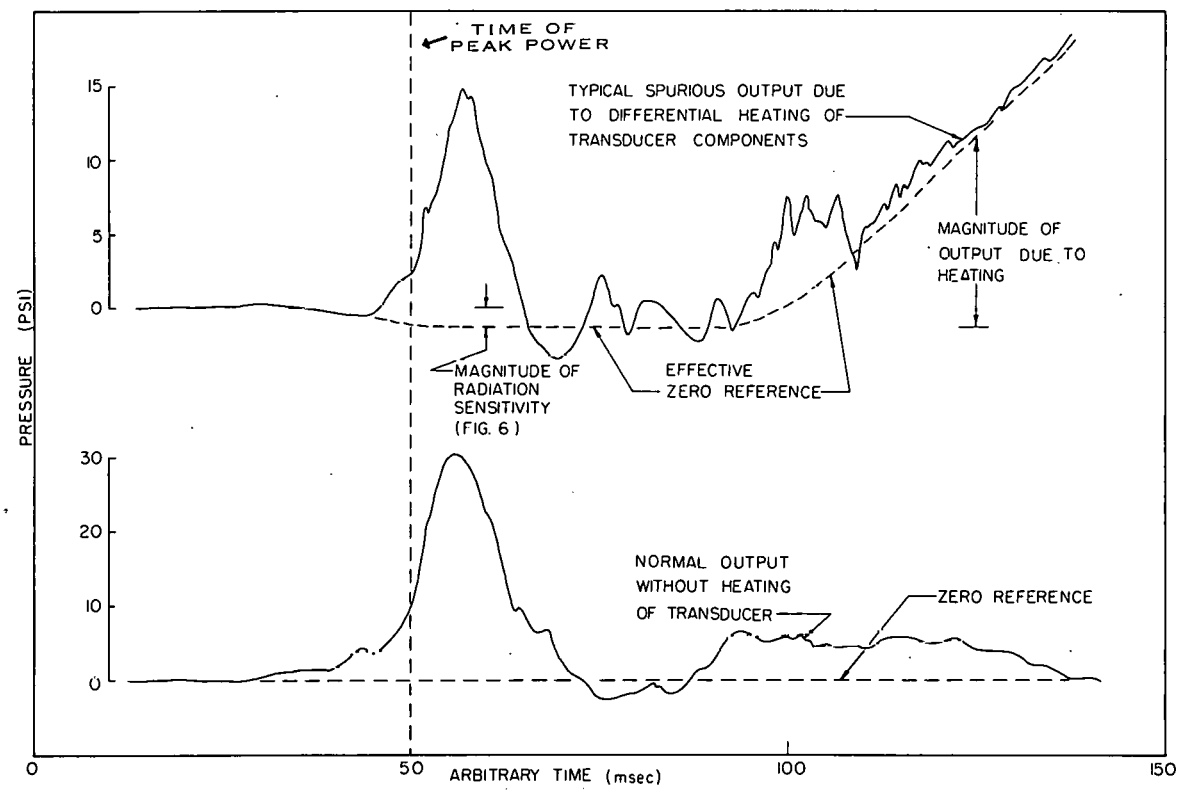

Fig. 7 Spurious output from a pressure transducer indicating the effects of differential heating of transducer components resulting from rapid changes in coolant temperature.

One additional factor should be noted even though it is not strictly an environmental effect. Many of the transducers used have diaphragms as part of the sensing mechanisms. Such diaphragms and their attendant structural components have natural or mechanical resonance frequencies(ω_r), and for most transducers the output is frequency dependent, especially for input (signal) frequencies near the mechanical resonant frequencies. The resonant frequencies vary considerably with transducer range and design. For the transducers used in these tests, the resonant frequencies were in the 0.5 to 20 kilocycle range (Table I). Transducer outputs as high as 200 times the output applying to the flat response region have been observed in some of the transducers used. In general, these transducers can be used to monitor pressure pulses with effective frequencies up to about 1/4 the resonant frequencies. For frequencies above this point the transducer output is frequency dependent as illustrated in Figure 8.

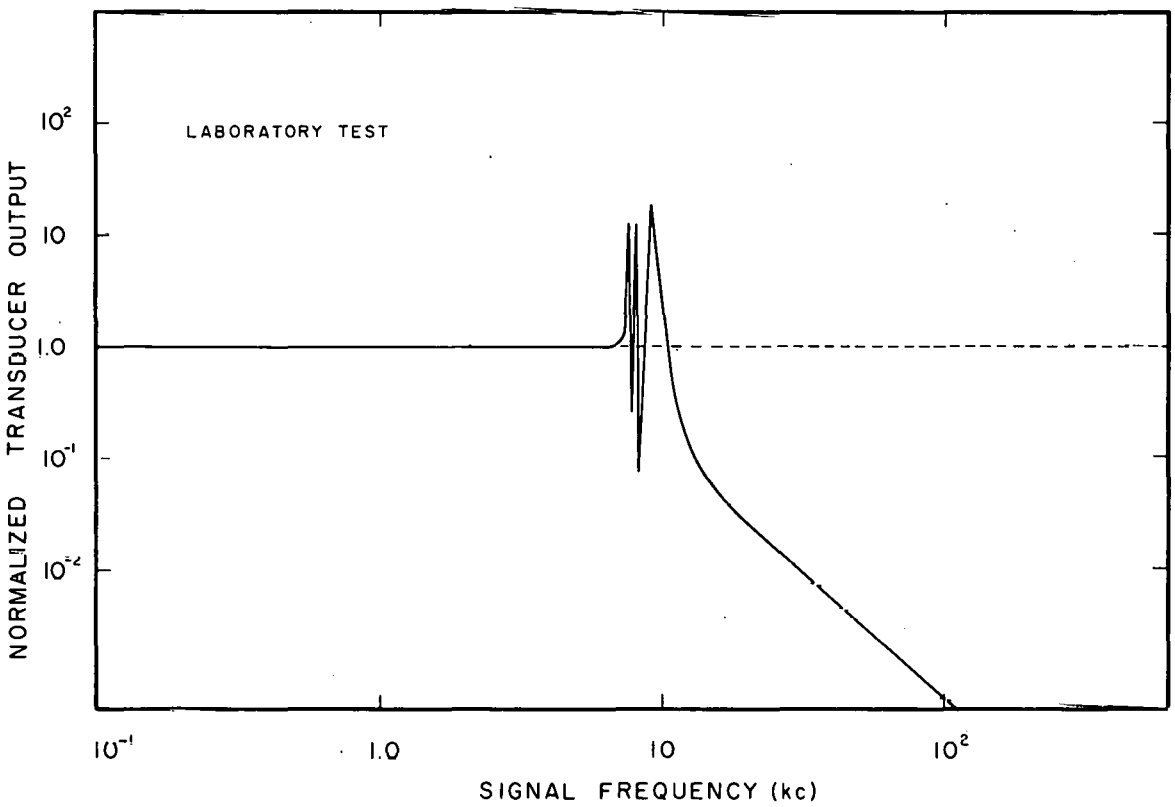

Fig. 8 Graphic representation of the response of a typical diaphragm-type transducer.

3.3 Transducer Locations

The majority of the pressure data was obtained with the pressure transducers mounted in the fuel assembly lower end boxes just external to the core. A few special tests were conducted in which pressure measurements were obtained at other positions within the reactor vessel and within a fueled assembly. Details of transducer locations for these special tests are described in connection with the presentation of the data.

3.4 Calibration Procedures

The pressure transducers were calibrated prior to the initiation of a test series. This calibration utilized a standard dead weight tester which provided checks on linearity, hysteresis, and transducing sensitivity. For those test series which extended over a period of several weeks, degenerative effects due to corrosion of the diaphragm and shorting of the sensing coils for reluctance transducers were noted. These effects contributed to a general decrease in the reliability of transducer response as noted in Appendix B.

4. SIGNAL CONDITIONING EQUIPMENT

The signal conditioning equipment primarily consisted of broad band dc amplifiers, 20 kc carrier amplifiers, and galvanometer current driver amplifiers. These amplifiers were capable of providing an output with less than 5% uncertainty from linearity drift and gain accuracy considerations in the frequency domain extending from dc to 5 kc. Although the zero level was maintained by a continuously variable control, changes in operational gain were available only in discrete steps. The equipment was calibrated on a weekly basis to guard against gain and bias drift and to provide a check on accuracy of calibration and proper logging of detector location and calibration changes.

5. RECORDING EQUIPMENT

Data obtained during the test series reported here were recorded on optical oscillographs. These oscillographs have a minimum response time (zero to full scale) of 150 μsec which was more than adequate for the pressure data obtained. Several problems are associated with the optical recording system. In particular, the trace deflection exceeds the available trace separation so that the traces frequently cross over one another. This is especially true for oscillatory outputs, as for example the ringing of pressure transducers. At high recording speeds, contrast is often poor, further aggravating the situation. Reduction of the data to legible (scaled) analog plots requires manual reproduction of the trace, as for example by use of a curve follower [5]. However, this equipment represented an established system and was one of the best available at the time. It is currently being replaced by analog-magnetic tape recording equipment of greater flexibility.

III. PRESENTATION OF DATA

1. SPERT I

1.1 Facility Description [6]

The Spert I facility is extensively described elsewhere. For present purposes it is sufficient to observe that the facility is composed of an open shield tank, 10 ft in diameter and 16 ft deep, installed below grade. For the tests described in this report a four ft diameter reactor tank 10.5 ft high was placed inside the shield tank. A pictorial cutaway of the facility with the reactor tank installed is shown in Figure 9. The reactor, moderator water, and all pressure transducers were placed in the reactor tank; the space between the reactor tank and the shield tank was empty. Thus, the surface of the reactor core was located less than two feet from a vessel boundary at the sides. For most tests the water level also was approximately two feet above the core.

As a consequence of the geometrical configuration, reflection phenomena appreciably affected the pressure-time history. For example, the acoustic transit time for reflection from the free surface and the fixed surface at the reactor tank is approximately 1 msec, so that the pressure behavior corresponding to times beyond 1 msec after the initiation of generation is a composite of the generated and reflected contributions. A detailed treatment of the laws governing reflection and the effects of reflection upon pressure generation can be found in most texts on acoustics [7, 8, 9]. For present purposes it will be sufficient to note that interpretation of the pressure data requires a consideration of the effects of reflection, especially negative reflection from the free surface. Other factors such as (a) the effects upon propagation velocity of system inhomogeneity due to the presence of steam in the moderator water (steam-water mixture) [10] and the metal plates immersed in the water [11], (b) geometric reduction in pressure magnitude with increasing distance from the source [12], and (c) directionality of the pressure source resulting from structural composition of the core, also must be considered.

1.2 Core Description [13]

The P-Core fuel assembly consisted of a 3-in. square array of 18 fuel plates, each nominally 3 in. wide and 24 in. long and composed of a 20-mil-thick fuel-bearing "meat" [a] clad with 5 mils of 304L stainless steel. Each fuel plate contained 28.6 gms of U-235 so that a fuel assembly had a total of 515 grams of U-235. The plates were brazed into an unfueled side plate which formed part of a rectangular container (Figure 10). The standard core consisted of 19 such fuel assemblies positioned in a grid plate as shown in Figure 11. Each fuel assembly was identified by a two digit number specifying the row and column in which the assembly was located. The central assembly, located in fuel position 44, contained the special poison rod used to initiate the transients.

[a] The meat section was composed of UO_2, 93.2% enriched in U-235 in a stainless steel matrix.

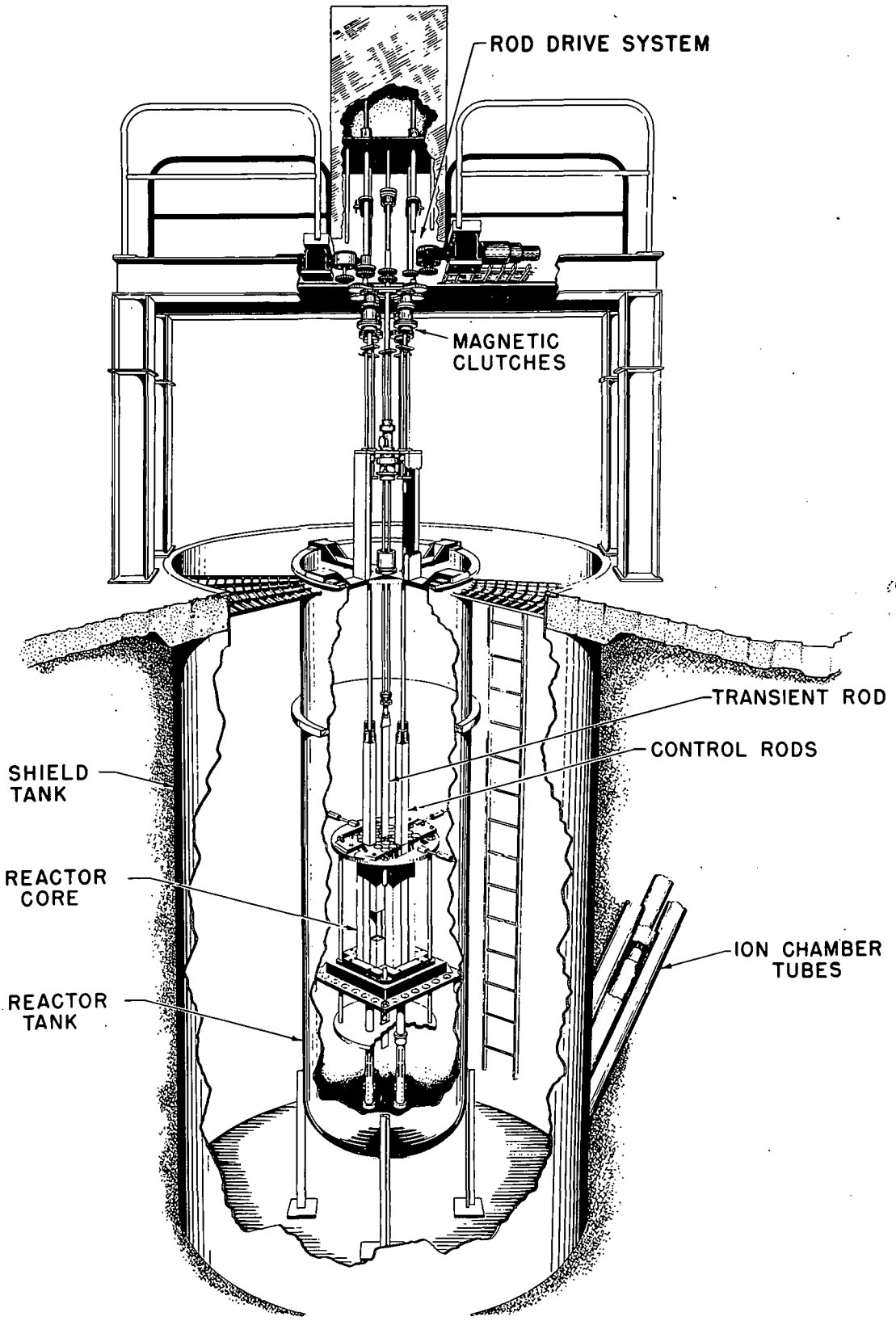

Fig. 9 Schematic representation of the Spert I facility showing the relative locations of the reactor tank, shield tank, and other system components.

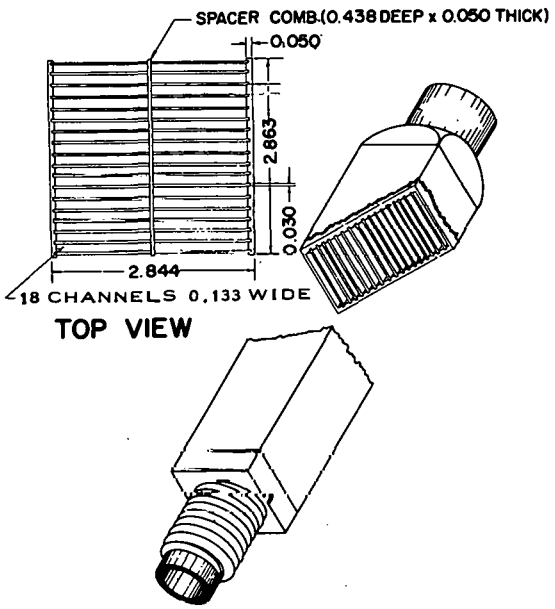

Fig. 10 Schematic representation of stainless steel P-Core fuel assembly.

Four fuel-poison control rod assemblies were located in fuel positions 24, 42, 46, and 64. Fuel plates were designated 1 through 18, beginning at the north of each assembly. For example the tenth plate from the north in assembly 44 is identified by the notation 44 10. Thermocouple locations were designated by vertical position of the thermocouple in inches above or below the core midplane, as for example 44 10 + 3. The plates were separated by a nominal 133 mils of moderator water. Further detail of the core design may be found in a previously published report [13].

The pressure transducers were placed in the lower end boxes for most tests. Their locations are specified uniquely by the fuel position number as 33, 35, etc. These notations will be used in referring to measuring locations applicable to the data presented below. The few exceptions applying to special tests are individually described.

A few pertinent parameters of value in evaluating the P-Core data are presented in Table II.

TABLE II

PERTINENT P-CORE CONSTANTS [14]

Item	Magnitude
Clad Material	Stainless Steel
Critical Mass U-235	7.6 kg
Total U-235	9.3 kg
H/U Ratio	120
M/W Ratio	0.3
Available K_{ex}	4.90 $
Temperature Defect 20° - 95°C	1.48 $
Isothermal Temperature Coefficient - 20°C	- 0.25 x $10^{-2}$$/°C
Isothermal Temperature Coefficient - 95°C	- 3.40 x $10^{-2}$$/°C
Average Void Coefficient C_V	- 9.9 x $10^{-4}$$/cm^3
Reduced Prompt Neutron Lifetime $\ell^*/\bar{\beta}$	2 x 10^{-3} sec
Water Channel Width	133 mils

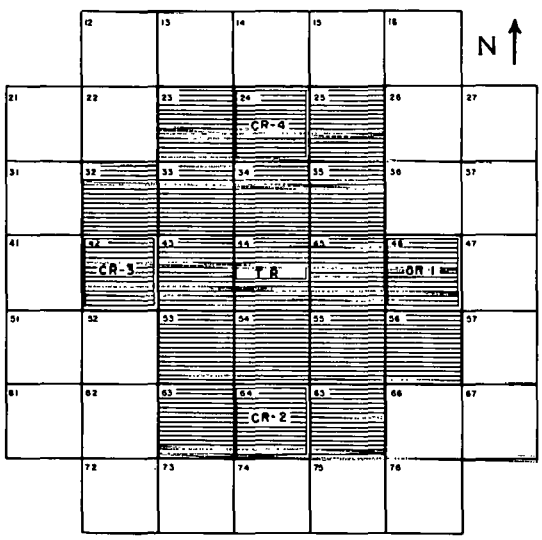

Fig. 11 Layout of Sport I reactor grid showing arrangement of fuel assemblies for the operational P-Core.

1.3 Data Presentation

1.31 General Considerations. The data presented below were recorded by use of an optical oscillograph. A photographic reproduction of an appropriate portion of a typical oscillographic record is shown in Figure 12. The traces numbering 0 through 27 are labeled at the left of the figure, and the

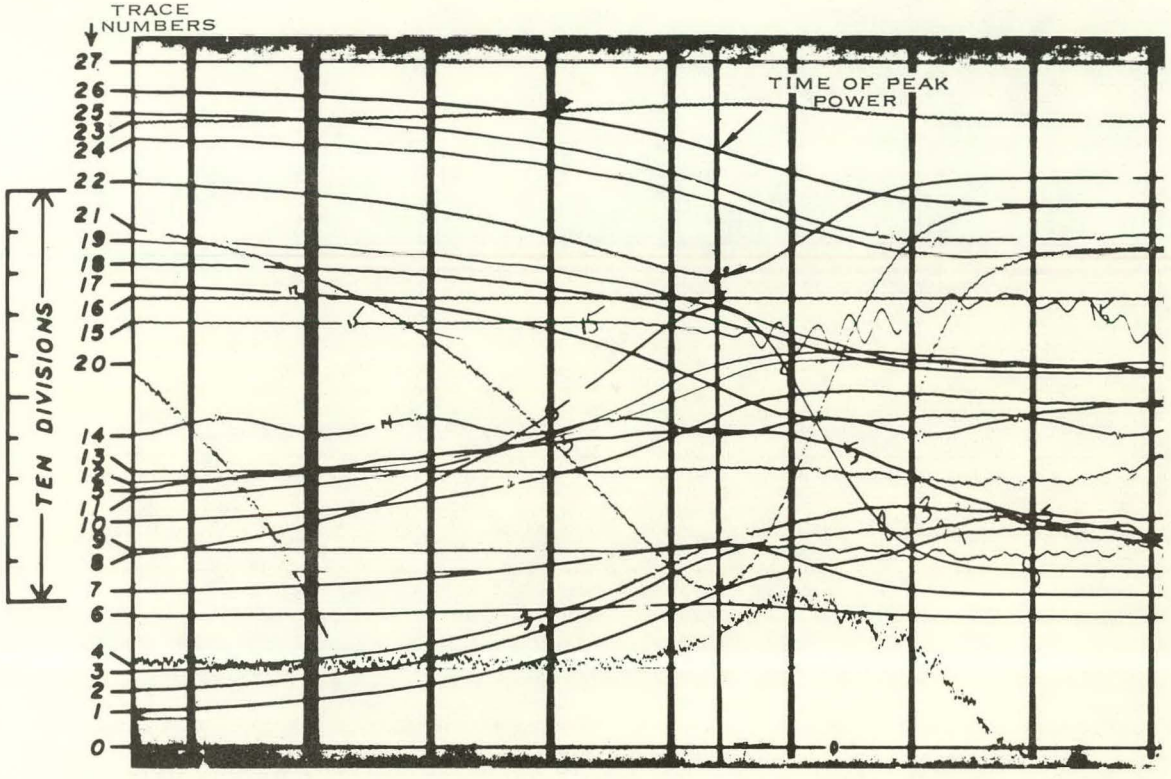

Fig. 12 Photographic reproduction of the original CEC record obtained for a typical Spert I transient.

calibration numbers required to obtain the appropriate magnitudes from the deflections shown in the oscillographic recording are given in Table III. The table also includes the trace identification as to sensor type and location. The vertical markers in Figure 12 are time lines which are spaced at 10-msec intervals with every tenth line accentuated. An additional vertical line has been placed on the figure to indicate the time of peak power.

Obtaining digital information from the oscillographic records is a slow and sometimes difficult procedure. It involves measurement of trace deflection followed by an appropriate normalization and conversion by use of a scale factor. The procedure is often complicated by overlapping of the traces, faintness of line definition when rate of deflection is high, etc. To facilitate analog to digital conversion a curve follower [5] was used, the output of which gave traces that were calibrated in both time and magnitude of the variable

TABLE III

IDENTIFICATION AND CALIBRATION DATA
FOR USE WITH THE PHOTOGRAPH OF OSCILLOGRAPHIC RECORD 0-08630 (Fig 12).

τ = 17 msec. θ_i = 20°C

Trace Number	Sensor Type	Location	Calibration Number
0 - 1	Thermocouple	44 18 -6	31.4°C/div.
0 - 2	Thermocouple	44 18 -3	30.6°C/div.
0 - 3	Thermocouple	44 18 +0	31.8°C/div.
0 4	Flowmeter	Above 35	None
0 - 5	Ion Chamber	Tube 1 (75 3/8")	0.766 dec/div.
0 - 6	Ion Chamber	Tube 3 (74-3/32")	455 Mw/div.
0 - 7	Ion Chamber	Tube 3 (74-3/32")	111 Mw/div.
0 - 8	Ion Chamber	Tube 3 (74 3/32")	21.8 Mw/div.
0 - 9	Transducer	33 end box	6.25 psi/div.
0 -10	Thermocouple	54 18 -6	31.9°C/div.
0 -11	Thermocouple	54 18 -3	30.0°C/div.
0 -12	Thermocouple	54 18 +0	31.8°C/div.
0 -13	Transducer	35 end box	6.25 psig/div.
0 -14	Rod Drop	44 trans. rod	None
0 -15	Transducer	55 end box	2.56 psig/div.
0 -16	Transducer	53 end box	12.8 psig/div.
0 -17	Thermocouple	44 18 +3	30.5°C/div.
0 -18	Thermocouple	65 18 +0	31.8°C/div.
0 -19	Thermocouple	65 18 -6	30.7°C/div.
0 -20	Ion Chamber	Tube 2 (64-1/16")	3.17 Mw/div.
0 -21	Ion Chamber	Tube 2 (64-1/16")	15.8 Mw/div.
0 -22	Ion Chamber	Tube 2 (64-1/16")	63.0 Mw/div.
0 -23	Transducer	Gamma tube	None
0 -24	Thermocouple	55 18 +0	31.0°C/div.
0 -25	Thermocouple	55 18 -3	30.6°C/div.
0 -26	Thermocouple	55 18 -6	31.4°C/div.
0 -27	Reference trace		None

involved. Use of special logarithmic converters and integrators designed for use with the curve follower permitted plotting of the data in special format, as, for example, log temperature, log energy, etc.

1.32 Analog Plots

(1) Time-History Correlations of Power Energy, Temperature, Flow and Pressure. During a reactor transient, pressure may be generated within the core as a result of various physical occurrences, eg, thermal expansion and change of state. Initially, the release of energy during a transient causes expansion of the fuel plates, followed shortly by moderator expansion as heat is transferred from the plates to the moderator. The expansion of either fuel or moderator creates a source of pressure within the system. For higher energy releases, higher temperatures are encountered and changes of state are possible, first in the moderator water via vaporization (boiling), and later in the fuel plates by means of melting and eventually by vaporization of the plates. Each of these change-of-state phenomena can occur only after an effective threshold temperature has been reached. Thus it appears reasonable to expect a correlation between such variables as energy, power, flow and temperature, and the resulting pressure generation.

The time-dependent behavior of these variables may be compared with the pressure behavior in Figure 13. The fuel-plate surface temperature closely follows the energy deposition within the plate until the boiling temperature is reached [a], indicating that for this transient little energy is transferred to the water by conduction and convection prior to boiling. When the plate temperature exceeds the boiling temperature, energy transfer from the plate to the water via boiling results in a significant reduction in the rate of temperature rise. The dashed curve superimposed over the temperature curve in this and subsequent figures is an approximation to the behavior of an "insulated" fuel plate. It has been obtained empirically from the energy curve by translating the time axis as required to compensate approximately for the delay between energy deposition and sensing of the deposition by the thermocouples. The translated energy curve was then normalized to the temperature curve in the exponential region. The deviation of the temperature from this approximate insulated plate behavior is a qualitative measure of the energy transfer from the plate to the water.

The initial deflection of the pressure trace is negative. There is some evidence that part of this negative deflection may be due to a net increase in volume of the fuel can [b] as a result of fuel plate expansion. A part of the

---

[a] Note that all temperature plots are logarithmic and are indicative of the temperature rise above ambient. The symbol θ is placed on the temperature curve with the horizontal bar at the value of $\Delta\theta$ corresponding to boiling, eg, 97° - 26°C = 71°C in Figure 13. The magnitude of the temperature rise corresponding to the boiling temperature is indicated in parentheses as ($\Delta\theta$ = 71°C). For an explanation of the trace designations such as 63 18-6 see item 2 above.

[b] For welded assemblies such as the P-Core and the Spert III C-Core, fuel plate expansion results in a net outward displacement of the fuel can side plates. The resultant volumetric increase may exceed the volumetric expansion of the fuel plates themselves. A resultant net flow of moderator into the assembly could cause a small decrease in the reference pressure level at the transducer location.

deflection is probably a result of radiation sensitivity of the transducer as indicated in Figure 13, where the component is so labelled and the dashed extension approximates the zero reference line from which pressure level probably should be measured. The caption will be omitted from subsequent figures since the features of this contribution are consistently similar and easily recognizable. The pressure behavior appropriately exhibits a moderate initial rise prior to the onset of boiling heat transfer, which is attributed to fuel plate and moderator expansion. Theoretically, for an open vessel, this contribution would decrease to zero at the time of peak power [15]. A subsequent larger pressure rise is closely correlated with the time of onset of boiling heat transfer, and, hence, may be reasonably associated with steam formation resulting from boiling. The plateau observed at the time of peak power is a consequence of the combination of these two pressure contributions (one increasing and one decreasing) in the vicinity of peak power.

The onset of flow indicating expulsion of moderator from the core correlates well with the pressure behavior (Figure 13). It should be noted here that the long term "fundamental" of the flow response has superimposed on it a higher frequency component ($\approx$100 cps) due to core vibration. Continuation of flow beyond the time of peak pressure is a result of inertial effects, and causes a decline of the pressure magnitude to a point below the initial reference level. For the flowmeter used in P-Core tests the magnitude of flow rate is proportional to the square root of the trace deflection shown (Section II).

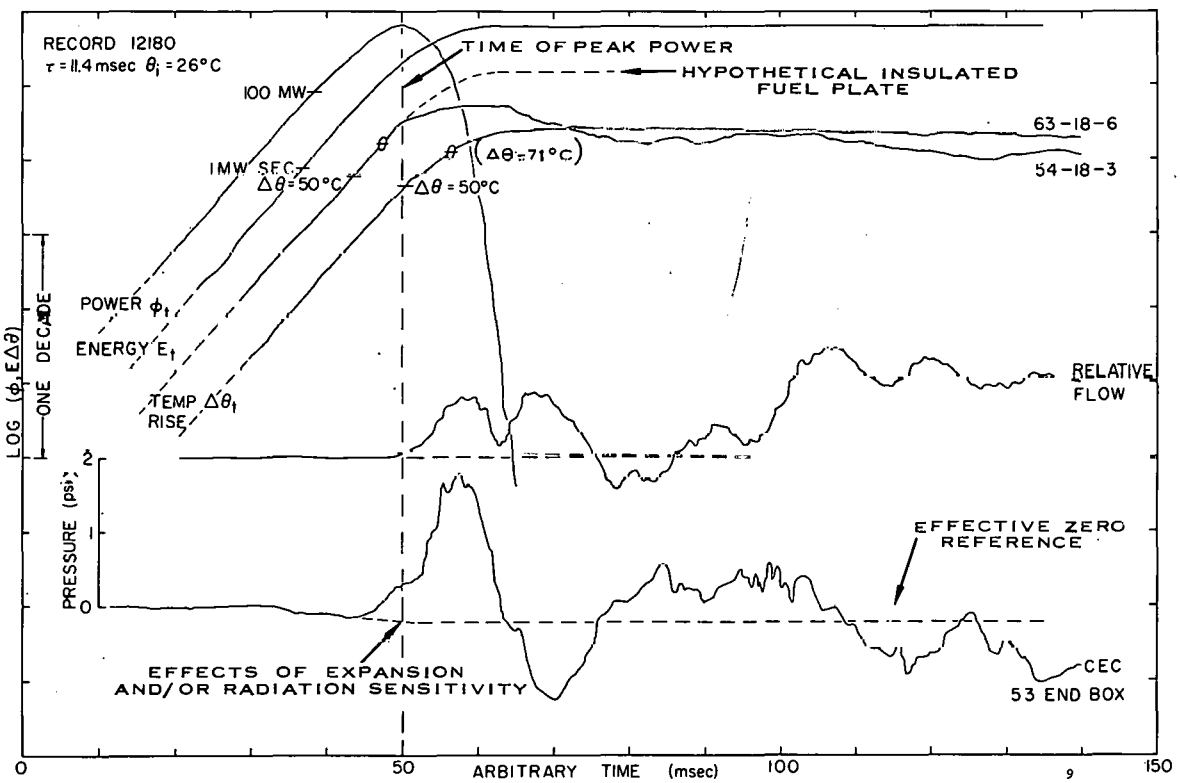

Fig. 13 A presentation of time histories for power, energy, fuel-plate surface temperature, pressure, and flow. The symbol θ on the temperature-time histories indicates the boiling temperature with the corresponding temperature rise shown in parentheses adjacent to one of the traces.

Data for a transient having a slightly shorter reactor period are shown in Figure 14. This figure also displays a temperature measurement obtained in the water channel between fuel plates. The data were obtained from a 5-mil butt-welded, chromel-alumel thermocouple shown schematically in Figure 15.

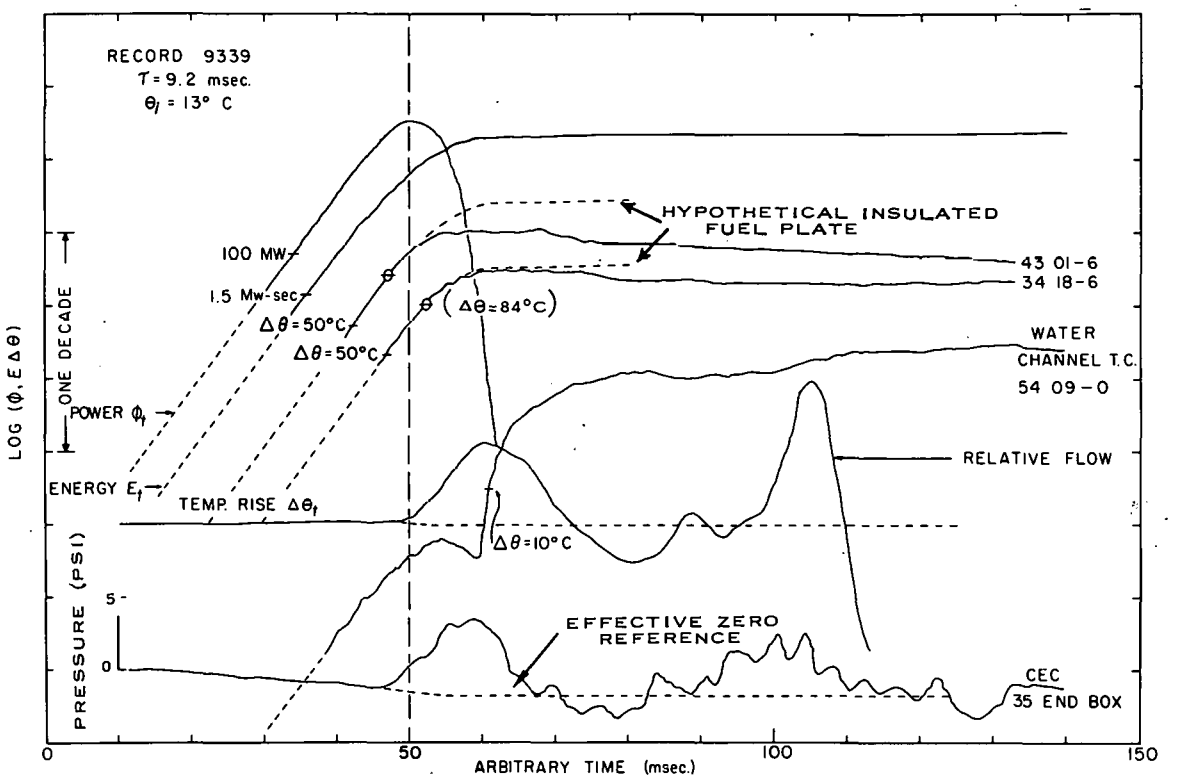

Fig. 14 A presentation of time histories for power, energy, fuel-plate surface temperature, pressure, and flow. The symbol θ on the temperature-time histories indicates the boiling temperature with the corresponding temperature rise shown in parentheses adjacent to one of the traces.

Data obtained with a device incorporating four such thermocouples spaced at 20-mil intervals in the water channel are shown in Figure 16. The nominal temperature rise indicated by these water channel thermocouples implies that for these transients most boiling is restricted to a very thin film of water adjacent to the fuel plates, as predicted from a simple calculation of heat transfer [16]. In the time interval preceding peak power, the temperature indication from all four water channel thermocouples rises simultaneously to a point about 7°C above the reference level, declines momentarily, and then continues to rise during the next 100 msec. This behavior is indicative of radiation heating of the thermocouples during the power generation cycle, followed later in time by a rise correlated with an increase in moderator temperature.

(2) Time-History Correlation of Pressure Behavior and Radial and Longitudinal Temperature Distributions. In the above correlations between the fuel-plate temperature and the pressure (Figures 13 and 14) the temperature data shown represent only a few isolated points within the reactor. To adequately

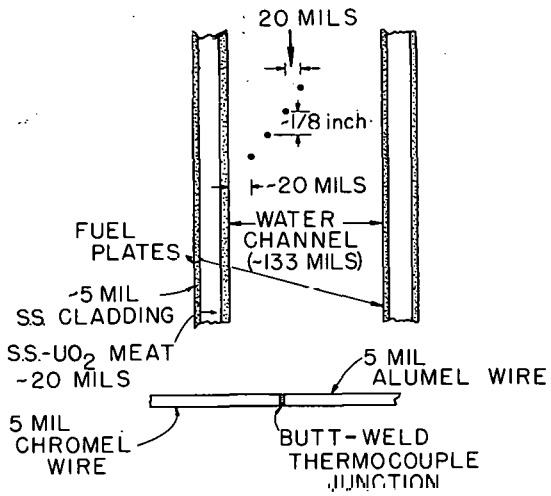

Fig. 15 Schematic representation of the placement of thermocouples for temperature measurements obtained between fuel plates in the Spert I P-Core fuel assembly.

represent conditions within the pressure source [a], it is necessary to consider the spatial distribution of temperature. In practice, it is possible to determine this spatial distribution only in a macroscopic sense, as, for example, from the radial and longitudinal temperature distributions obtained within the core during the 17-msec transient shown in Figures 17, 18, and 19. Again a correlation between the occurrence of heat transfer from the plate (deviation from the insulated plate behavior) and the generation of pressure may be observed [b]. Similar data for reactor periods of 9.8 and 6.7 msec are displayed in Figures 20 through 23. From these data the importance of the size of the pressure source, ie, the volume of the core contributing to the

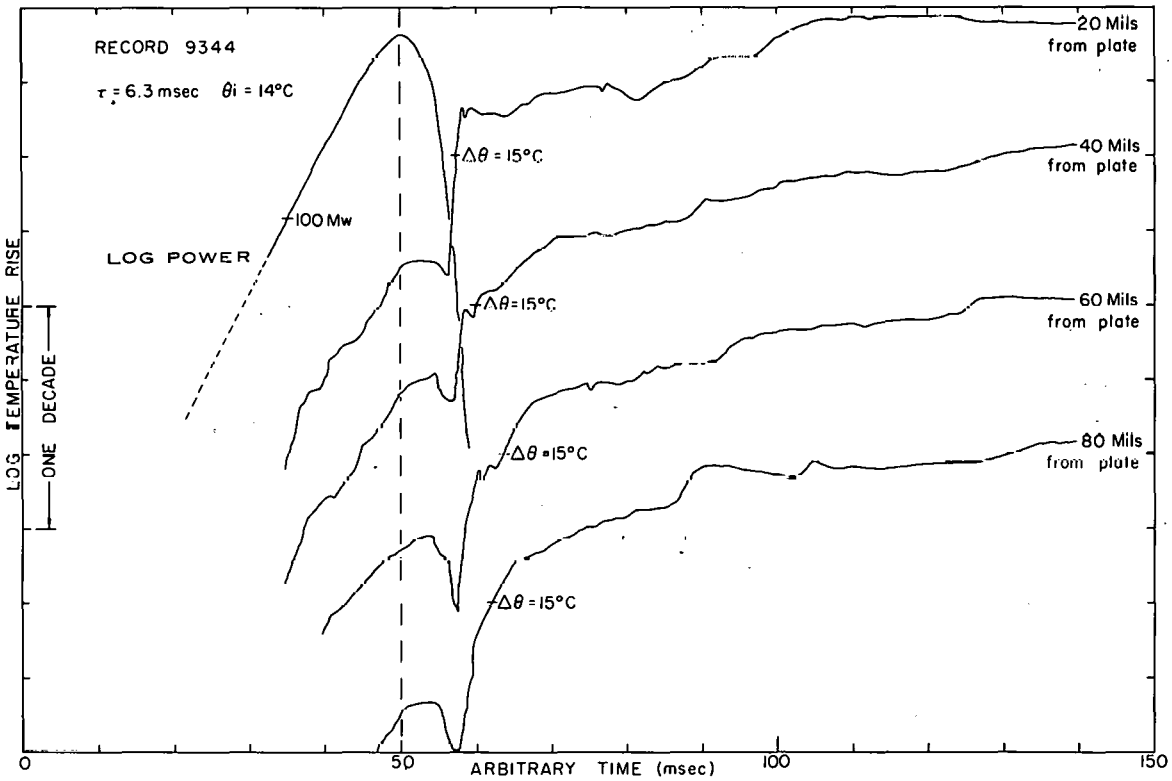

Fig. 16 Temperature-time histories obtained from butt-welded thermocouples in the water channel between fuel plates of the Spert I P-Core assembly.

[a] The pressure source will be defined as that portion of the reactor core which contributes significantly to the generation of pressure.

[b] The space-time distribution of the onset of boiling correlates very closely with the static neutron flux profile.

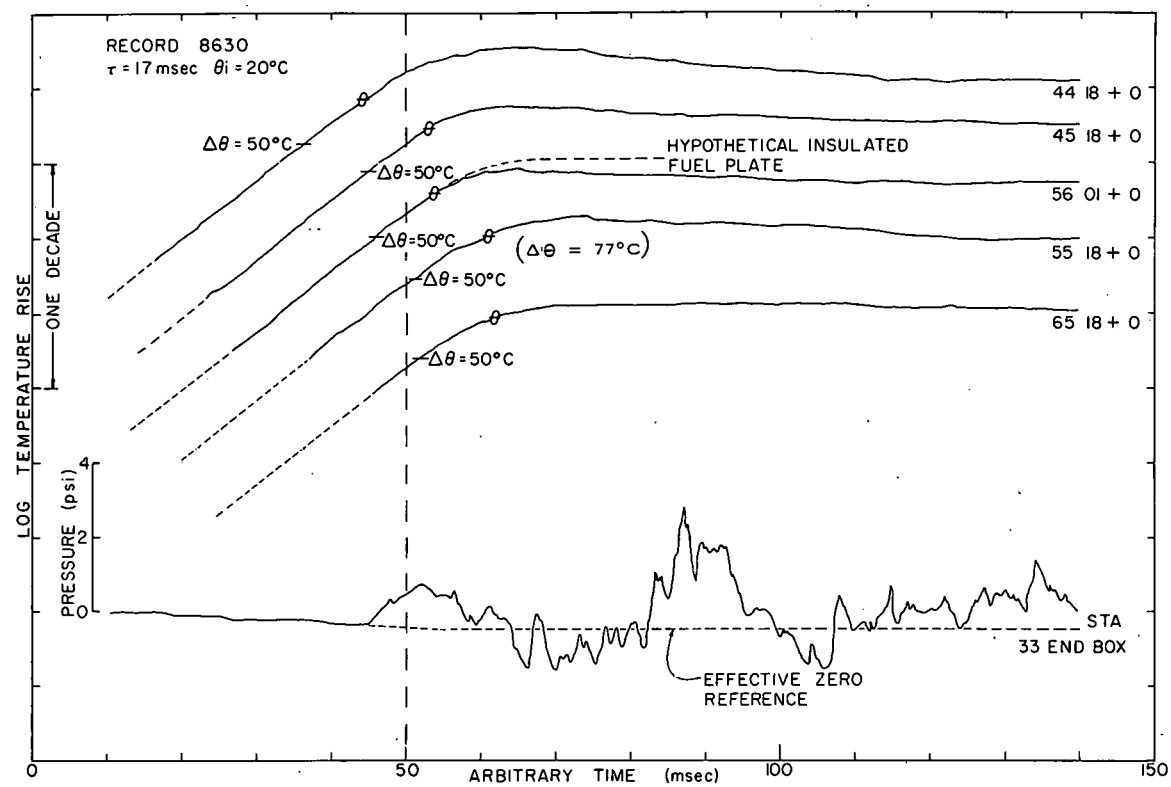

Fig. 17 A presentation of fuel-plate surface temperature-time histories at various radial positions and the pressure-time history. The symbol θ on the temperature-time histories indicates the boiling temperature with the corresponding temperature rise shown in parentheses adjacent to one of the traces.

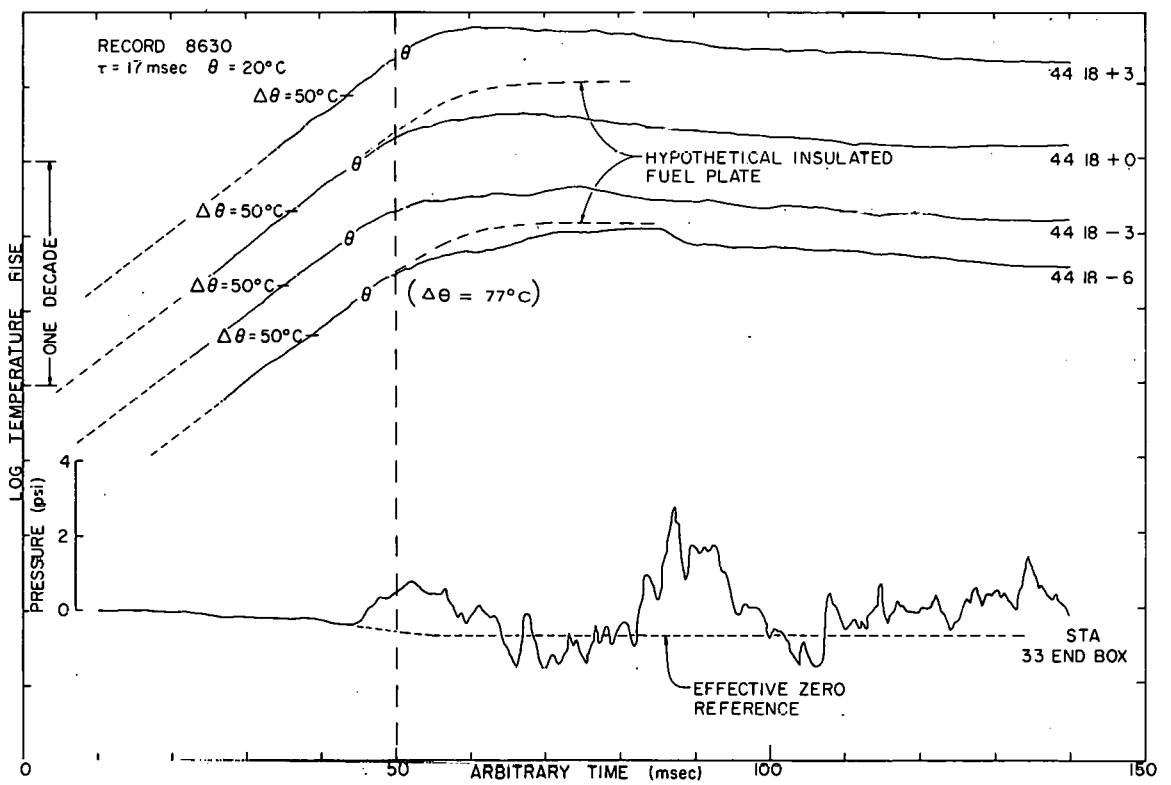

Fig. 18 A presentation of fuel-plate surface temperature-time histories at various longitudinal positions along a fuel plate and the pressure-time history. The symbol θ on the temperature-time histories indicates the boiling temperature with the corresponding temperature rise shown in parentheses adjacent to one of the traces.

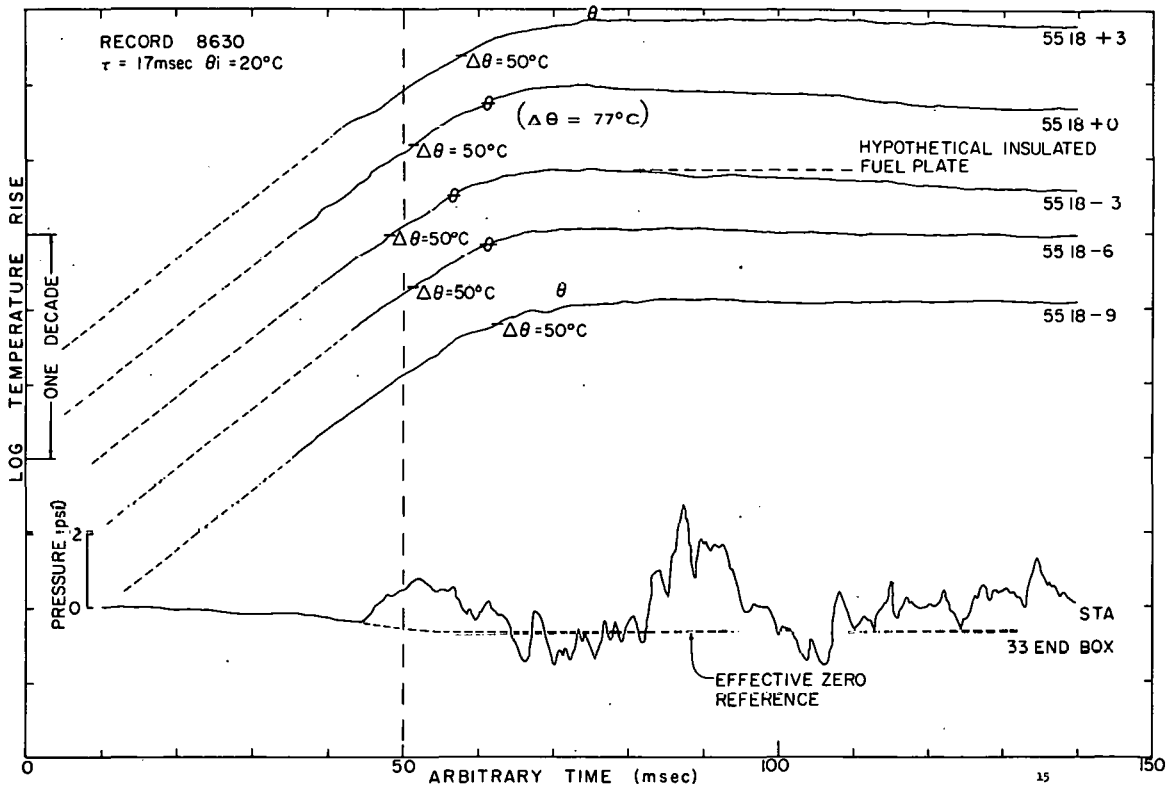

Fig. 19 A presentation of fuel-plate surface temperature-time histories at various longitudinal positions along a fuel plate and the pressure-time history. The symbol θ on the temperature-time histories indicates the boiling temperature with the corresponding temperature rise shown in parentheses adjacent to one of the traces.

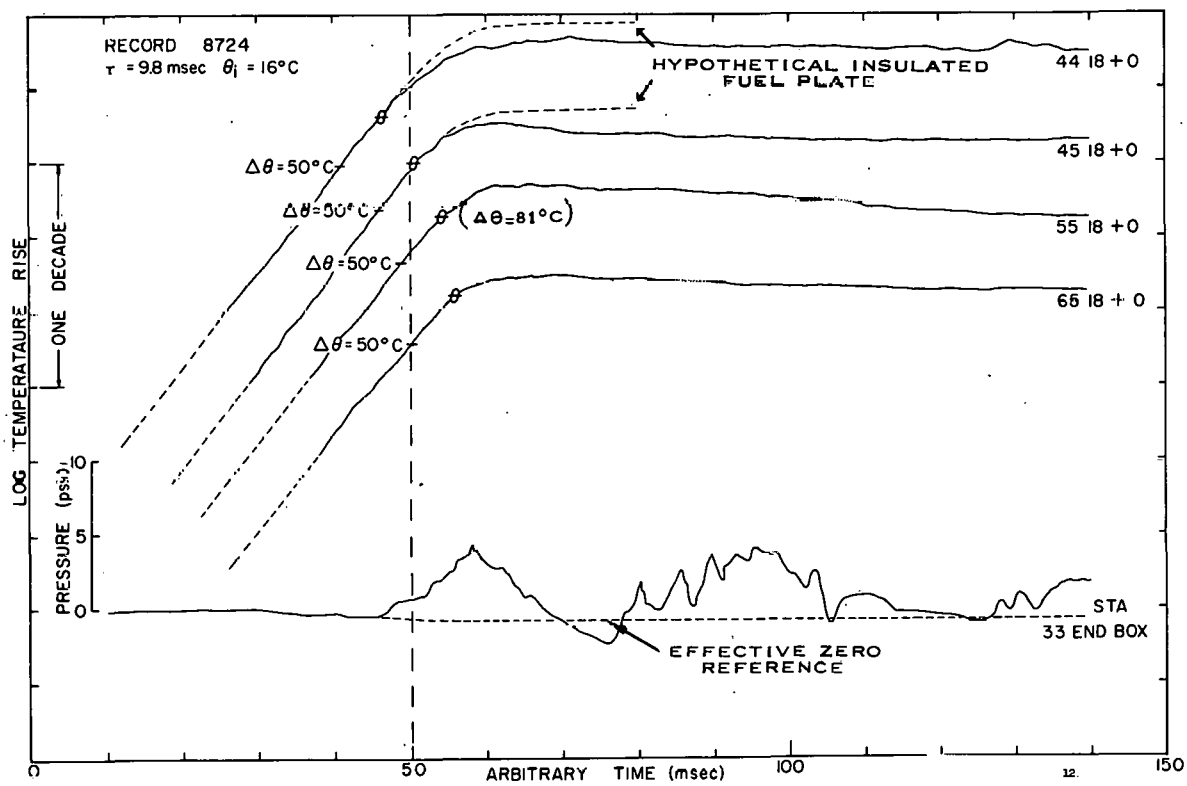

Fig. 20 A presentation of fuel-plate surface temperature-time histories at various radial positions and the pressure-time history. The symbol θ on the temperature-time histories indicates the boiling temperature with the corresponding temperature rise shown in parentheses adjacent to one of the traces.

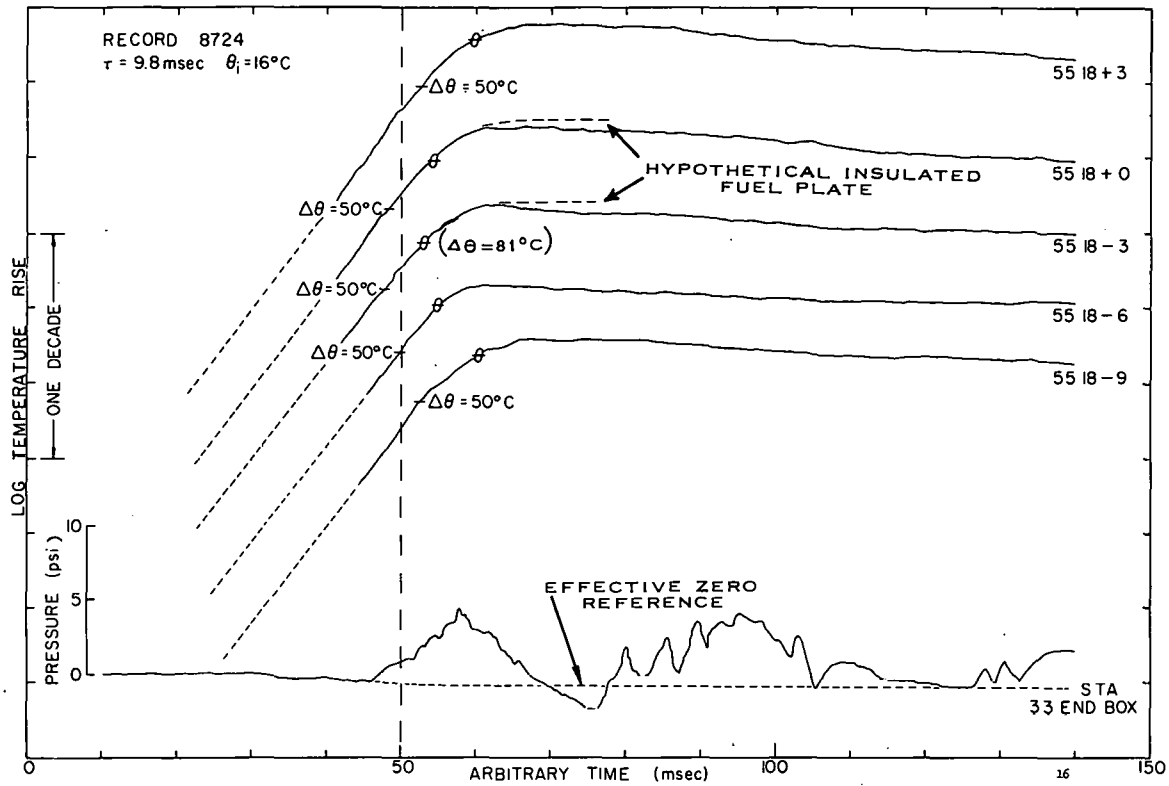

Fig. 21 A presentation of fuel-plate surface temperature-time histories at various longitudinal positions along a fuel plate and the pressure-time history. The symbol θ on the temperature-time histories indicates the boiling temperature with the corresponding temperature rise shown in parentheses adjacent to one of the traces.

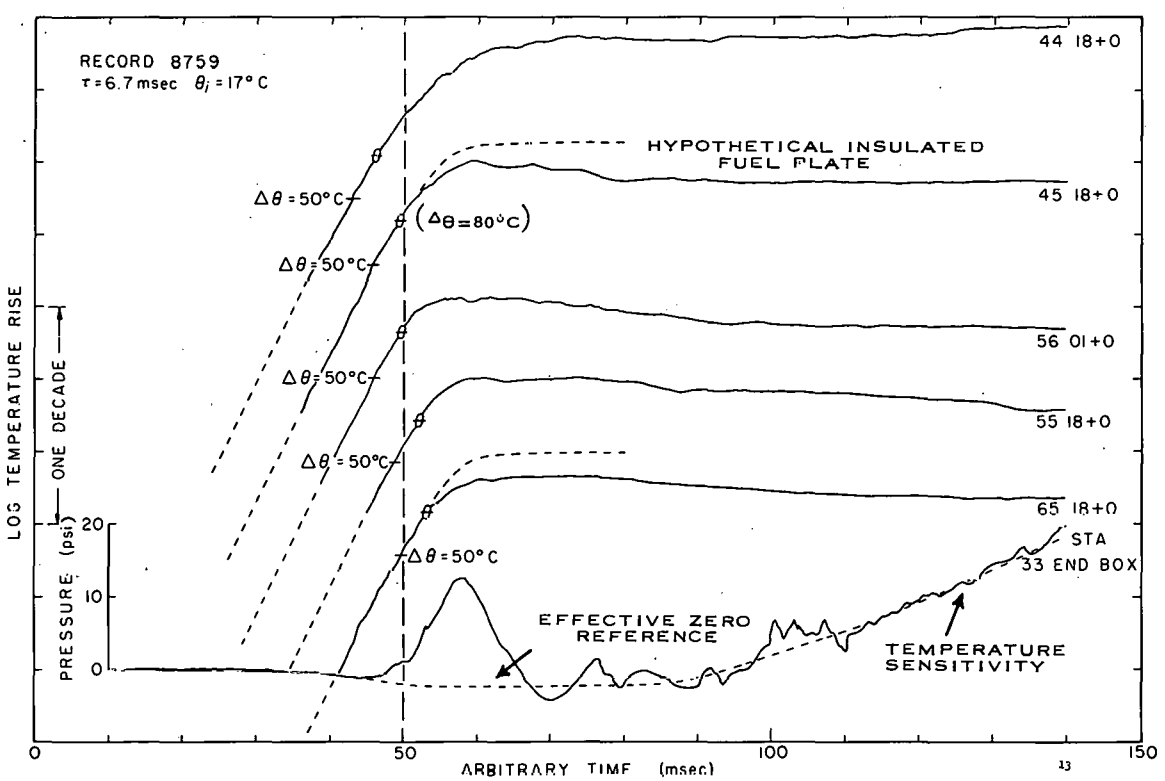

Fig. 22 A presentation of fuel-plate surface temperature-time histories at various radial positions and the pressure-time history. The symbol θ on the temperature-time histories indicates the boiling temperature with the corresponding temperature rise shown in parentheses adjacent to one of the traces.

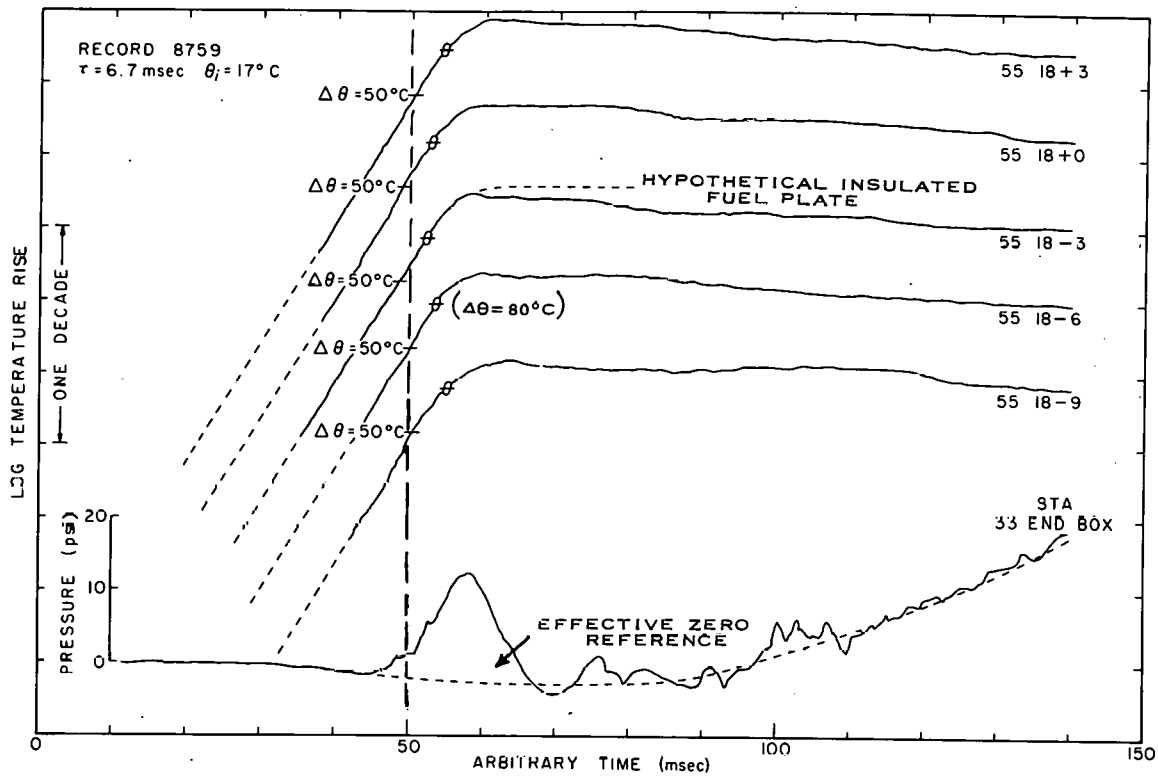

Fig. 23 A presentation of fuel-plate surface temperature-time histories at various longitudinal positions along a fuel plate and the pressure-time history. The symbol θ on the temperature-time histories indicates the boiling temperature with the corresponding temperature rise shown in parentheses adjacent to one of the traces.

generation of pressure can be noted. For example, the central assembly sometimes indicates heat transfer over a limited central region at a point in time preceding the first observable deflection of the pressure trace. This behavior is due to (a) the high geometrical losses incident to pressure transmission from a small central source to the end box location, and (b) low sensitivity of the transducer used [a]. However, whenever boiling heat transfer is observed over an appreciable fraction of the core, it is always accompanied by a perceptible rise in pressure level.

For the shortest period transient shown (Figure 22) expulsion of hot liquid from the core causes a long-term rise in indicated pressure level subsequent to the initial pressure peak. This spurious output results from differential heating of the transducer components and is not indicative of true pressure level. The dashed line drawn through these data indicates qualitatively the location of the zero reference [b].

The data of Figure 24 further illustrate the dependence of pressure generation upon heat transfer by showing the magnitude of the deviations of the fuel-plate surface temperature from the insulated-plate behavior at various

[a] A sufficiently sensitive pressure sensor would have indicated a very small increase in pressure at this time.

[b] Similar base lines are indicated in later plots, generally without specific identification, since the nature of the contribution due to temperature sensitivity is usually quite apparent.

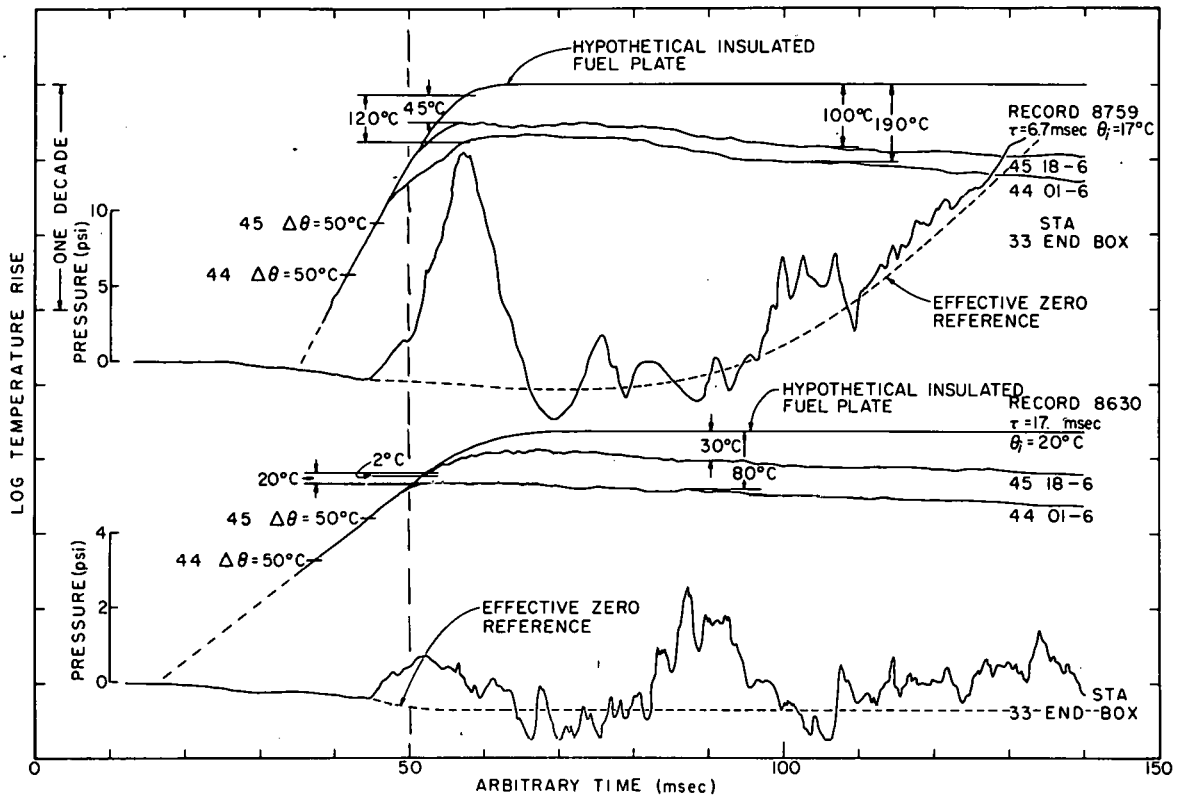

Fig. 24 Representative pressure-time histories for P-Core transients indicating typical deviations from the behavior of a hypothetical insulated fuel plate.

times in the course of pressure generation. Again, part of the deflection of the pressure trace for the short period transient is a spurious output resulting from temperature sensitivity of the transducer (eg, beyond $\approx$ 70 msec). It is difficult to determine the true level of pressure generation in this time interval.

The data of Figure 25 display a close correlation between temperature and pressure behavior for reactor transients having a boiling initial temperature. A general decrease in fuel-plate surface temperatures closely associated with the secondary pressure pulse is clearly evident. Discontinuties associated with sharp increases in temperature also can be observed in the data. These temperature increases are probably a result of interruption of heat transfer by formation of a film blanket adjacent to the fuel plate. One such discontinuity is visible in trace 55 01-9 in the lower half of Figure 25 where the postulated interruption of heat transfer results in a cessation of pressure generation as would be expected.

(3) Effects of Miscellaneous Variables Upon Pressure Generation. The dependence of the pressure behavior upon reactor period is shown in Figures 26 and 27 for ambient and boiling initial temperatures. The general pressure behavior is the same for both initial conditions and reactor periods shown. It consists of a primary pressure peak followed by a pressure decline and secondary pressure peaks of lesser magnitude. This behavior is typical of all Spert I cores as may be seen by reference to the data presented in Appendix A. As the reactor period decreases, the magnitude of the pressure

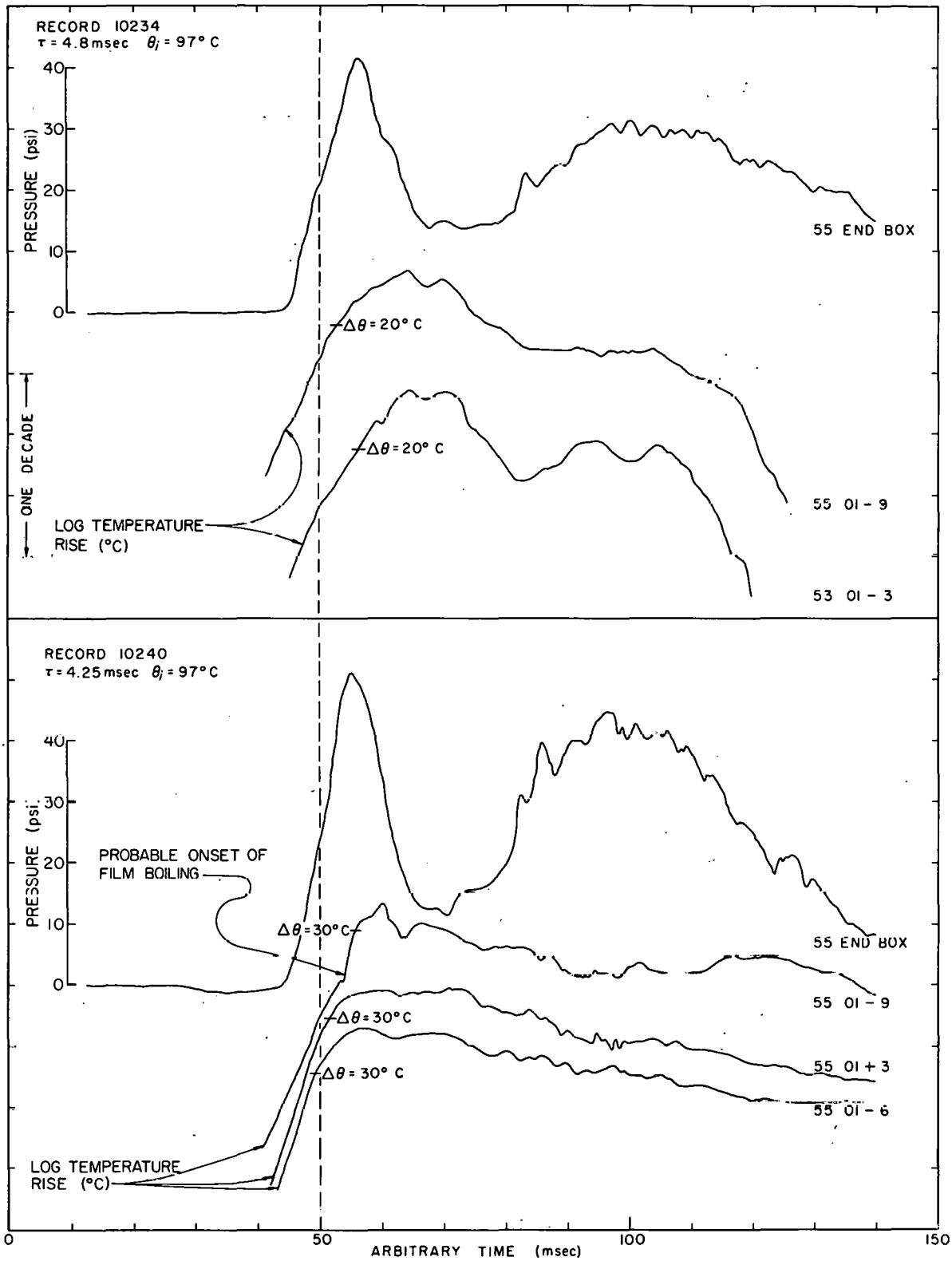

Fig. 25 Representative temperature- and pressure-time histories for boiling reactor transients showing correlations between the occurrence of heat transfer from the fuel plate to the moderator water and the resultant pressure generation.

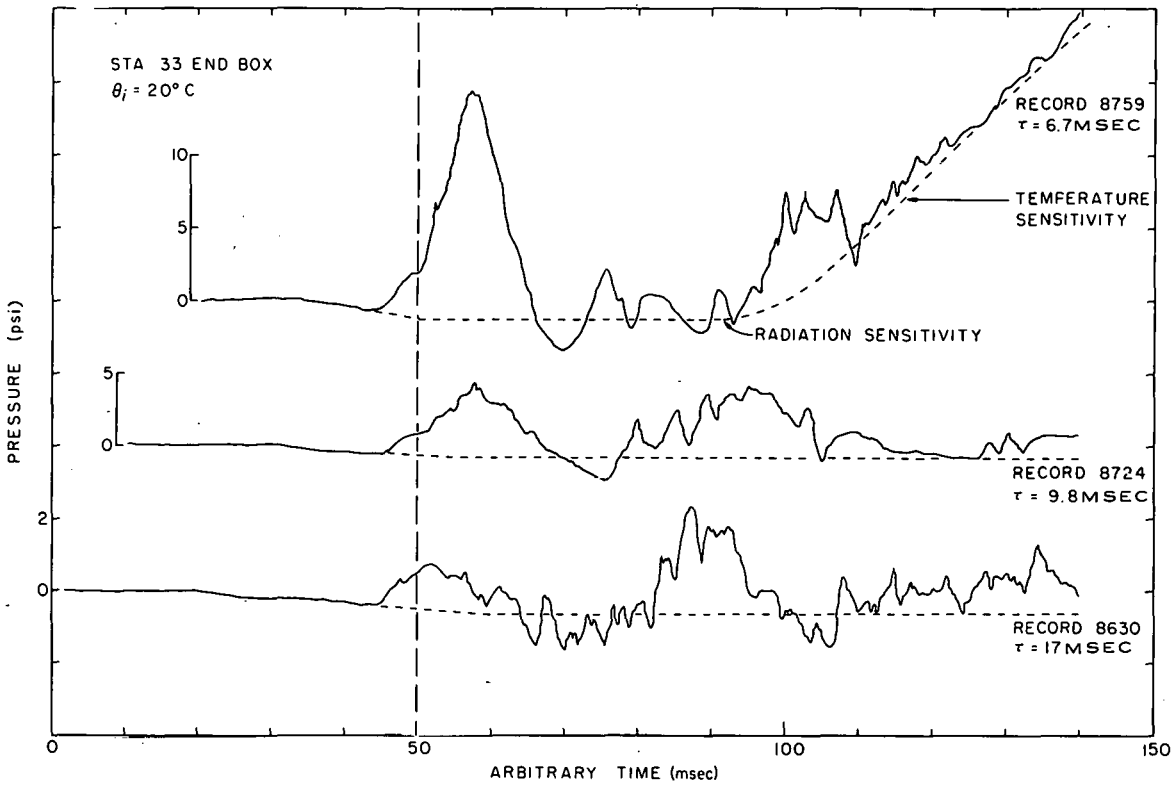

Fig. 26 Representative pressure-time histories for ambient temperature reactor transients showing the dependence upon reactor period. (Note effects of radiation and temperature sensitivity upon the reference pressure level.)

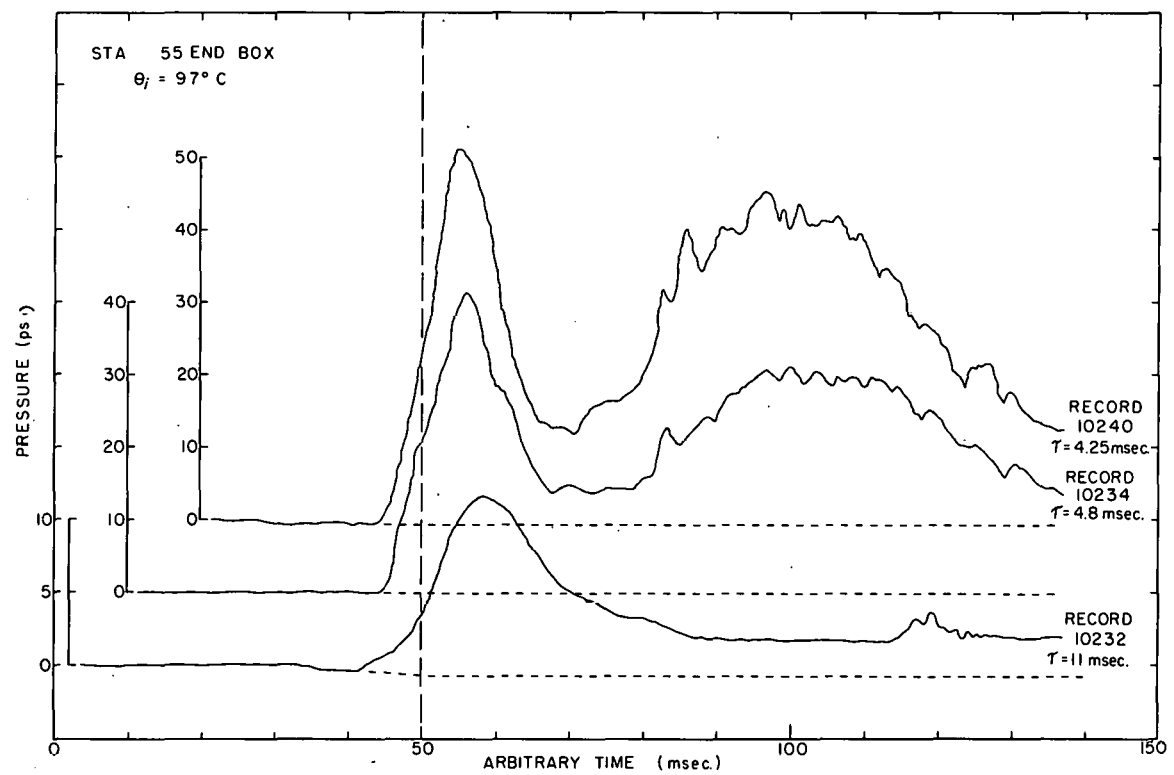

Fig. 27 Representative pressure-time histories for boiling reactor transients showing the dependence upon reactor period.

peak increases, the pulse duration (time at half maximum) decreases, and the pressure peak moves nearer to the time of peak power. Pressure levels are materially higher for the boiling initial temperatures.

The dependence of the pressure magnitude and time behavior upon position in the reactor tank also was investigated. Transducer locations for the test series are shown schematically in Figure 28. The pressure-time behavior for three positions within the reactor tank and for reactor periods of 13.1 msec and 6.6 msec are shown in Figures 29 and 30, respectively. The effects of radiation and temperature sensitivities which are especially apparent in the data obtained at the side of the core are virtually nonexistent at the tank wall. The detail or "fine structure" in the pressure response, which is very pronounced in the data at the side of the core, represents high frequency components which are rapidly attenuated during propagation. The data obtained in the end box and at the tank wall display a much smoother pressure-time history. The pressure-time behavior at the tank wall is shown as a function of reactor period in Figure 31.

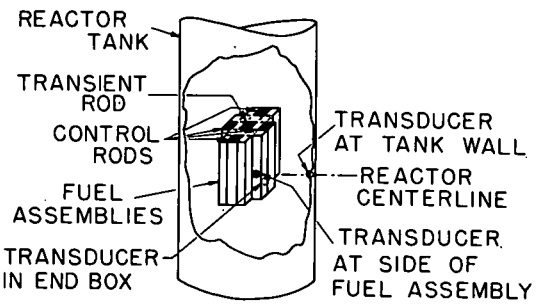

Fig. 28 Schematic representation of transducer locations for investigation of directional aspects of pressure generation.

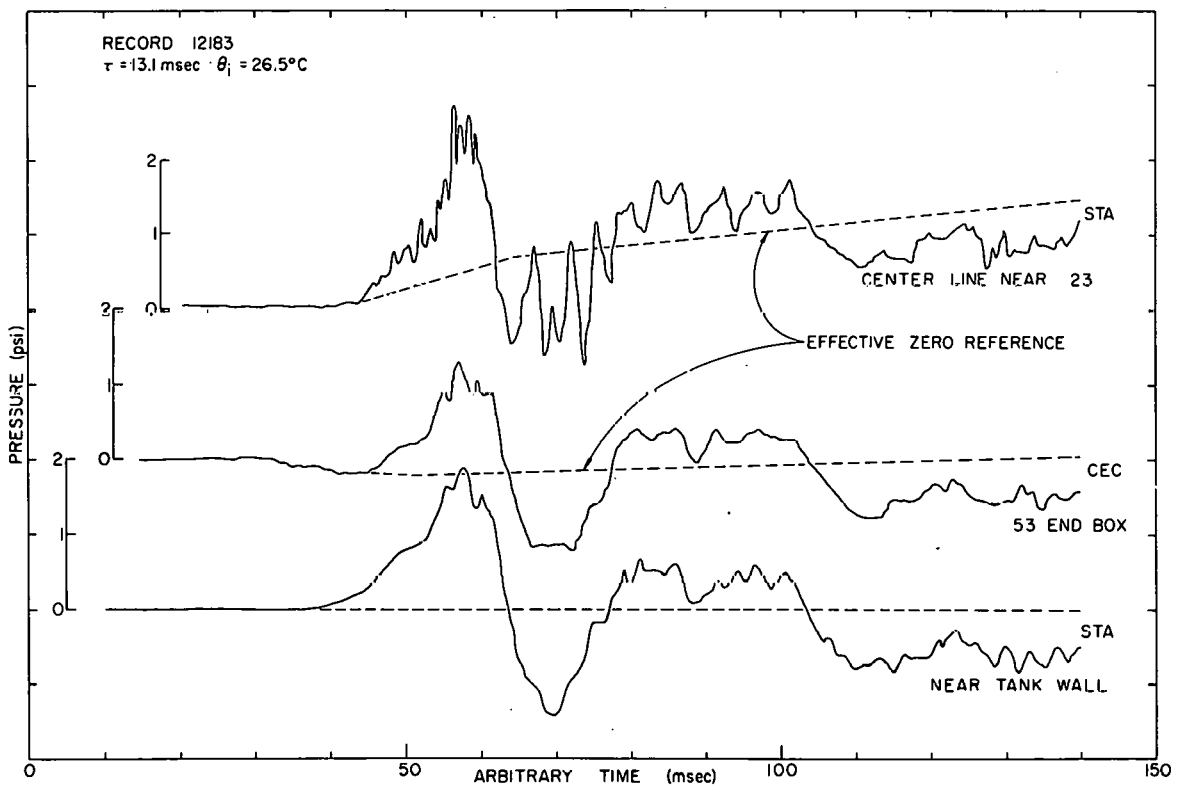

Fig. 29 Representative pressure-time histories obtained at various locations within the reactor tank for a nominal 13-msec reactor period.

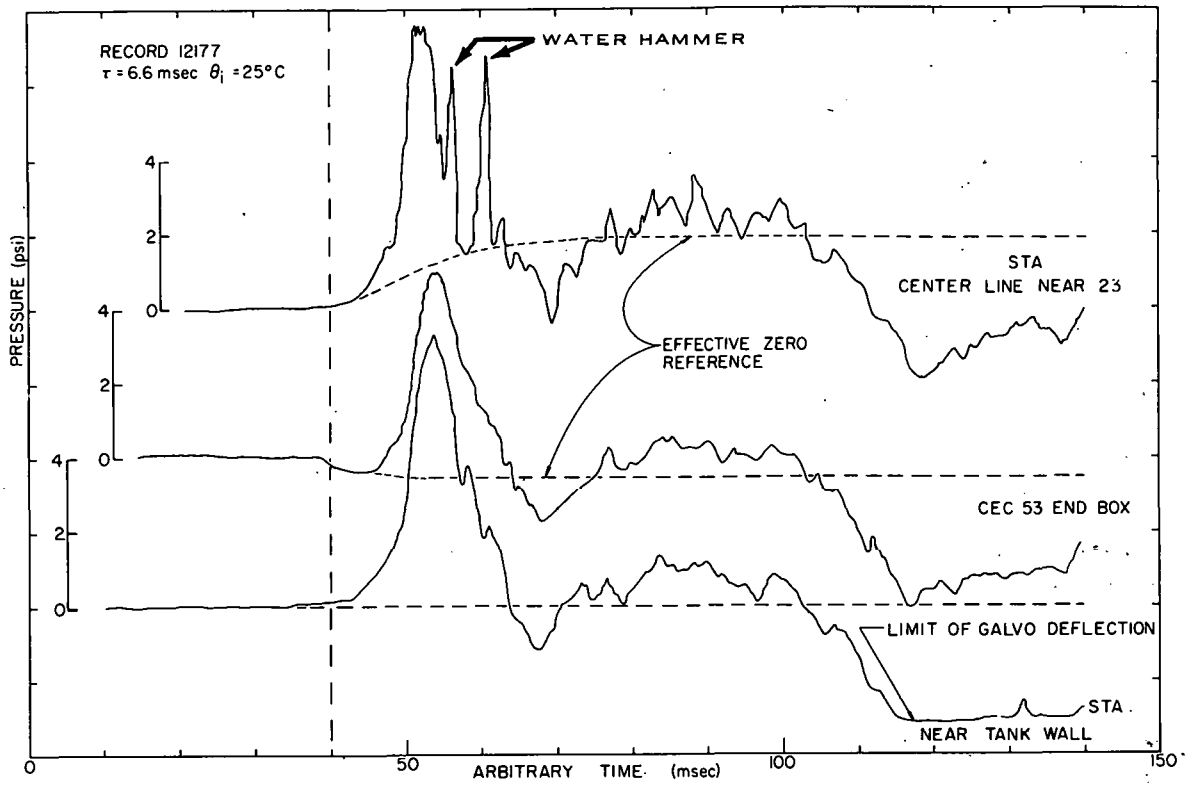

Fig. 30 Representative pressure-time histories obtained at various locations within the reactor tank for a nominal 6.6-msec reactor period.

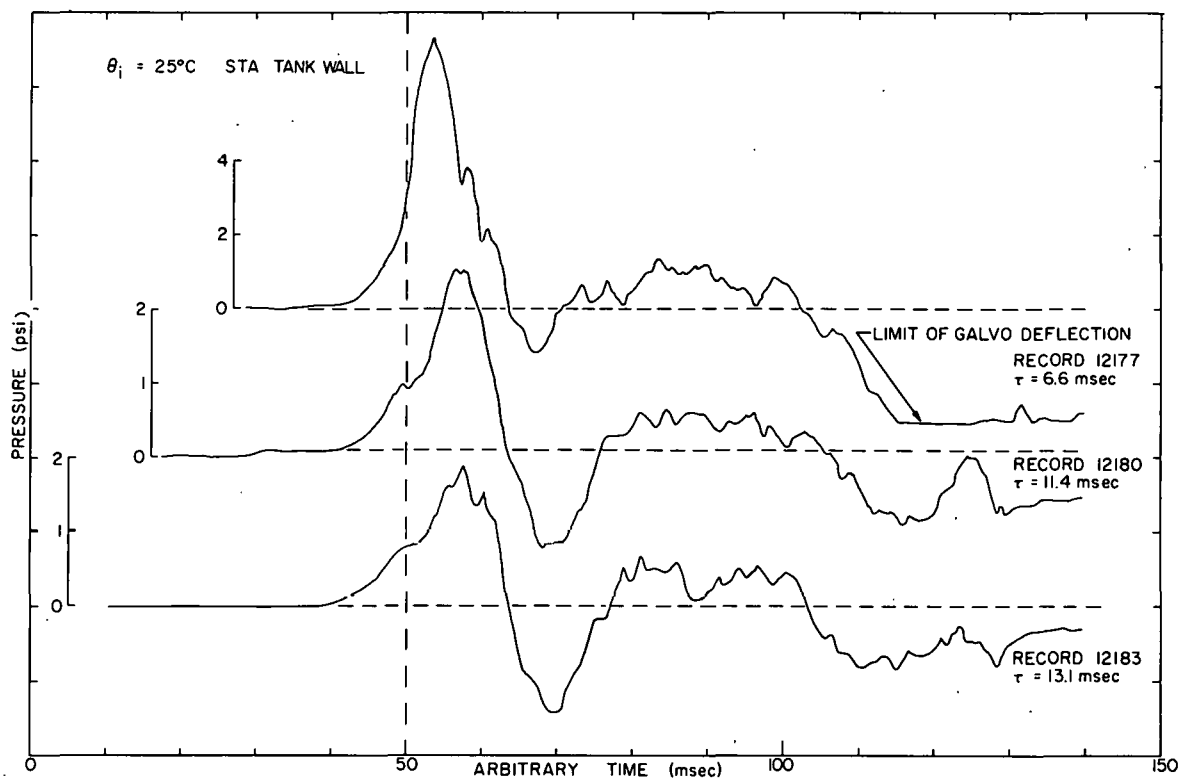

Fig. 31 Pressure-time histories obtained at the wall of the reactor tank for various reactor periods.

The effects of reflection from the free surface may be observed in the data of Figure 32. The data presented were obtained in the upper end box ($\approx$ 2 ft from the water surface) and the lower end box ($\approx$ 4 ft from the water surface) of fuel assembly 53. The pressure-time behaviors are remarkably similar, but the magnitudes differ by about a factor of two. This behavior is due in part to differences in the magnitudes of the reflected (negative) pressure components at the two measuring locations. These traces are indicative of data obtained in a number of transients as shown by the information presented in Table IV.

(4) Rise Time of the Pressure Pulse. The rise time of the pressure pulse will be defined here as the time required for the pressure magnitude to increase from 10% to 90% of the peak. There are isolated instances in the data where rapidly rising pressure spikes occured. These spikes result from local water-hammer effects (Figure 30) and represent only minor energy concentration. The primary pressure pulses which contain most of the energy have rise times in excess of 1 msec for all transients. Since the pressure levels do not exceed 60 psi for any P-Core transient, the pressure pulses obtained were not shock waves [a] in any sense and propagated at normal acoustic velocities. [17]

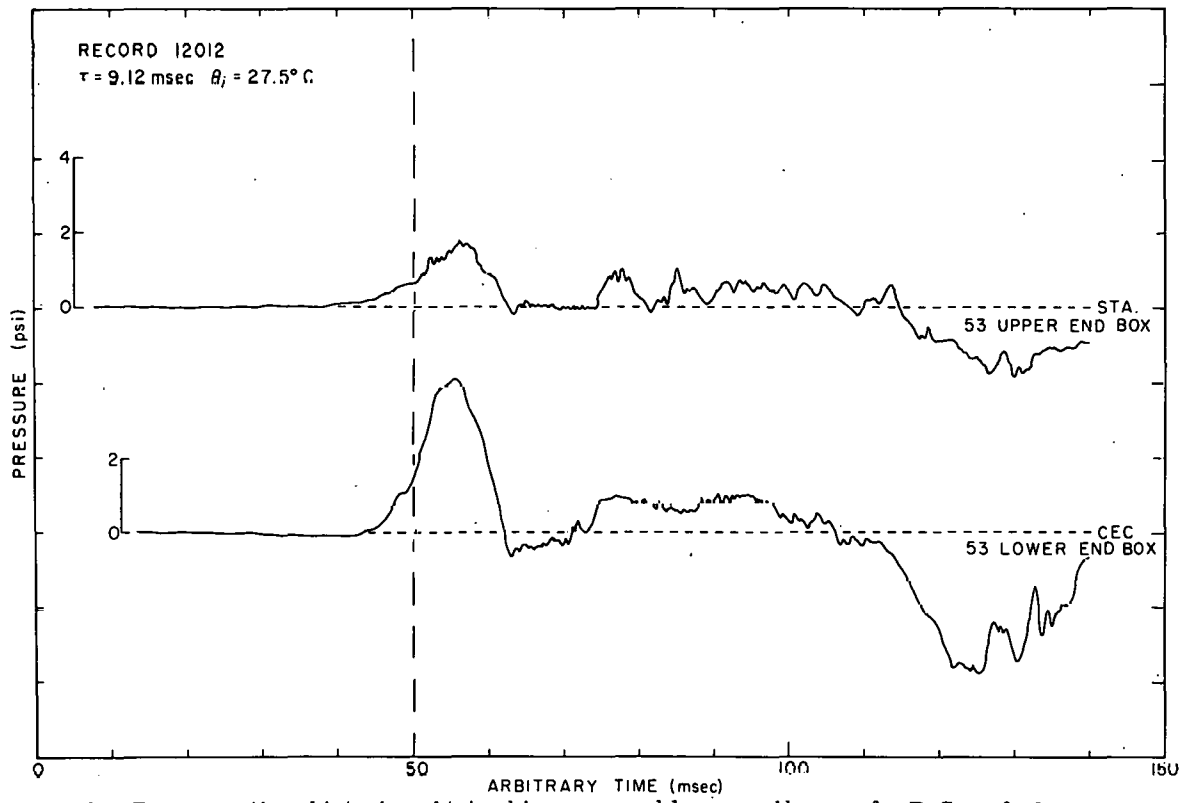

Fig. 32 Pressure-time histories obtained in upper and lower end boxes of a P-Core fuel assembly.

[a] There are two prevalent definitions of a shock wave. The more rigorous definition specifies a shock wave as having a velocity of propagation exceeding the local sonic velocity and a very short rise time (usually <5 μsec). For practical purposes this implies a pressure magnitude of several kilobars. A second definition loosely classifies any sharp fronted pressure wave (rise time <5 μ sec) as a shock wave regardless of the pressure magnitude.

TABLE IV

COMPARISON OF PEAK PRESSURES IN UPPER AND LOWER END BOX LOCATIONS

Record	Reactor Period (msec)	Pressure (psi) Upper End Box	Pressure (psi) Lower End Box	Ratio (Lower/Upper)
12007	9.3	1.9	4.1	2.2
12012	9.1	1.7	4.2	2.5
12018	9.6	1.8	4.3	2.4
12046	12.4	1.0	2.1	2.1
12051	12.4	0.66	2.1	3.2
12056	9.25	1.66	3.8	2.2
12061	8.8	1.9	4.1	2.2
12066	8.9	1.8	4.5	2.5
AVERAGE				2.4

The pressure-time histories are free of the effects of reflection for only about 1 msec after the beginning of pressure generation. For all subsequent times the observed pressure is a composite of an initial (prompt) pressure contribution and a reflected (delayed) contribution. The observed rise time is thus not necessarily the same as would be observed in a system where reflections could not affect pressure magnitude at the measuring location during pressure generation.

From the data obtained with this core, there does not appear to be any simple correlation between the timing of the power and pressure peaks or their respective time-dependent magnitudes. If the leading edge of the pressure pulse is approximated by an exponential function (see Appendix A-4), the "effective period" of this exponential is much less than the reactor period. The dynamic pressure behavior appears to be more closely related to the hydrodynamic, thermodynamic, and acoustic properties of the core than it is to the time history of the power level.

1.33 Cross Plots. The peak-pressure and pressure-at-peak-power data obtained during testing with the P-Core are summarized in Table V. The observed repeatability of the data for peak pressure is of the order of ± 30% [a]. Data for pressure at the time of peak power show considerably more scatter, primarily as a result of the very small trace deflections corresponding to the low pressure magnitudes involved.

[a] Factors affecting reliability of the data are discussed further in Appendix B.

TABLE V

SUMMARY OF P-CORE PRESSURE DATA

Record Number	Initial Temperature (°C)	Reactor Period (msec)	Transducer Type	Transducer Location	Pressure at Peak Power (psi)	Peak Pressure (psi)
8630	20	16.5	STA	33 end box	0.2	1.2
			CEC	35 end box	0.7	1.0
			ULT	55 end box	0.6	1.0
8720	15	11.4	STA	33 end box	1.3	2.0
			CEC	35 end box	1.0	1.7
			ULT	55 end box	2.2	2.3
8724	16	9.8	STA	33 end box	1.2	5.0
			CEC	35 end box	1.6	6.2
			ULT	55 end box	2.0	5.7
8759	17	6.7	STA	33 end box	2.6	14.0
			CEC	35 end box	2.5	18.6
			ULT	55 end box	3.1	15.7
8795	18	5.5	STA	33 end box	6.0	23.4
			CEC	35 end box	5.5	19.6
			ULT	55 end box	6.2	18.0
8814	17	4.7	STA	33 end box	5.2	30.7
			CEC	35 end box	5.0	27.5
			ULT	55 end box	5.5	26.0
9339	13	9.2	CEC	35 end box	1.7	5.2
9344	14	6.3	STA	33 end box	2.5	16.0
			CEC	35 end box	3.1	12.3
			STA	53 end box	2.7	15.9
9422	15	11.3	CEC	35 end box	1.2	3.7
			STA	53 end box	0.9	3.9
9425	7	9.8	CEC	35 end box	1.2	6.3
			STA	53 end box	1.7	7.3
10232	97	11.0	CEC	35 end box	2.5	12.5
			STA	55 end box	3.8	8.6
10234	97	4.8	CEC	35 end box	16.0	35.0
			STA	55 end box	20.5	41.3
10240	97	4.25	CEC	35 end box	19.0	52.2
			STA	55 end box	23.2	51.8
11994	25.75	19.2	CEC	53 end box	0.3	0.4
12007	27	9.3	STD	side of core	2.7	4.2
			STA	53 u-end box	0.5	1.9
			CEC	53 end box	1.4	4.1

TABLE V (cont'd)

SUMMARY OF P-CORE PRESSURE DATA

Record Number	Initial Temperature (°C)	Reactor Period (msec)	Transducer Type	Transducer Location	Pressure at Peak Power (psi)	Peak Pressure (psi)
12012	27	9.1	STD	side of core	3.2	4.2
			STA	53 u-end box	1.0	1.8
			CEC	53 end box	3.0	4.3
12018	28	9.6	STD	side of core	2.2	4.4
			STA	53 u-end box	0.5	1.7
			CEC	53 end box	1.5	4.2
12041	27	19.1	STD	side of core	0.4	0.8
12046	27	12.4	STD	side of core	1.0	2.8
			STA	53 u-end box	0.3	0.7
			CEC	53 end box	0.7	2.0
12051	28	12.4	CEC	53 end box	---	2.1
12056	28	9.25	STD	side of core	2.5	4.1
			STA	53 u-end box	---	1.6
			CEC	53 end box	1.5	3.8
12061	26	8.8	STD	side of core	2.5	4.0
			STA	53 u-end box	0.8	2.1
			CEC	53 end box	1.9	3.9
12066	27	8.9	STD	side of core	2.1	4.0
			STA	53 u-end box	1.0	1.8
			CEC	53 end box	1.7	4.5
12080	27	17.0	CEC	53 end box	0.3	0.5
12177	25	6.6	CEC	53 end box	1.3	5.3
			STA	tank wall	1.6	7.2
12180	26	11.4	STA	tank wall	0.5	2.5
			CEC	53 end box	0.4	1.9
12183	26	13.1	STA	tank wall	0.5	1.9
			CEC	53 end box	0.4	1.5

The data have been plotted as a function of reciprocal period in Figures 33 and 34 for ambient initial temperature and in Figures 35 and 36 for boiling initial temperature. Peak pressure and pressure at peak power are plotted as functions of total energy release and energy release to time of peak power in Figures 37 and 38, respectively. For convenience of reference, lines having specific slopes have been drawn through the data with the slopes indicated on the plots.

The primary application of these data is associated with studies of reactor behavior for those transients which do not cause permanent damage to the core. For such transients the primary mechanism of energy transfer is by means of conduction and/or boiling heat transfer from the intact metal plates.

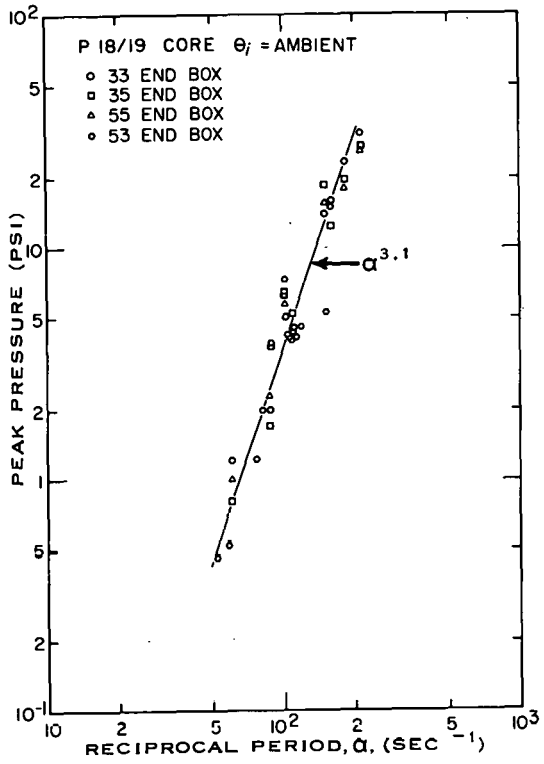

Fig. 33 Peak transient pressure in various lower end boxes as a function of reciprocal reactor period for ambient initial temperature.

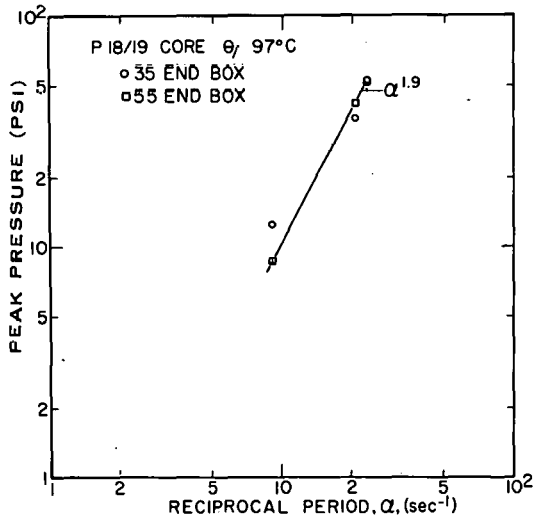

Fig. 35 Peak transient pressure in various lower end boxes as a function of reciprocal reactor period for boiling initial temperature.

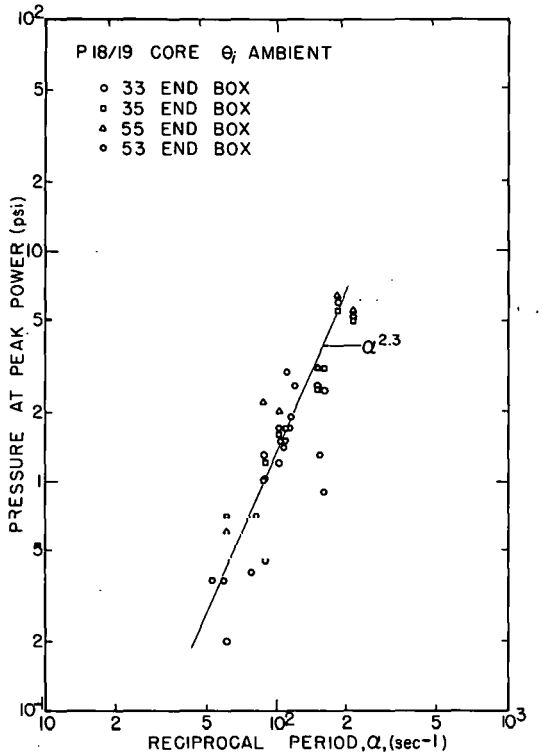

Fig. 34 Transient pressure at time of peak power in various lower end boxes as a function of reciprocal reactor period for ambient initial temperature.

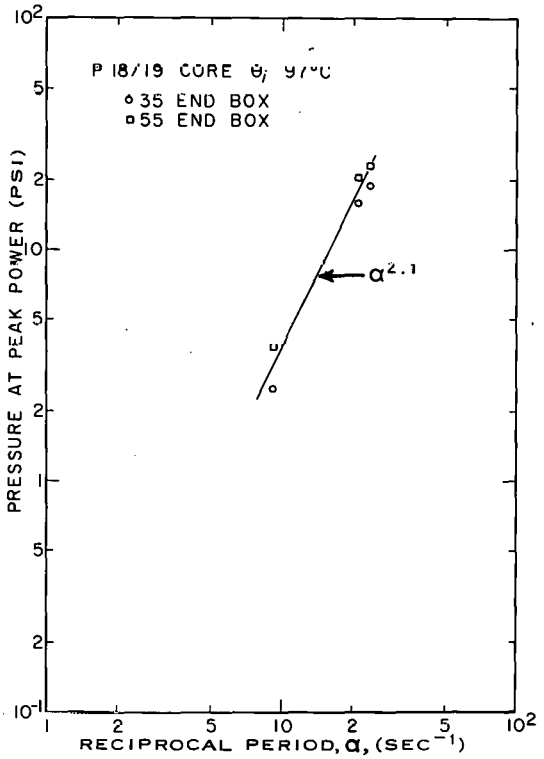

Fig. 36 Transient pressure at time of peak power in various lower end boxes as a function of reciprocal reactor period for boiling initial temperature.

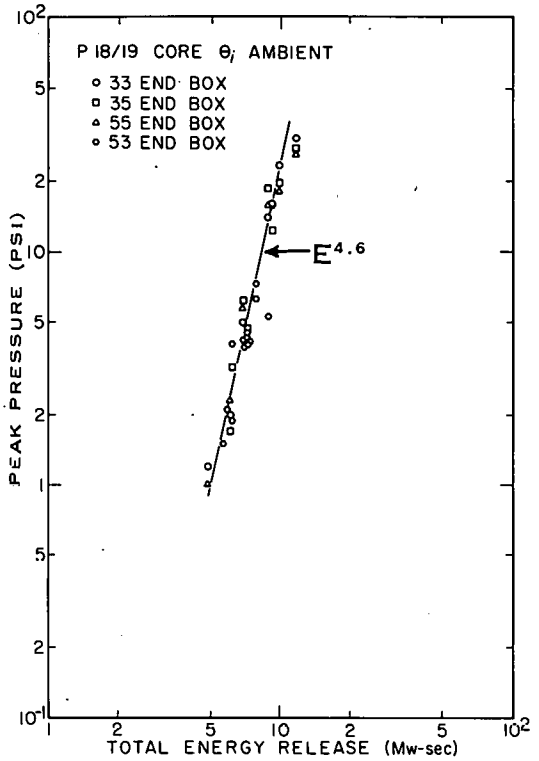

Fig. 37 Peak transient pressure in various lower end boxes as a function of total nuclear energy release for ambient initial temperature.

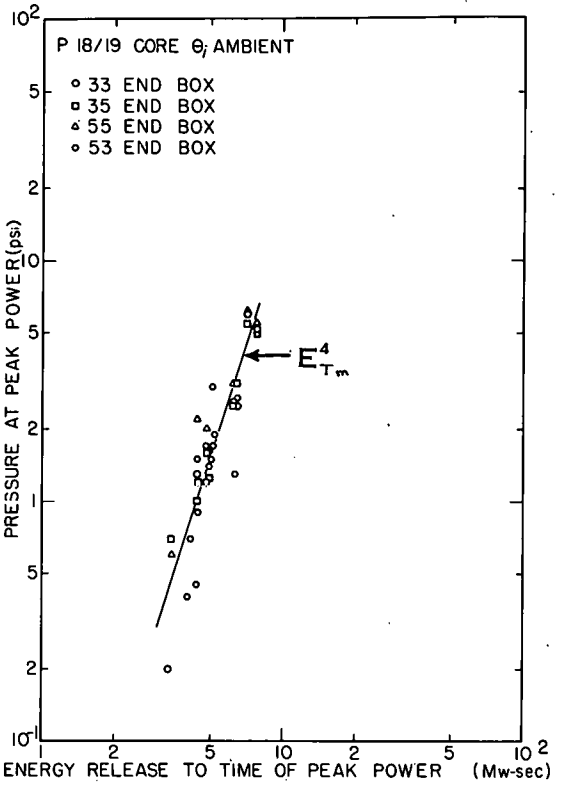

Fig. 38 Transient pressure at time of peak power in various lower end boxes as a function of nuclear energy release to time of peak power for ambient initial temperature.

However, as the transient energy release increases (larger α), a threshold for gross core melting must eventually be reached, whereupon a new geometry for heat transfer will be created (metal droplets in water) and a new type of pressure source will exist. It is not possible at present to specify a definitive value of α for which such effects might be expected. Hence, extrapolation of the data to larger α is not advisable. As a case in point, the Spert I D-Core data obtained during a fiducial series [18] may be compared with data obtained during the destructive [19] test. The pressure pulse obtained during the fiducial series was similar to the P-Core pressure pulse displayed above. However, the pressure behavior obtained during the destructive test shows two distinct pressure pulses. The first pulse occurred near the time of peak power and had a magnitude approximately equal to that given by extrapolation of the fiducial data. The second pulse occurred some 15 msec after peak power and had a peak pressure two orders of magnitude greater than the first pulse. This second pulse could not be obtained by extrapolation of the earlier data and probably resulted from the development of a new type of pressure source similar to the one indicated above.

2. SPERT III

2.1 Facility Description [20]

Since a complete description of the Spert III facility can be found elsewhere, only a brief outline will be given here. The facility consists of the reactor vessel assembly and auxiliary equipment as shown in Figure 39. The reactor vessel is shown pictorially in Figure 40. It has an inside diameter of four ft, an overall height of about 19 ft, and is designed to operate at a static

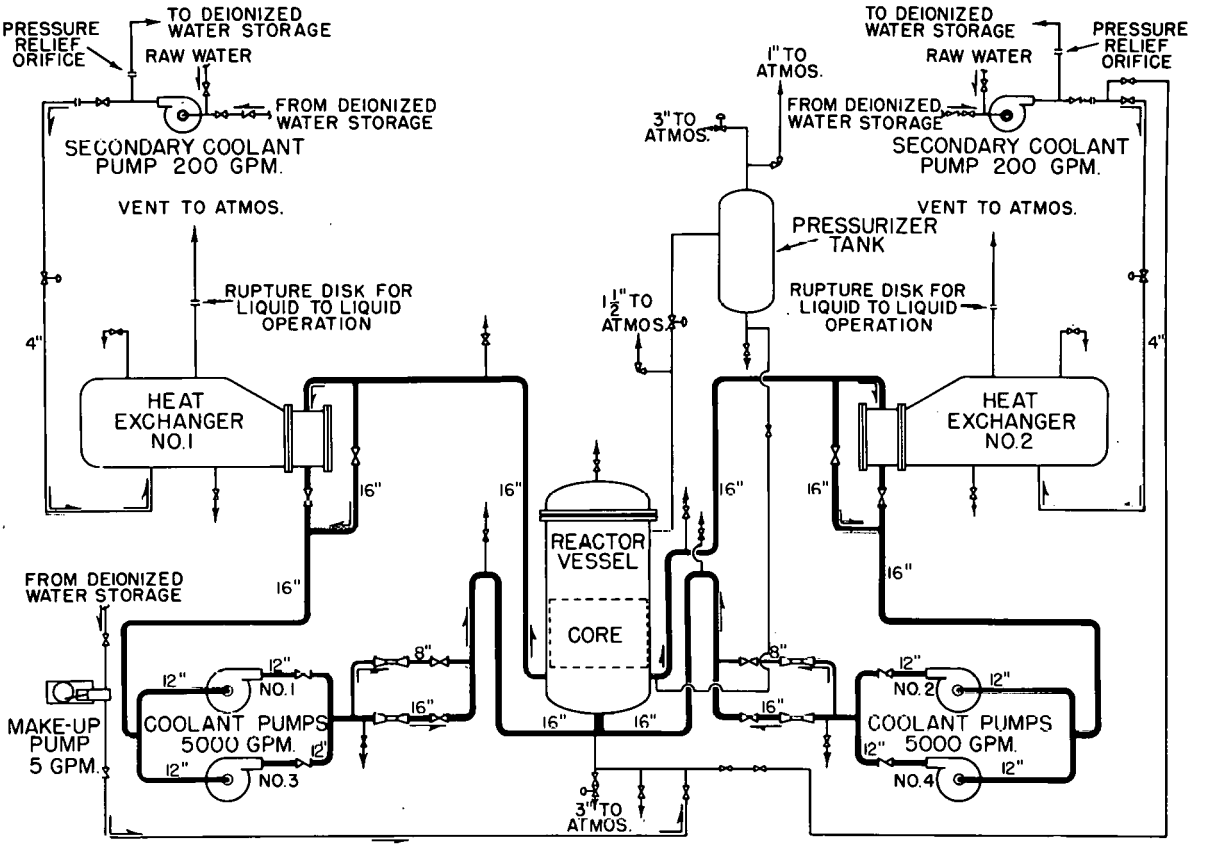

Fig. 39 Schematic representation of Spert III facility showing the reactor vessel and auxiliary equipment.

pressure of 2500 psi at 670°F. The vessel shell is 3.5 in. thick and is built up by a number of thinner sections (laminar construction) the inner of which is clad with 0.125 in. of 304L stainless steel. The vessel head is of forged construction and is of the modified-hemispherical, full-opening, bolted type. The control rod drive assemblies are mounted on the head.

The core skirt and grid assemblies are supported by one of the thermal shields from a point near the bottom of the vessel. The upper grid is designed to permit insertion or removal of up to 15 fuel assemblies without removal of the vessel head. This fuel handling is accomplished by utilizing the four 6-in.-diameter access ports in the head. The head also has five 1.5-in.-diameter openings to accept the control rod drives. There are six 4-in.-diameter ports in the vessel shell near the top of the vessel which are used for removal of instrument leads. Coolant is introduced through two 16-in.-diameter lines at the bottom tee and is removed through six 8-in.-diameter exit nozzles near the top of the vessel. The vessel is covered with 3 in. of Foamglas insulation and enclosed within a lead gamma shield, 6 in. thick.

2.2 Core Description [21]

The Spert III fuel assembly is shown schematically in Figure 41. It is a plate-type stainless steel unit very similar to the P-Core fuel assembly (Section III-1). It consists of stainless steel clad fuel plates brazed to side plates for support. The assembly has a central stiffener plate which effectively

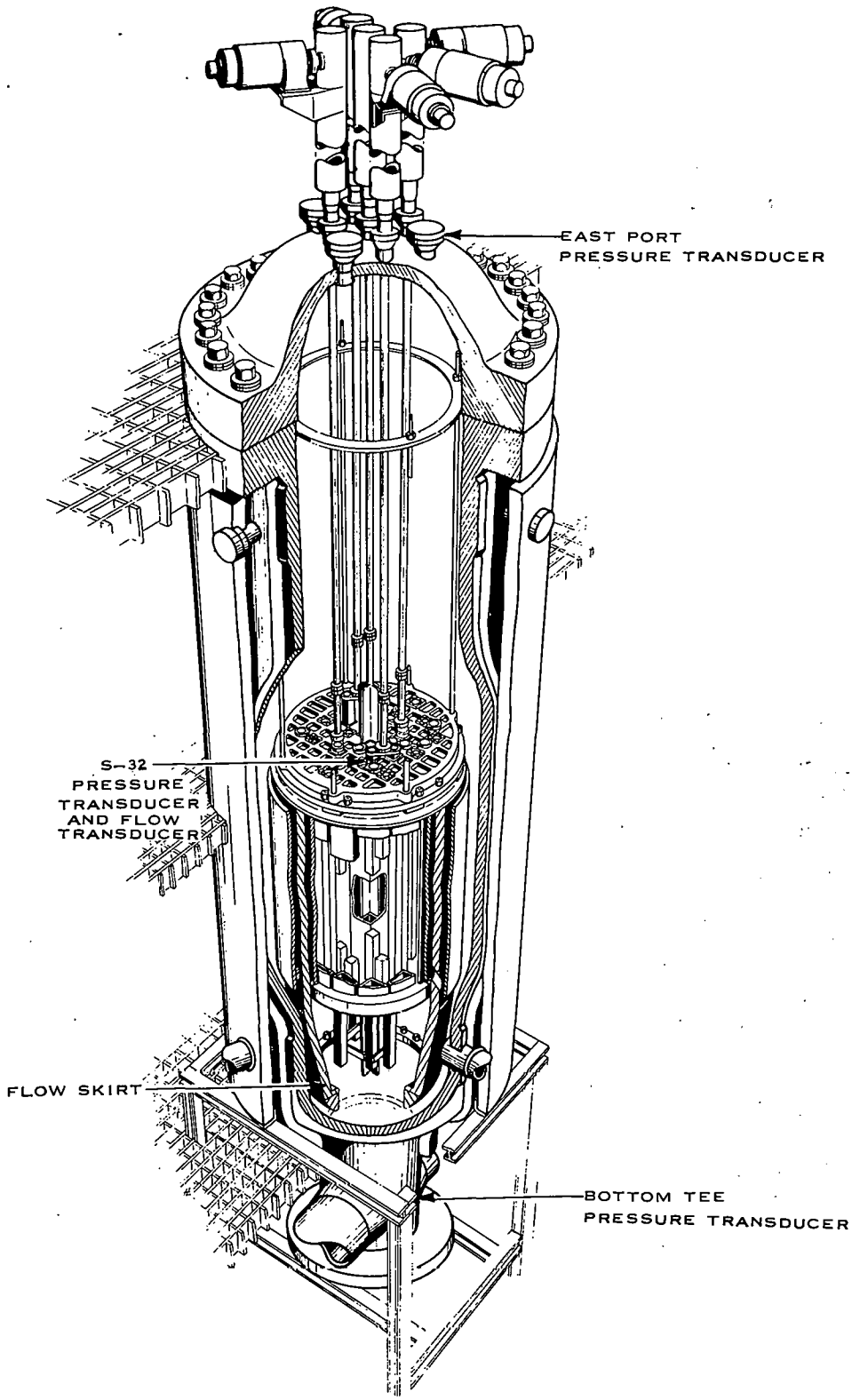

Fig. 40 Schematic representation of Spert III Reactor vessel assembly showing the location of pressure transducers.

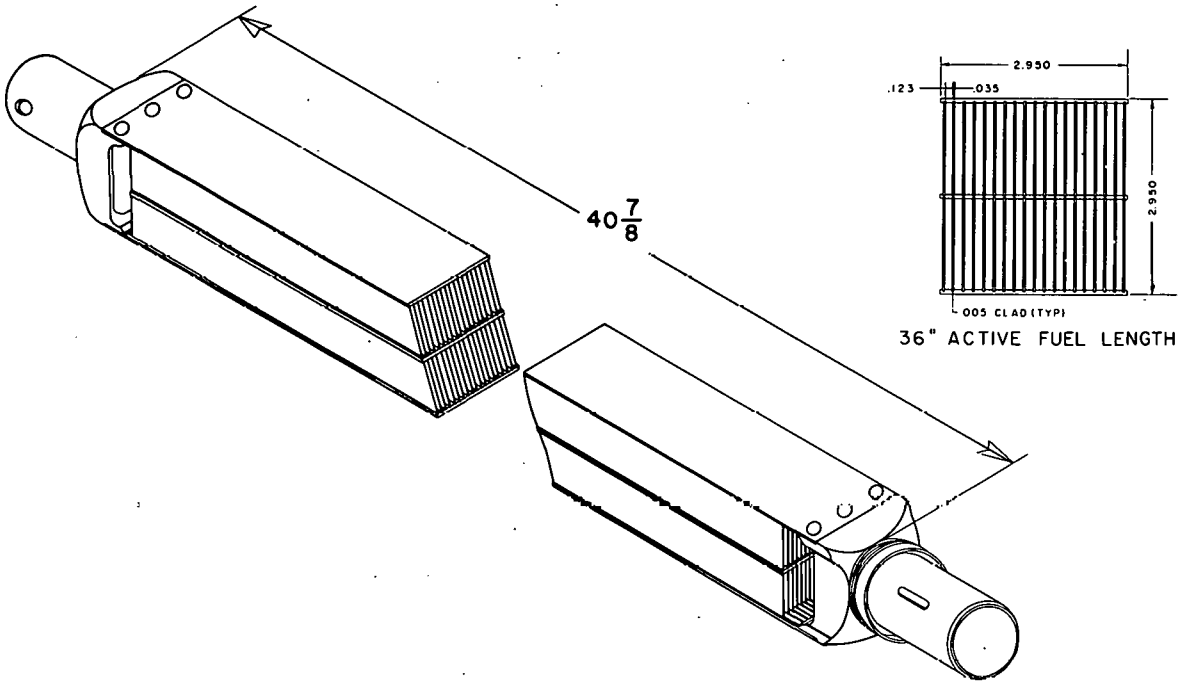

Fig. 41 Schematic representation of a standard, stainless steel, Spert III fuel assembly.

divides each plate into two sections. Each fuel plate has a 20 mil thick meat section of 93.2% enriched UO_2 in a stainless steel matrix. The fuel bearing region is clad in 5 mils of 304L stainless steel. There are two basic assemblies. The regular 19-plate assembly is 3 x 3 x 36 in. and has a fuel content of 638 grams (33.6 grams/plate). A smaller 16-plate assembly is 2.5 x 2.5 x 36 in. and has a fuel content of 442 grams (27.6 grams/plate).

The control rod assemblies are of the fuel-poison type with a fueled lower section and a B^{10} stainless-steel alloy upper section. The assembly, which is shown schematically in Figure 42, contains 14 fuel plates identical to those in the small assembly described above. The operational reactor consists of 40 of the 19-plate assemblies, four of the smaller 16-plate assemblies, and eight of the 14-plate control rod assemblies, resulting in a total loading of 30.6 kg of U-235. The operational configuration is shown in Figure 43 where positions of the control rods and the orientation of the typical fuel assemblies are indicated. All assemblies in a given quadrant are loaded with the plates parallel to the typical assembly shown, and all quadrants are identical, except for orientation of the fuel plates. Quadrants are designated by the letters N, S, E, and W, and fuel assemblies are further identified by letter and number as N 31, E 31, etc. Thermocouple locations are identified by plate number (number 1 nearest transient rod blade) and vertical distance from the center line of the core, as N 31 A1-9. The letter A or B designates which half of the assembly the thermocouple is in, side A being the side nearest to the transient rod blade.

A few pertinent parameters of value in evaluating the Spert III data are presented in Table VI.

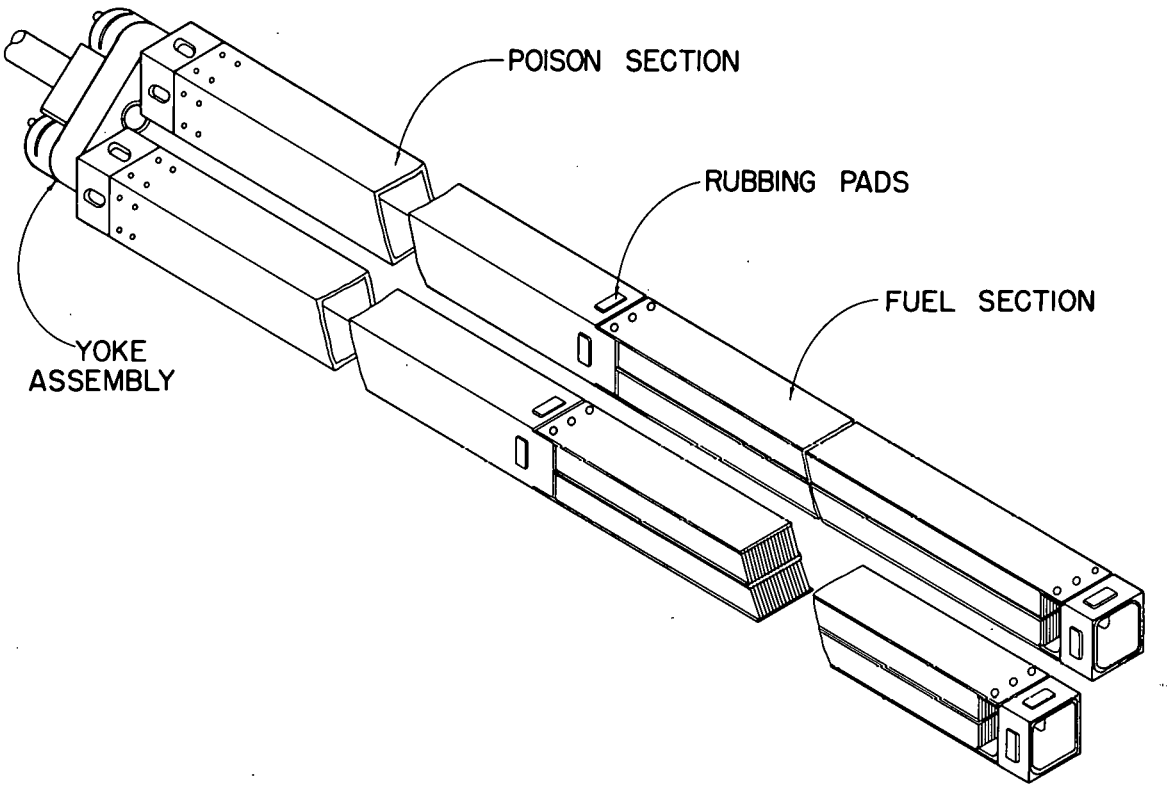

Fig. 42 Schematic representation of a Spert III fuel-poison control rod assembly.

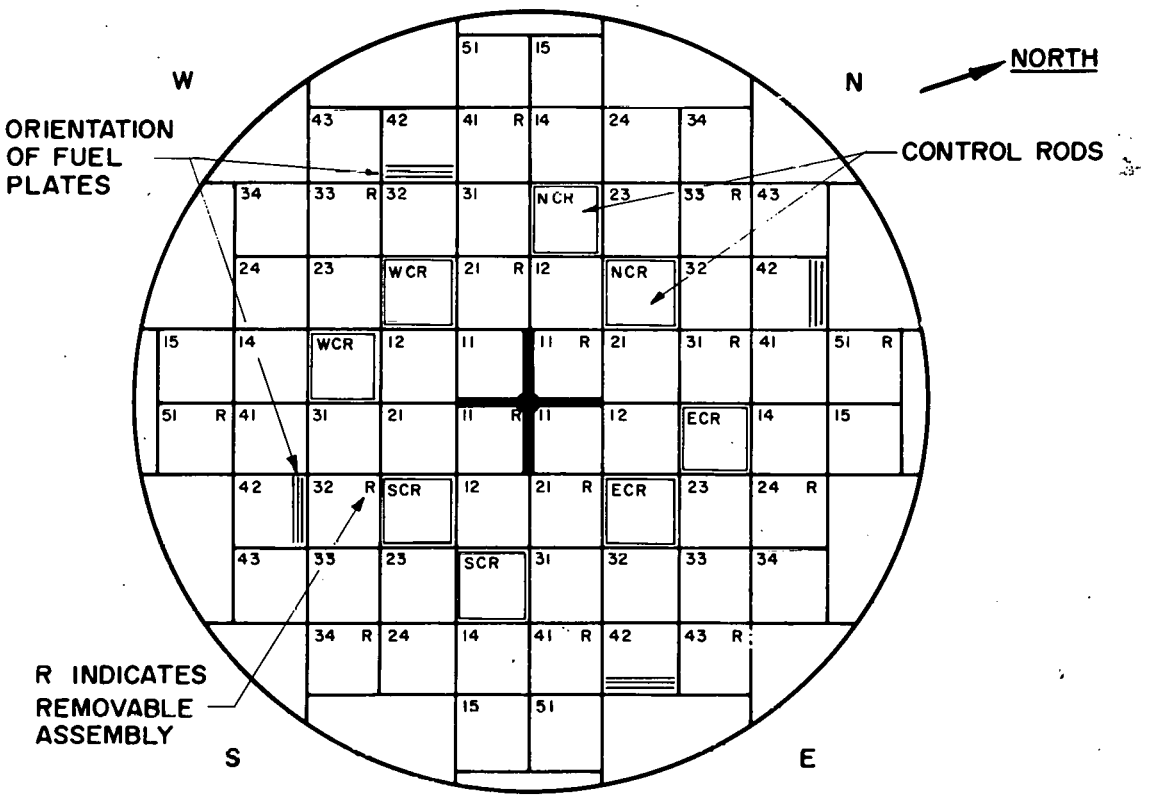

Fig. 43 Layout of Spert III reactor grid showing orientation of fuel plates for a typical fuel assembly in each quadrant.

TABLE VI

PERTINENT SPERT III, C-CORE CONSTANTS [22]

Item	Magnitude or Type
Clad Material	Stainless Steel
Critical Mass U-235	14.6 kg
Total U-235	30.6 kg
H/U	107
M/W	0.38
Available K_{ex} 21°C	20.5$
Temperature defect	
21 - 260°C	8.5$
21 - 343°C	18.0$
Isothermal temperature Coefficient (2500 psig)	
27°C	-0.011 $/°C
38°C	-0.016 $/°C
95°C	-0.030 $/°C
149°C	-0.041 $/°C
204°C	-0.057 $/°C
260°C	-0.081 $/°C
316°C	-0.150 $/°C
343°C	-0.290 $/°C
Pressure Coefficient 0 - 2500 psig at 27°C	$+ 1.4 \times 10^{-4}$ $/psig
Pressure gain 0 - 2500 psig at 27°C	+ 0.35 $
Ave Void Coefficient †	2.0×10^{-4} $/cm^3
Reduced prompt neutron lifetime $\ell^*/\bar{\beta}$	3×10^{-3} sec
Water Channel Width	128 mils

† Average of data obtained for a uniform distribution of void over the core volume and in the temperature range $29°C \leq \theta \approx \leq 316°C$.

2.3 Data Presentation

2.31 General Considerations. Data obtained during Spert III transient testing were also recorded on optical oscillographs and processed in a manner identical to that previously described for Spert I data. The Spert III facility provides the capability for operation at high temperature and at initial system pressures up to 2500 psig. The transient data reported here are primarily data for initial pressures in excess of atmospheric. These data have been obtained for two reactor conditions. For the first condition, the reactor vessel was completely filled with water, and was referred to as "liquid full". The other condition of interest is that in which an air space was deliberately maintained at the top of the vessel. This reactor condition was referred to as "air dome", and data thus obtained will be so designated.

As a consequence of the pressurization of the system, boiling was suppressed for most long period transients ($\tau \approx 20$ msec). For high system pressurization (P_i = 2500 psig) boiling was very limited (or absent) for even the shortest period transients ($\tau \approx 10$ msec). Consequently, most of the data of interest were obtained at the shorter reactor periods.

The data presentation format will be similar to that used for the Spert I data, except for those variations required to include the additional variables such as initial system pressure, coolant flow rate, and initial system temperature.

2.32 Analog Plots

(1) Time History Correlations for Power, Energy, Temperature, Flow, and Pressure. The time behavior of pressure may be compared with that of power, energy, temperature, and flow (moderator expulsion) in Figures 44 through 47. In these data the magnitude of the saturation temperature is placed adjacent to the symbol, θ, once on each figure to indicate the magnitude of the temperature rise at which boiling can occur. The pressure generation, due to fuel plate expansion, can be seen best for the intermediate and high initial pressures where boiling occurs at higher temperatures, hence, allowing more expansion prior to boiling. The correlation between the time at which boiling heat transfer is observed (ie, the time at which the temperature behavior deviates sharply from the insulated plate behavior) and the time of an increase in slope of the pressure trace also may be seen in these data. The transducer used to monitor pressure in these transients was located in the upper end box of fuel assembly S 32.

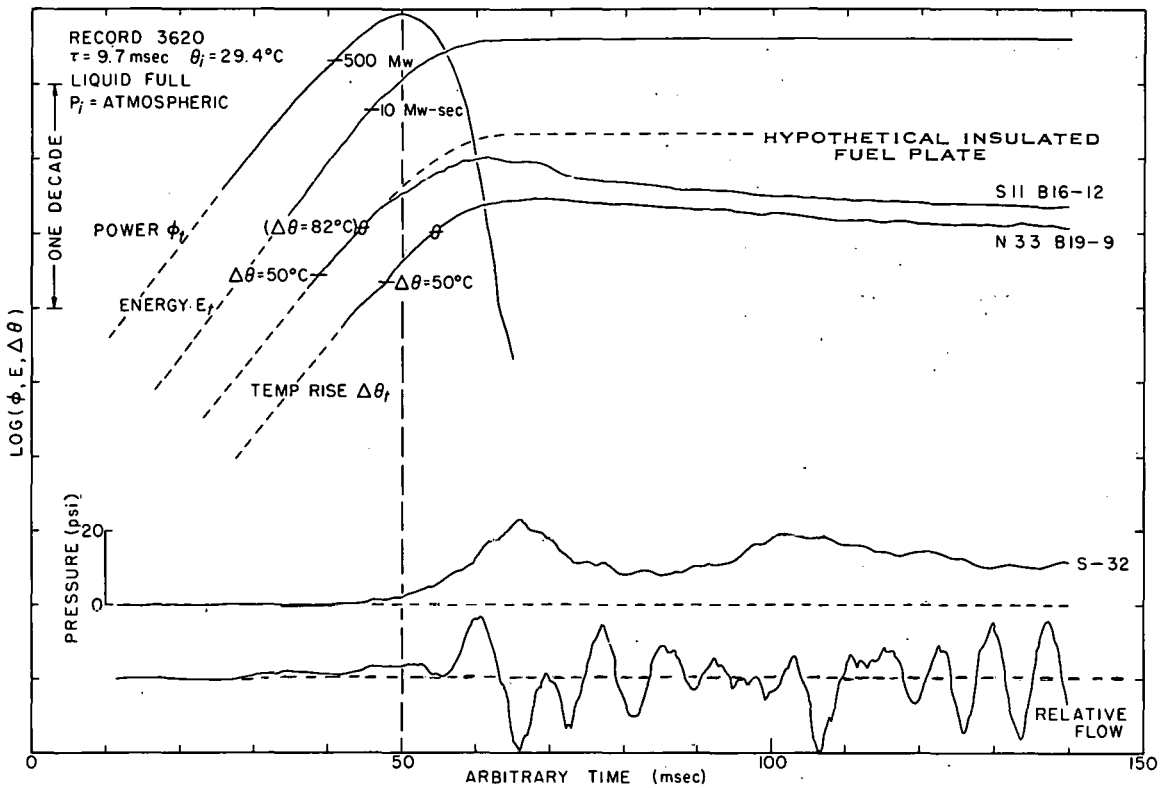

Fig. 44 A presentation of time histories for power, energy, fuel-plate surface temperature, pressure, and flow. The symbol θ on the temperature-time histories indicates the boiling temperature with the corresponding temperature rise shown in parentheses adjacent to one of the traces.

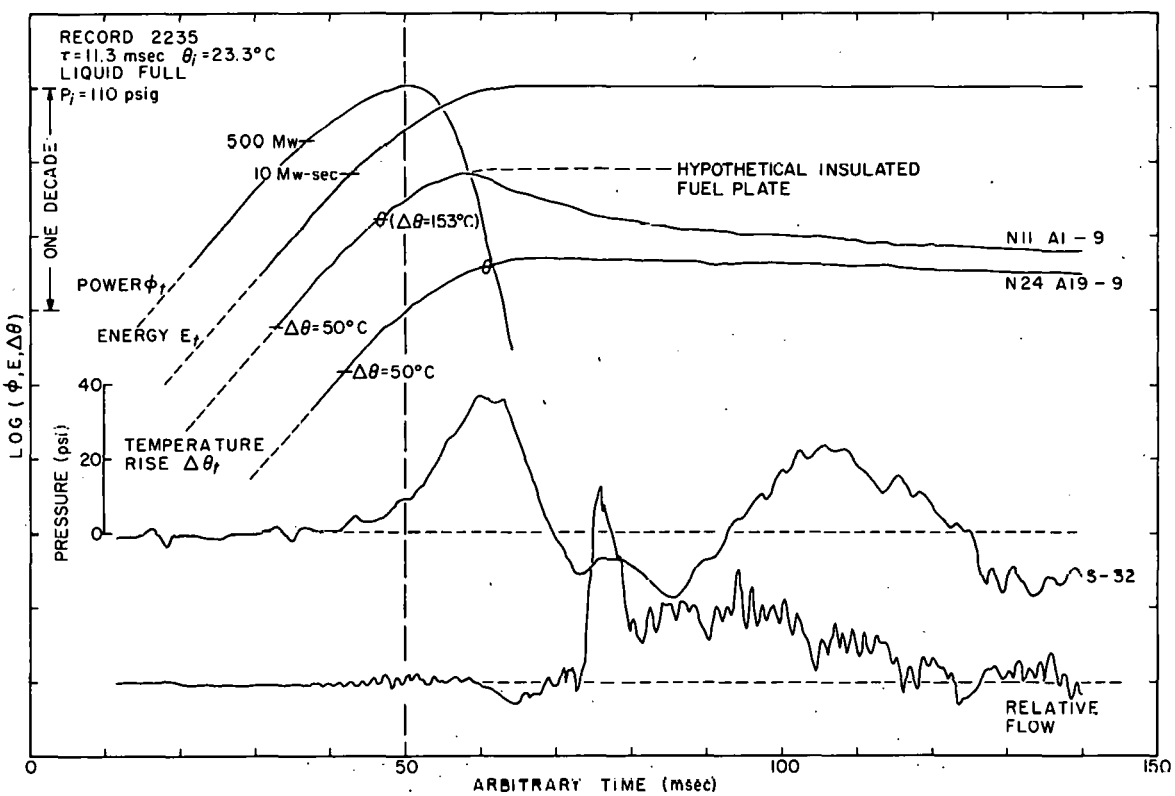

Fig. 45. A presentation of time histories for power, energy, fuel-plate surface temperature, pressure, and flow for a specific initial pressure with the reactor vessel liquid full. The symbol θ on the temperature-time histories indicates the boiling temperature with the corresponding temperature rise shown in parentheses adjacent to one of the traces.

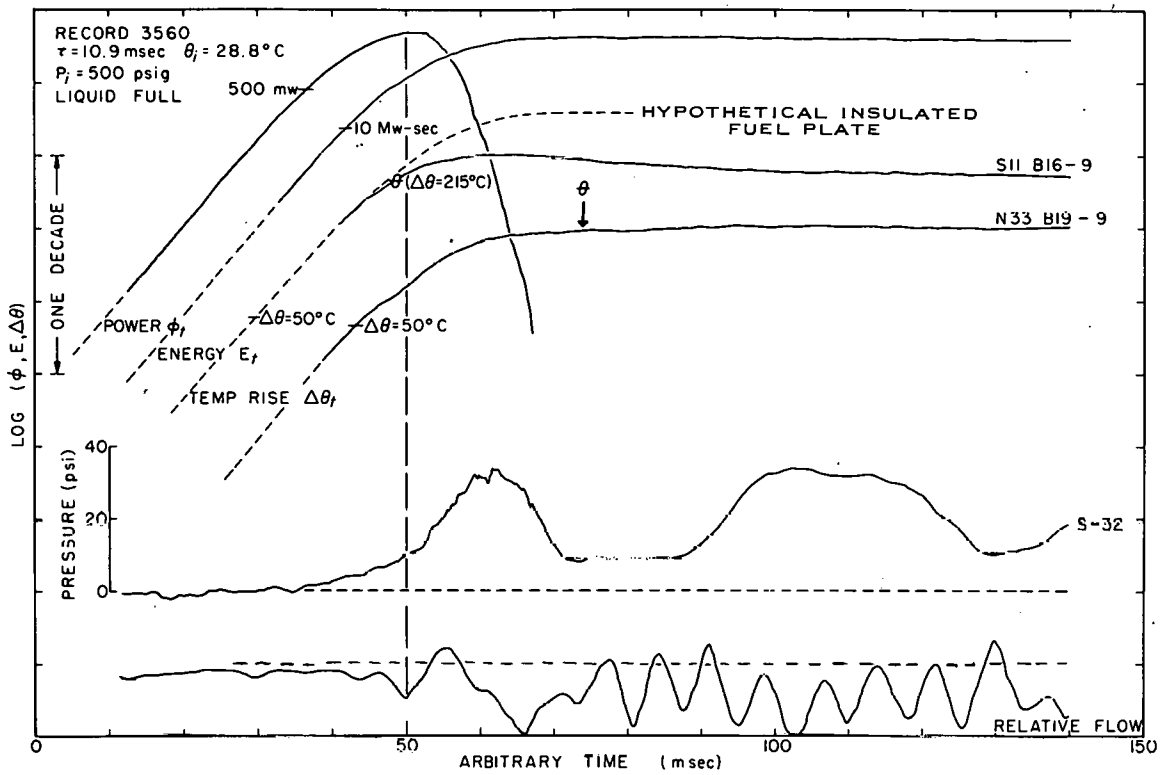

Fig. 46 A presentation of time histories for power, energy, fuel-plate surface temperature, pressure, and flow for a specific initial pressure with the reactor vessel liquid full. The symbol θ on the temperature-time histories indicates the boiling temperature with the corresponding temperature rise shown in parentheses adjacent to one of the traces.

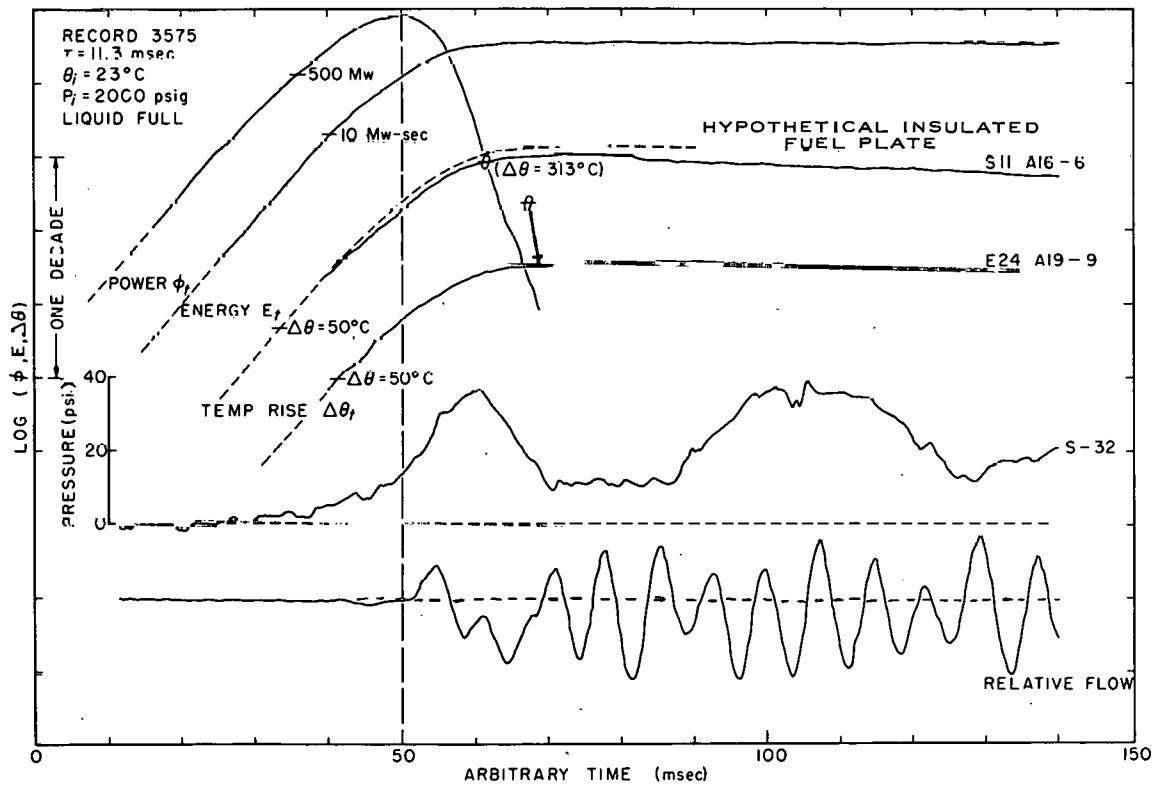

Fig. 47. A presentation of time histories for power, energy, fuel-plate surface temperature, pressure, and flow for a specific initial pressure with the reactor vessel liquid full. The symbol θ on the temperature-time histories indicates the boiling temperature with the corresponding temperature rise shown in parentheses adjacent to one of the traces.

The flowmeter data in Figures 44 and 45 display a prominent 125 cps component which is evident in transients conducted over the entire range of initial pressure and reactor period. As for the P-Core, this component results from vibratory motion of the core; the frequency of oscillation is the characteristic frequency of the core structure. An additional high frequency component is evident in the trace of Figure 45. This component results from excitation of the natural frequency of the flowmeter which is about 700 cps. The fundamental response of the flowmeter which is indicative of the actual flow from the assembly may be obtained by integrating through these spurious resonance components [a]. Correlation between pressure and flow response is similar to that observed for Spert I.

(2) Time History Correlation of Pressure Behavior and Radial and Longitudinal Temperature Distributions. The gross core temperature distribution can be inferred from the data in Figures 48 through 53. In these data a dashed line has been drawn vertically through the symbols, θ, to aid in establishing the time at which boiling is possible. The correlation between indicated heat transfer and the pressure generated is excellent; the spatial-time distribution in onset of boiling closely resembles the static flux distribution as in the Spert I data.

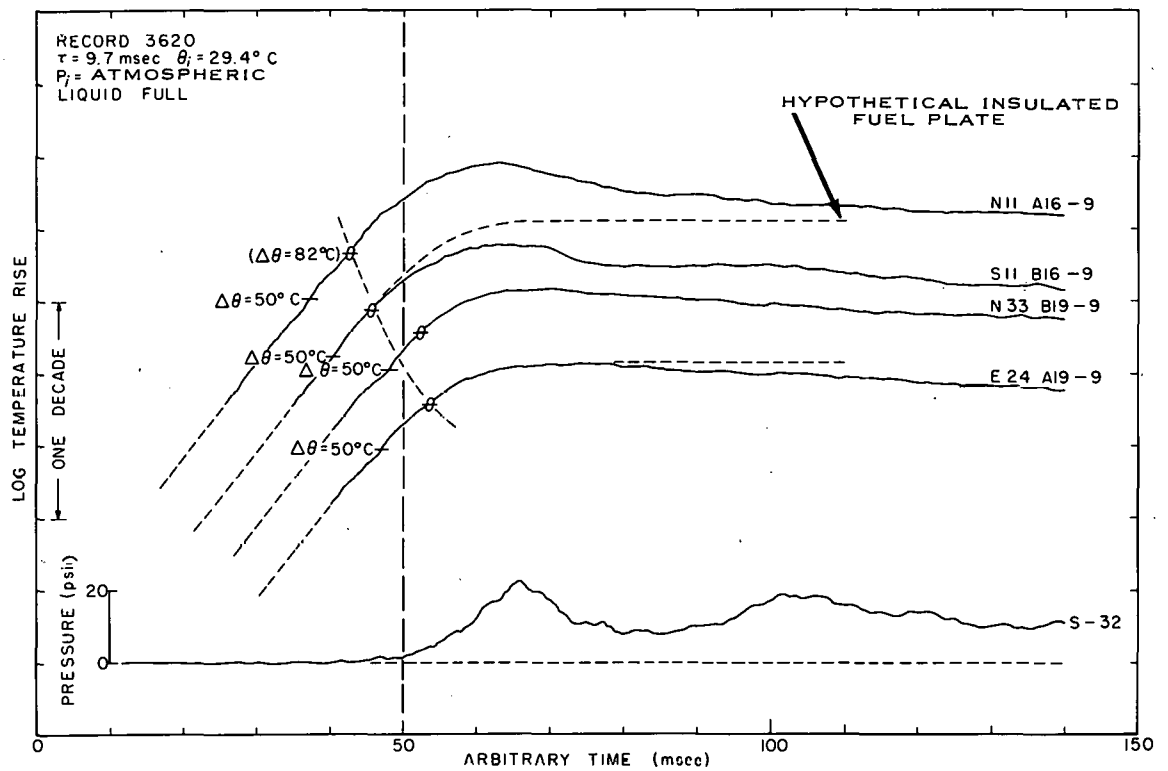

Fig. 48 A presentation of fuel-plate surface temperature-time histories at various radial positions and the pressure-time history. The symbol θ on the temperature-time histories indicates the boiling temperature with the corresponding temperature rise shown in parentheses adjacent to one of the traces.

[a] As for the P-Core, the flow transducer used is such that the actual flow rate is proportional to the square root of the trace deflection. Since the flow rates are to be used here only for qualitative comparison, the actual flow rates have not been computed.

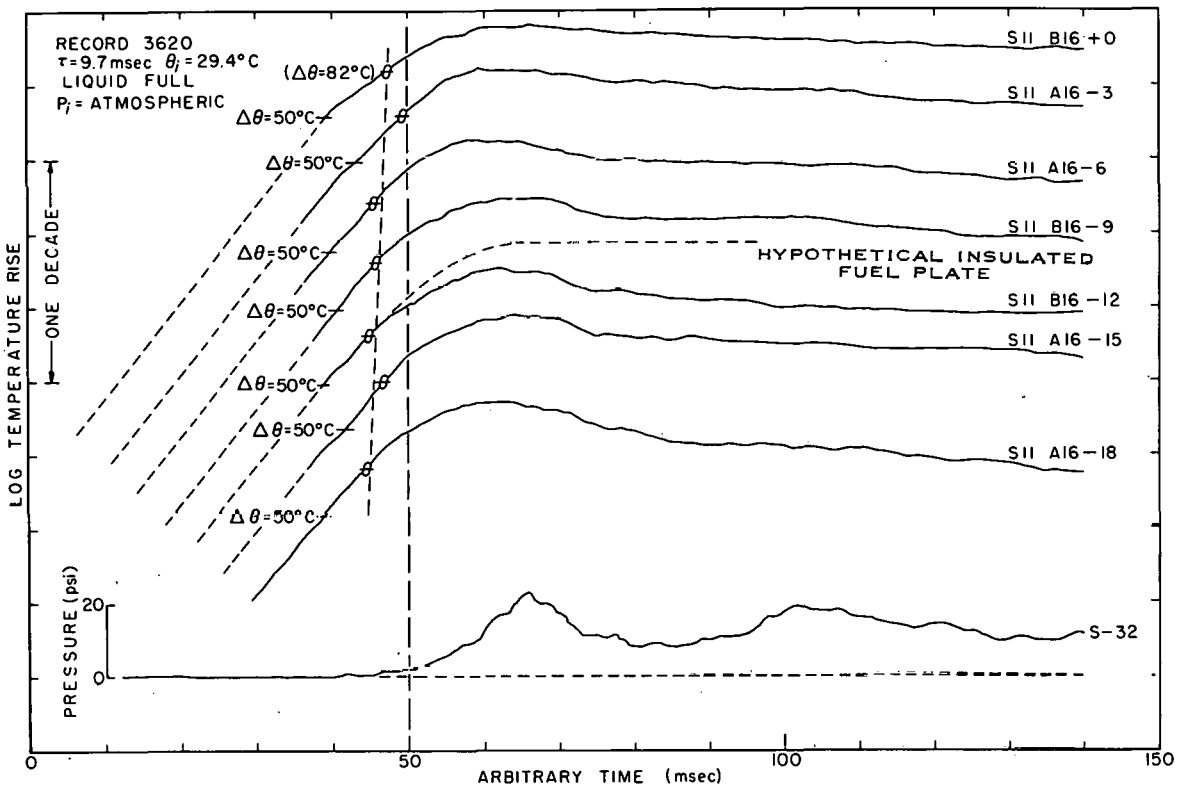

Fig. 49 A presentation of fuel-plate surface temperature-time histories at various longitudinal positions along a fuel plate and the pressure-time history. The symbol θ on the temperature-time histories indicates the boiling temperature with the corresponding temperature rise shown in parentheses adjacent to one of the traces.

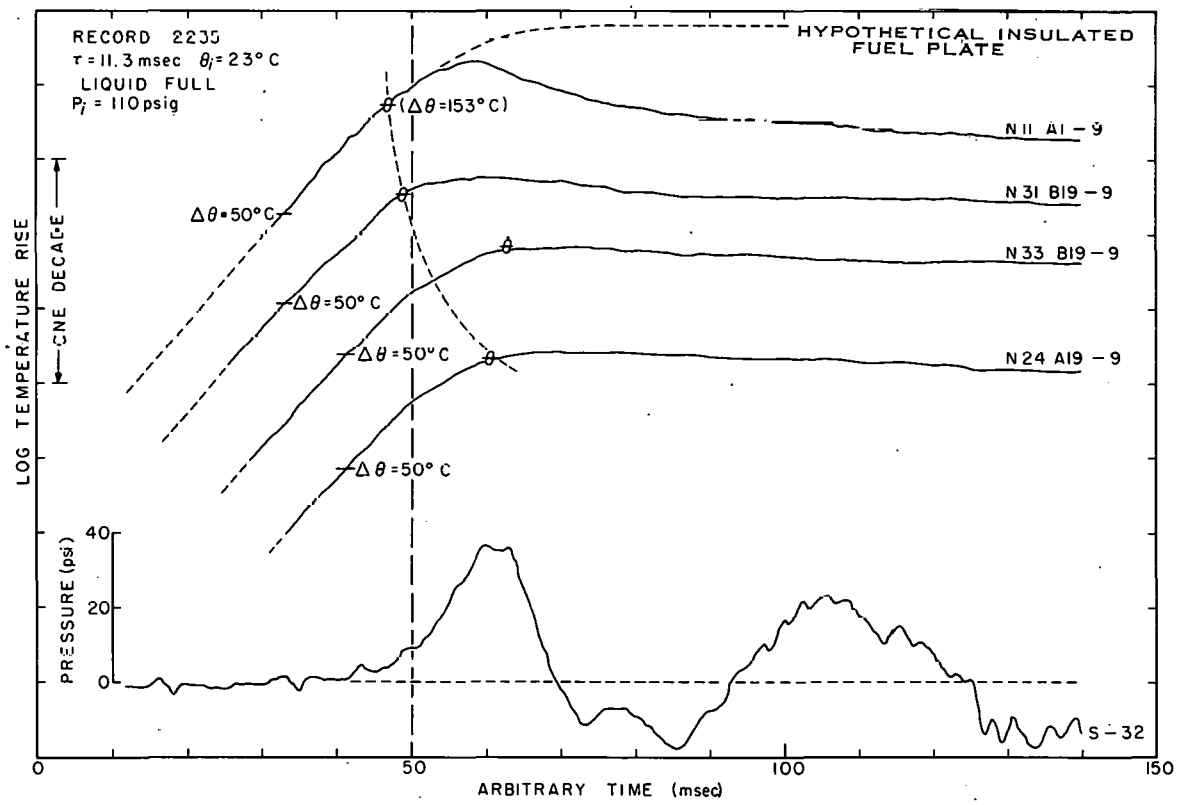

Fig. 50 A presentation of fuel-plate surface temperature-time histories at various radial positions and the pressure-time history for a specific initial pressure with the reactor vessel liquid full. The symbol θ on the temperature-time histories indicates the boiling temperature with the corresponding temperature rise shown in parentheses adjacent to one of the traces.

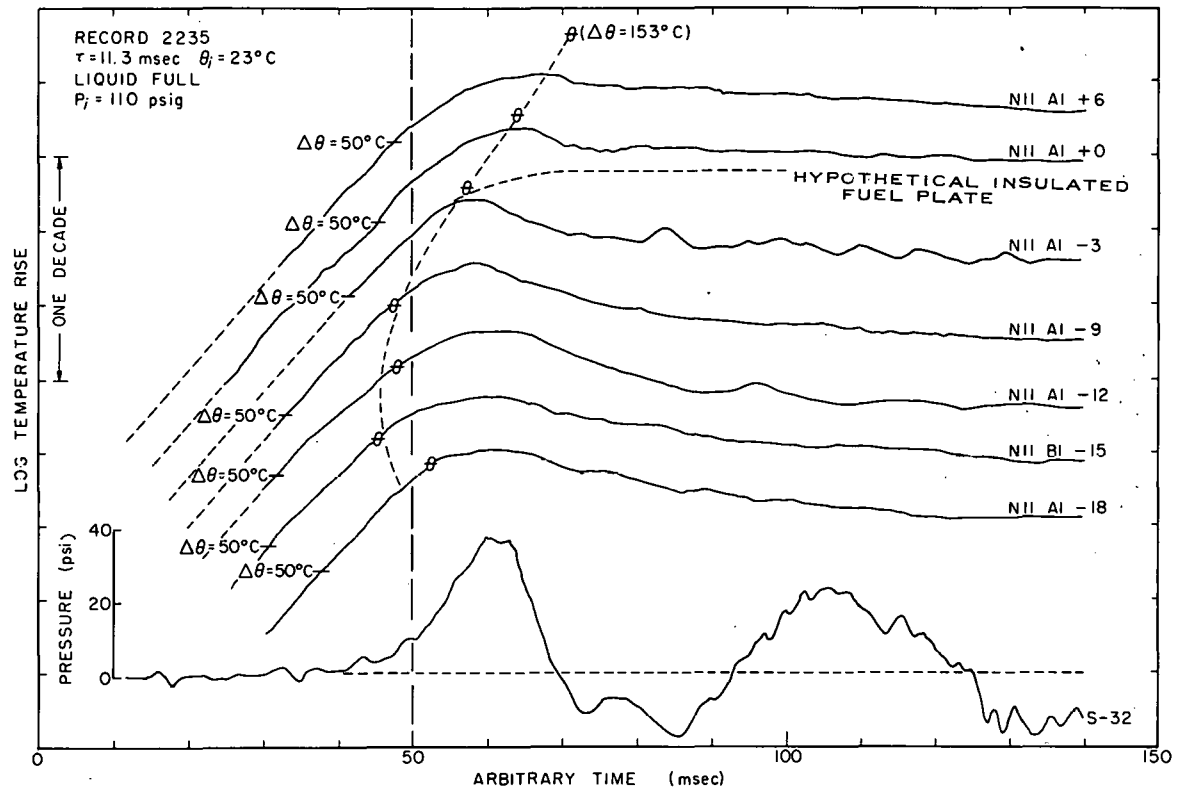

Fig. 51 A presentation of fuel-plate surface temperature-time histories at various longitudinal positions along a fuel plate and the pressure-time history for a specific initial pressure with the reactor vessel liquid full. The symbol θ on the temperature-time histories indicates the boiling temperature with the corresponding temperature rise shown in parentheses adjacent to one of the traces.

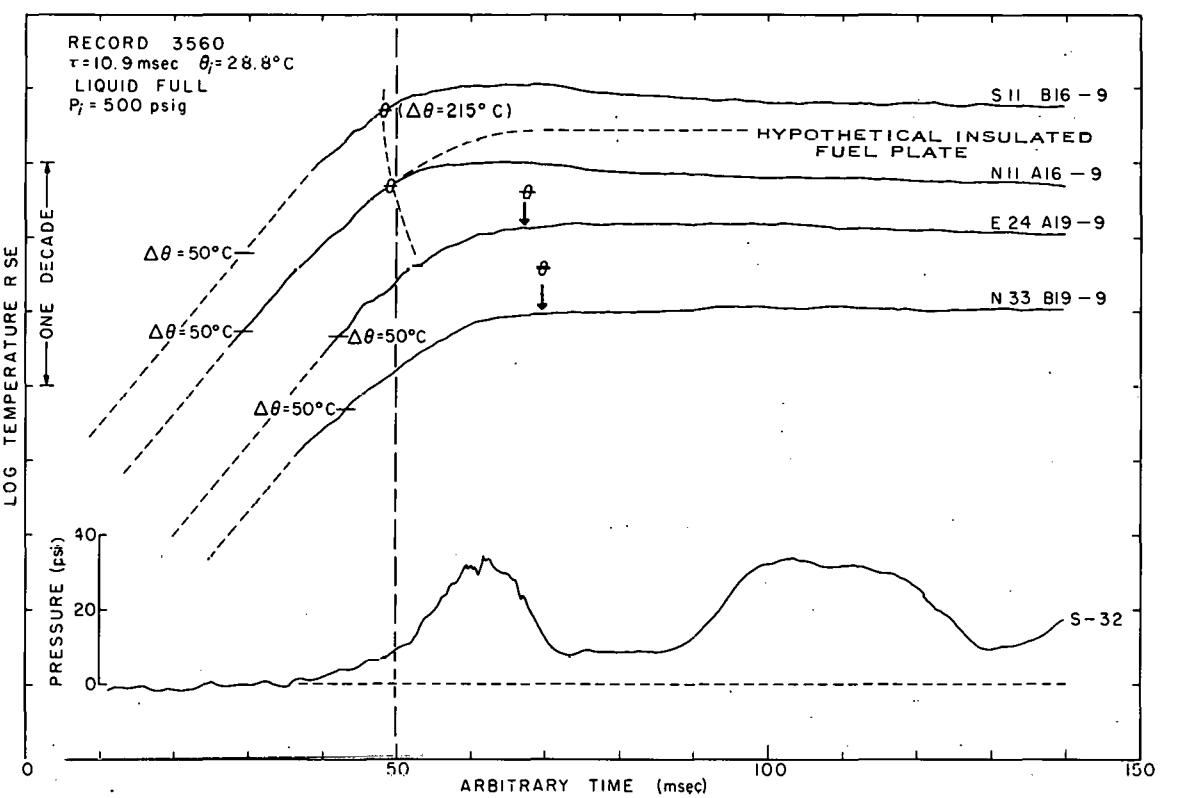

Fig. 52 A presentation of fuel-plate surface temperature-time histories at various radial positions and the pressure-time history for a specific initial pressure with the reactor vessel liquid full. The symbol θ on the temperature-time histories indicates the boiling temperature with the corresponding temperature rise shown in parentheses adjacent to one of the traces.

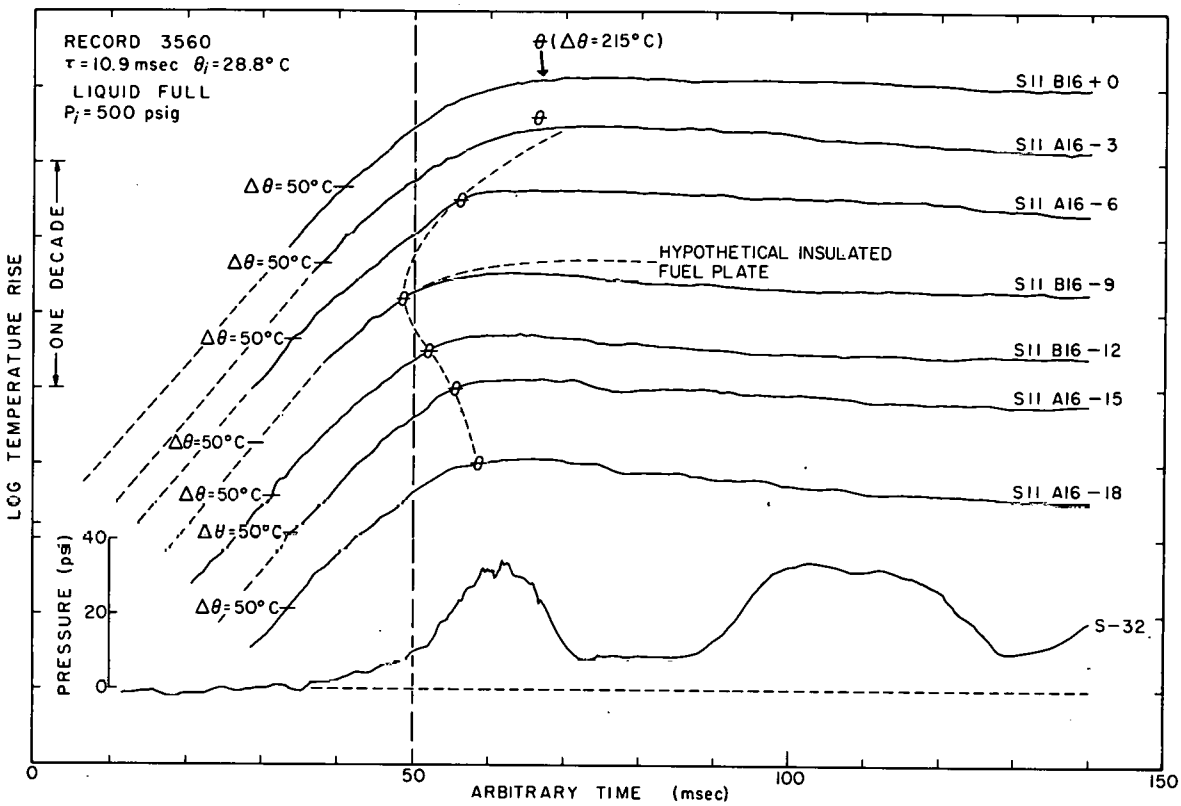

Fig. 53 A presentation of fuel-plate surface temperature-time histories at various longitudinal positions along a fuel plate and the pressure-time history for a specific initial pressure with the reactor vessel liquid full. The symbol θ on the temperature-time histories indicates the boiling temperature with the corresponding temperature rise shown in parentheses adjacent to one of the traces.

An improvement in heat transfer with moderate pressurization may be observed in Figures 50 and 51. It is accompanied by a proportionate increase in pressure level as may be seen by comparison with the data of Figures 48 and 49. Suppression of boiling in peripheral regions of the core is evident at higher system pressures as may be observed in Figures 52 and 53 (see also Figures 46 and 47).

Similar longitudinal and radial temperature data for a transient with an air dome in the vessel are presented in Figures 54 through 56. The initial pressure during this transient was 110 psig, but similar trends were observed for all pressurized transients with an air dome. Although the temperature-time histories appear very similar to those obtained for liquid full reactor transients (Figures 45, 50, and 51), the pressure-time histories are markedly different. The magnitude of the pressure peak is less than half as large for the air dome transient, and the pressure-time behavior is similar to that obtained for the longer period ($\tau \approx 20$ msec) Spert I transients (Figure 17). The flowmeter response also is more similar to that for a Spert I transient than for the liquid full pressurized transients. This behavior results from the pressure relief afforded at the interface between the air dome and the water in the vessel. The lower stiffness of the air dome (relative to water) permits displacement of the interface and enhances flow from the core required for reactor shutdown.

(3) Effects of Miscellaneous Variables Upon Pressure Generation. Power and energy behavior for 10-msec air dome and liquid full reactor transients are compared in Figure 57. The liquid full data are shown in the upper curve; the air dome data are shown in the lower curve in each instance. The data indicate a higher energy release and peak power for transients in which the

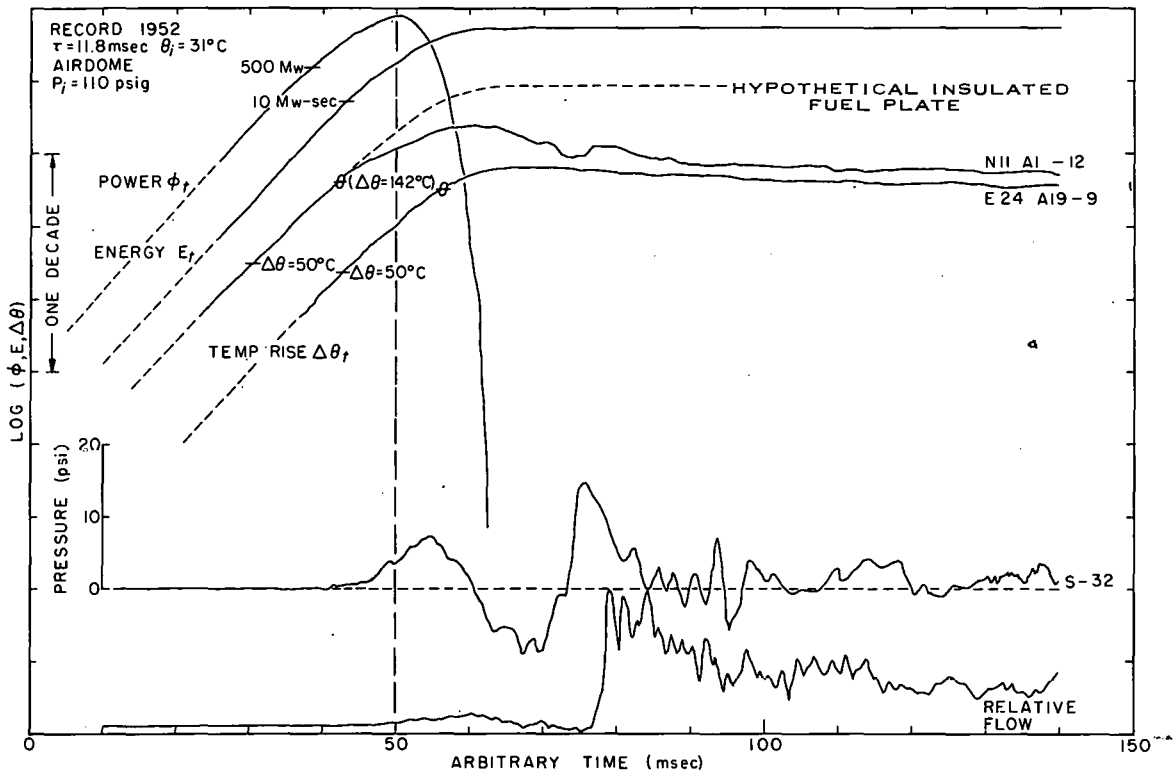

Fig. 54 A presentation of time histories for power, energy, fuel-plate surface temperature, pressure, and flow for a specific initial pressure with an air dome in the reactor vessel. The symbol θ on the temperature-time histories indicates the boiling temperature with the corresponding temperature rise shown in parentheses adjacent to one of the traces.

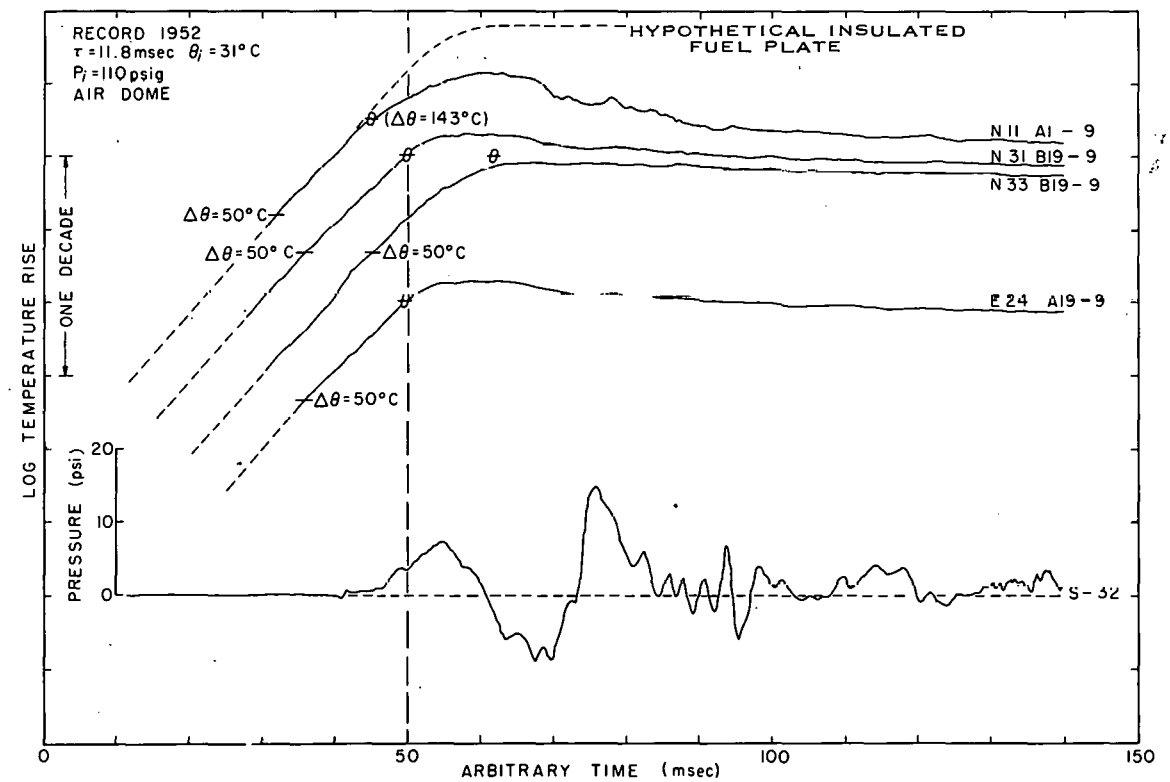

Fig. 55 A presentation of fuel-plate surface temperature-time histories at various radial positions and the pressure-time history for a specific initial pressure with an air dome in the reactor vessel. The symbol θ on the temperature-time histories indicates the boiling temperature with the corresponding temperature rise shown in parentheses adjacent to one of the traces.

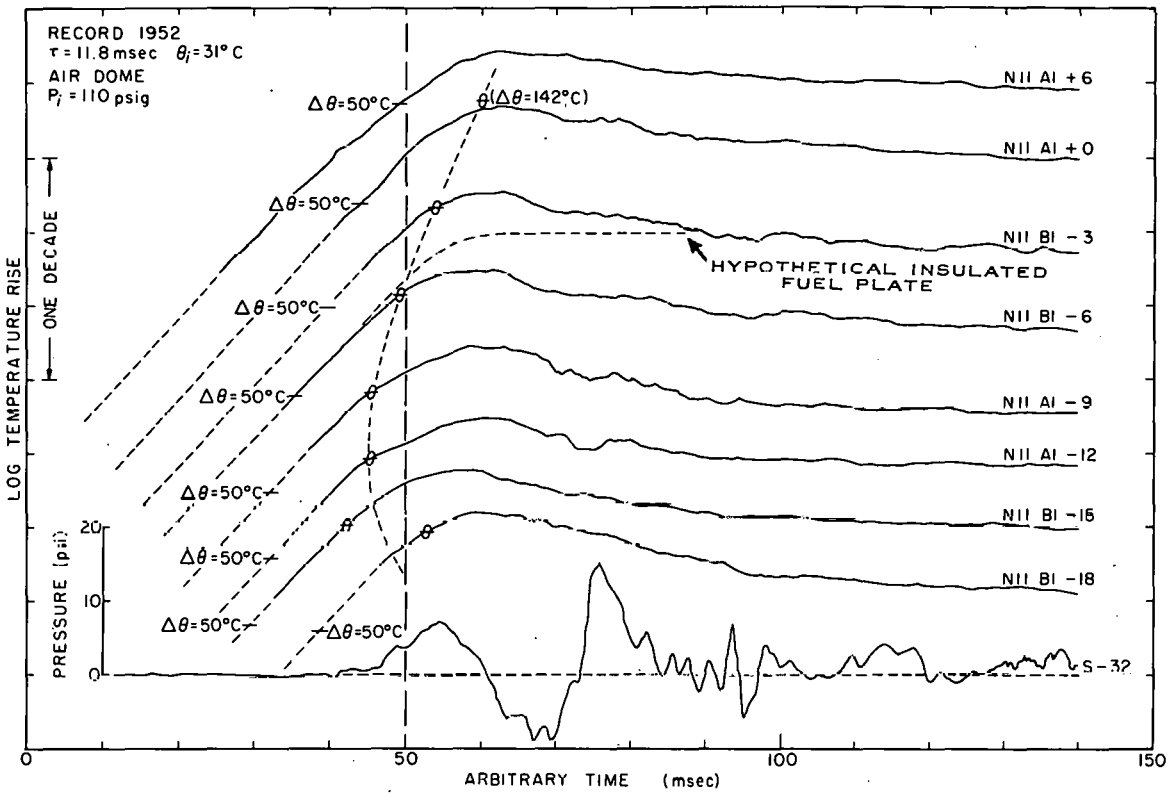

Fig. 56 A presentation of fuel-plate surface temperature-time histories at various longitudinal positions along a fuel plate and the pressure-time history for a specific initial pressure with an air dome in the reactor vessel. The symbol θ on the temperature-time histories indicates the boiling temperature with the corresponding temperature rise shown in parentheses adjacent to one of the traces.

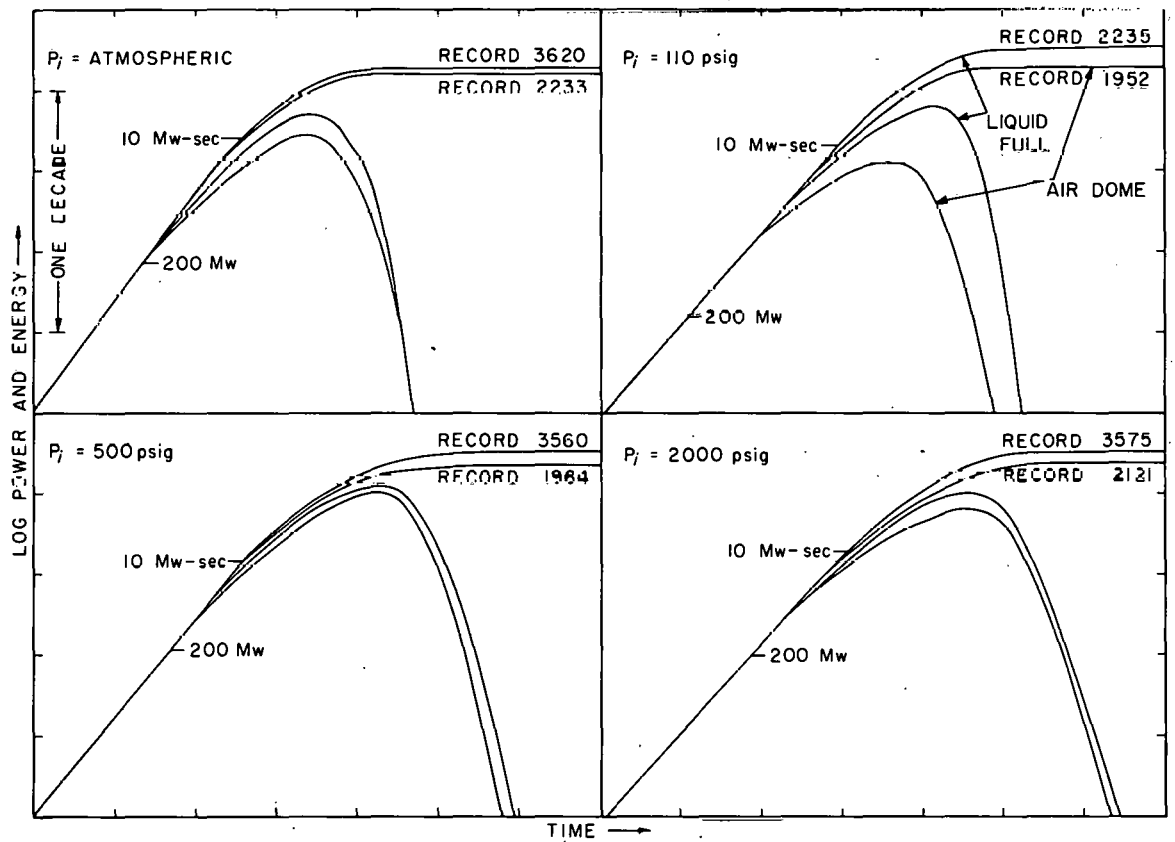

Fig. 57 Representative power and energy-time histories for reactor transients conducted with the reactor vessel liquid full and with an air dome in the vessel.

vessel was liquid full. The differences between behaviors are greatest at intermediate initial pressures for this reactor period and initial temperature. Additional data obtained from similar transients are shown in Table VII.

TABLE VII

SUMMARY OF PEAK POWER, PEAK PRESSURE, AND TOTAL ENERGY RELEASE FOR AIR DOME AND LIQUID FULL SPERT III TRANSIENTS

Reactor Vessel	Reactor Period (msec)	Initial Temperature (°C)	Initial Pressure (psig)	Peak Power (Mw)	Peak Pressure (psi)	Total Energy Release (Mw sec)
Liquid Full	10	22	Atmospheric	830	20	19.5
	10	23	110	1500	40	26.0
	10	29	500	950	38	28.5
	10	23	2000	920	35	26.5
	20	22	Atmospheric	275	4	12.5
	20	28	110	235	6	13.0
Air Dome	10	28	Atmospheric	670	7	18.5
	10	31	110	860	6	21.5
	10	28	500	890	6	25.0
	10	24	1900	800	5	23.8
	20	27	Atmospheric	282	2	11.7
	20	28	110	283	No Dflec.	13.7

The effects of changes in initial temperature upon several variables are shown in Figures 58 through 60. The reactor period for these transients was approximately 20 msec, hence, the level of pressure response was low. In Figure 58, a dotted line has been drawn through the pressure data to integrate through the noise and hum components and indicate roughly the contribution due to pressure. For the conditions represented in the data of Figures 58 through 60 (P_i=110, psig $\tau \approx$ 20 msec, $28 \leq 0_i \leq 127$°C, vessel liquid full) boiling is largely suppressed at low initial temperatures, but becomes a significant contributor at high initial temperature. The magnitude of the pressure peak is correspondingly higher at the higher initial temperature, and the rate of decline of the power level is greater indicating greater negative reactivity feedback. Peak transient pressures obtained for other reactor periods and initial pressures are summarized in Table VIII.

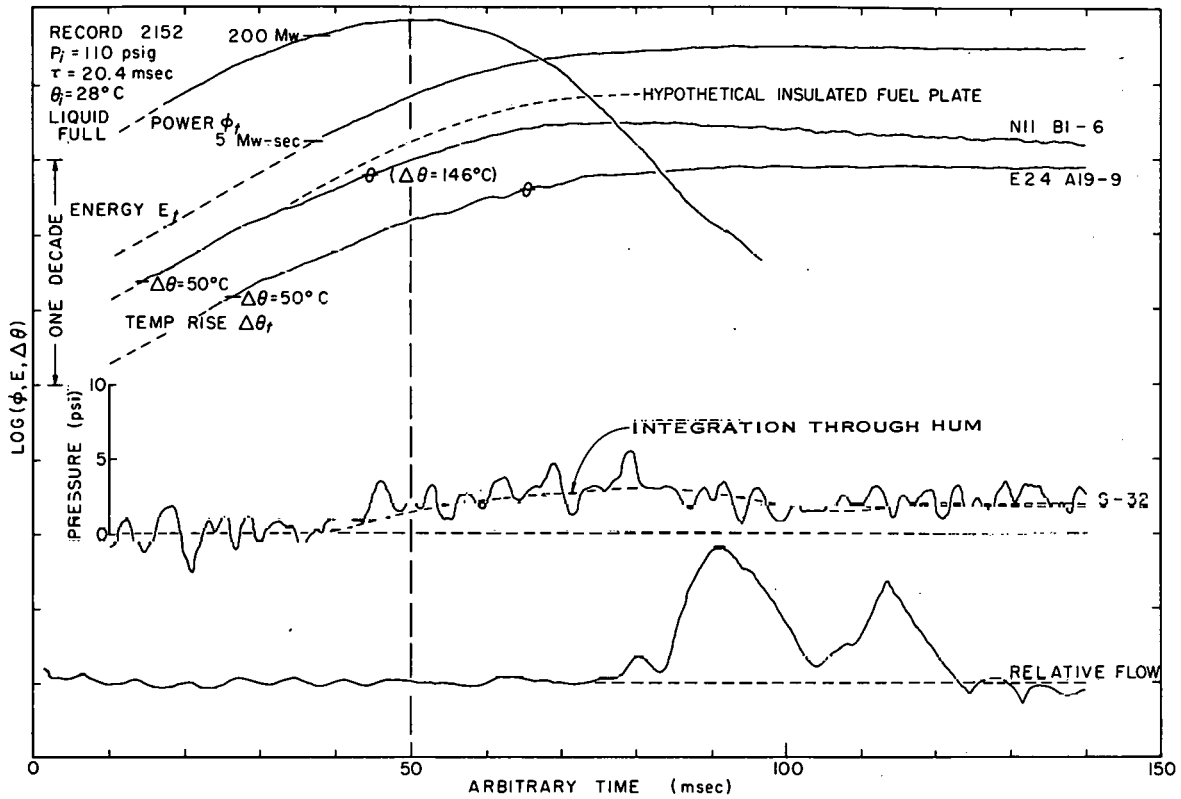

Fig. 58 A presentation of time histories for power, energy, fuel-plate surface temperature, pressure, and flow for a specific initial pressure with the reactor vessel liquid full. The symbol θ on the temperature-time histories indicates the boiling temperature with the corresponding temperature rise shown in parentheses adjacent to one of the traces.

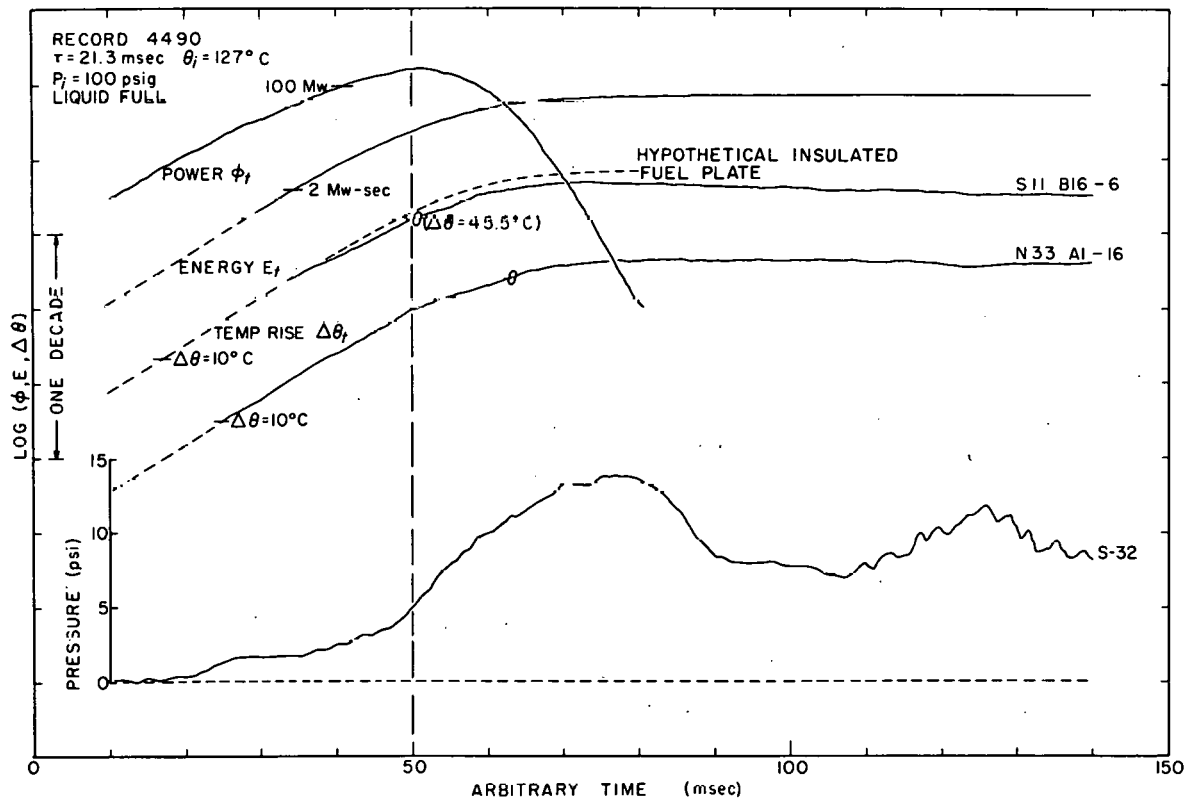

Fig. 59 A presentation of time histories for power, energy, fuel plate surface temperature, and pressure, for a specific initial pressure with the reactor vessel liquid full. The symbol θ on the temperature-time histories indicates the boiling temperature with the corresponding temperature rise shown in parentheses adjacent to one of the traces.

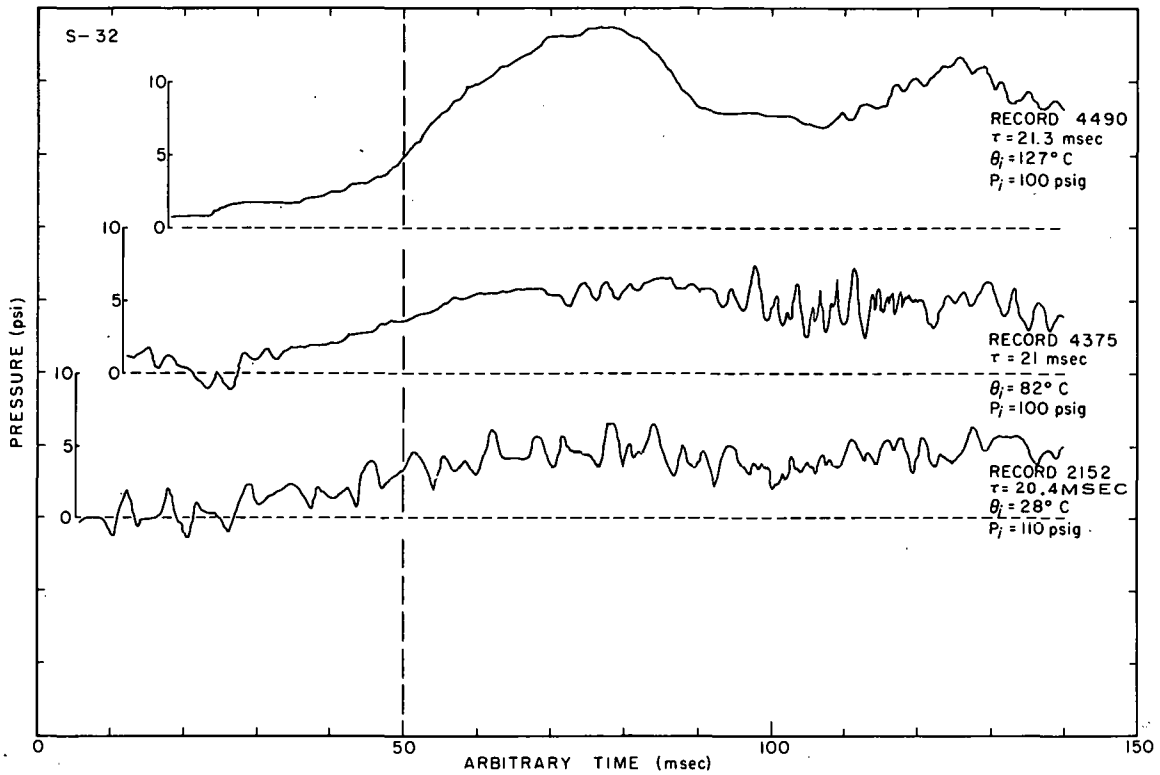

Fig. 60 Representative pressure-time histories for various initial system temperatures.

The dependence of the pressure-time history upon coolant flow rate is indicated in Figure 61. The pressure behavior is very similar for all flow rates observed except the 20,000 gpm flow rate. This anomalous behavior at high flow rate may indicate an interference with the development of good boiling heat transfer as a result of high flow velocities. However, the data available are not extensive enough to establish a precise explanation of the effect. The peak transient pressure data for various flow rates and measuring locations are summarized in Table IX.

The dependence of pressure generation upon reactor period is shown in Figures 62, 63, and 64 for initial pressure up to 500 psig. The long period pressure behavior ($\tau \approx 20$ msec) shows a long-term pressure rise of moderate magnitude modulated by 60 and 120 cycle hum. For the 500 psig initial pressure the complete suppression of boiling is evident from the pressure profile (Figure 64). However, the 10-msec transients prominently indicate the effects of boiling after an initial pressure contribution resulting from expansion effects.

The data of Figures 65, 66, and 67 are indicative of the variation of pressure with measuring location in the reactor vessel. The magnitude of the pressure level varies only slightly with position; the pressure-time histories are very similar for all locations. The suppression of boiling is again evident in the data for 2500 psig initial pressure (Figure 67), where the prominence of the pressure peaks is much diminished over that observed at lower initial pressure (Figures 65 and 66) and the pressure behavior is indicative primarily of a long-term pressure rise due to expansion.

TABLE VIII

SUMMARY OF PEAK PRESSURE DATA FOR
20 MSEC LIQUID FULL SPERT III TRANSIENTS OBTAINED AT
VARIOUS INITIAL TEMPERATURES FOR SPECIFIED INITIAL PRESSURES

Static Pressure (psig)	Initial Temperature (°C)	Peak Transient Pressure (psi)		
		S-32	Bottom Tee	East Port
Atmospheric	22	3.7	-	2.7
	60	2.7	-	-
	90	3.2	-	3.3
50	22	4.9	5.5	4.4
	60	2.7	-	3.0
	90	7.0	-	6.0
	127	21.7	-	20.8
100	28	6.5	-	-
	82	6.2	-	7.8
	127	14.8	-	15.3
200-250	30	7.6	10.2	-
	116	13.5	-	13.6
	154	15.3	-	-
500	21	7.5	8.6	13.0
	205	12.1	-	-
1000	23	7.8	13.8	13.0
	205	14.1	-	-
2500	21	16.2	12.6	16.0
	101	10.1	-	15.0
	205	14.1	-	13.8

The gradual change in the pressure behavior with initial system pressure is more evident in the data of Figure 68, where it becomes quite evident that the pressure-time history is really composed of two parts, a low frequency component resulting from expansion and a higher frequency "steam contribution" which is superimposed on (or modulates) this long-term fundamental. The data display remarkable similarities, with a first peak at about 50 msec followed by a periodic oscillation of about 17 to 20 cps. This oscillatory behavior is a consequence of coupling between the reactor vessel and the water within the vessel [a]. Energy transfered to the vessel wall is stored in the form of strain

[a] A power oscillation parallels the pressure oscillation indicating a correlated change in system reactivity; all power traces plotted have been terminated arbitrarily after the first peak.

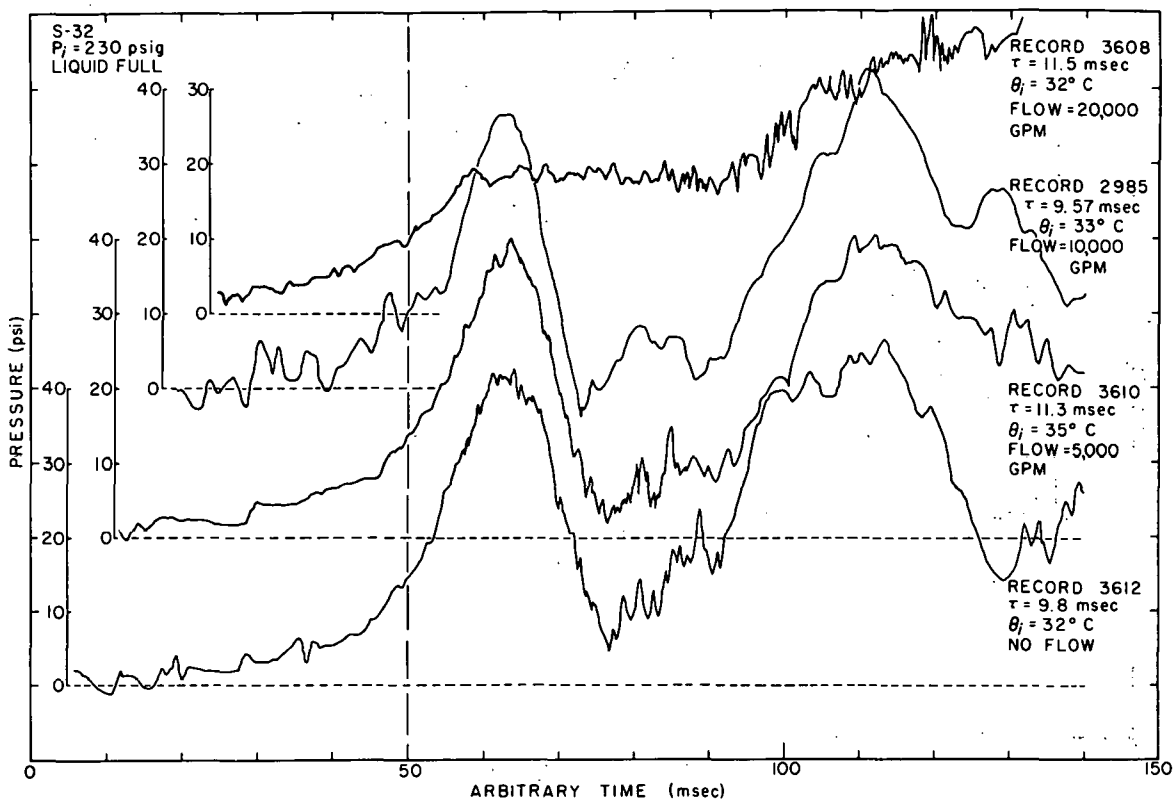

Fig. 61 Representative pressure-time histories for various reactor coolant flow rates.

TABLE IX

PEAK PRESSURE AS A FUNCTION OF FLOW RATE FOR 10-MSEC REACTOR TRANSIENTS AT 230 PSIG INITIAL SYSTEM PRESSURE

Flow Rate (gpm)	Initial Pressure (psig)	Peak Pressure (psi)		
		S-32	East Port	Bottom Tee
No flow	230	61.8	-	80.7
5,000	230	56.7	-	54.7
10,000	235	45.6	-	46.4
20,000	230	19.1 (40)*	20.2 (40)*	-

(*) Pressures indicated are the pressure at the time the peak occurred for lower flow rates and the ultimate pressure is shown in parentheses.

until the primary pressure pulse has passed and is returned to the system in the form of flow and pressure as the vessel walls return to their undisturbed position. The characteristic frequency of oscillation is determined by the mass and stiffness of both the vessel and the water in the vessel.

For static pressures below 100 psig, the coupling between the water and the vessel is weak enough that local water-hammer effects are prominently visible

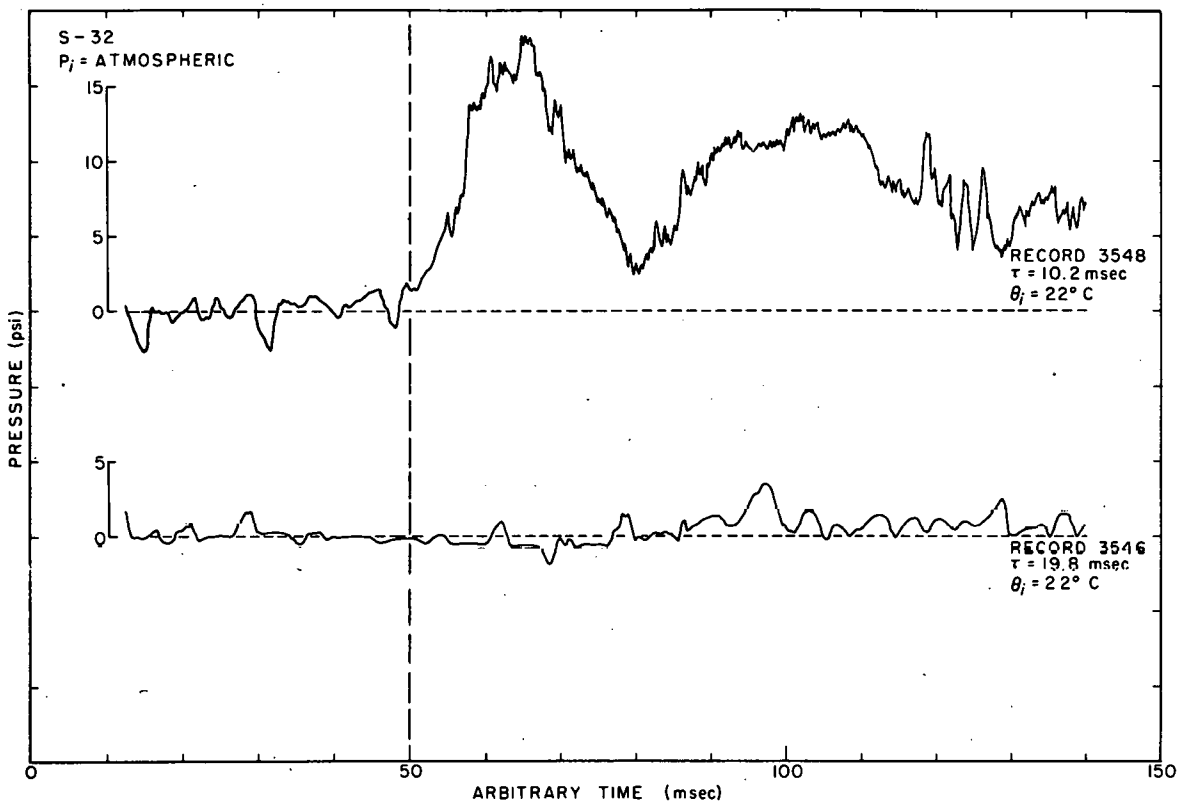

Fig. 62 Representative pressure-time histories for various reactor periods and atmospheric initial system pressure.

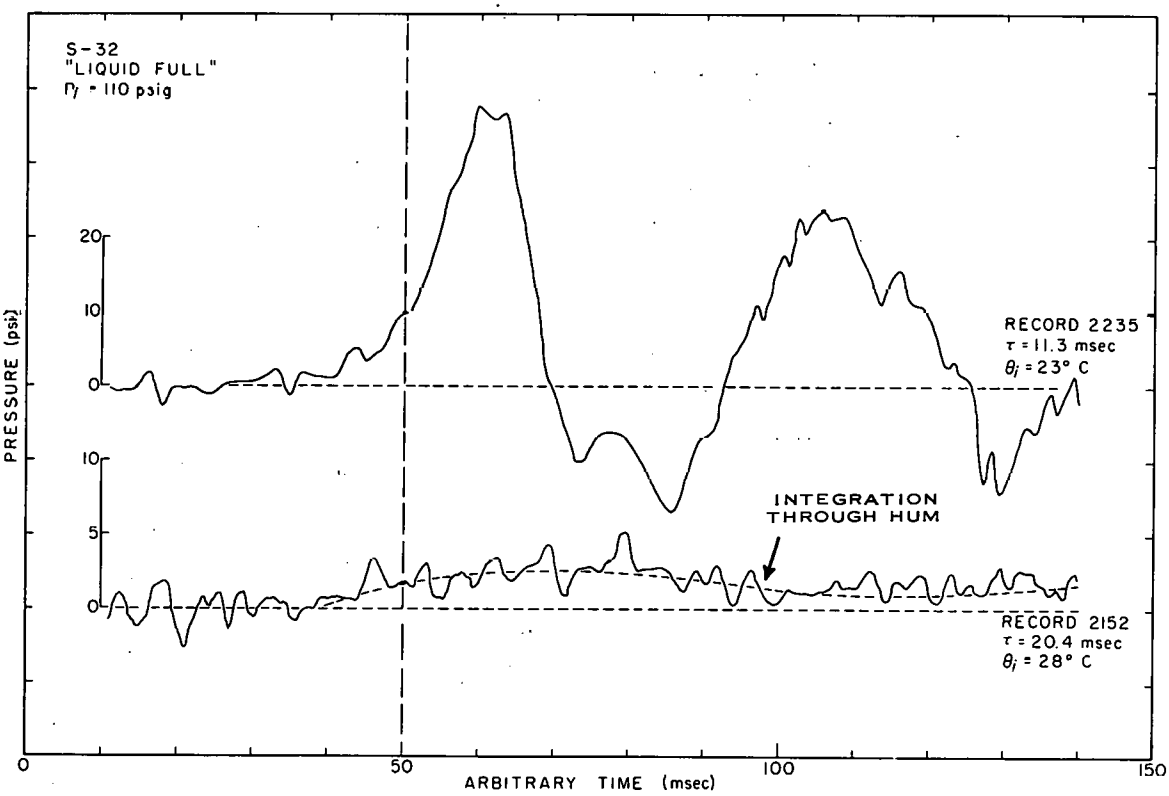

Fig. 63 Representative pressure-time histories for various reactor periods and 230 psig initial system pressure.

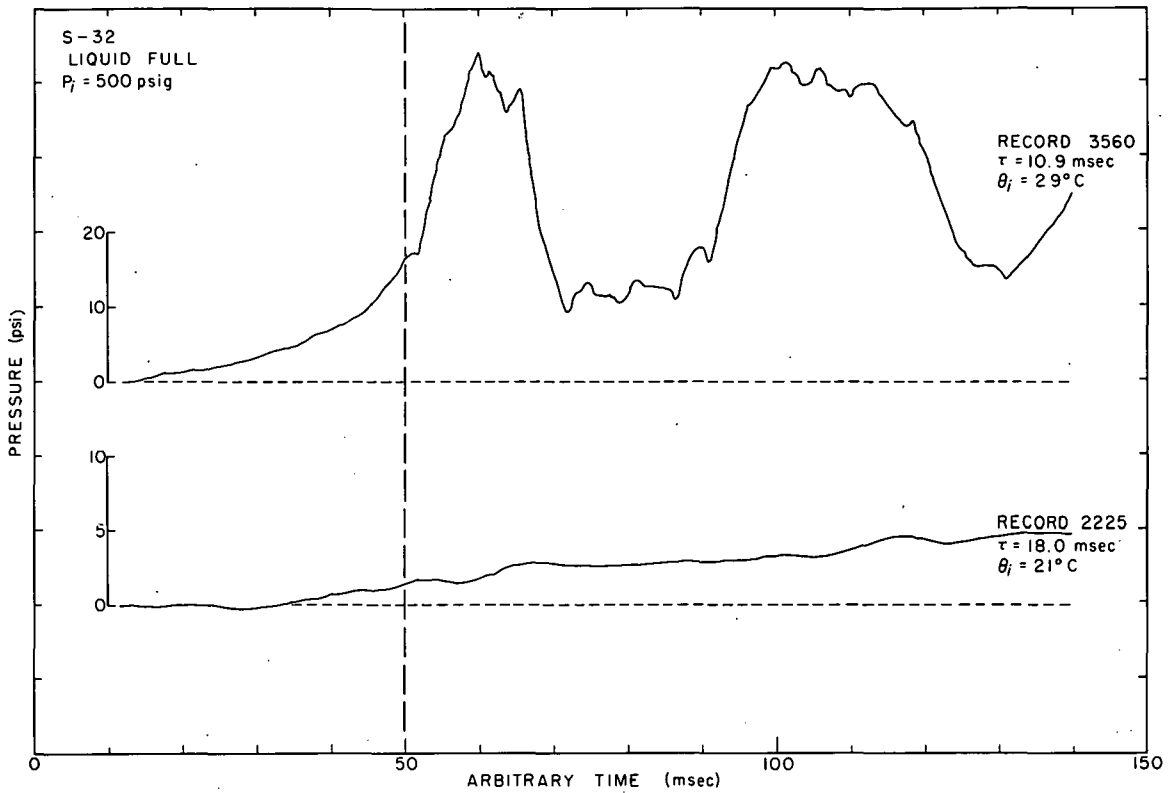

Fig. 64 Representative pressure-time histories for various reactor periods and 500 psig initial system pressure.

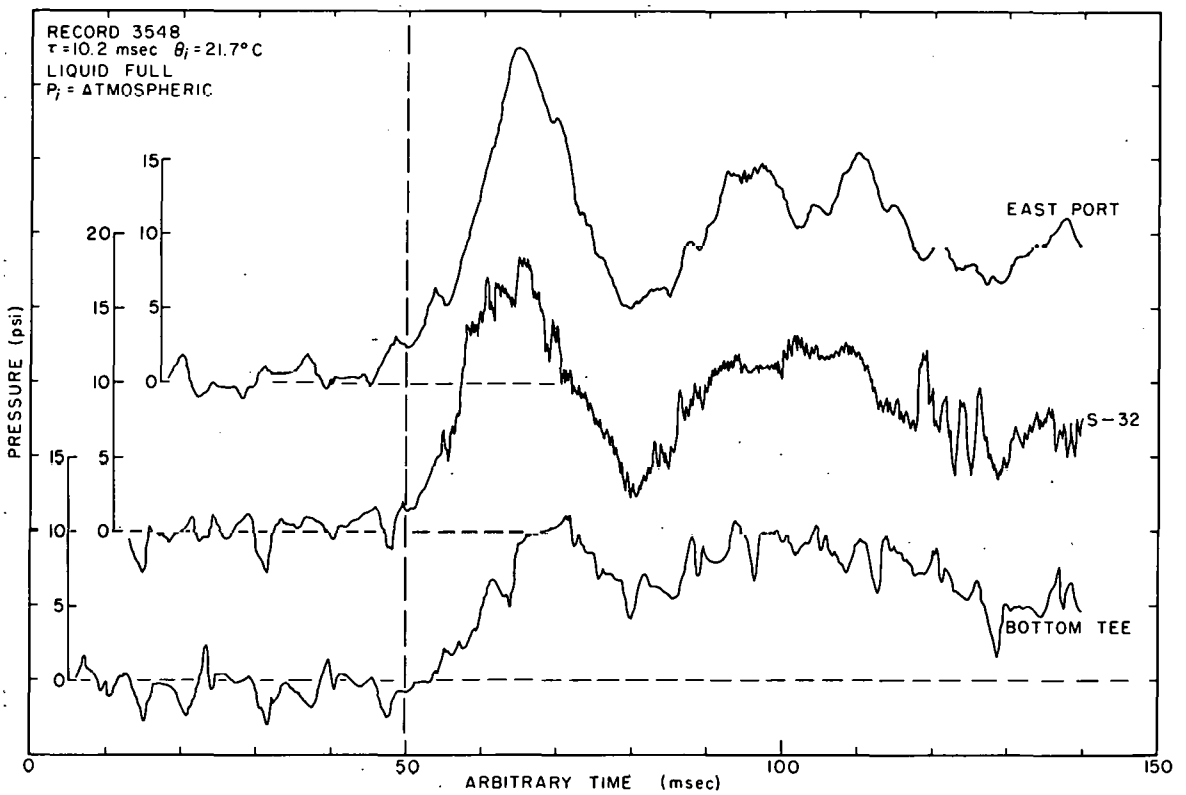

Fig. 65 Representative pressure-time histories for various locations in the Spert III reactor vessel and atmospheric initial system pressure.

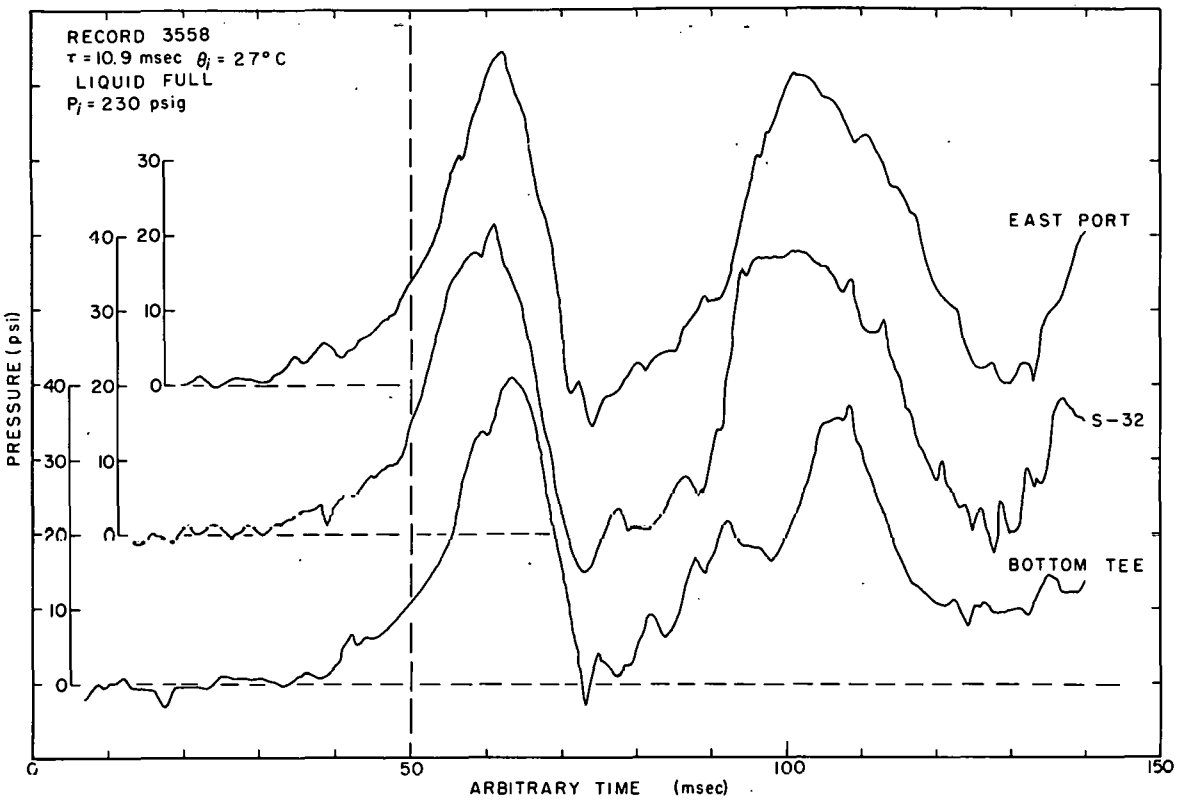

Fig. 66 Representative pressure-time histories for various locations in the Spert III reactor vessel and 230 psig initial system pressure.

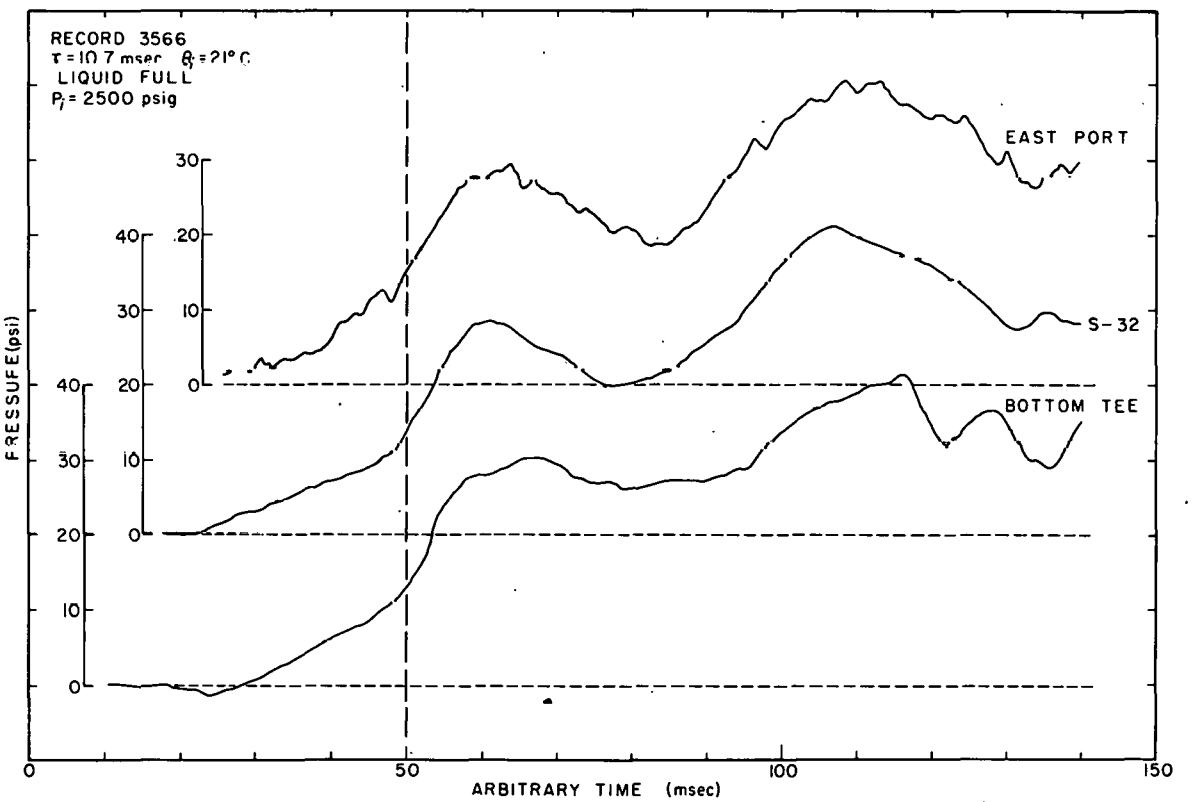

Fig. 67 Representative pressure-time histories for various locations in the Spert III reactor vessel and 2500 psig initial system pressure.

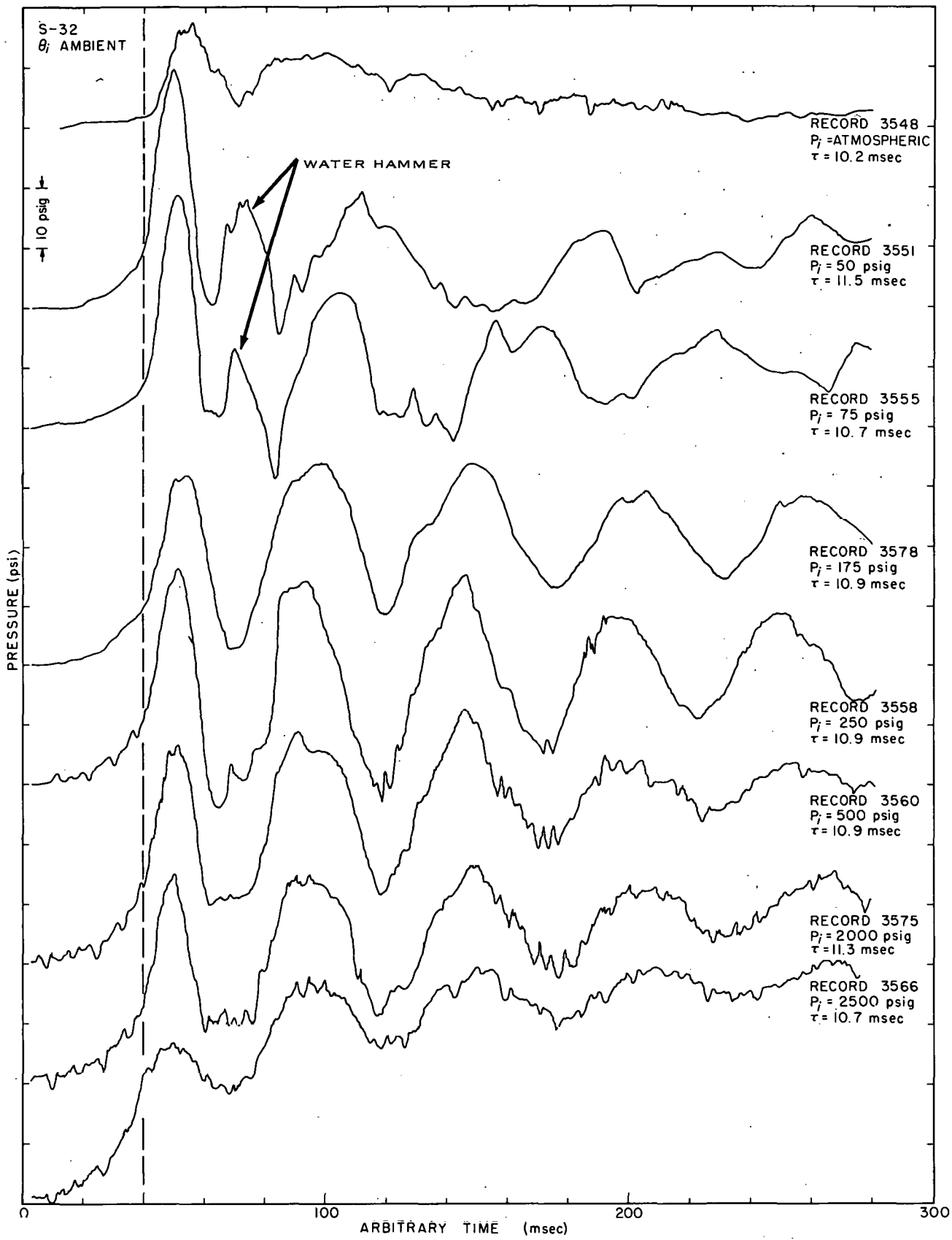

Fig. 68 Representative pressure-time histories for reactor transients conducted at various initial system pressures.

in the data. The frequency of oscillation of both water hammer and vessel ringing increases with increasing pressure until at 230 psig the water hammer is almost completely absent and the ringing approaches the characteristic frequency of the vessel ($\approx$ 20 cps). At 500 psig and above any existing air bubbles entrapped in the system are forced into solution thereby further improving the system coupling.

The data of Figure 69 are indicative of the reproducibility of the pressure data as observed during repeated transients at about 230 psig initial pressure. Since considerable difficulty had been experienced in eliminating air bubbles from the system, a special test series was conducted in November 1960. In this test sequence considerable care was exercised to remove air bubbles from the system so that is was bubble free. No water changes were permitted during the test sequence. Data from these tests are shown by the top three pressure-time histories in Figure 69, The lower two time histories were obtained during tests conducted in July 1960 where water conditions were not so closely controlled. Comparisons of the data indicate marked variations, as for example peak pressures varying from a low of 34 psi to a high of 57 psi. However, the long-term pressure rise at times well beyond peak power compares within $\pm$ 10% of the mean, thus eliminating concern for errors in calibration. The inference is that the differences in magnitude of the primary peaks are a consequence of differences in composition of the reactor system. The variation in timing between peak pressure and peak power ($\approx$9 msec to 12 msec) suggests a variation in stiffness (or bulk modulus) of the water between transients. This is further indicated by the variation in ringing frequency which is emphasized by the dashed line in Figure 69.

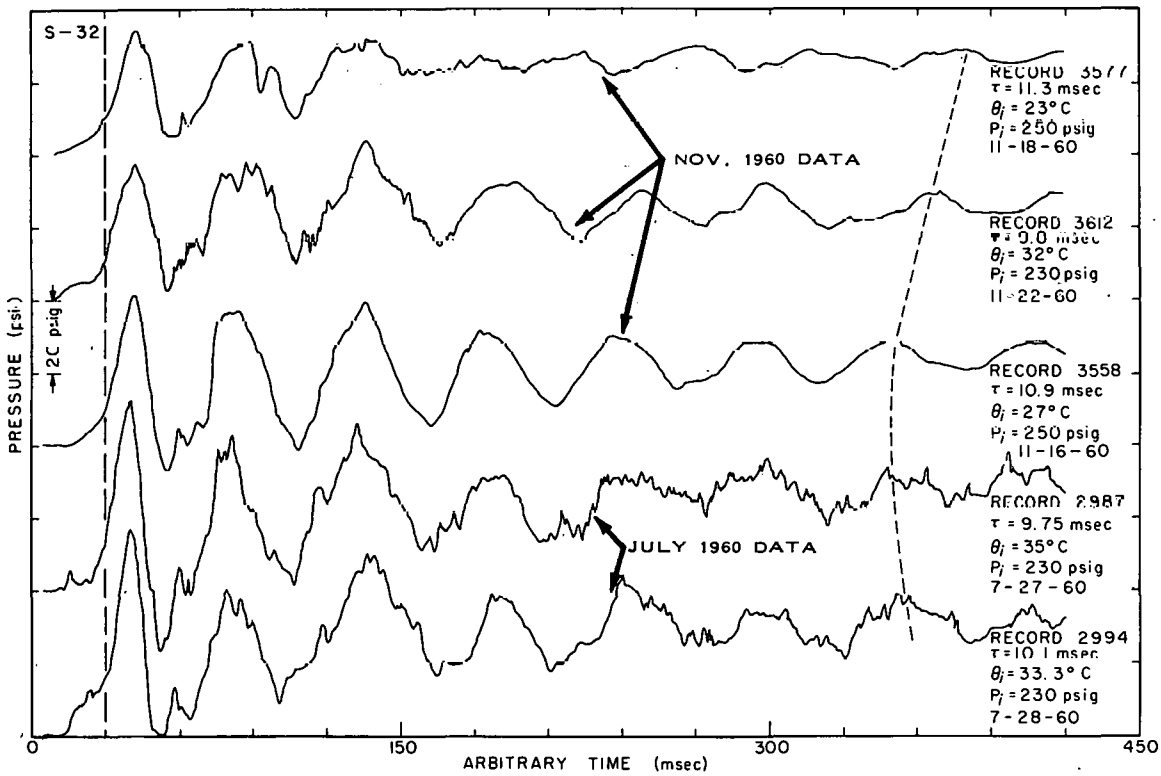

Fig. 69 Representative pressure-time histories showing the degree of repeatability for various transients with similar initial conditions.

The data clearly show the variations to be as pronounced for the November reactor transients, wherein the water conditions were controlled, as for earlier transients in which the water condition was not controlled. Further, the earliest reactor transient in the November series (Record 3558) has the cleanest fundamental and highest ringing frequency, while later transients show a progressively less pure fundamental and lower ringing frequency. It is probable that buildup of radiolytic gas during operation and subsequent entrapment of gas bubbles within the vessel is responsible for this behavior. Further precautions are required if the effects of bubble entrapment upon pressure generation are to be eliminated.

(4) Rise Time of the Pressure Pulse. The rise times of the pressure pulses observed in Spert III are similar to those obtained at Spert I. Local water-hammer effects originating primarily within the fuel assemblies are evident in the data in the form of a few sharp rising pressure spikes. However, the primary pressure pulses always have rise times in excess of 1 msec, and peak pressures of less than 90 psi. Thus, the pressure pulses observed are not shock waves and will propagate at normal acoustic velocities (Section III-1).

As for Spert I, there appears to be no simple correlation between pressure magnitude and power level. If the leading edge of the pressure pulse is approximated by an exponential function, the "effective period" of the function is considerably shorter than the reactor period and is ostensibly determined by the hydrodynamic, thermodynamic, and acoustic properties of the core-vessel environment.

2.33 Cross Plots. Pressure data obtained during testing at Spert III are summarized in Table X. Overall repeatability of the data is of the order of ± 30%, with the exception of a few 20-msec transients where reproducibility was of the order of ± 50% (Appendix B). The peak pressure data obtained during the November 1960 test series with the vessel liquid full have been plotted in Figure 70. The data points represent the magnitude of the first pressure peak since this peak in all instances is the maximum short term or transient pressure observed [a]. The dashed line drawn through the data indicates a peaking in this distribution at intermediate initial system pressures. The decline in magnitude of this first peak at high initial system pressures probably results from suppression of boiling.

The solid line shown represents the highest pressure observed. It is coincident with the dashed line for initial system pressures below 100 psig. Above 100 psig this magnitude exceeds that of the first peak indicating that the composite of the expansion rise and the secondary peak exceeds the magnitude of the first peak. To avoid cluttering the figure, the data points for this maximum observed pressure magnitude are not shown.

---

[a] Because of the long-term expansion rise upon which the transient or steam pressure contribution is superimposed, the magnitude attained by pulses subsequent to the first pulse occasionally exceeds that of the first pulse. However, the rise above the base pressure (due to expansion) is always greatest for the first peak.

TABLE X

SUMMARY OF SPERT III PRESSURE DATA

Record Number	Initial Temperature (°C)	Reactor Period (msec)	Initial Pressure (psig)	Vessel	Reactor Coolant Flow (gpm)	Transducer Location	Pressure at Peak Power (psi)	Peak Pressure (psi)
1595	26.5	18.5	atmospheric	airdome	None	Bottom Tee	---	2.5
1676	26.5	10.7	atmospheric	airdome	None	Bottom Tee	5.0	14.0
1863	24.0	11.9	atmospheric	airdome	None	S 32	---	5.4
1948	31.0	14.0	110	airdome	None	Bottom Tee	---	7.4
1952	31.0	11.7	110	airdome	None	S 32	---	6.5
						Bottom Tee	6.5	26.2
1955	34.0	11.4	atmospheric	airdome	None	Bottom Tee	---	13.5
1964	28.0	10.8	500	airdome	None	S 32	---	6.5
						Bottom Tee	6.5	13.1
1967	31.0	11.0	atmospheric	airdome	None	S 32	---	3.2
						East Port	4.9	12.3
2067	27.0	11.3	1000	airdome	None	S 32	---	4.8
						East Port	---	14.1
2121	24.0	11.6	1900	airdome	None	S 32	3.2	4.8
						Bottom Tee	8.8	13.2
2127	26.5	10.9	atmospheric	airdome	None	S 32	3.2	5.1
						Bottom Tee	---	8.8
2152	27.8	20.4	110	liquid full	None	S 32	3.5	6.4
2225	21.1	18.0	500	liquid full	None	S 32	4.7	7.4
						Bottom Tee	6.4	8.6
						East Port	---	13.0
2227	23.0	18.2	1000	liquid full	None	S 32	---	7.7
						Bottom Tee	6.4	13.8
						East Port	5.2	13.0
2230	23.4	16.2	1900	liquid full	None	S 32	4.0	11.8
						Bottom Tee	4.3	13.4
						East Port	6.2	15.6
2233	28.4	10.9	atmospheric	airdome	None	S 32	3.3	6.7
						Bottom Tee	8.6	12.5
						East Port	---	9.9
2235	23.3	11.3	110	liquid full	None	S 32	10.5	43.0
						Bottom Tee	6.4	35.8
						East Port	5.2	38.0
2237	25.6	10.8	1000	liquid full	None	S 32	15.6	36.2
						Bottom Tee	12.5	41.0
						East Port	7.8	31.3
2240	25.6	10.7	1900	liquid full	None	S 32	10.8	30.5
						Bottom Tee	13.0	32.4
						East Port	11.5	36.5
2246	27.3	10.8	atmospheric	airdome	None	S 32	---	3.3
						Bottom Tee	---	6.9
2968	25.6	22.1	230	liquid full	None	S 32	---	7.6
						Bottom Tee	4.3	10.0
2972	25.7	22.2	230	liquid full	5000	S 32	---	5.0
						Bottom Tee	4.3	8.6
2974	33.4	22.9	230	liquid full	10,000	S 32	---	11.7
						Bottom Tee	4.3	13.0
2977	31.1	21.1	255	liquid full	20,000	S 32	---	7.6
						Bottom Tee	---	13.0
2980	32.2	23.5	230	liquid full	20,000	S 32	---	10.6
						Bottom Tee	6.0	9.5

TABLE X (cont'd)

SUMMARY OF SPERT III PRESSURE DATA

Record Number	Temperature (°C)	Reactor Period (msec)	Initial Pressure (psig)	Vessel	Reactor Coolant Flow (gpm)	Transducer Location	Pressure at Peak Power (psi)	Peak Pressure (psi)
2982	28.3	10.0	230	liquid full	5,000	S 32	13.2	56.7
						Bottom Tee	11.3	54.7
2985	32.7	9.57	235	liquid full	10,000	S 32	11.6	45.6
						Bottom Tee	11.3	46.4
2987	34.8	9.75	230	liquid full	10,000	S 32	15.2	55.7
						Bottom Tee	13.0	60.7
2990	28.3	10.4	255	liquid full	20,000	S 32	10.1	27.9
						Bottom Tee	10.9	28.2
2994	32.4	10.1	230	liquid full	None	S 32	16.2	61.8
						Bottom Tee	41.2	80.7
3103	31.1	25.2	230	liquid full	20,000	S 32	5.1	17.5
						Bottom Tee	4.7	17.1
3107	33.3	20.0	2500	liquid full	20,000	S 32	---	18.0
						Bottom Tee	7.2	21.4
3109	32.8	20.0	2500	liquid full	None	S 32	---	10.3
						Bottom Tee	10.3	16.3
3115	33.3	9.3	2500	liquid full	20,000	S 32	17.0	30.9
						Bottom Tee	2.1	30.0
3165	28.9	19.1	20	liquid full	None	S 32	---	5.0
						Bottom Tee	---	4.7
3167	23.9	21.0	atmospheric	airdome	None	Bottom Tee	---	8.6
3546	21.7	19.8	atmospheric	liquid full	None	S 32	---	3.7
						East Port	---	2.7
3548	21.7	10.2	atmospheric	liquid full	None	S 32	1.9	19.1
						Bottom Tee	---	13.2
						East Port	2.5	19.9
3550	22.4	18.4	50	liquid full	None	S 32	3.9	4.9
						Bottom Tee	2.9	5.5
						East Port	2.0	4.3
3551	22.4	11.5	50	liquid full	None	S 32	6.7	39.0
						Bottom Tee	5.7	37.2
						East Port	8.2	40.7
3553	23.9	18.5	75	liquid full	None	S 32	3.1	4.9
						Bottom Tee	---	5.9
						East Port	4.3	5.7
3555	23.9	10.65	75	liquid full	None	S 32	9.2	40.6
						Bottom Tee	6.9	39.8
						East Port	11.1	44.9
3557	26.7	18.7	250	liquid full	None	S 32	2.9	7.8
						Bottom Tee	4.9	12.2
						East Port	4.3	8.2
3558	26.7	10.9	250	liquid full	None	S 32	10.8	43.5
						Bottom Tee	11.8	44.3
						East Port	13.7	44.6
3560	28.9	10.9	500	liquid full	None	S 32	12.6	36.6
						Bottom Tee	13.2	37.4
						East Port	13.6	38.9
3562	20.6	10.25	175	liquid full	None	S 32	12.2	40.6
						Bottom Tee	9.8	40.0
						East Port	11.1	46.0
3564	20.6	16.95	2500	liquid full	None	S 32	5.5	16.2
						Bottom Tee	5.5	12.6
						East Port	6.1	16.0
3566	20.6	10.74	2500	liquid full	None	S 32	15.6	29.2
						Bottom Tee	17.1	32.5
						East Port	14.5	29.3
3575	22.8	11.3	2000	liquid full	None	S 32	14.2	37.2
						Bottom Tee	12.0	35.4
						East Port	14.5	41.2

TABLE X (cont'd)

SUMMARY OF SPERT III PRESSURE DATA

Reactor Number	Initial Temperature (°C)	Reactor Period (msec)	Initial Pressure (psig)	Vessel	Reactor Coolant Flow (gpm)	Transducer Location	Pressure at Peak Power (psi)	Peak Pressure (psi)
3577	22.8	11.3	250	liquid full	None	S 32	11.8	36.6
						Bottom Tee	10.8	38.0
						East Port	10.4	36.6
3578	23.3	11.3	1175	liquid full	None	S 32	9.8	37.2
						Bottom Tee	8.6	36.1
						East Port	12.3	39.5
3608	32.3	11.5	230	liquid full	20,000	S 32	10.5	19.1
						East Port	12.8	20.2
3610	35.0	11.35	230	liquid full	5,000	S 32	10.5	39.2
						East Port	13.2	41.2
3612	30.2	11.25	200	liquid full	None	S 32	13.0	37.7
						East Port	13.5	39.9
3614	33.3	20.6	230	liquid full	5,000	S 32	---	13.0
						East Port	2.5	13.2
4620	29.5	9.7	atmospheric	liquid full	None	S 32	2.8	21.2
						East Port	7.1	22.4
4314	60.0	22.6	50	liquid full	None	S 32	2.68	2.6
						East Port	---	3.0
4323	82.2	22.7	atmospheric	liquid full	None	S 32		3.7
						East Port	---	6.6
4375	82.0	21.05	100	liquid full	None	S 32	4.2	6.1
						East Port	4.2	7.8
4399	90.0	20.0	atmospheric	liquid full	None	S 32	---	3.2
						East Port	---	3.3
4414	90.0	19.7	50	liquid full	None	S 32	3.2	6.9
						East Port	---	6.0
4476	116.0	18.0	200	liquid full	None	S 32	6.7	13.5
						East Port	4.5	13.6
4490	126.5	21.3	100	liquid full	None	S 32	7.5	14.8
						East Port	5.7	15.3
4548	126.5	19.9	50	liquid full	None	S 32	8.5	21.7
						East Port	9.0	20.8
4571	154.5	21.6	200	liquid full	None	S 32	4.6	15.3
4770	185.0	22.0	200	liquid full	None	S 32	7.2	22.6
4827	205.0	24.1	500	liquid full	None	S 32	5.2	12.1
4961	204.0	19.7	1000	liquid full	None	S 32	3.4	14.0
5028	205.0	18.9	2500	liquid full	None	S 32	3.2	14.1
						East Port	3.6	13.8
5040	101.0	19.6	2500	liquid full	None	S 32	4.82	10.0
						East Port	4.8	15.0
5044	101.0	23.9	2500	liquid full	16,000	S 32	5.83	16.1
						East Port	3.9	10.5

The data plotted for a 20-msec reactor period is again the maximum observed pressure. In this instance boiling is suppressed for all but the shortest reactor periods; the pressure magnitude results primarily from expansion effects.

Data obtained with an air dome in the reactor vessel are shown in Figure 71. These data also are for a reactor period of about 10 msec. In this instance little, if any, peaking is indicated. The magnitude of pressure with the air dome present is much less than that obtained with the vessel liquid full ($P_{AD} \approx 0.3\ P_{LF}$). This behavior results primarily from the pressure relief (and thus flow) afforded at the liquid-gas interface, which permits earlier nuclear shutdown and negative pressure reflection from the gas-water interface.

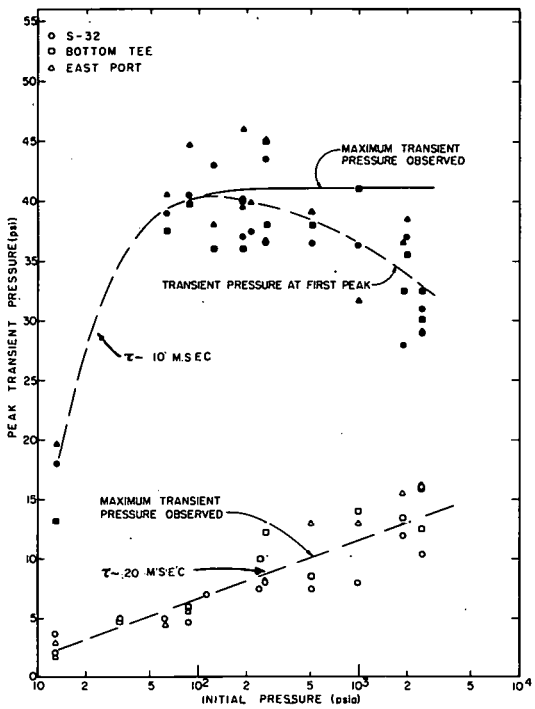

Fig. 70 Peak transient pressure as a function of initial system pressure for ambient initial temperature reactor transients, conducted with the reactor vessel liquid full.

The magnitude of the first peak has been plotted as a function of reciprocal reactor period in Figures 72, 73, and 74 [a]. Lines of specific slope have been drawn through the data with the slope indicated in each instance. As observed for Spert I data (Section III-1) extrapolation of these data to shorter reactor periods is not advisable. As before, the nature of the pressure source may be expected to change from an array of integral plates prior to core melting to a dispersion of fuel droplets or mist in water subsequent to the onset of gross core melting. The change in nature of the source must be expected to produce a change in magnitude of the pressure generated.

[a] Similar plots could be drawn for the maximum observed pressure. They have not been drawn here since they are similar to the first peak data.

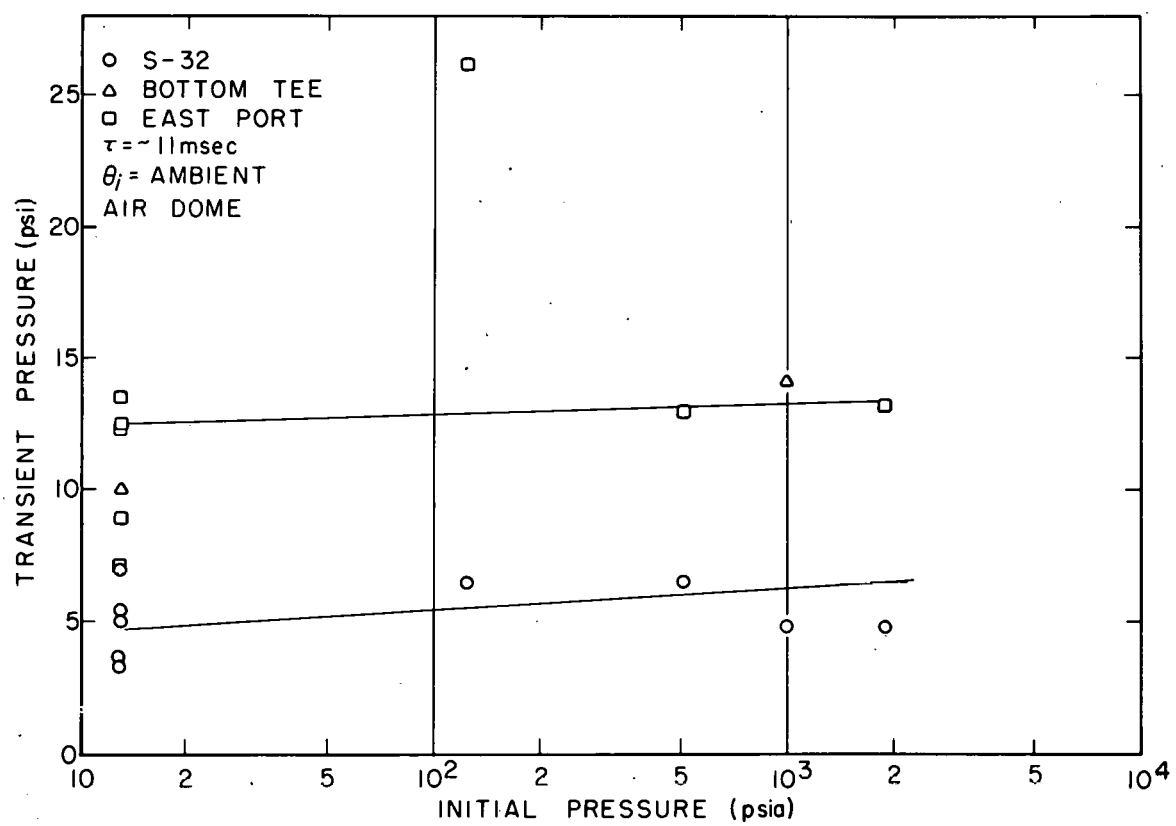

Fig. 71 Peak transient pressure as a function of initial system pressure for ambient initial temperature reactor transients, conducted with an air dome in the reactor vessel.

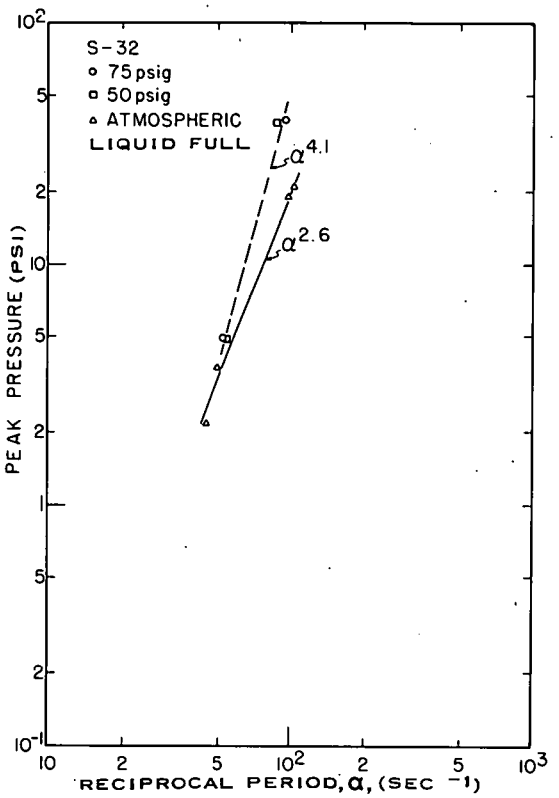

Fig. 72 Peak transient pressure as a function of reciprocal reactor period for ambient initial temperature reactor transients and various initial system pressures.

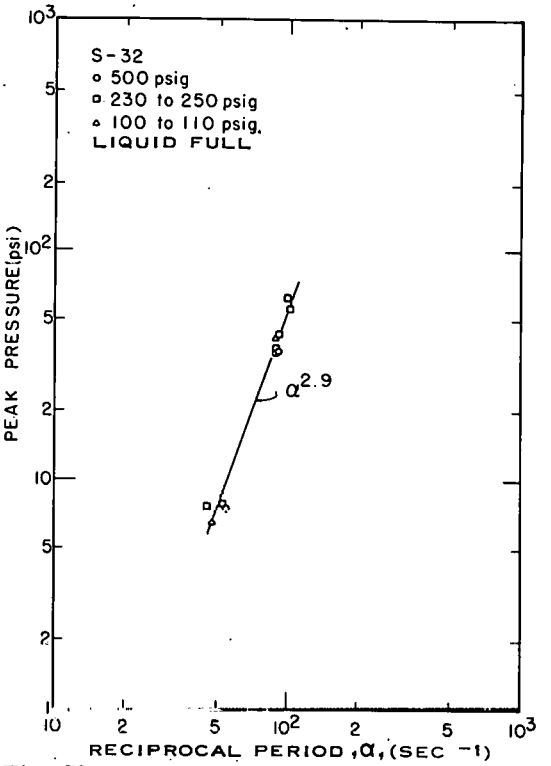

Fig. 73 Peak transient pressure as a function of reciprocal reactor period for ambient initial temperature reactor transients and various initial system pressures.

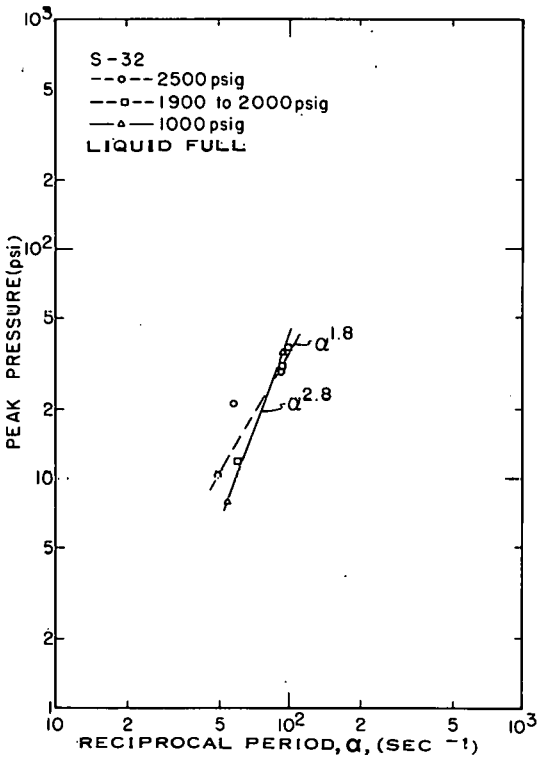

Fig. 74 Peak transient pressure as a function of reciprocal reactor period for ambient initial temperature reactor transients and various initial system pressures.

The dependence of peak pressure upon initial temperature for 20-msec reactor transients is shown in Figures 75, 76, and 77. At low initial pressure (Figure 75) a decrease in peak transient pressure with increasing initial temperature is observed for initial temperatures below 50° C. Beyond 50° C the peak pressure rises monotonically with increasing initial temperature. At intermediate initial pressures, the data represent a monotonic increase of peak transient pressure with increasing initial temperature (Figure 76). For high initial pressure the peak transient pressure is virtually independent of initial temperature over the range of variation in these tests ($20°C < \theta < 220°C$). Data of this type are not available for 10-msec transients and it is not apparent whether similar results would be obtained for other initial conditions. Additional data will be required before satisfactory explanation of this behavior can be given.

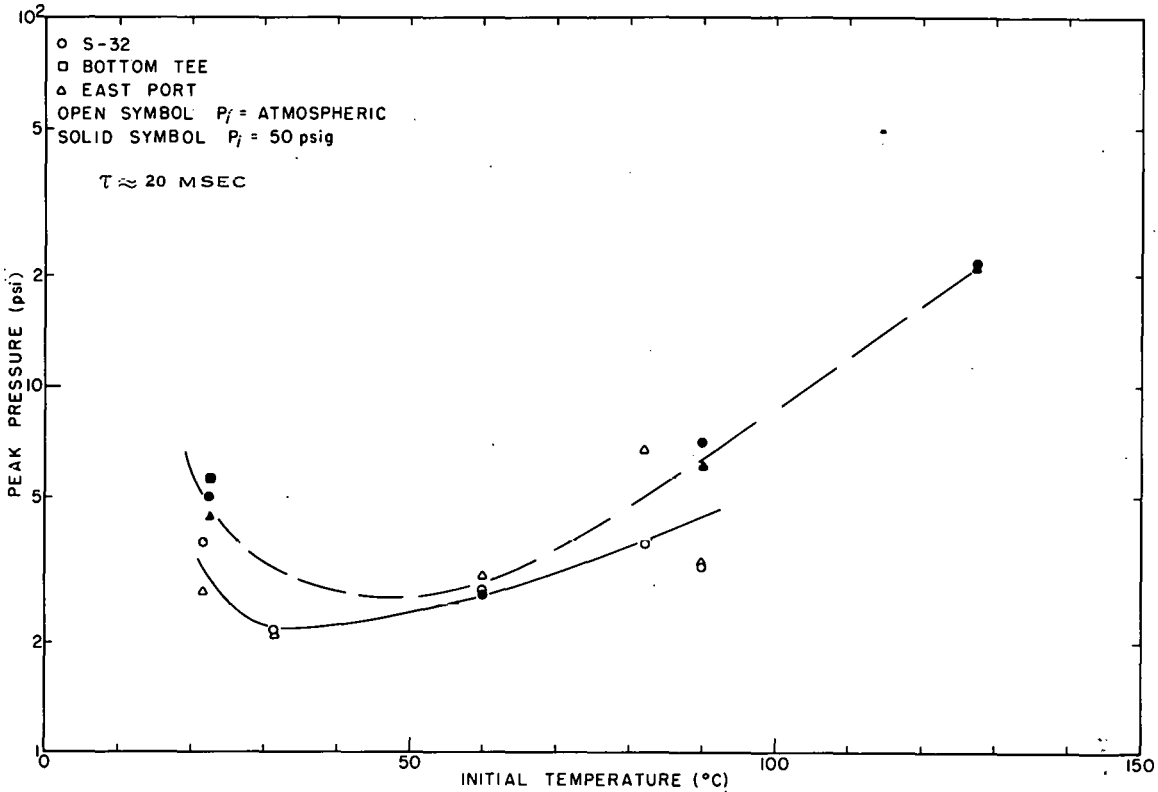

Fig. 75 Peak transient pressure as a function of initial system temperature for a liquid full reactor vessel and various initial system pressures.

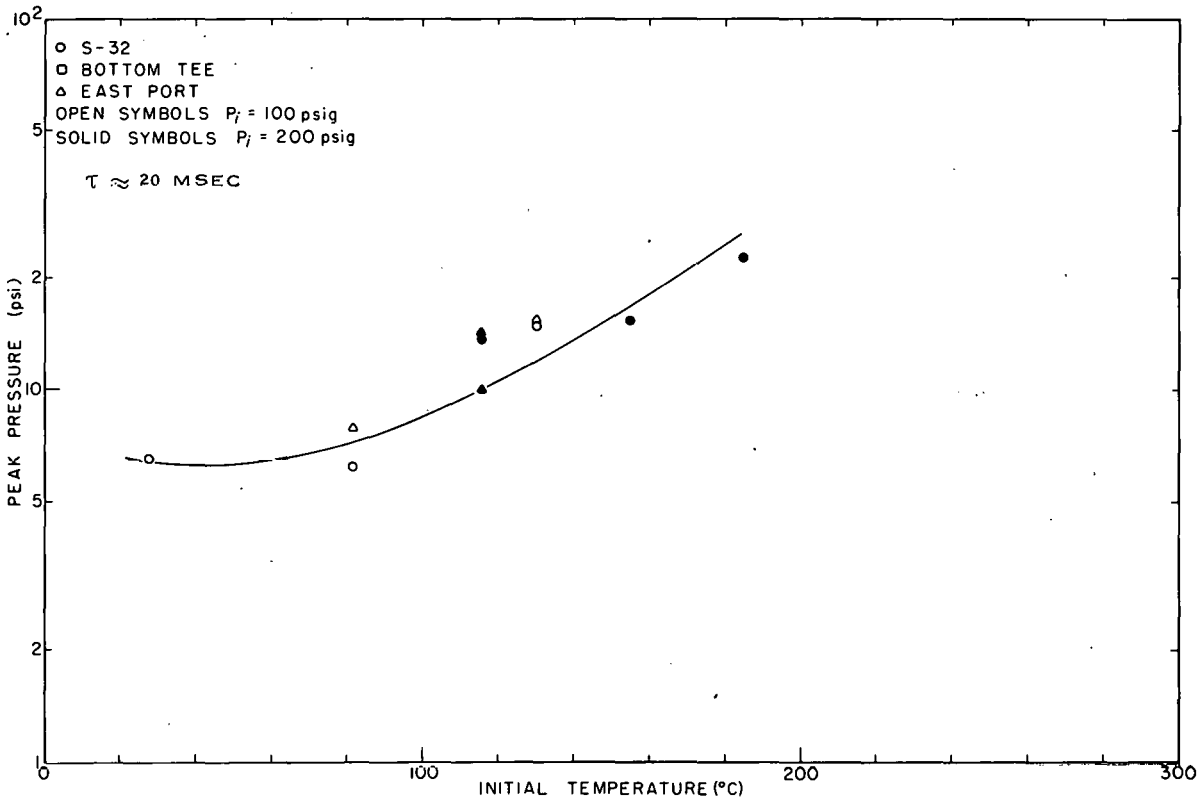

Fig. 76 Peak transient pressure as a function of initial system temperature for a liquid full reactor vessel and various initial system pressures.

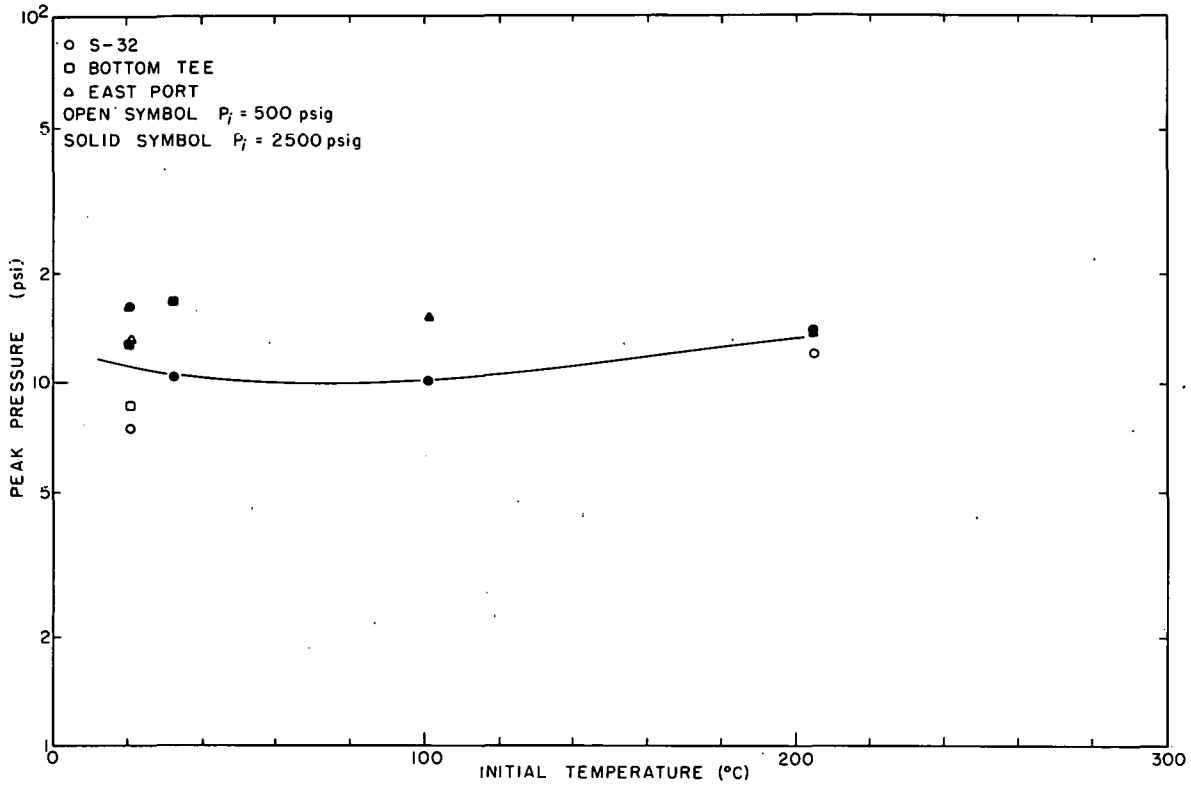

Fig. 77 Peak transient pressure as a function of initial system temperature for a liquid full reactor vessel and various initial system pressures.

3. DATA FROM OTHER SPERT I CORES

The data obtained with the aluminum A- and B-Cores and the stainless steel BSR-II Core in the Spert I facility are discussed in detail in Appendix A. The data obtained were similar in most respects to the data reported in sections III-1 and -2. However, a few special tests were conducted which present information of a type not previously discussed. A brief summary of these special tests will be given in this section. Further details are given in Appendix A.

3.1 A-Core Tests

During A-Core testing, a special test was conducted which investigated the relationship of the pressure within the pressure source (a fuel assembly) to the pressure outside the source. The test results indicated that the pressure levels were moderately higher within the assembly than in a fuel assembly end box. The internal pressures were about a factor of 3 higher than external pressures at an 8-msec reactor period, with the divergence apparently increasing with decreasing reactor period. In order to obtain measurements within the fuel assembly it was necessary to remove part of the fuel plates, thus enlarging the flow channel within the assembly. Possible perturbations in pressure behavior due to this change in geometrical configuration have not been investigated in detail. Such considerations could materially affect the results observed.

In another test series various wetting agents and gaseous additives were introduced into the moderator water. For reactor periods of approximately

18 msec and 10 msec, the data indicate that both the magnitude and the time-history of pressure behavior are very little affected by the presence of these additives.

When the height of water head above the core was increased, an appreciable increase in magnitude of the pressure was observed. This behavior results from a delay in the arrival at the measuring location of the negative reflection from the free surface. The increase in pressure with increasing water head is present at both low ($\approx$ 20°C) and high (boiling) initial temperature. All data presented were obtained at 20-msec reactor periods. Investigation of the effects of water head upon pressure behavior is continuing at Spert IV.

Although several transients were conducted at boiling initial temperature, calibration difficulties affected the data to such an extent that it is difficult to draw any definite conclusions concerning the dependence of pressure magnitude upon reactor period. However, the analog data obtained do indicate a broadening of the pressure pulse with increasing initial temperature.

3.2 B-Core Tests

The primary variable investigated with the B-Cores was metal-to-water ratio (which affects the void coefficient of reactivity) and core dimensions. Most of the transients were obtained for reactor periods of 15 msec or longer as a consequence of fuel-plate damage observed during early 10-msec transients. The time-histories indicate a variation in time of peak pressure relative to time of peak power. The pressure peak occurs after time of peak power for the high void coefficient B 24/32 core, and very near time of peak power for the low void coefficient B 12/64 core. These data reflect the importance of boiling in the sequence of events leading to reactor shutdown. Boiling is a minor contributor to shutdown for the high void coefficient B 24/32 core at reactor periods of 10 msec and longer. However, the B 12/64 core requires boiling void formation to achieve shutdown for a 10-msec reactor period.

3.3 BSR-II Core Tests

The data obtained with the BSR-II Core do not indicate any trends not previously observed in the P-Core.

IV. SUMMARY

The transient pressure data presented in this report were obtained from plate-type, light-water-moderated reactors, during self-limiting power excursions for which there was no permanent damage to the core. Extrapolation of the results to reactor transients having materially higher energy release should be made with appropriate caution due to changes which are known to occur in the nature of the pressure source [19] when gross core melting or vaporizing of the fuel is encountered.

Precise measurement of the transient pressure response is complicated by sensitivity of the detector to such environmental factors as nuclear radiation, acceleration, differential heating of transducer components, etc. Measurement of transient pressures of a few tens of psi in systems pressurized initially to thousands of psi is especially difficult. Improvements in the transducer mechanism, which reduce the spurious response resulting from environmental sensitivities and resonance effects within the transducer, have materially improved the reliability of data and should continue to improve this reliability in future tests. The reproducibility of the pressure magnitudes obtained in the test series reported herein has improved with experience from about a factor to two in earliest tests conducted in 1955 to about $\pm$ 30% for the most recent tests.

The range of parameters involved in the tests is summarized in Table XI. For these tests the peak pressures observed were always less than 100 psi and the rise times were in excess of 1 msec.

For most of the power excursion tests reported here, the pressure peak occurred a few milliseconds after the power peak, the time interval being a function of reactor period, void coefficient, and other related variables. For the low void coefficient B 12/64 core, the pressure peak sometimes occurred coincident with or slightly before the power peak.

The pressure pulse was not truly an exponential function. However, if the pressure behavior during the interval of most rapid increase in pressure were approximated by an exponential function, the resultant effective period of the pressure pulse would be consistently less than the reactor period, the usual ratio being of the order of one to three (ie, $\tau_p/\tau_\phi \approx 1/3$). The pressure-time history appears to depend primarily upon the hydrodynamic, thermodynamic, and acoustic parameters of the reactor environment.

The effects of size of the pressure source upon pressure generation are evident in the data. Pressure magnitude is closely correlated to the diameter of the region of prime energy (heat) transfer for a given core, and increases with an increase in size of the pressure source. The pressure magnitude also increases roughly in accordance with the effective temperature at which energy transfer (eg, steam formation) occurs.

TABLE XI

RANGE OF VARIABLES APPLICABLE TO SPERT TESTS REPORTED IN THIS DOCUMENT

Reactor Vessel	Initial Temperature	Initial Pressure	Minimum Reactor Period
Open	7 - 97°C	Atmospheric	$\approx$ 4.5 msec
Closed	21 - 205°C	Atmospheric to 2500 psi	$\approx$ 9.5 msec

The generation and transmission of pressure are in accordance with the

behavior expected from acoustical considerations. The effects of reflection from the system boundaries can be observed in the data as a reduction in magnitude of the pressure. The pressure pulse is transmitted through the plate-water environment about as efficiently as it is transmitted in a direction parallel to the plates, which result is predicted by Heuter and Bolt [11] for the ratio of plate thickness to acoustic wave length applicable to these tests. The data indicate a reasonable symmetry in the pressure distribution within the system.

There is some evidence of directionality in the pressure generated at the source, and at shorter reactor periods this directionality should be intensified with a resultant modification in the generated spatial pressure distribution.

The time histories of pressure, power, energy, and temperature indicate a close correlation among these primary variables. However, the pressure response must be compared with the spatial as well as the time dependence of these variables, especially in the case of temperature behavior. The existence of a contribution to the pressure generation due to fuel plate and moderator expansion and the resulting displacement of the fuel assembly side plates and moderator can be observed in the data. Such expansion contributions are most apparent in pressurized, liquid-full systems where boiling may be suppressed. In tests for which complete suppression of boiling was attained, the pressure behavior exhibited a long-term asymptotic rise similar to the energy-time history. In tests for which boiling was not completely suppressed, the expansion contribution is followed by a more prominent contribution attributed to energy transfer resulting in steam formation.

Since the two stainless steel cores (P- and C-Cores) were very similar, a comparison of the data obtained is of interest in determining the effects of enclosing the system. The transient pressure level was usually greater for the enclosed (but unpressurized) system than for the open system. The differences in observed pressure behavior between open and enclosed systems appear to be greatest for long reactor periods and low initial temperatures.

Data obtained with pressure transducers mounted inside a modified fuel assembly in an open system indicate that pressure levels within a fuel assembly are somewhat higher than those measured at the core periphery. The data indicate that the internal to external pressure ratio increases with increasing energy release, so that such considerations may become increasingly important at shorter reactor periods.

The pressure pulses observed during these tests were definitely not "shock" waves. That is, the rise times were long (> 1 msec compared to $< 5\ \mu$sec for shock waves), and the levels were low (tens of psi compared to thousands of psi for the usual definition of shock waves). However, as the total energy release is increased by decreasing the reactor period, the rise time of the pressure pulse also decreases. It is not clear whether or not these pulses will become shock waves.

It should be emphasized that an understanding of the pressure-time relationship would not solve all the problems incident to the study of reactor kinetics. The pressure behavior is primarily a measure of the form of energy transfer and the rate at which it occurs. The nuclear heat generated initially within the fuel during a reactor transient must eventually be shared with other com-

ponents of the system. The attendant heat flow is indicated to some extent by the transient temperature response, and ultimately results in the production of mechanical energy (or work) of which the pressure behavior is a prime indicator. The precise nature of the conversion mechanism and the conversion efficiency are complex functions of both the system design and the total energy release. A thorough knowledge of the pressure-time behavior can facilitate understanding of the problem of energy partition, and may ultimately provide vital answers concerning the nature of system response and the reasons for system failure.

V. REFERENCES

1. W. H. Giedt and D. L. Rall, Design and Development of a Fuel Plate Surface Thermocouple for Special Power Excursion Reactor Tests, IDO-16388 (February 1957).

2. F. L. Bentzen, Spert-I Instrumentation, IDO-16316 (March 1957) pp 13-14.

3. S. P. Harris and C. F. Bumpus, Jr., Pressure and Temperature Instrumentation for Dynamic Measurements in the KEWB Program, A Summary Report, NAA-SR-4790 (November 1960).

4. F. Schroeder, (ed.) Spert Project Quarterly Technical Report for October, November, December 1959, IDO-16616 (August 1960) pp 21-24.

5. Materials Testing Reactor - Engineering Test Reactor Technical Branches Quarterly Report, October 1 - December 31, 1962, IDO-16857 (March 1963) pp 49-50.

6. T. R. Wilson, An Engineering Description of the Spert-I Reactor Facility, IDO-16318 (June 1957) pp 13-16.

7. P. M. Morse, Vibration and Sound, Second Edition, New York: McGraw-Hill, 1948.

8. Theodor F. Hueter and Richard T. Bolt, Sonics, New York: John Wiley and Sons Inc., 1955.

9. American Institute of Physics Handbook, Section Editors: Bruce H. Billings and others; Coordinating Editor: Dwight E. Gray, Second Edition, New York: McGraw-Hill, 1963.

10. H. B. Karplus, Propagation of Pressure Waves in a Mixture of Water and Steam, ARF-4132-12 (1961).

11. Hueter and Bolt, op. cit., Chapter 7.

12. Morse, op. cit., Chapter VII.

13. G. O. Bright, (ed.), Quarterly Progress Report (for) July, August, September 1958, IDO-16512 (May 1959) pp 22-25.

14. S. G. Forbes et al, Analysis of Self-Shutdown Behavior in the Spert I Reactor, IDO-16528 (July 1959) p 18.

15. G. O. Bright et al, An Elementary Model for Reactor Burst Behavior, IDO-16393 (August 1957).

16. W. A. Horning and H. C. Corben, Theory of Power Transients in Spert I Reactor, IDO-16446 (August 1957) pp 78-81.

17. Ref. 9, Section 2, p 231 and Section 3, p 38.

18. A. H. Spano and R. W. Miller, Spert I Destructive Test Program Safety Analysis Report, IDO-16790 (June 1962) pp 36-75.

19. R. W. Miller et al, Report on the Spert I Destructive Test on an Aluminum, Plate-Type, Water-Moderated Reactor, IDO-16883 (to be published).

20. R. E. Heffner and T. R. Wilson, Spert III Reactor Facility, IDO-16721 (October 1961).

21. F. Schroeder et al, The Spert III Reactor Nuclear Start-up, IDO-16586 (March 1960).

22. F. Schroeder, (ed.) Spert Project Quarterly Technical Report for October, November, December 1959, IDO-16616 (August 1960) pp 4-18.

23. Wilson, op. cit., pp 13-16.

24. Forbes, loc. cit.

25. J. C. Haire, Subcooled Transient Tests in the Spert I Reactor - Experimental Data, IDO-16342 (July 1958).

26. G. O. Bright, (ed.) Reactor Projects Branch Quarterly Progress Report (for) July, August, September 1957, IDO-16416 (October 1957) pp 10-40.

27. L. A. Stephan, Transient Tests of the BSR-II Core in the Spert I Facility, IDO-16768 (April 1963).

28. F. Schroeder, (ed.) Spert Project Quarterly Technical Report (for) April, May, June 1960, IDO-16640 (April 1961) pp 3-9.

29. J. C. Haire, Subcooled Transient Tests in the Spert I Reactor - Experimental Data, IDO-16342 (July 1958) pp 14-22.

APPENDIX A - ADDITIONAL SPERT I DATA

1. A-CORE EXPERIMENTS

1.1 Core Description [23]

The first core operated in Spert I was an aluminum-clad core designated the A-core. The A-Core fuel assembly was in many respects similar to the P-Core assembly [a]. It consisted of 17 fuel plates brazed to nonfueled side plates and supported by two stiffener plates as shown in Figure 78. Each fuel plate was thus divided into three sections designated 1, 2, and 3 from east to west as shown in Figure 79. Fuel plates were designated by number from 1 to 17 beginning at the north of the assembly as for the P-Core. An additional digit specified which of the three sections of the plate was involved as 44 172 (Figure 79). Vertical position of a thermocouple was expressed in inches above or below centerline with a letter N or S to specify the side of the plate on which the thermocouple was mounted. The plates consisted of a 20-mil-thick U-Al meat (93.5% enriched in U-235) clad with 20 mils of aluminum. The fuel loading was 9.9 gms U-235 per plate, or 168 gms per 17 plate assembly. Overall dimensions of the assembly were 2.96 in. square by 32-5/8 in. long (active length 24-5/8 in.--see Figure 78). Twenty-eight assemblies completed the operational core as shown in Figure 79.

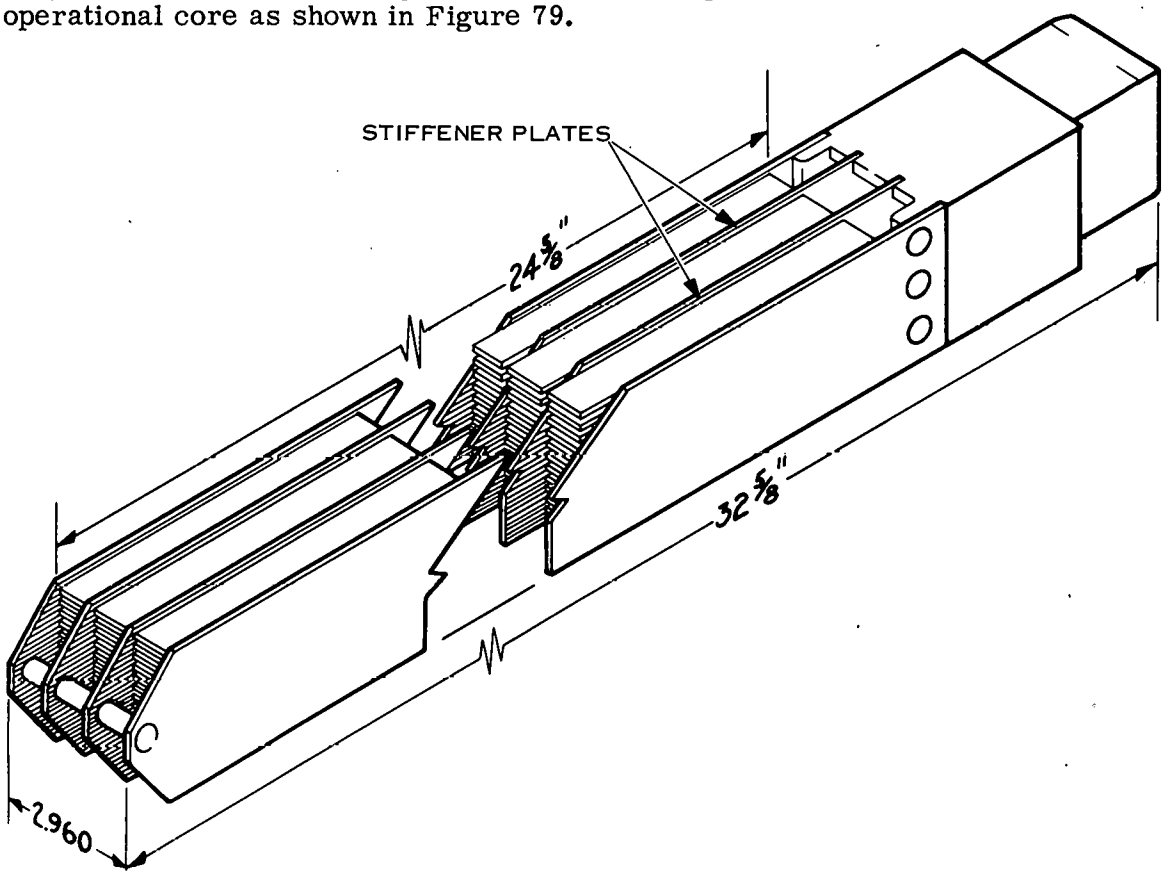

Fig. 78 Schematic representation of aluminum clad A-Core fuel assembly.

[a] See Section III-1 for a description of P-Core and the Spert I facility.

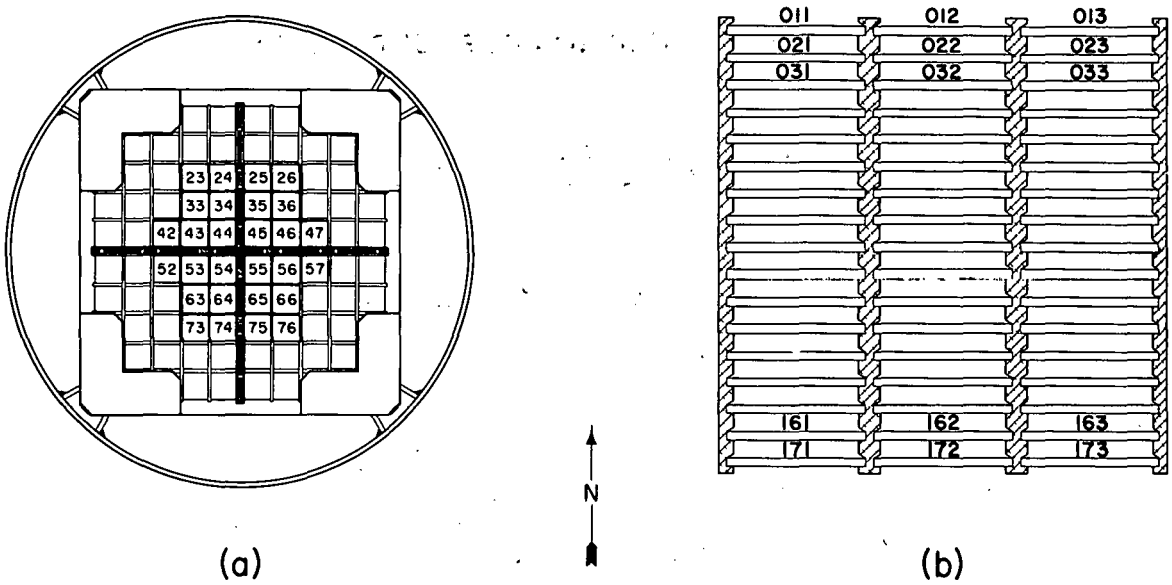

Fig. 79 Layout of Spert I reactor grid showing arrangement of fuel assemblies for the operational A-Core.

A few parameters pertinent to evaluation of the A-Core data are presented in Table A-1.

1.2 Data Presentation

1.21 General Considerations. The data obtained with the A-Core are similar in most respects to those obtained with the P-Core. There were, however, a few special experiments performed with this core, eg, those investigating the effects of moderator additives and height of water above the core (water head). Those data similar to P-Core data already considered will be presented with a minimum of comment and are intended for use in further substantiating effects previously noted. Data pertaining to special experiments will be discussed in more detail.

TABLE A-1

PERTINENT A-CORE CONSTANTS [24]

Item	Magnitude
Clad Material	Aluminum
Critical Mass U-235	3.9 kg
Total U-235	4.7 kg
H/U Ratio	320
M/W Ratio	0.79
Available K_{ex}	5.20$
Temperature defect 20 - 95°C	1.47$
Isothermal Temperature Coefficient 20°C	-0.67×10^{-2} $/°C
Isothermal Temperature Coefficient 95°C	-2.7×10^{-2} $/°C
Average Void Coefficient - C_V	-4.6×10^{-4} $/cm^3
Reduced Prompt Neutron Lifetime ℓ^*/β	7×10^{-3} sec
Water Channel Width	116 mils

1.22 Analog Plots. The data presented were obtained from the original oscillographic traces by using an analog curve follower as previously described (Section II).

(1) Time-History Correlations for Power, Energy, Temperature Flow, and Pressure. The time behaviors of pressure, temperature, power, energy, and flow may be compared in Figures 80 and 81 for 18-msec and 8-msec reactor periods, respectively. The correlations between pressure and temperature behavior (heat transfer) are again evident. The pressure peak for the

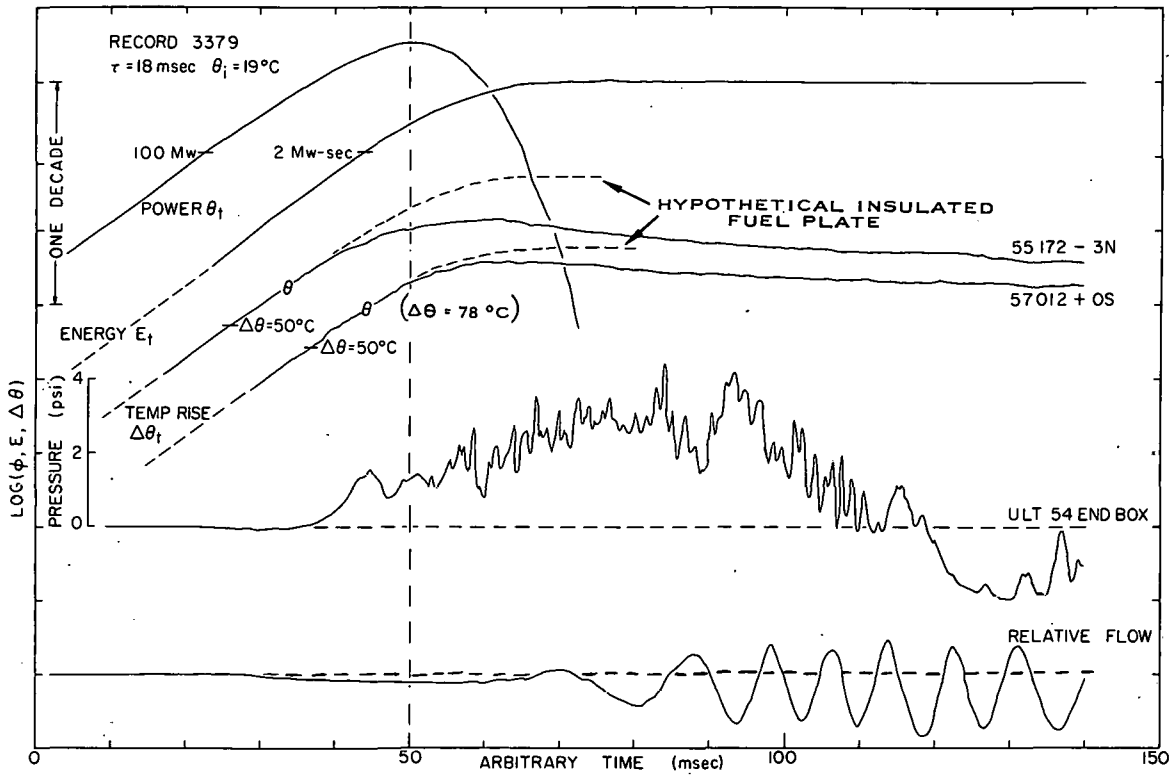

Fig. 80 A presentation of time histories for power, energy, fuel-plate surface temperature, pressure, and flow. The symbol θ on the temperature-time histories indicates the boiling temperature with the corresponding temperature rise shown in parentheses adjacent to one of the traces.

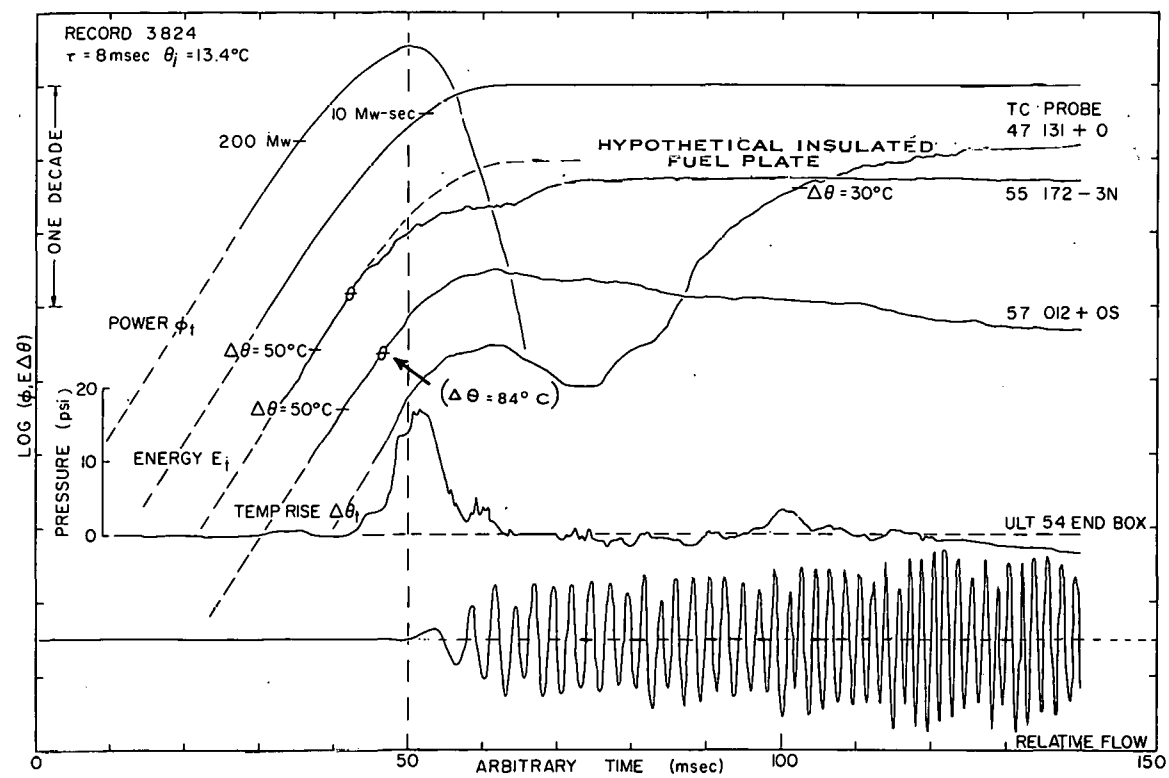

Fig. 81 A presentation of time histories for power, energy, fuel-plate surface temperature, pressure, and flow. The symbol θ on the temperature-time histories indicates the boiling temperature with the corresponding temperature rise shown in parentheses adjacent to one of the traces.

A-Core (Figure 81) occurs somewhat earlier with respect to peak power than it did for the P-Core, (Figure 26) but the pressure-time history is very similar to the P-Core pressure-time history. A temperature probe located in a water channel has an output very similar to that observed for the P-Core, except that the delay between heating of the plate and heating of the moderator is slightly longer for the A-Core. The flow traces indicate the usual correlation between pressure and flow, ie, the flow lags the pressure generation and is greater for shorter period transients [a].

(2) Time-History Correlation of Pressure Behavior with Radial and Longitudinal Temperature Distributions. Corresponding radial and longitudinal temperature distributions are shown in Figures 82 through 85. In these data an anomalous behavior may be observed in some of the temperature traces. These anomalies appear as vertical discontinuities in the temperature traces at 56 172 + ON and 44 172 + OS in Figure 85. These discontinuities may not represent actual temperature changes, ie, they may be a consequence of a change in effective depth of the junction of the thermocouple within the cladding as the cladding expands upon heating. These discontinuities are observed only with the use of peened thermocouples (Section II-2).

(3) Effects of Miscellaneous Variables Upon Pressure Generation. The dependence of pressure response upon reactor period is shown in Figures 86 and 87 for ambient and boiling initial temperatures. Prior to the time of peak power, 60 and 120 cycle hum from the electronics is very evident

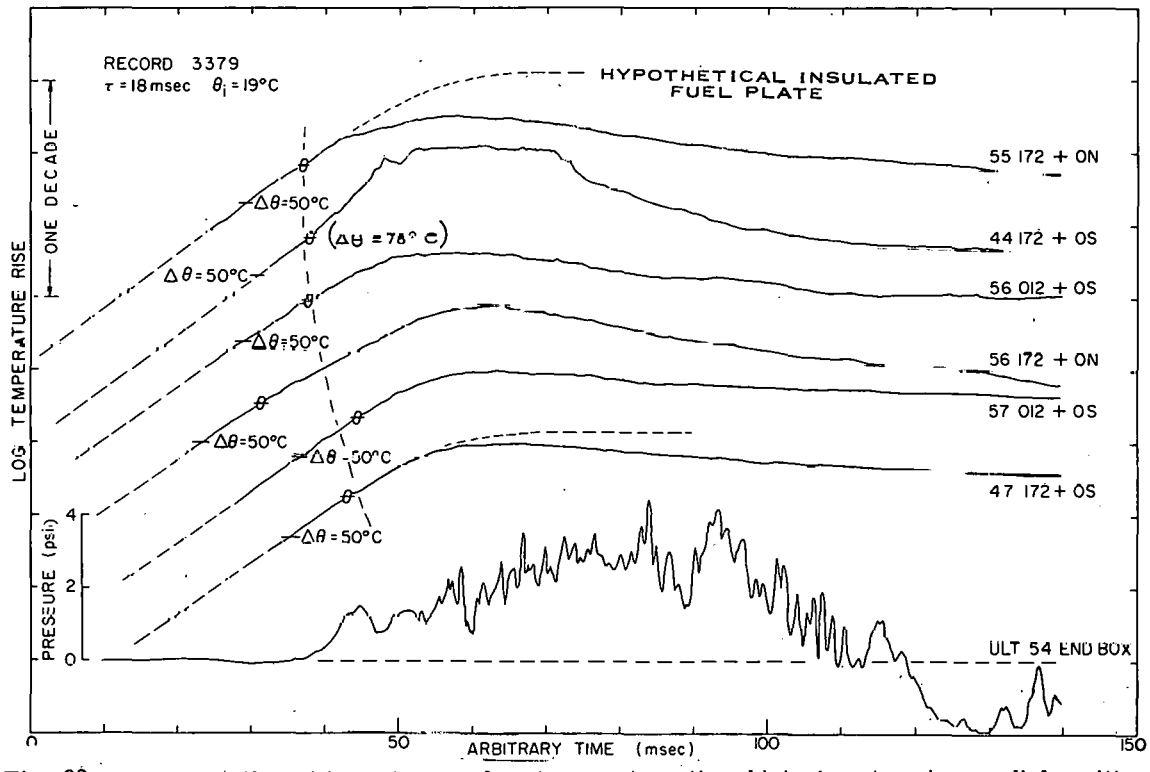

Fig. 82 A presentation of fuel-plate surface temperature-time histories at various radial positions and the pressure-time history. The symbol θ on the temperature-time histories indicates the boiling temperature with the corresponding temperature rise shown in parentheses adjacent to one of the traces.

[a] Note that for these flowmeters increasing flow is shown by a higher output frequency as seen by comparing Figures 80 and 81.

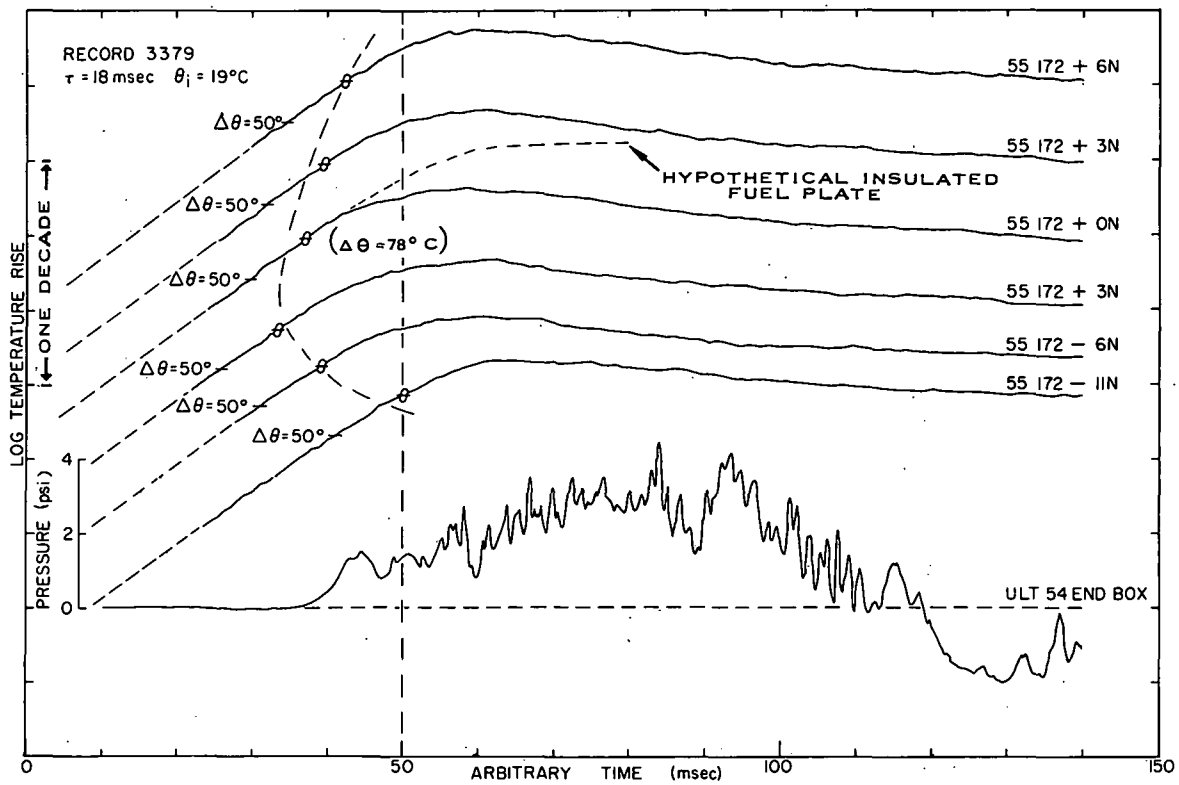

Fig. 83 A presentation of fuel-plate surface temperature-time histories at various longitudinal positions along a fuel plate and the pressure-time history. The symbol θ on the temperature-time histories indicates the boiling temperature with the corresponding temperature rise shown in parentheses adjacent to one of the traces.

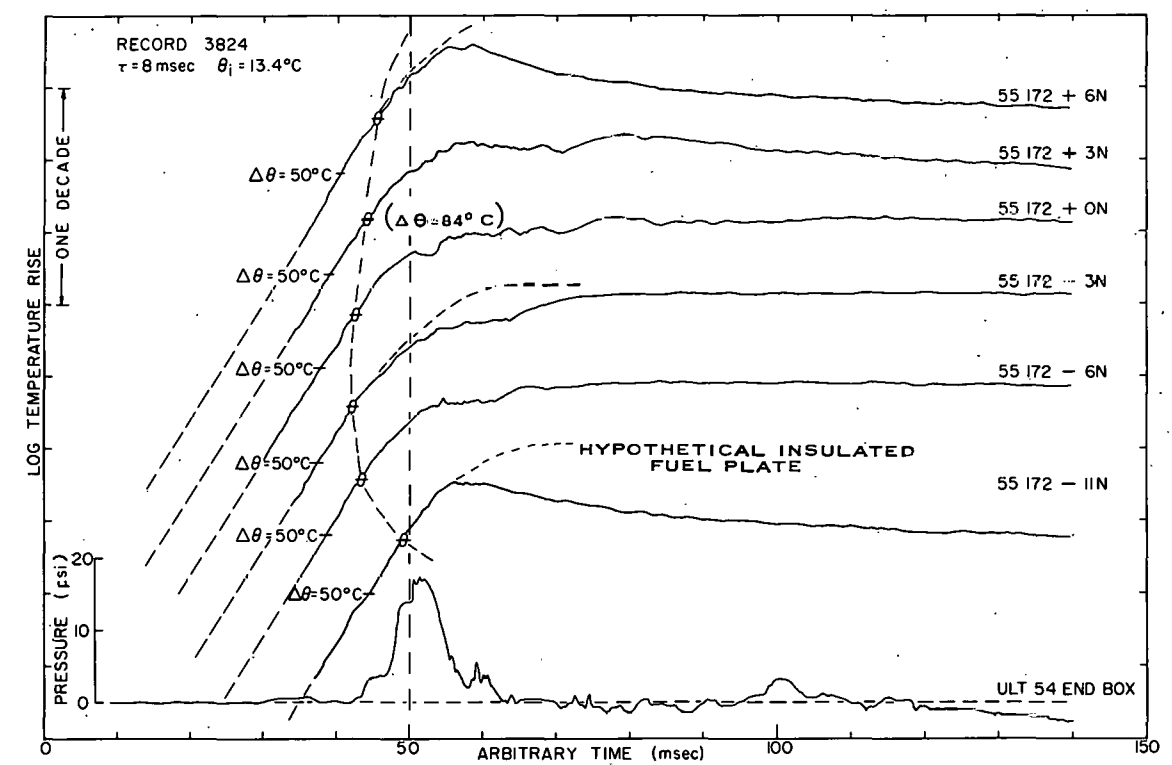

Fig. 84 A presentation of fuel-plate surface temperature-time histories at various longitudinal positions along a fuel plate and the pressure-time history. The symbol θ on the temperature-time histories indicates the boiling temperature with the corresponding temperature rise shown in parentheses adjacent to one of the traces.

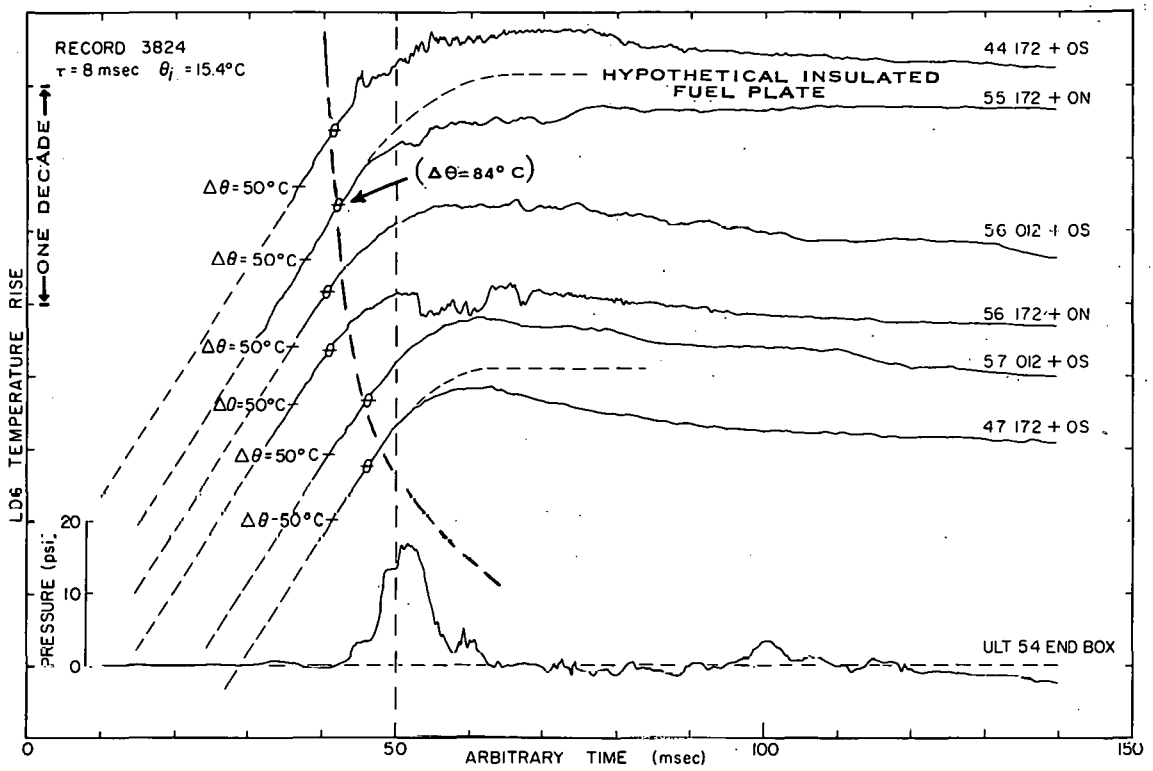

Fig. 85 A presentation of fuel-plate surface temperature-time histories at various radial positions and the pressure-time history. The symbol θ on the temperature-time histories indicates the boiling temperature with the corresponding temperature rise shown in parentheses adjacent to one of the traces.

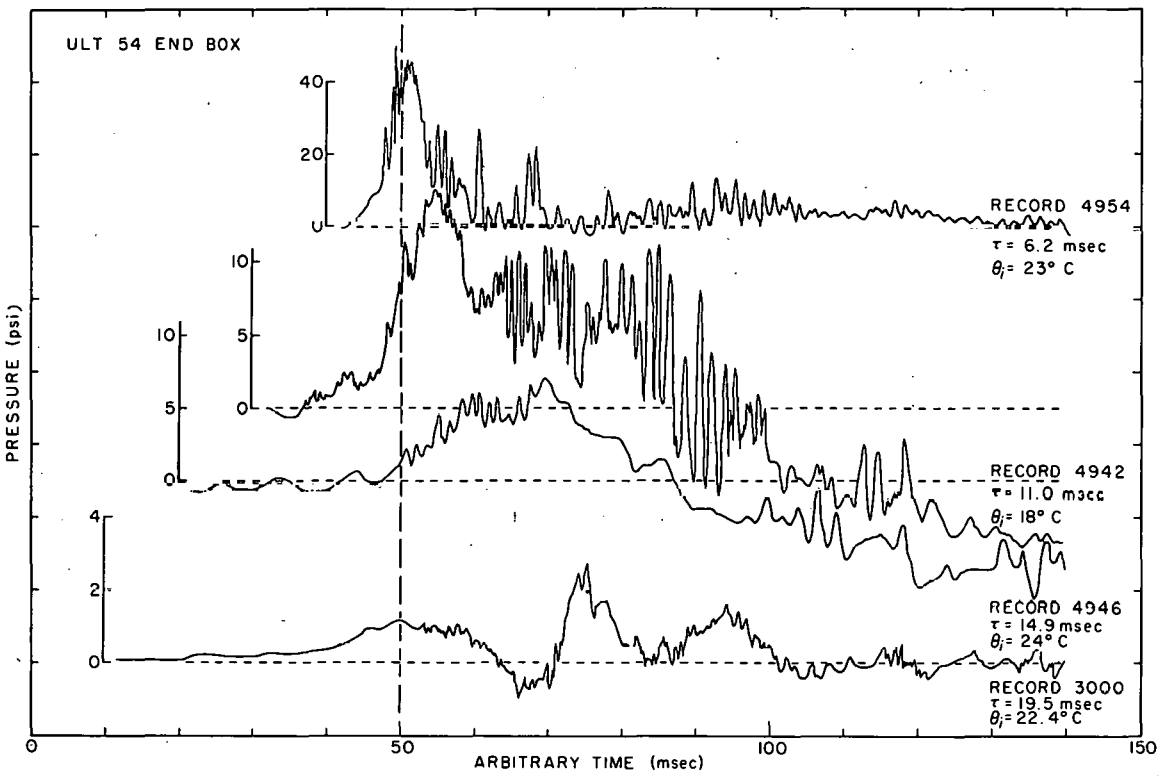

Fig. 86 Representative pressure-time histories for ambient temperature reactor transients at various reactor periods.

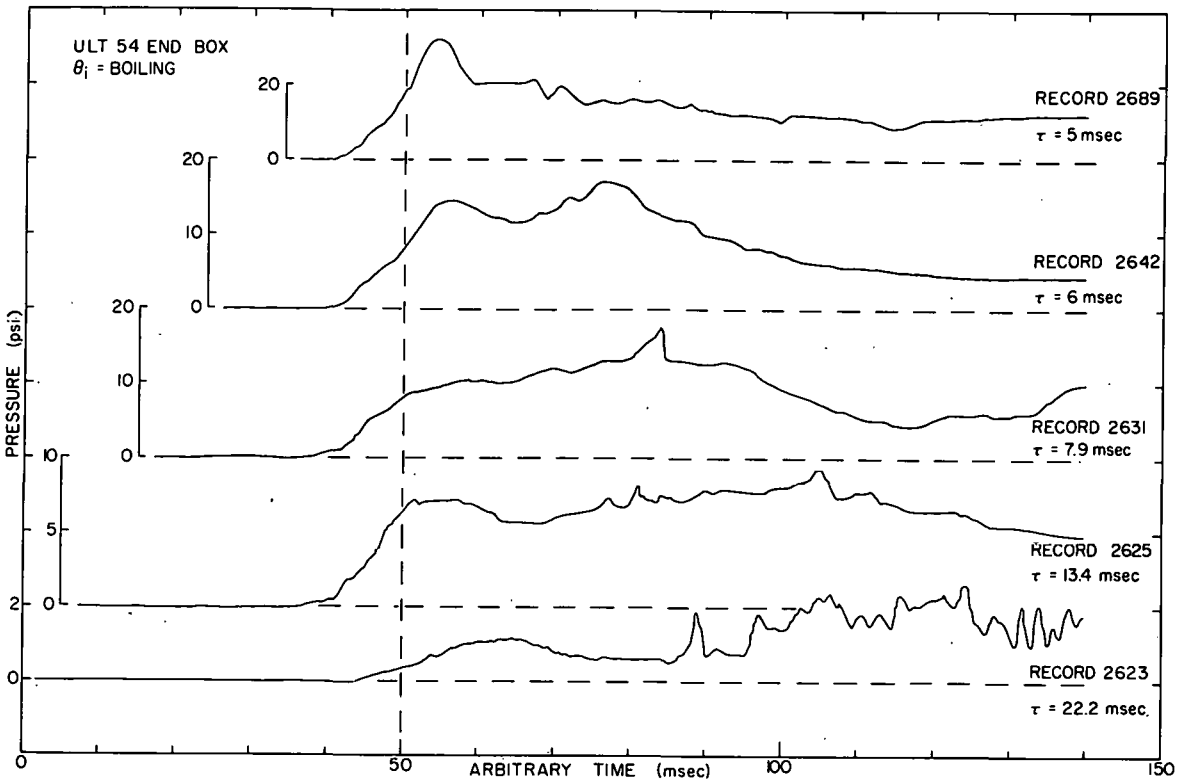

Fig. 87 Representative pressure-time histories for boiling reactor transients at various reactor periods.

in the traces of Figure 86. A rather striking change in the pressure behavior with a change in the reactor period is apparent. It consists primarily of a narrowing of the primary pressure pulse with decreasing reactor period, a shift in time of peak pressure nearer to the time of peak power, and a notable increase in pressure level. While the changes are less pronounced for the boiling transients (Figure 87), they are still clearly in evidence. Additional data of this type are shown in Figures 88 and 89, where the initial temperature is the primary parameter [a]. There appears to be little consistency in the dependence of pressure level upon initial temperature for these boiling transients [b].

The influence of the height of water head above the core upon pressure behavior is shown in Figures 90 and 91. The only data available were obtained for long reactor periods. They indicate a pronounced increase in pressure magnitude with increasing height of water head as would be expected from acoustical considerations (eg, the negative reflection from the free surface is delayed in time so that the peak rises higher). The trend is about as evident for boiling initial temperature as for ambient initial conditions (Figure 90). It also is evident for transients in which carbon dioxide gas was used as an additive to the moderator water (Figure 91). Investigation of this head effect is continuing at Spert IV.

---

[a] Since only a few transients were obtained at elevated initial temperature, some variation in reactor period was unavoidable for these plots.

[b] Pressure magnitudes are probably less accurate for these transients than for the P-Core data as a result of calibration or procedural difficulties (see item 1.23).

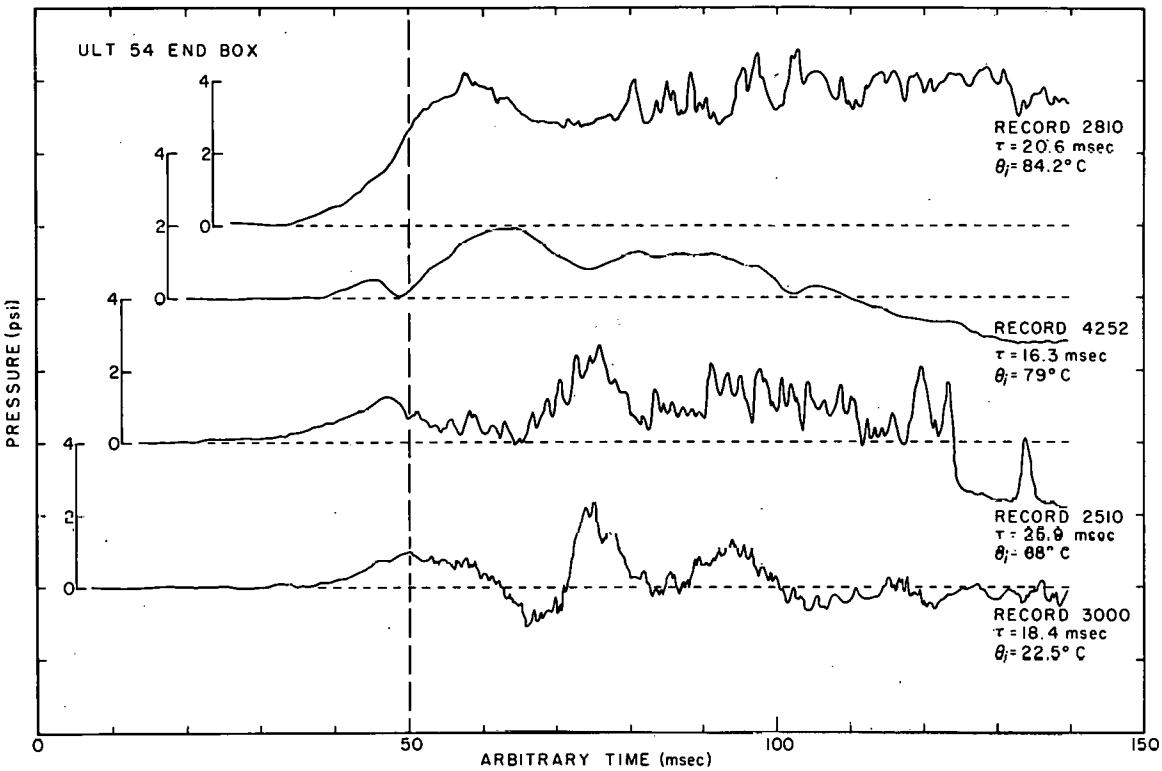

Fig. 88 Representative pressure-time histories for various initial temperatures and a nominal 20-msec reactor period.

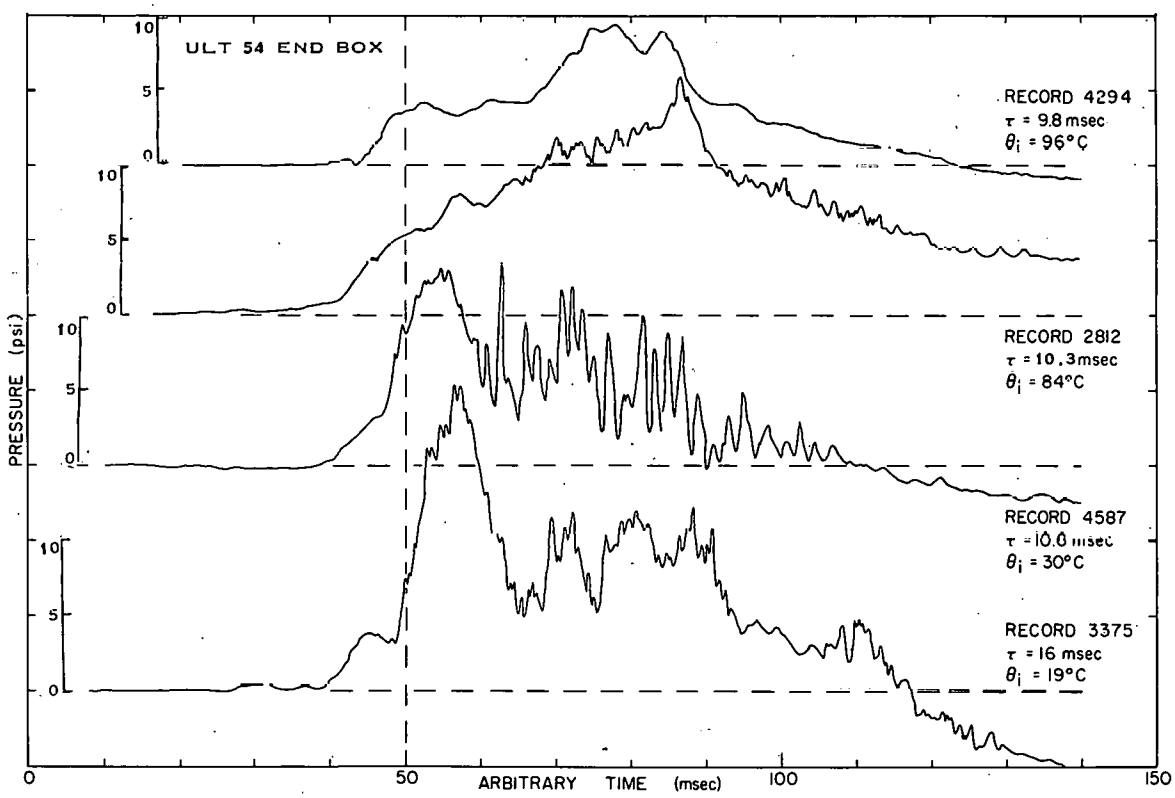

Fig. 89 Representative pressure-time histories for various initial temperatures and a nominal 10-msec reactor period.

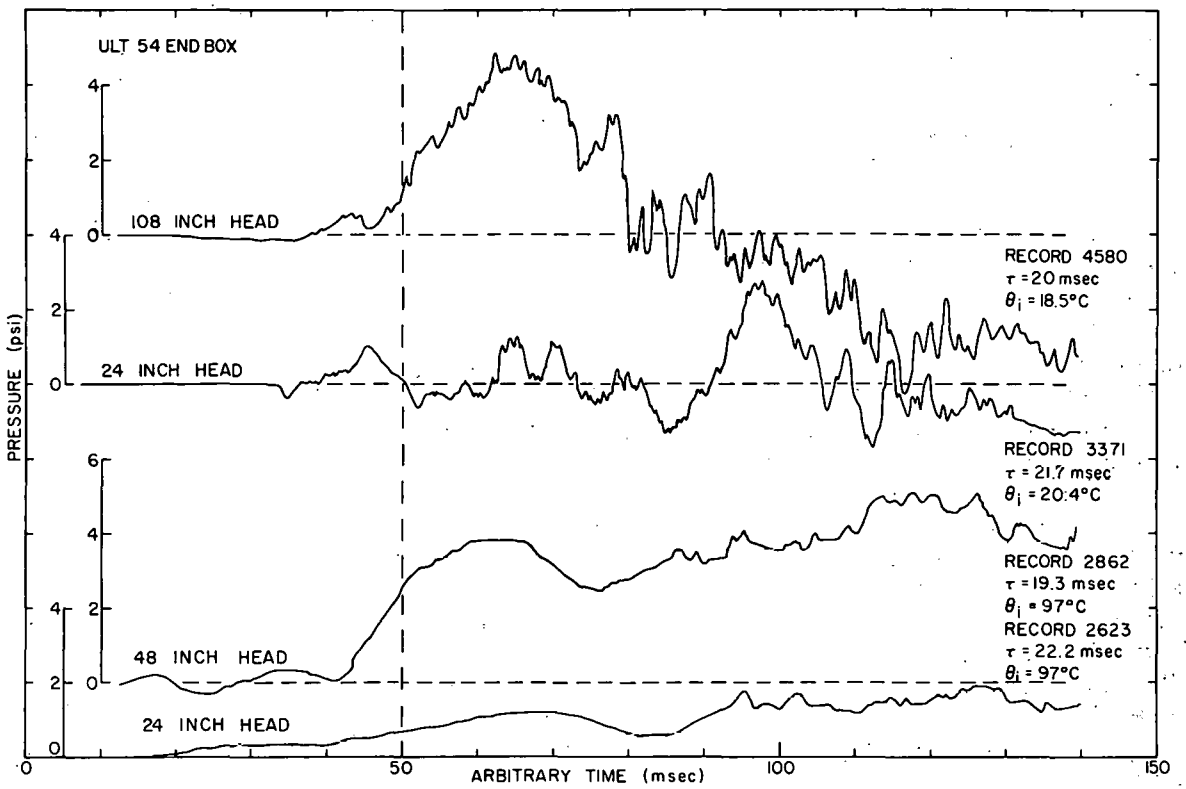

Fig. 90 Representative pressure-time histories for various depths of water head above the reactor core with pure water moderator.

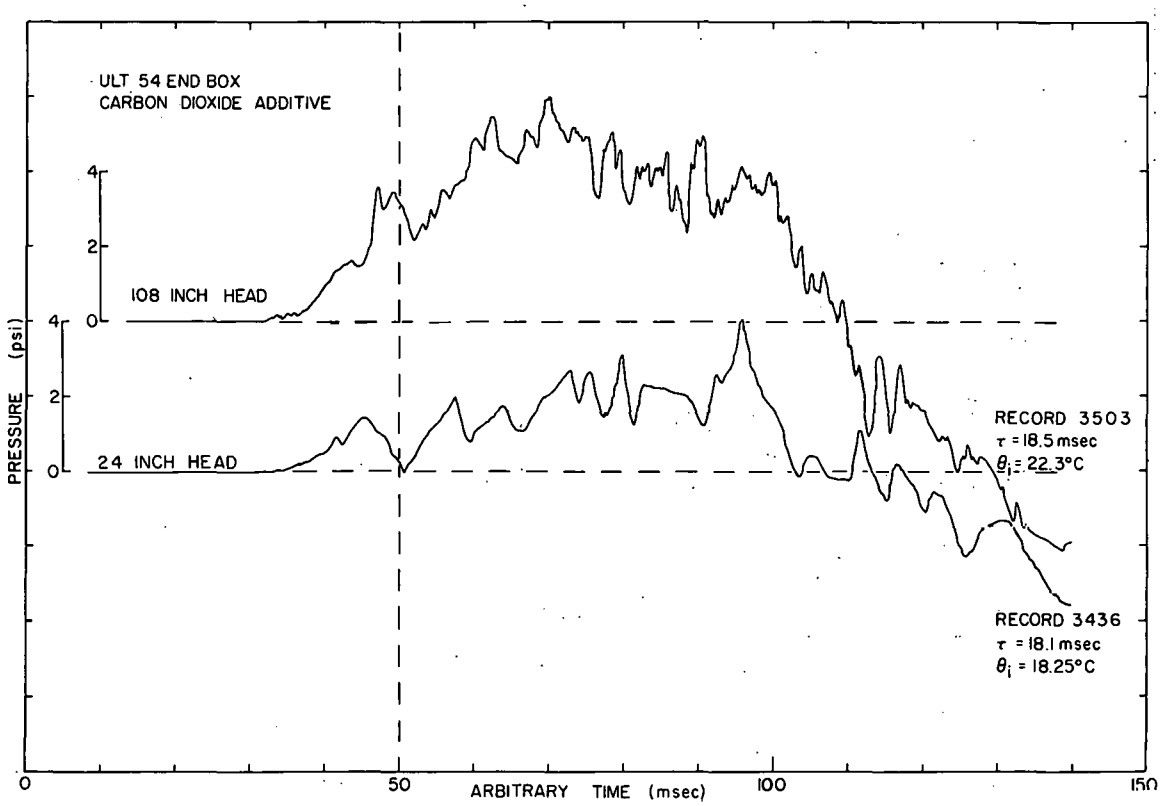

Fig. 91 Representative pressure-time histories for various depths of water head above the reactor core with carbon dioxide additive in the moderator.

A special test series considered the effects of introducing various additives into the moderator water. These additives were primarily either wetting agents or gas bubbles. For both the 18-msec transients (Figure 92) and the 10-msec transients (Figure 93) there seems to be very little difference in pressure behavior with additives present from that observed with pure water as moderator.

(4) Pressure Level Within The Pressure Source. During testing with the A-Core, measurement of the pressure level within the pressure source was attempted. The special fuel assembly used is shown in Figure 94. It consisted of a standard fuel can with part of the fuel removed to permit installation of pressure transducers vertically at + 6 in., + 0 in., - 3 in., - 6 in., and - 12 in. referred to as positions 1 through 5, respectively. This special assembly was placed in fuel location 66. A pressure transducer also was placed in the lower end box of the fuel assembly.

Analog data obtained with this assembly are shown in Figure 95. Two of the time histories are missing from the data; position 1, which exceeded allowable full-scale deflection and, hence, yielded little or no applicable information, and position 6 which was inoperative for this transient. The radiation sensitivity at position 3 is indicated by the dashed reference line. The data indicate slight differences in the time at which the pressure pulse was first sensed by the various transducers, but are of the same general shape and of approximately equal magnitude for all measuring locations. Data obtained in the 66 lower end box are an order of magnitude lower than those within the assembly. However, the 66 end box data were consistently

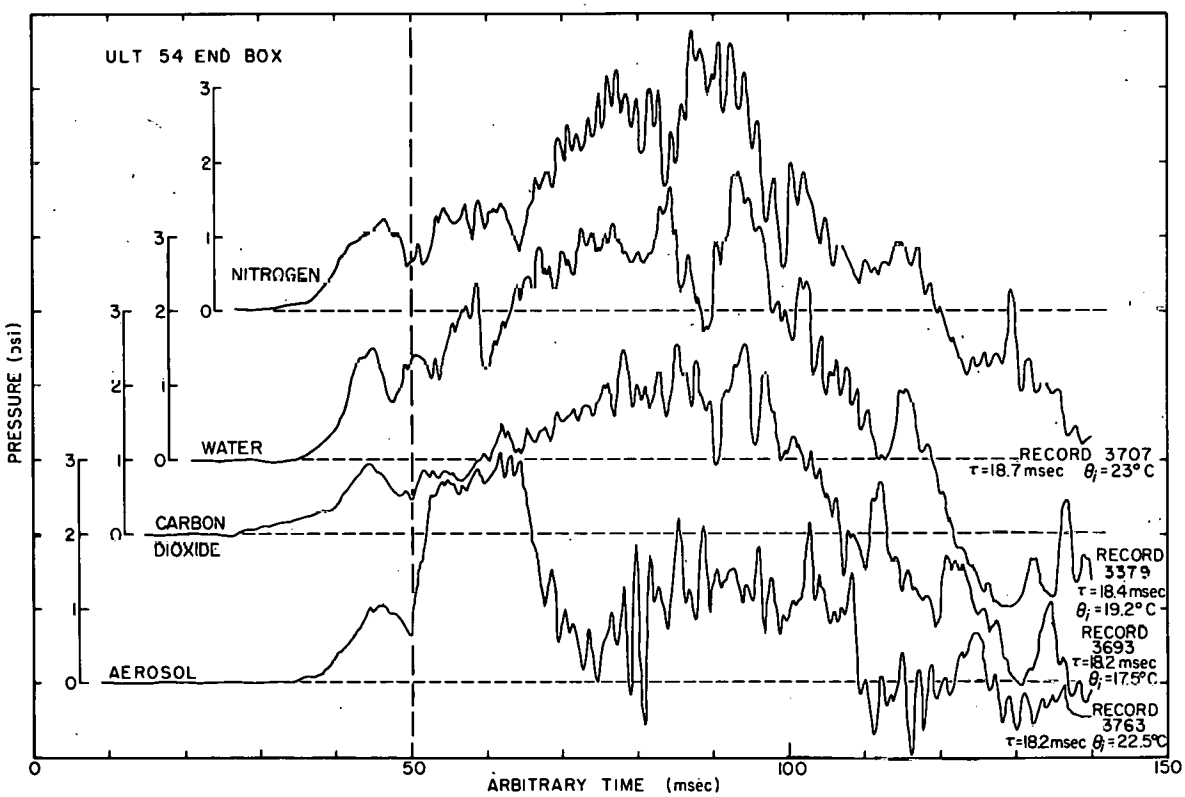

Fig. 92 Representative pressure-time histories with various moderator additives present for a nominal 20-msec reactor period.

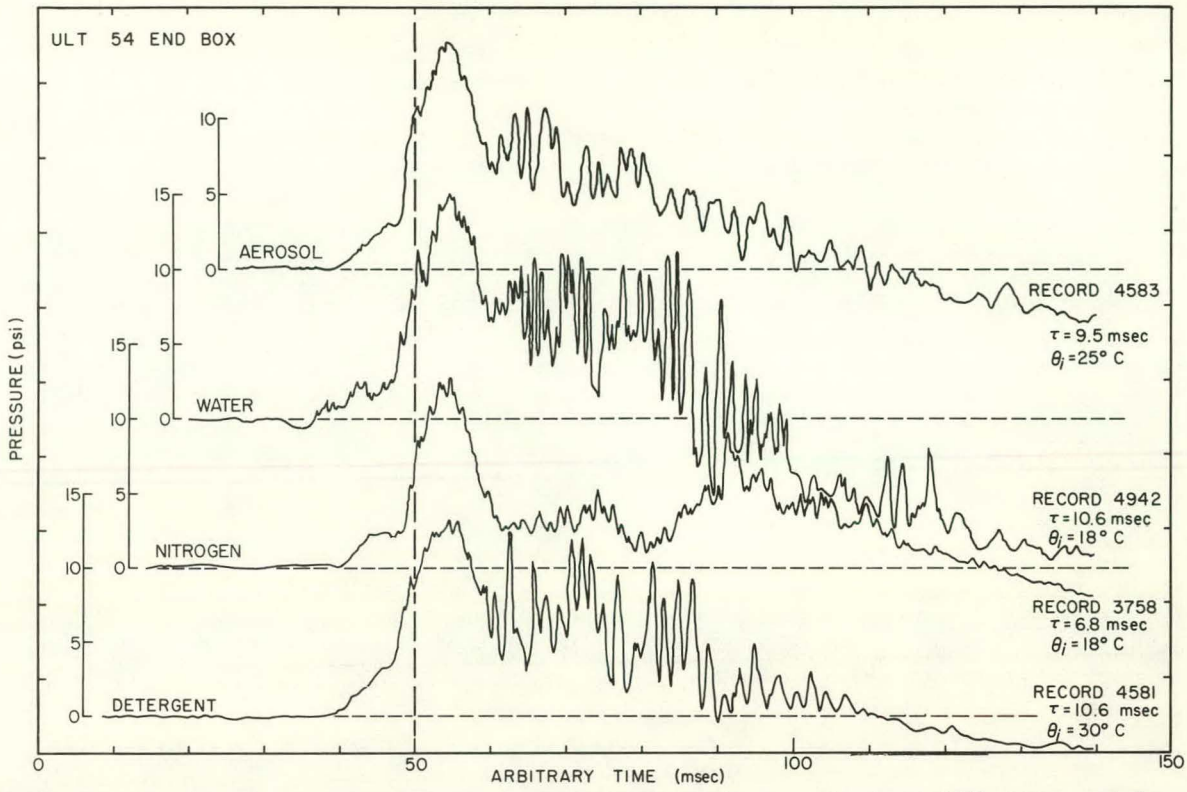

Fig. 93 Representative pressure-time histories with various moderator additives present for a nominal 10-msec reactor period.

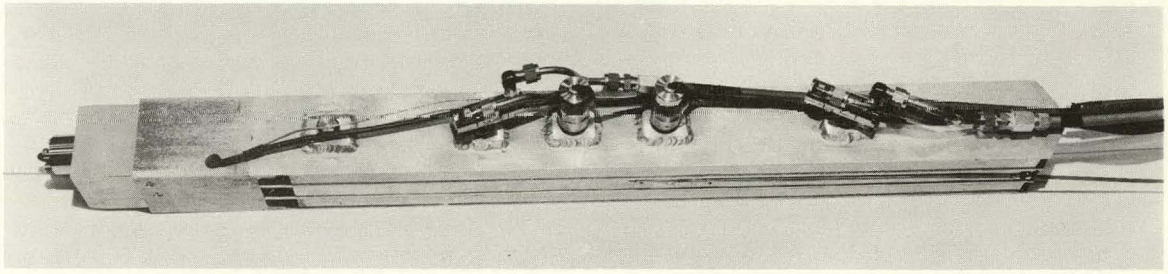

Fig. 94 Photograph of a special Spert I A-Core fuel assembly with pressure transducers mounted in a side plate and in the lower end box.

a factor of 3 below the data obtained at other end box locations, as shown in Figure 96, indicating a probable calibration problem. Thus, the pressure level within the assembly appears to be about a factor of 3 higher than pressures at the end box locations for an 8-msec transient in the A-core. [a]

The data for these transients have been plotted as a function of reciprocal period in Figures 97, 98, and 99. Data points obtained with moderator additives present are indicated by an appropriate symbol as for other A-Core data. Lines

---

[a] Removal of some of the fuel plates from the assembly to permit installation of the pressure transducers affected the width of the flow channel in this region. The effects of this change upon pressure generation has not been investigated sufficiently to permit quantitative specification of the perturbations introduced.

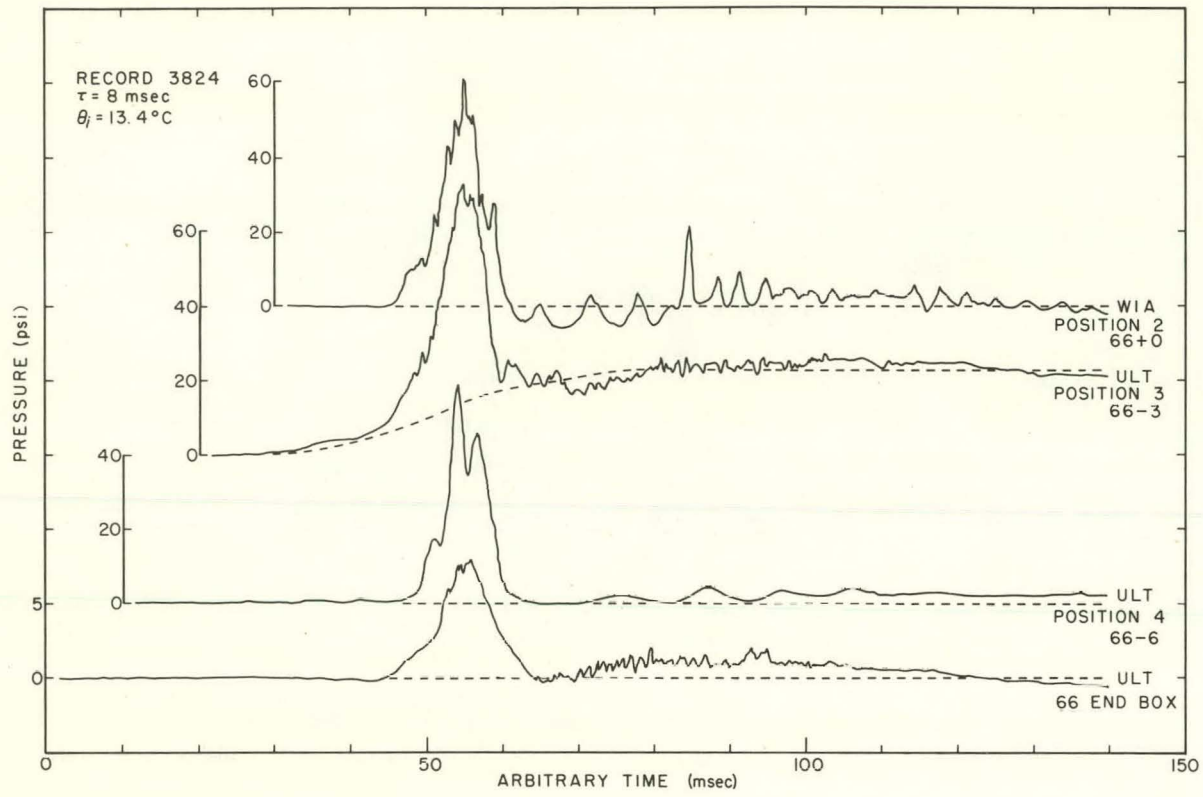

Fig. 95 Representative pressure-time histories obtained inside a special Spert I fuel assembly.

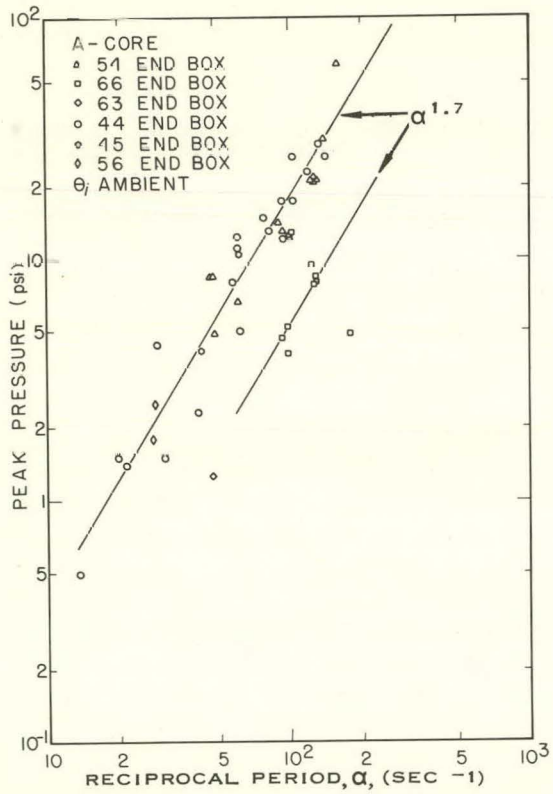

Fig. 96 Peak transient pressure in various lower end boxes as a function of reciprocal reactor period.

indicative of the slope of the data have been drawn as appropriate and are shown compositely in Figure 100. The symmetry of the core about the flux peak (- 3 in.) is evident. A line representing the average of the end box data also is shown for purposes of comparison. The differences in slope between the end box and interior measuring locations imply greater differences in pressure magnitude at these locations for shorter reactor periods.

The data are further displayed as a function of longitudinal position within the assembly in Figure 101 for pure water moderator, and in Figure 102 with moderator additives present [a].

---

[a] The -15-in. position corresponds to the average of the end box data rather than the measurement in the 66 end box because of the calibration problem noted earlier.

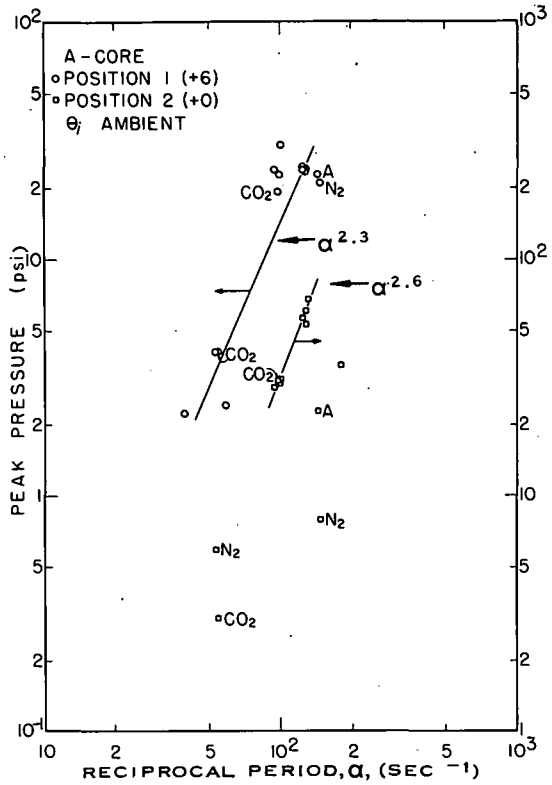

Fig. 97 Peak transient pressure at longitudinal positions 1 and 2 inside an A-Core fuel assembly as a function of reciprocal reactor period.

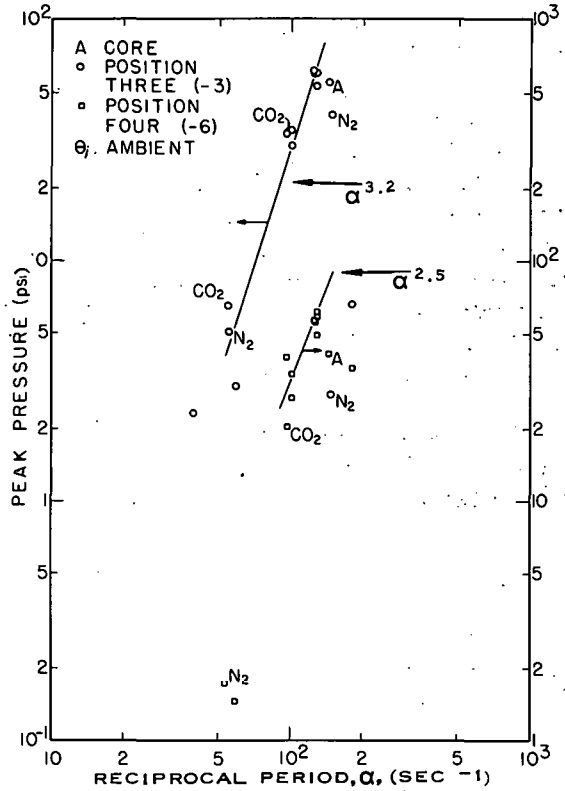

Fig. 98 Peak transient pressure at longitudinal positions 3 and 4 inside an A-Core fuel assembly as a function of reciprocal reactor period.

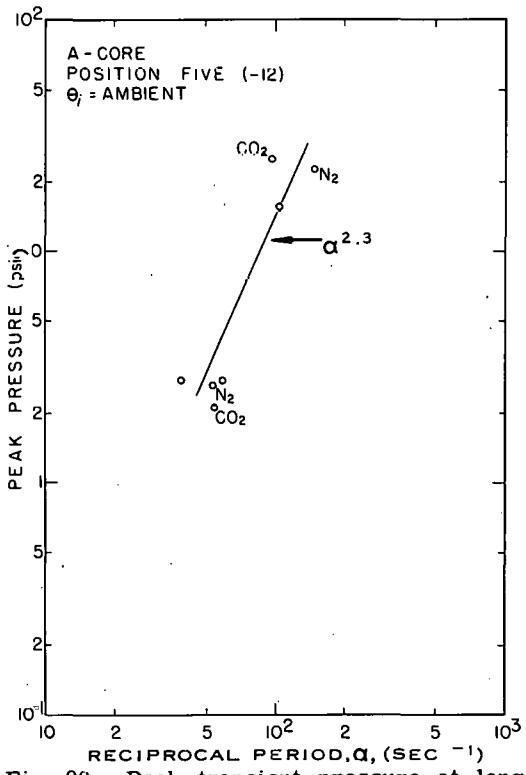

Fig. 99 Peak transient pressure at longitudinal position 5 inside an A-Core fuel assembly as a function of reciprocal reactor period.

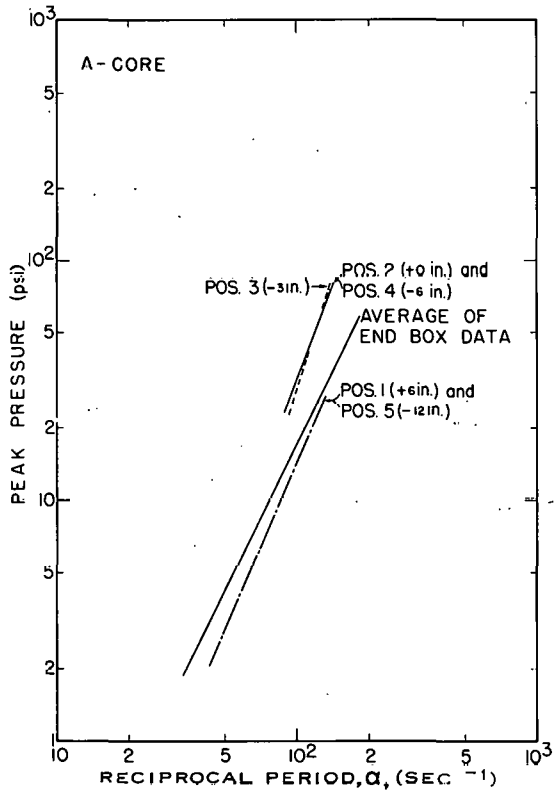

Fig. 100 Peak transient pressure inside an A-Core fuel assembly and in a lower end box as a function of reciprocal reactor period.

1.23 Cross Plots. Pressure data obtained in A-Core testing are summarized in Table A-2. These data were the first obtained at Spert and display the poorest reproducibility, which generally is about ± 50% for a given transducer. Data obtained during boiling reactor transients are less consistent than those for ambient temperature reactor transients. However, careful examination of the boiling data indicates better consistency within a given test sequence than was obtained between two different test sequences, implying a procedural problem probably related to calibration. The transducers used, eg, the Ultradyne and Wianko transducers, utilized a 20-kc carrier; the differences between responses for various transducers are probably attributable to differences in capacitive shunting of the signal during calibration in air and operation of the transducer in water.

The data obtained have been plotted as a function of reciprocal reactor period in Figures 103, 104, and 105. The effect of moderator additives on peak pressure is indicated in Figure 104, where a slight reduction in pressure

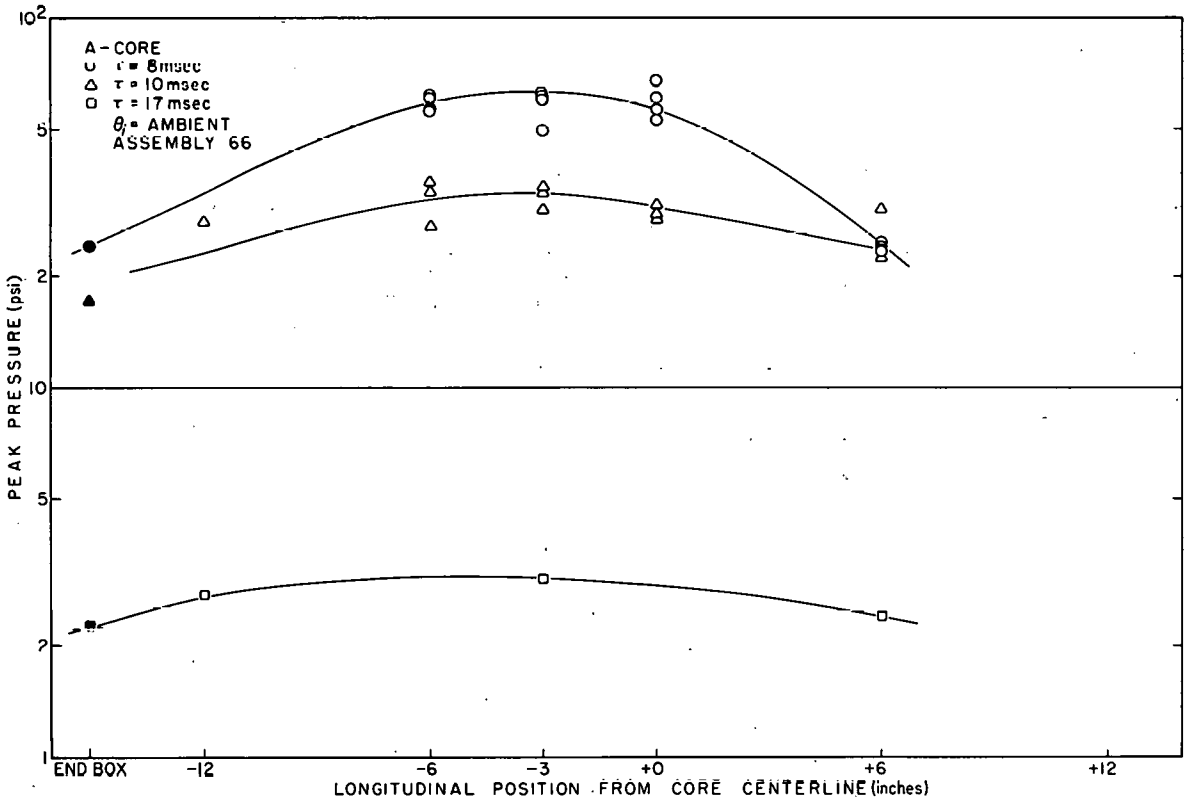

Fig. 101 Peak transient pressure inside an A-Core fuel assembly as a function of longitudinal position in the assembly with pure water moderator.

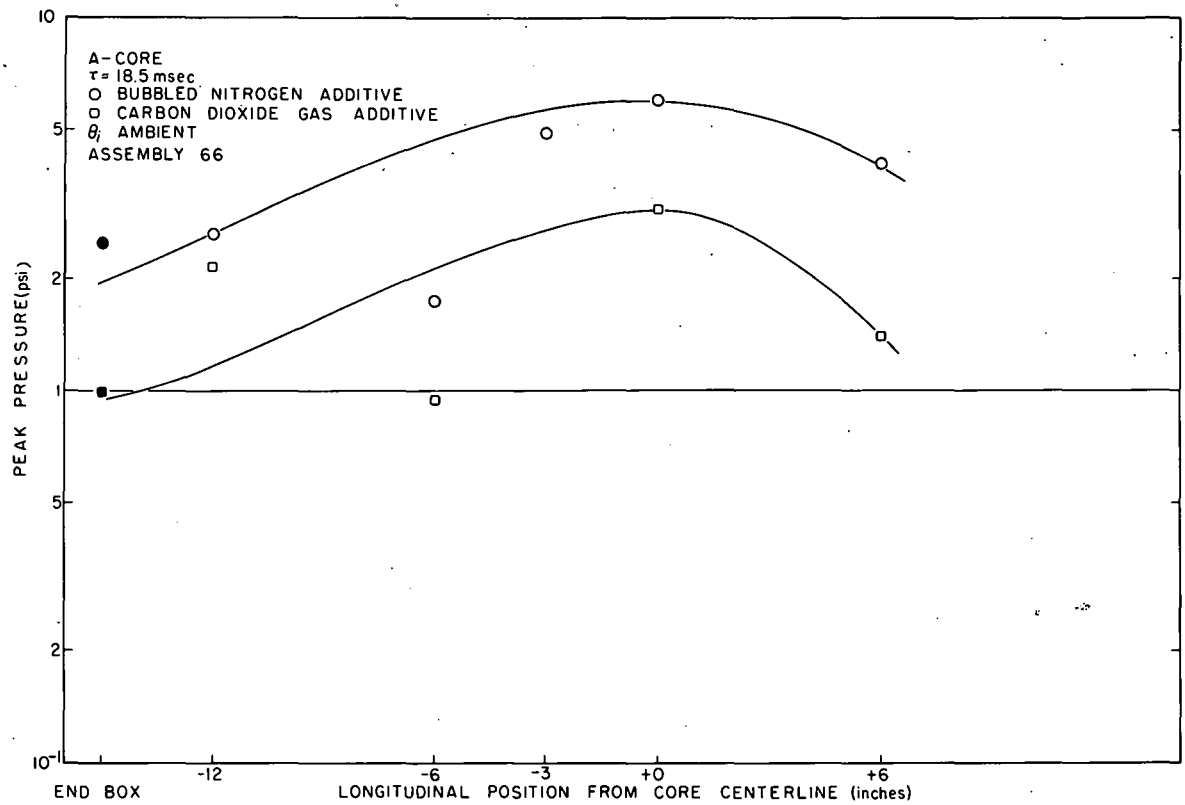

Fig. 102 Peak transient pressure inside an A-Core fuel assembly as a function of longitudinal position in the assembly with moderator additives present.

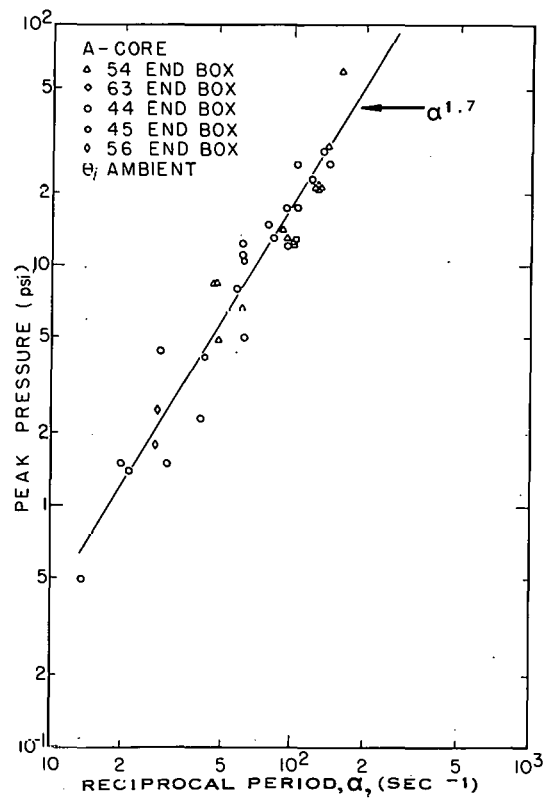

Fig. 103 Peak transient pressure in various lower end boxes as a function of reciprocal reactor period with pure water moderator.

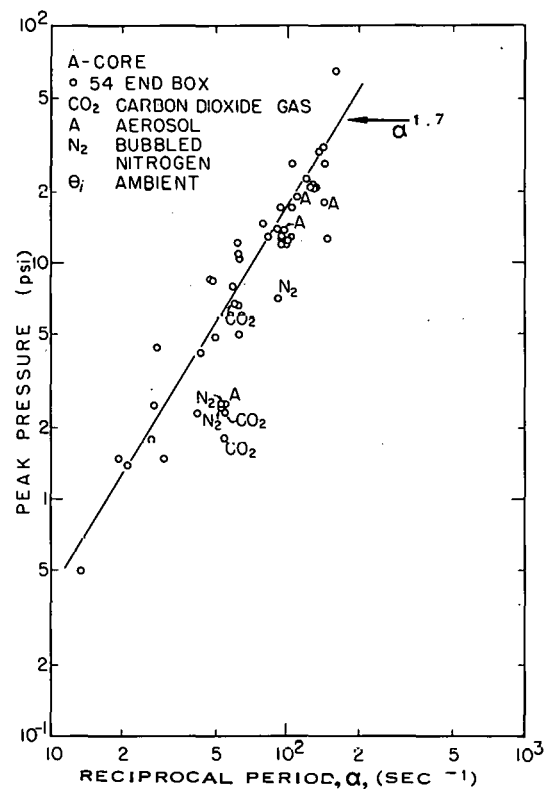

Fig. 104 Peak transient pressure in various lower end boxes as a function of reciprocal reactor period with and without moderator additives.

TABLE A-2

SUMMARY OF A-CORE PRESSURE DATA

Record Number	Initial Temp. (°C)	Reactor Period (msec)	Moderator ** Additive and Water Head	PXD Transducer Type-Location	Pressure at Peak Power (psi)	Peak Pressure (psi)
1429 *	20	36	24 in.	CEC 56 end box	---	2.5
1431	19	35	24 in.	ULT 44 end box	---	4.4
1436	22	37	24 in.	CEC 56 end box	----	1.8
1438	22	33	24 in.	ULT 44 end box	---	1.5
1464	18	16	24 in.	ULT 44 end box	---	5.0
1466	18	17	24 in.	ULT 44 end box	---	8.0
1469	20	16	24 in.	ULT 44 end box	---	11.0
1470	20	16	24 in.	ULT 44 end box	---	12.3
1469	15	10.4	24 in.	ULT 44 end box	---	12.0
1500	17	12	24 in.	ULT 44 end box	---	13.0
1502	17	12.7	24 in.	ULT 44 end box	---	14.7
1513	16	10.6	24 in.	ULT 44 end box	---	17.3
1515	18	9.5	24 in.	ULT 44 end box	---	17.3
1529	20	7.4	24 in.	ULT 44 end box	---	29.6
1530	16	7.0	24 in.	ULT 44 end box	---	26.5
1830	22	74	24 in.	ULT 44 end box	---	0.5
2232	18	8.3	24 in.	ULT 44 end box	---	23.0
2510	28	24	24 in.	ULT 45 end box		2.3
2843	26	23	24 in.	ULT 45 end box	---	4.2
2845	28	15.8	24 in.	ULT 45 end box	---	10.5
2510	67.9	25.9	24 in.	ULT 45 end box	0.6	2.3
				ULT 54 end box	0.3	1.7
				ULT Tank Wall	0.1	1.1
				ULT 63 end box	0.5	1.9
				ULT 73 end box	0.3	1.9
2623	97	22.2	24 in.	ULT 45 end box	0.4	1.1
				ULT 54 end box	0.4	1.2
2625	97	13.4	24 in.	ULT 45 end box	4.2	5.7
				ULT 54 end box	6.4	7.2
				ULT 73 end box †	0.6	1.2
				ULT Tank Wall †	0.3	0.6
2627	97	11.5	24 in.	ULT 45 end box	7.0	7.8
				ULT 73 end box	1.0	1.7
				ULT Tank Wall	0.5	0.9
2629	96.7	9.04	24 in.	ULT 45 end box	9.7	21.8
				ULT Tank Wall	2.6	3.5
				ULT 73 end box	2.2	7.2
2631	97	7.9	24 in.	ULT 45 end box	12.3	26.0
				ULT 54 end box	8.2	17.0
				ULT 73 end box	2.5	3.0
				ULT Tank Wall	3.8	4.5
2636	96.7	6.3	24 in.	ULT 45 end box	16.2	28.3
				ULT 54 end box	12.4	19.2
				ULT Tank Wall	6.4	7.0
				ULT 73 end box	3.7	4.8
2642	97	6.0	21 in.	ULT 45 end box	7.2	15.3
				ULT 54 end box	7.0	14.3
				ULT 73 end box	2.0	6.3
				ULT Tank Wall	7.3	7.8
2681	96.8	8.26	25 in.	ULT 45 end box	12.7	29.0
				ULT 54 end box	8.5	18.3
				ULT Tank Wall	1.7	2.0
				ULT 73 end box	2.9	5.3
2685	96.5	5.65	25 in.	ULT 54 end box	12.5	21.6
				ULT Tank Wall	3.5	6.8
				ULT 73 end box	5.3	14.7

TABLE A-2 (cont'd)

SUMMARY OF A-CORE PRESSURE DATA

Record Number	Initial Temp. (°C)	Reactor Period (msec)	Moderator ** Additive and Water Head	PXD Transducer Type Location	Pressure at Peak Power (psi)	Peak Pressure (psi)
2687	96.9	5.76	26 in.	ULT 45 end box	7.0	16.4
				ULT 54 end box	4.5	8.2
				ULT Tank Wall	3.0	6.0
				ULT 73 end box	2.1	5.4
2689	97	5.0	26 in.	ULT 45 end box	32.0	57.0
				ULT 54 end box	18.5	31.0
				ULT 73 end box	6.5	16.3
				ULT Tank Wall	3.7	7.0
2810	84.2	20.65	25 in.	ULT 45 end box	2.1	4.2
				ULT 54 end box	1.9	3.1
				ULT Tank Wall	---	0.5
				ULT 63 end box	1.5	3.4
				ULT 73 end box	---	0.8
2812	84	10.3	24 in.	ULT 45 end box	7.3	18.4
				ULT 54 end box	4.7	16.9
				ULT Tank Wall	0.5	0.8
				ULT 63 end box	7.9	10.3
				ULT 73 end box	0.8	2.0
3373	18.8	16.95	24 in.	ULT position 1 ***	1.7	2.4
				ULT position 3 ***	1.5	3.0
				ULT position 4 ***	1.4	---
				ULT position 5 ***	2.5	2.7
				ULT 66 end box	6.7	11.2
3379	19.2	25.6	24 in.	ULT position 1 ***	1.0	2.2
				ULT position 3 ***	1.5	2.3
				ULT position 4 ***	0.5	0.7
				ULT position 5****	2.3	2.7
				ULT 66 end box	2.6	2.6
3384	20.8	9.57	24 in.	ULT position 1 ***	0.8	---
				ULT position 4 ***	5.0	---
				ULT position 5 ***	15.7	28
				ULT 66 end box	7.6	12.7
				ULT 54 end box	8.5	26.0
3436	18	18.1	CO_2-24 in.	ULT 54 end box	1.2	2.3
3438	18.6	16.74	CO_2-24 in.	ULT 54 end box	1.3	6.7
3503	22	18.5	CO_2-108 in.	ULT 54 end box	2.0	5.3
3650	96	18.9	CO_2-24 in.	ULT 54 end box	3.0	9.2
3693	17.5	18.27	CO_2-24 in.	ULT position 1 ***	0.4	1.3
				WIA position 2 ***	1.1	3.0
				ULT position 3 ***	4.2	6.4
				ULT position 4 ***	0.4	0.9
				ULT position 5 ***	1.4	2.1
				ULT 66 end box	0.3	0.3
				ULT 54 end box	0.2	1.8
3696	20	9.8	CO_2-24 in.	ULT position 1 ***	6.0	18.5
				WIA position 2 ***	9.3	33.5
				ULT position 3 ***	6.0	30.0
				ULT position 4 ***	3.7	25.0
				ULT position 5 ***	7.4	25.3
				ULT 66 end box	0.3	1.8
3707	23	18.7	N_2-24 in.	ULT 54 end box	0.4	2.5
				ULT position 1 ***	1.0	2.2
				WIA position 2 ***	2.5	5.0
				ULT position 4 ***	0.8	1.2
				ULT position 5 ***	2.2	2.5
3709	27	10.8	N_2-24 in.	ULT 54 end box	3.8	7.0
				ULT position 1 ***	9.0	20.3
				WIA position 2 ***	12.0	31.5
				ULT position 3 ***	7.0	26.5
				ULT position 4 ***	5.3	21.5
				ULT position 5 ***	10.0	21.0

TABLE A-2 (cont'd)

SUMMARY OF A-CORE PRESSURE DATA

Record Number	Initial Temp. (°C)	Reactor Period (msec)	Moderator ** Additive and Water Head	PXD Transducer Type Location	Pressure at Peak Power (psi)	Peak Pressure (psi)
3756	15.75	18.7	N_2-24 in.	ULT position 1 ***	0.2	4.0
				WIA position 2 ***	0.9	5.9
				ULT position 3 ***	1.8	4.8
				ULT position 4 ***	0.2	1.7
				ULT position 5 ***	1.4	2.6
				ULT 66 end box	0.2	0.6
				ULT 54 end box	0.3	2.4
3758	17.9	6.78	N_2-24 in.	ULT 54 end box	5.6	12.5
				ULT 66 end box	2.1	4.5
				ULT position 1 ***	10.2	21.1
				WIA position 2 ***	2.1	7
				ULT position 3 ***	10.5	40.4
				ULT position 4 ***	5.6	28.3
				ULT position 5 ***	9.0	22.8
3763	22.5	18.2	Aerosol 24 in.	ULT 54 end box	0.5	2.5
				ULT 66 end box	0.2	0.3
				ULT position 1 ***	1.3	4.8
				WIA position 2 ***	3.8	4.5
				ULT position 3 ***	3.0	5.8
				ULT position 4 ***	0.7	1.5
				ULT position 5 ***	2.3	3.4
3765	24	10.2	Aerosol 24 in.	ULT 54 end box	11.0	13.6
				ULT 66 end box	3.0	3.3
				ULT position 1 ***	14.0	24.0
				WIA position 2 ***	8.0	27.0
				ULT position 3 ***	9.7	24.0
				ULT position 4 ***	7.5	21.7
				ULT position 5 ***	10.0	16.0
3772	24	9.0	Aerosol 24 in.	ULT 54 end box	18.8	18.8
				ULT 66 end box	1.5	6.3
				ULT position 1 ***	37.0	48.0
				WIA position 2 ***	15.0	72.0
				ULT position 3 ***	20.0	35.0
				ULT position 4 ***	21.0	45.0
3780	13.5	6.95	Aerosol 24 in.	ULT position 1 ***	5.2	22.8
				WIA position 2 ***	8.7	55.5
				ULT position 3 ***	10.0	55.0
				ULT position 4 ***	2.4	41.0
				ULT 66 end box	2.2	6.9
				ULT 54 end box	12.8	17.9
3822	9.8	10.0	24 in.	ULT 66 end box	1.8	4.0
				ULT 54 end box	6.3	12.0
				ULT position 1 ***	9.4	22.7
				WIA position 2 ***	10.5	29.6
3822	9.8	10.0	24 in.	ULT position 3 ***	15.1	30.1
				ULT position 4 ***	3.6	27.0
3847	15.4	5.55	24 in.	WIA position 2 ***	---	35.6
				ULT position 3 ***	---	6.6
				ULT position 4 ***	---	35.6
				ULT 66 end box	---	4.3
3849	17.8	7.96	24 in.	ULT position 1 ***	20.4	24.6
				WIA position 2 ***	40.3	67.5
				ULT position 3 ***	31.3	60.0
				ULT position 4 ***	18.1	55.5
				ULT 66 end box	4.9	8.0
				ULT 54 end box	19.2	20.5
3851	20.8	10.5	24 in.	ULT position 1 ***	11.9	23.8
				WIA position 2 ***	19.2	28.7
				ULT position 3 ***	20.6	33.8
				ULT position 4 ***	30.8	35.9
				ULT 66 end box	3.4	4.6
				ULT 54 end box	11.2	12.9

TABLE A-2 (cont'd)

SUMMARY OF A-CORE PRESSURE DATA

Record Number	Initial Temp. (°C)	Reactor Period (msec)	Moderator ** Additive and Water Head	PXD Transducer Type Location	Pressure at Peak Power (psi)	Peak Pressure (psi)
3931	22.6	10.0	24 in.	ULT 54 end box	9.2	12.3
				ULT 66 end box	1.6	5.1
				ULT position 1 ***	9.5	30.2
				WIA position 2 ***	6.7	30.8
				ULT position 3 ***	15.1	34.8
				ULT position 4 ***	6.7	33.8
3933	24.6	7.82	24 in.	ULT 54 end box	11.8	20.4
				ULT 66 end box	2.9	7.7
				ULT position 1 ***	18.4	23.9
				WIA position 2 ***	13.3	53.0
				ULT position 3 ***	22.3	49.0
				ULT position 4 ***	17.2	61.0
3927	27.7	7.82	24 in.	ULT 54 end box	18.6	21.5
				ULT 66 end box	3.1	7.7
				ULT position 1 ***	18.2	23.4
				WIA position 2 ***	19.7	60.5
				ULT position 3 ***	20.8	60.0
				ULT position 4 ***	11.1	58.0
3939	30.4	8.04	24 in.	ULT 54 end box	13.6	20.8
				ULT 66 end box	3.9	9.3
				ULT position 1 ***	18.2	23.6
				WIA position 2 ***	17.2	56.0
				ULT position 3 ***	22.2	61.5
				ULT position 4 ***	12.3	56.5
4252	79.0	16.3	24 in.	ULT 54 end box	0.1	2.0
4254	78.0	8.4	24 in.	ULT 54 end box	9.0	---
4294	96.0	9.8	24 in.	ULT 54 end box	3.5	9.5
4580	18.5	20.0	108 in.	ULT 54 end box	1.0	4.8
4587	30.0	10.6	detergent 24 in.	ULT 54 end box	9.0	12.5
4940	15.2	21.1	24 in.	ULT 54 end box	---	8.4
4942	18.0	11.0	24 in.	ULT 54 end box	7.5	13.8
				WIA Tank Wall	2.5	10.0
4944	20.0	7.1	24 in.	ULT 54 end box	27.3	30.8
				WIA Tank Wall	8.7	10.5
4946	24.0	14.9	24 in.	ULT 54 end box	1.1	6.5
				WIA Tank Wall	1.0	1.0
4950	21.5	20.4	24 in.	WIA Tank Wall	0.5	1.6
				ULT 54 end box	2.4	8.4
4954	23.0	6.2	24 in.	ULT 54 end box	54.8	64.0
				WIA Tank Wall	10.5	11.5

* Data for the first 19 transients listed were obtained directly from a previous report [25].

** All transients had pure water as moderator unless an additive is specified.

*** Measurement locations in special fuel assembly modified to incorporate pressure transducers.

† In some instances data obtained at the 66 end box, 73 end box and tank wall locations are radically different from the data obtained at other end box locations due to problems inherent to calibration and high temperature operation of the transducer system.

appears to result from introducing the additives, especially in the case of gaseous additives. However, most of the differences fall within the range of reproducibility of the data, and the results are by no means conclusive.

Data for boiling initial temperatures (Figure 105) clearly show the increased scatter in the data for these transients. The data as obtained are shown in the right half of the figure. Arbitrary normalization of the data as required to bring results for a given transducer into agreement with itself in two successive

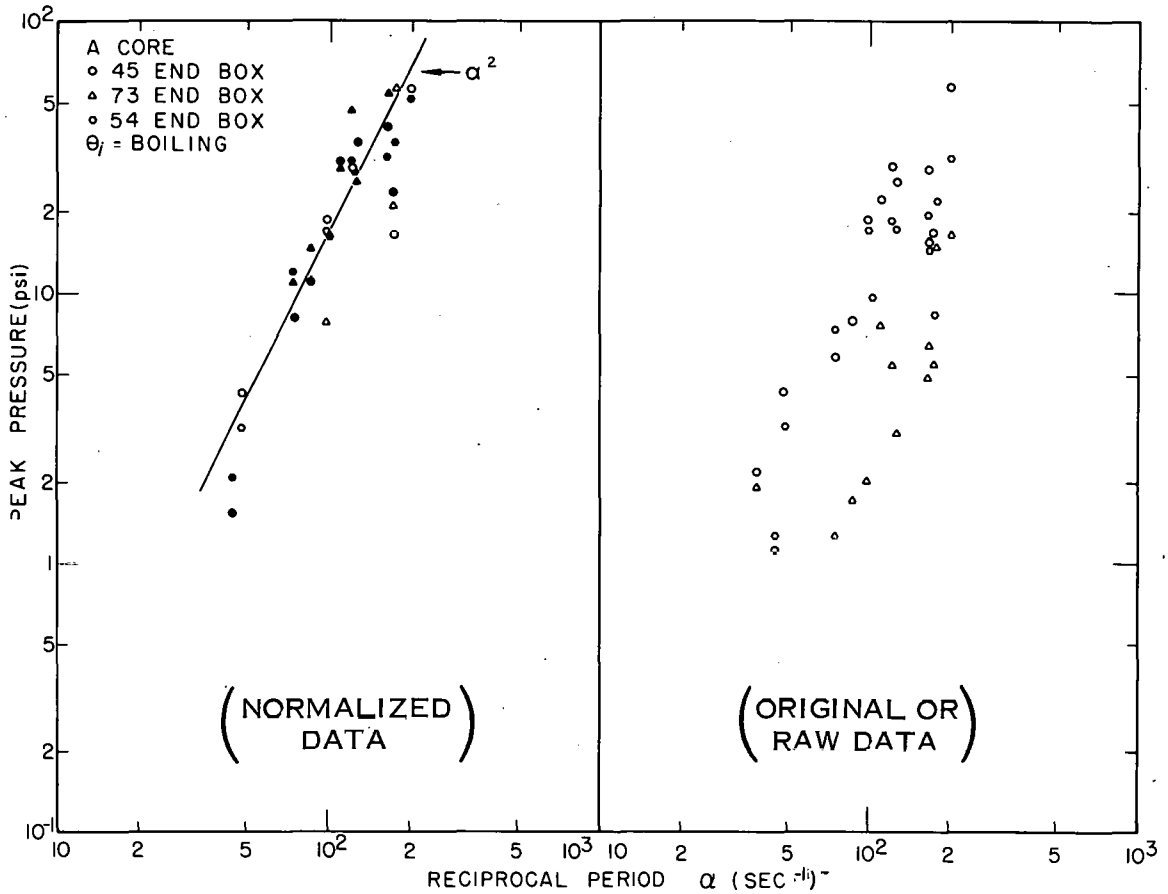

Fig. 105 Raw data and normalized data for peak transient pressures in various lower end boxes during boiling reactor transients.

test series gives the results indicated in the left half of the figure [a]. It is not implied that this normalization is justified, or is the correct normalization. The plot is included primarily to illustrate the observation that the scatter observed may be reasonably attributed to procedural (or calibration) problems rather than to limitations inherent in the transducer response.

2. B-CORE EXPERIMENTS

2.1 Core Description [26]

The B-core fuel assembly was a versatile assembly of removable aluminum fuel plates permitting variations in the plate spacing. Four fuel plates (numbers 4, 10, 16, and 22) were brazed to the unfueled side plates providing a rigid assembly. Additional plates were inserted in slots in the side plates to complete the assembly. Three specific configurations were used, viz, all 24 plates loaded, every third plate removed (leaving 16 plates), and all even numbered plates loaded (12 plates).

---

[a] Note that the 73 end box data required an additional normalization (multiplication by 2.5) to bring them into agreement with data for the other end boxes. This factor of 2.5 could be accounted for by failure to record a change in gain setting.

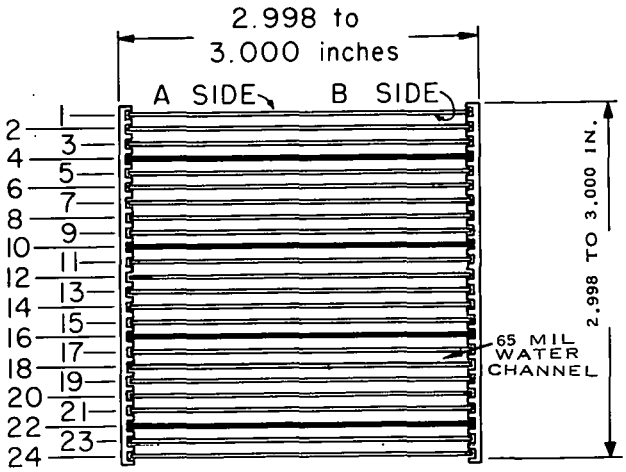

B 24/32
ALL 24 FUEL PLATES
LOADED

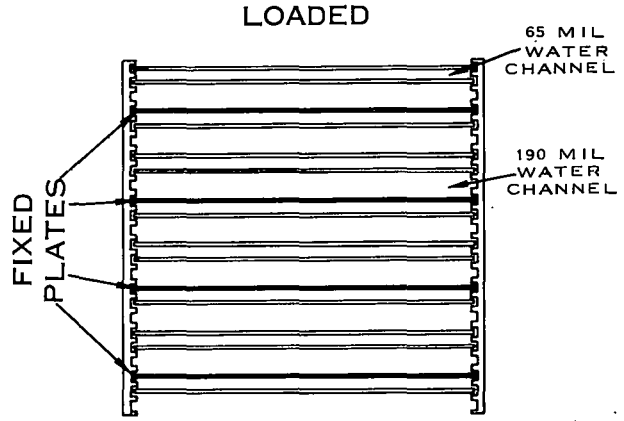

B 16/40
EVERY THIRD PLATE
REMOVED

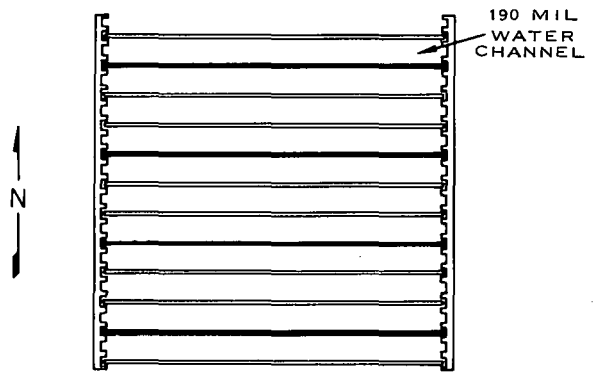

B 12/64
ALL EVEN NUMBERED
FUEL PLATES LOADED

Fig. 106 Schematic representation of fuel assemblies for the three B-Cores.

The resulting configurations are shown in Figure 106. The B 16/40 core had a non-symmetrical array of fuel in each assembly with alternate narrow (65 mil) and wide (190 mil) water channels. All fuel plates were 2.75 in. wide and 24-5/8 in. long with a 20-mil U-Al meat (93.5% enriched in U-235) containing 7 gm of aluminum. The geometrical configurations of the three B-Cores are shown in Figure 107, where the numbering sequence for fuel locations is shown. The fuel plates within a given assembly were designated and numbered from 1 to 12, 16, or 24, numbered appropriately from north to south. Thermocouple locations were further identified by longitudinal position from core centerline and a letter, A or B, indicating whether the thermocouple was on the north or south side of the plate.

Parameters pertinent to evaluation of data from the B-Cores are summarized in Table A-3.

2.2 Data Presentation

2.21 General Considerations. These data are similar in most respects to those obtained with other Spert I cores: the presentation of the data will be similar, except where comparisons between the three cores are appropriate. Since fuel-plate damage was observed at reactor periods of about 10 msec, the majority of the data for these cores was obtained at longer reactor periods ($\tau \approx 15$ to 20 msec).

2.22 Analog Plots. (1) Time-History Correlations for Power, Energy, Temperature, Flow and Pressure. The time behaviors of pressure, temperature, energy, power, and flow may be compared in Figures 108, 109, and 110 for

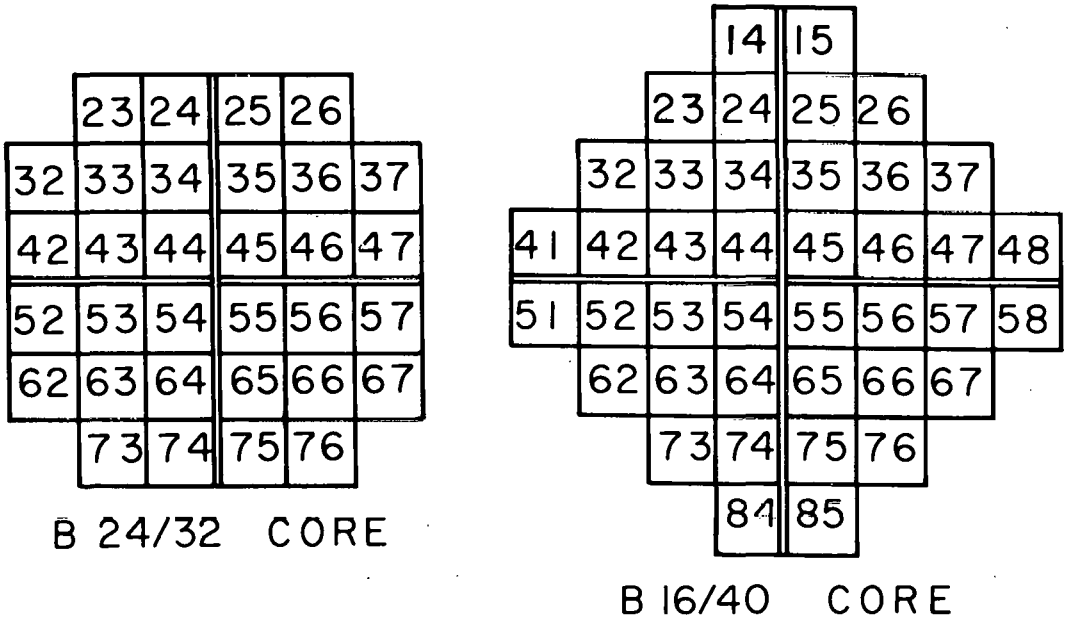

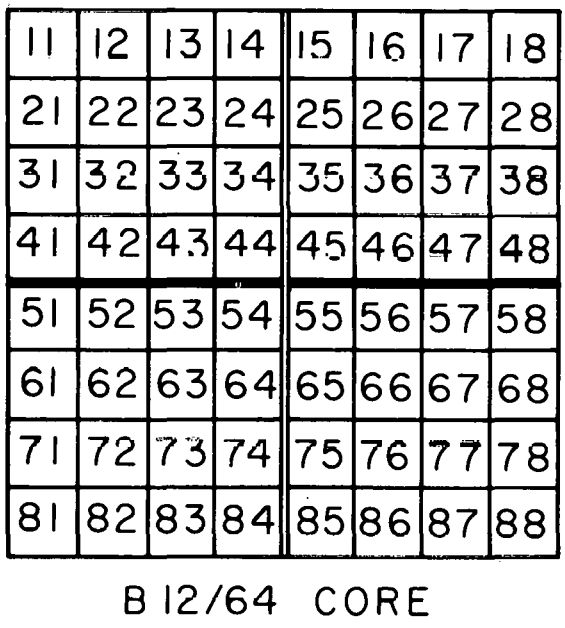

Fig. 107 Layout of Spert I reactor grid showing arrangement of fuel assemblies for the three operational B-Cores.

TABLE A-3

PERTINENT B-CORE CONSTANTS

Core	Magnitude		
	B 12/64	B 16/40	B 24/32
Clad materials	Al	Al	Al
Critical mass U-235	4.3 kg	3.6 kg	4.3 kg
Total U-235 loaded	5.4 kg	4.5 kg	5.4 kg
H/U ratio	760	540	270
M/W ratio	0.46	0.63	1.14
Available excess reactivity	4.3 $	5.6 $	6.6 $
Temperature defect 20°- 95°C	1.44 $	1.67 $	1.73 $
Isothermal temperature coefficient 20°C	-1.8×10^{-2} $/°C	-1.7×10^{-2} $/°C	-1.1×10^{-2} $/°C
Isothermal temperature coefficient 95°C	-2.0×10^{-2} $/°C	-3.4×10^{-2} $/°C	-3.4×10^{-2} $/°C
Average void coefficient, C_v	-0.93×10^{-4} $cm^3	-2.9×10^{-4} $/cm^3	-7.3×10^{-4} $/cm^3
Reduced prompt neutron lifetime $\ell^*/\bar{\beta}$	11×10^{-3} (sec)	10×10^{-3} (sec)	7×10^{-3} (sec)
Channel width	190 mils	65,190 mils	65 mils

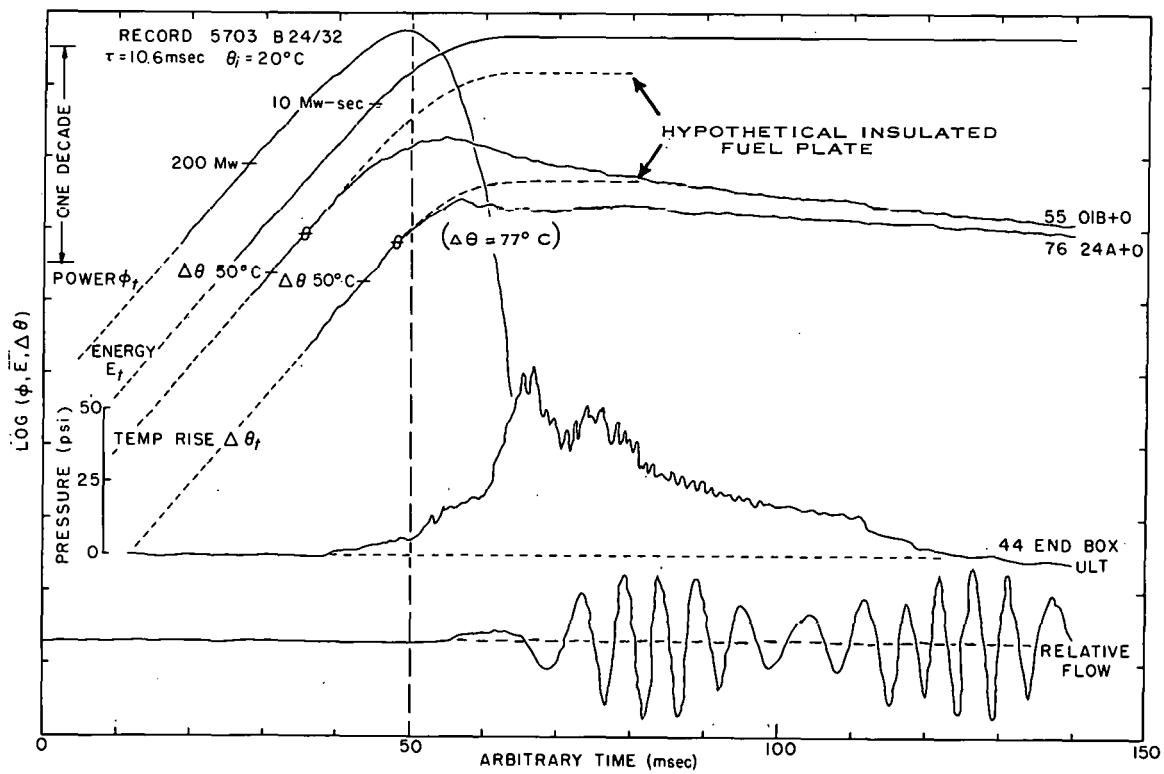

Fig. 108 A presentation of time histories for power, energy, fuel-plate surface temperature, pressure, and flow. The symbol θ on the temperature-time histories indicates the boiling temperature with the corresponding temperature rise shown in parentheses adjacent to one of the traces.

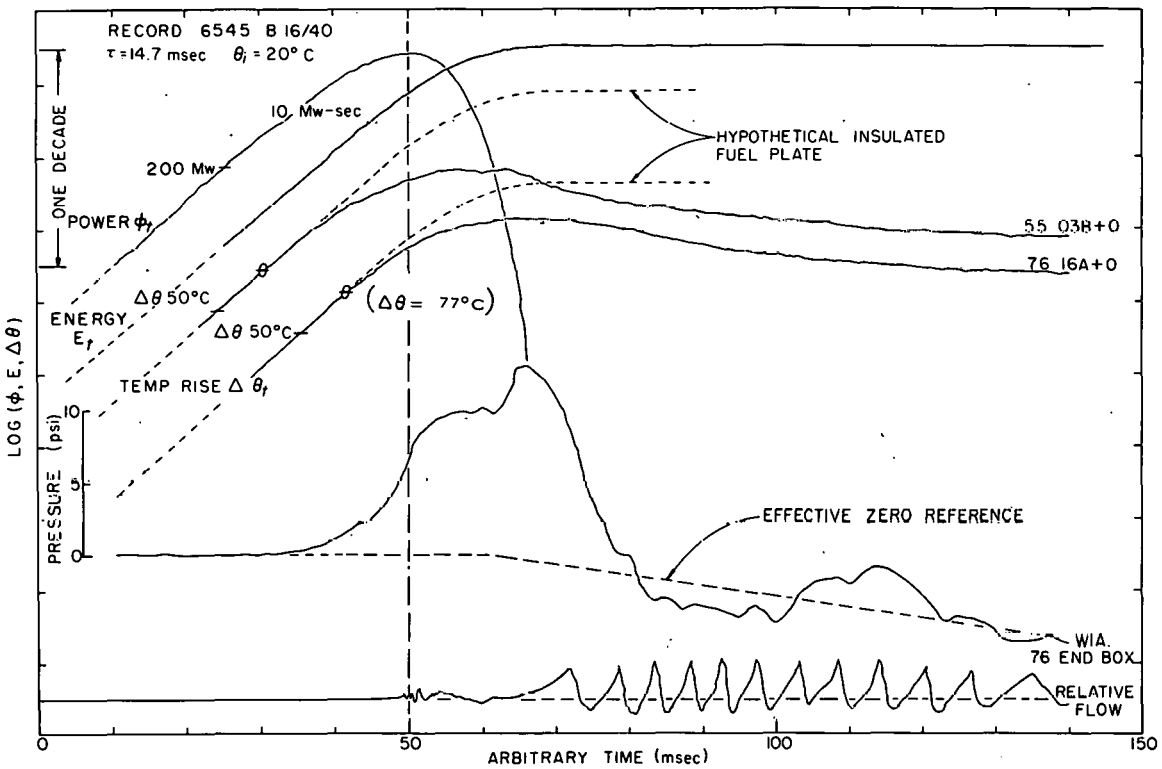

Fig. 109 A presentation of time histories for power, energy, fuel-plate surface temperature, pressure, and flow. The symbol θ on the temperature-time histories indicates the boiling temperature with the corresponding temperature rise shown in parentheses adjacent to one of the traces.

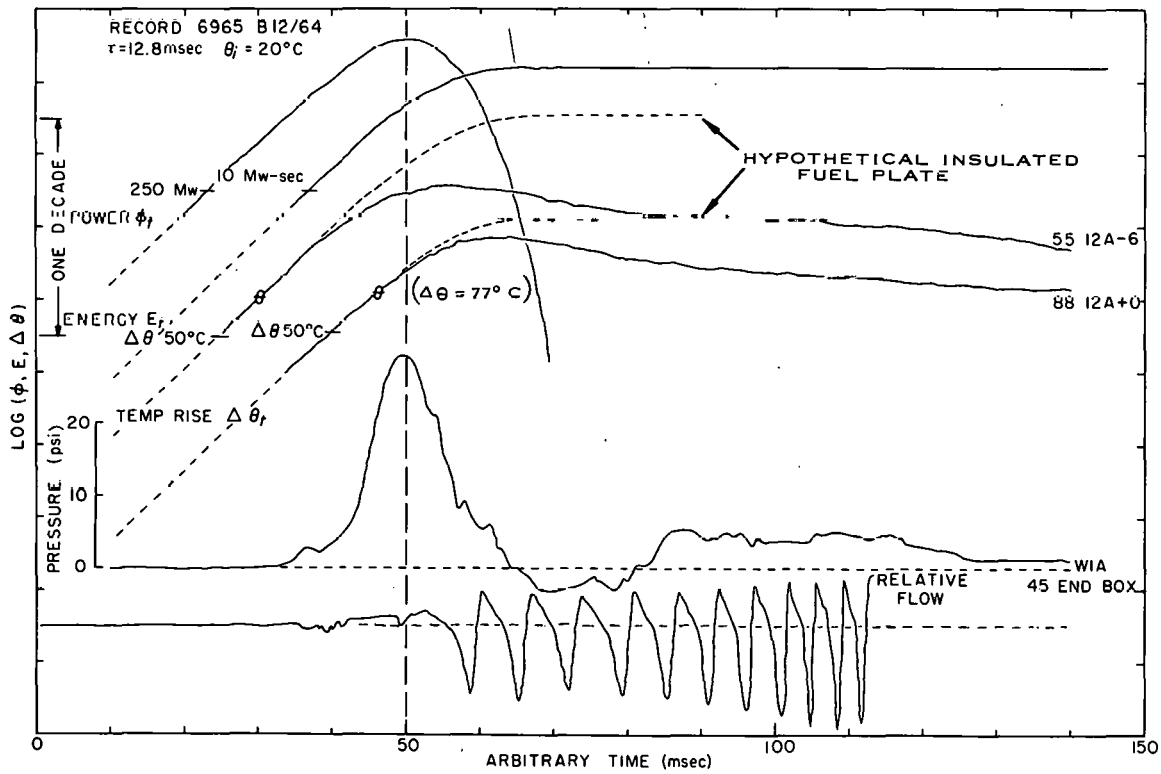

Fig. 110 A presentation of time histories for power, energy, fuel-plate surface temperature, pressure, and flow. The symbol θ on the temperature-time histories indicates the boiling temperature with the corresponding temperature rise shown in parentheses adjacent to one of the traces.

the B 24/32, B 16/40, and B 12/64 cores, respectively. Boiling heat transfer occurs near the time of peak power for these cores, and the magnitudes of the generated pressures are quite high. Consequently, the contributions to pressure resulting from fuel-plate expansion can seldom be observed directly [a]. Correlation between heat transfer and pressure generation is similar to that for other cores. The B 12/64 pressure peak occurs much nearer to time of peak power than do those for the other B-Cores as a consequence of its smaller void coefficient (Table A-3). Flow behavior parallels that of pressure in other cores. The gradual decrease in the reference pressure level, which is quite evident in the data of Figure 109, results from temperature sensitivity of the transducer.

(2) Time-History Correlations of Pressure with Radial and Longitudinal Temperature Distributions. Radial and longitudinal temperature distributions for each core may be compared with the respective pressure behaviors in Figures 111 through 122. Data for both long and short reactor periods are included. Correlation between boiling heat transfer and pressure generation is similar to that observed in other cores. There are, however, several instances in the data shown where a question has arisen concerning calibration of the

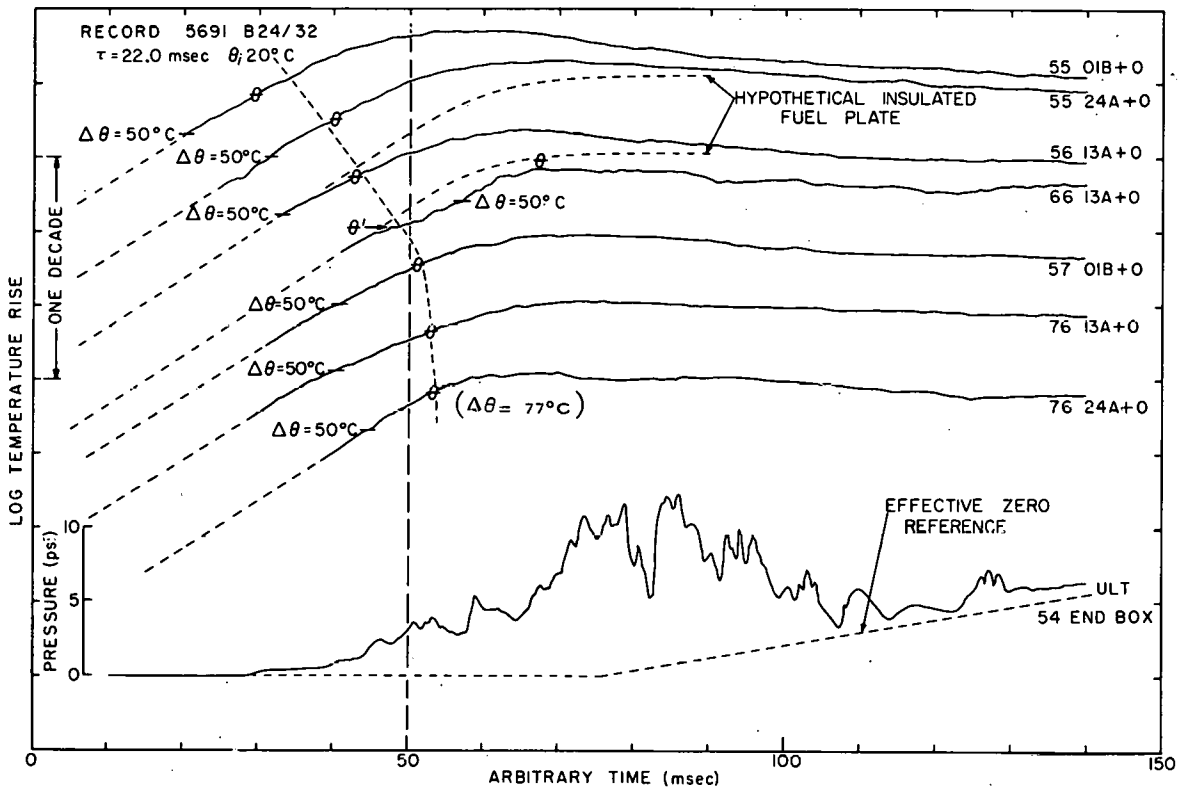

Fig. 111 A presentation of fuel-plate surface temperature-time histories at various radial positions and the pressure-time history. The symbol θ on the temperature-time histories indicates the boiling temperature with the corresponding temperature rise shown in parentheses adjacent to one of the traces.

[a] To assure recording of the higher B-Core pressure peaks without exceeding the allowable deflection of the oscillographic traces, the electronic gain setting was reduced. Hence, the deflections corresponding to expansion pressures were very slight.

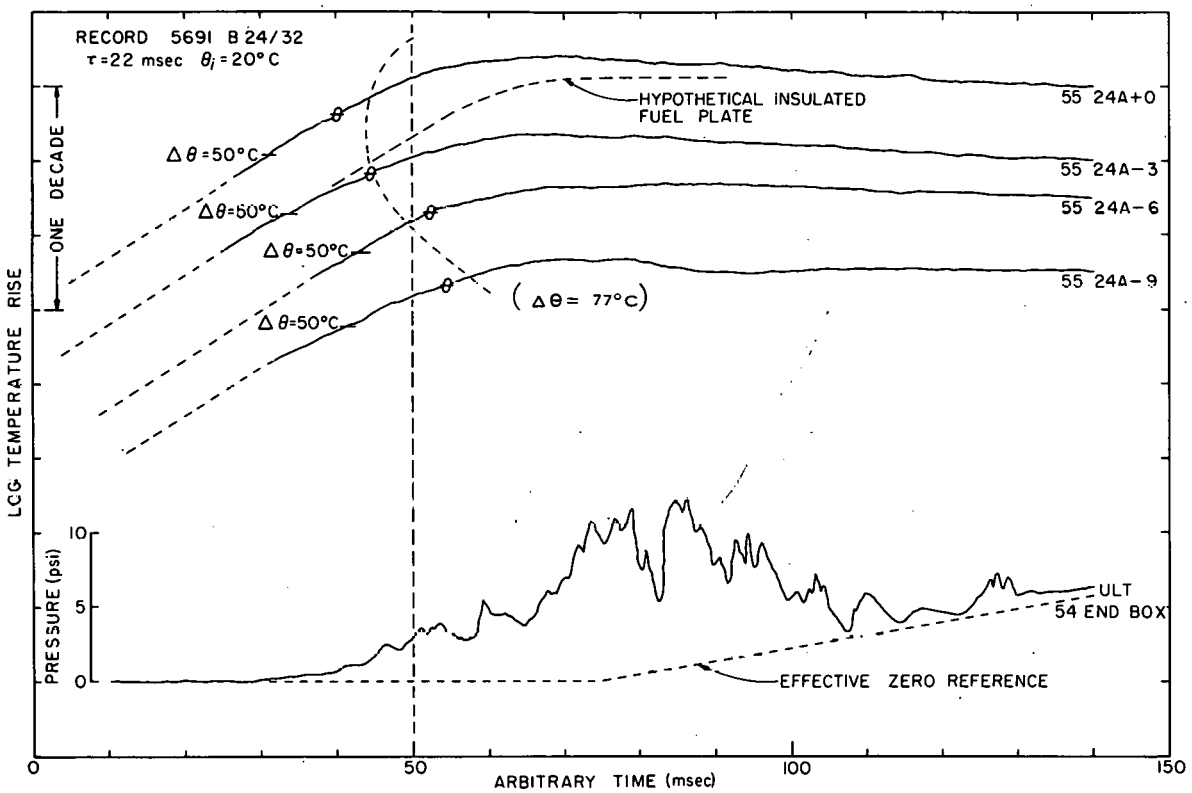

Fig. 112 A presentation of fuel-plate surface temperature-time histories at various longitudinal positions along a fuel plate and the pressure-time history. The symbol θ on the temperature-time histories indicates the boiling temperature with the corresponding temperature rise shown in parentheses adjacent to one of the traces.

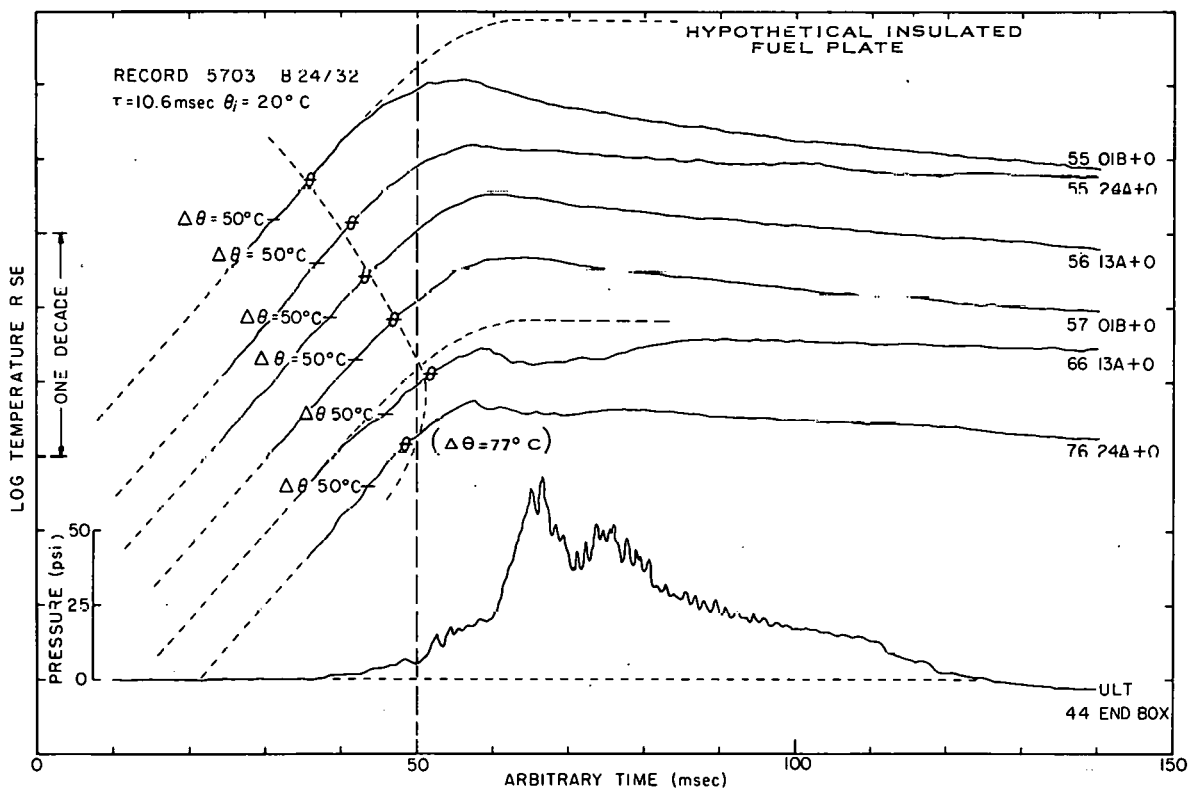

Fig. 113 A presentation of fuel-plate surface temperature-time histories at various radial positions and the pressure-time history. The symbol θ on the temperature-time histories indicates the boiling temperature with the corresponding temperature rise shown in parentheses adjacent to one of the traces.

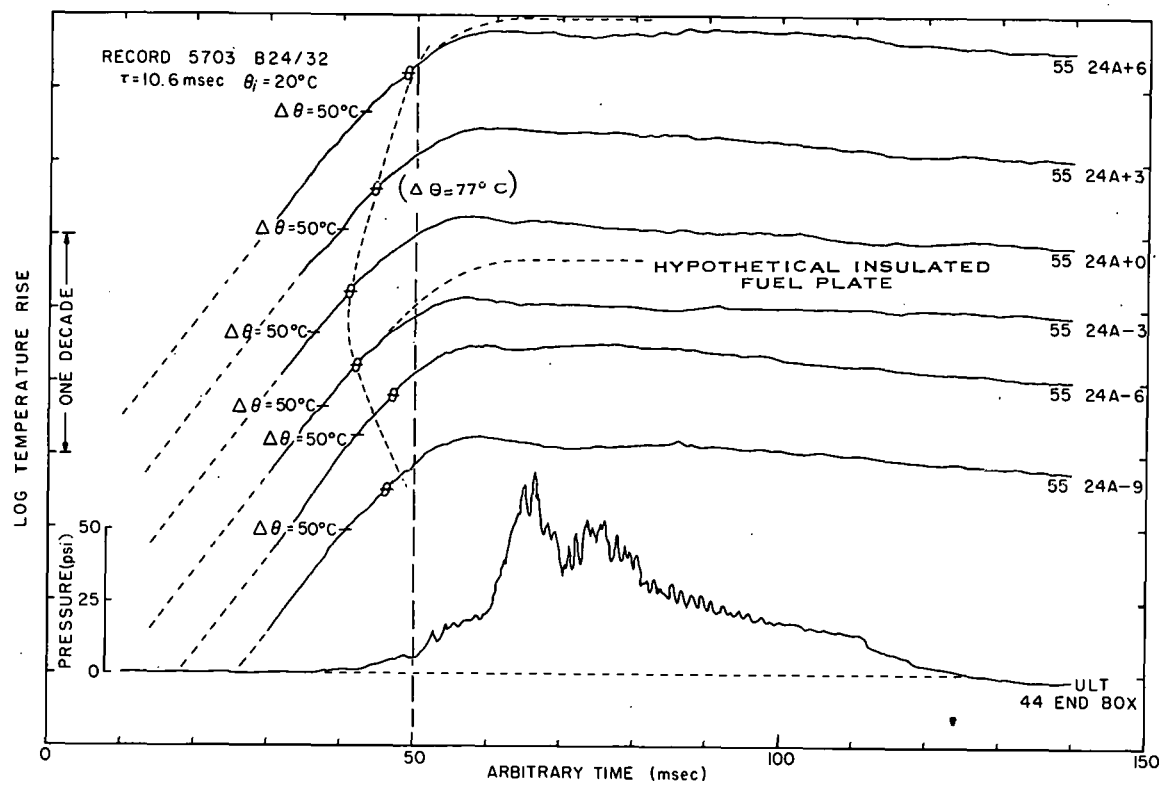

Fig. 114 A presentation of fuel-plate surface temperature-time histories at various longitudinal positions along a fuel plate and the pressure-time history. The symbol θ on the temperature-time histories indicates the boiling temperature with the corresponding temperature rise shown in parentheses adjacent to one of the traces.

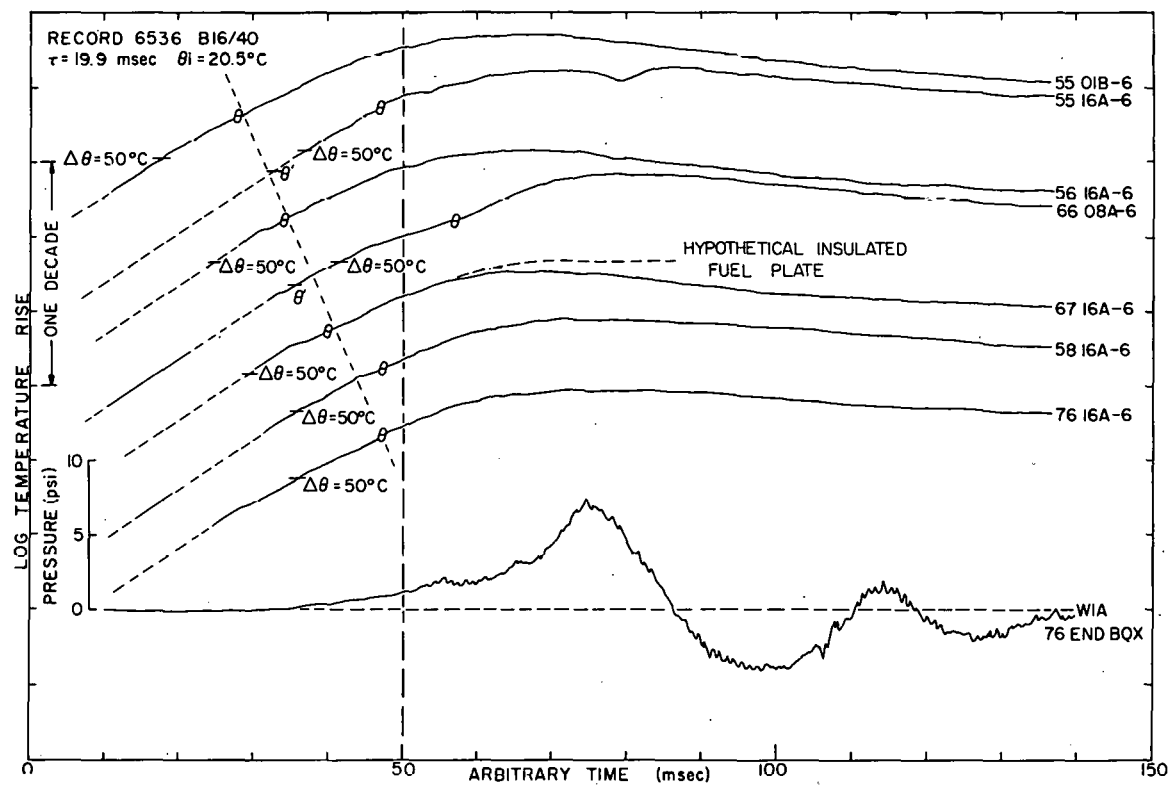

Fig. 115 A presentation of fuel-plate surface temperature-time histories at various radial positions and the pressure-time history. The symbol θ on the temperature-time histories indicates the boiling temperature with the corresponding temperature rise shown in parentheses adjacent to one of the traces.

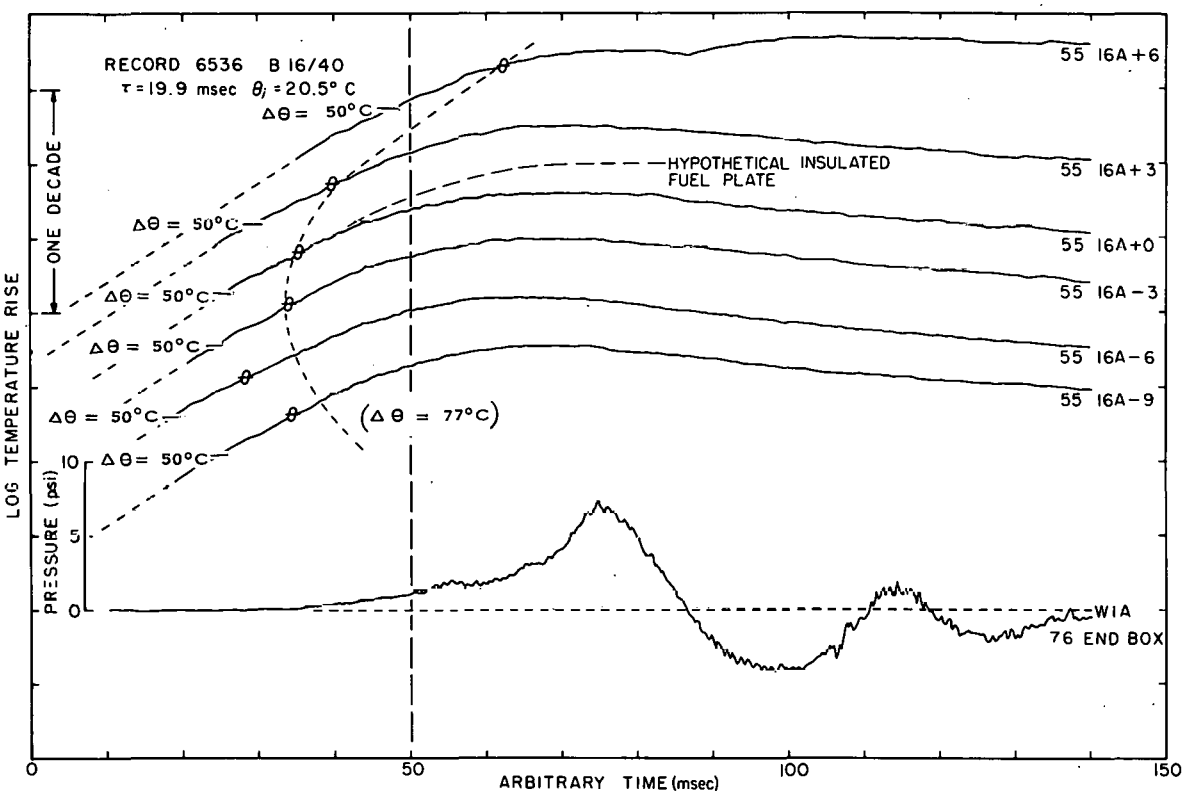

Fig. 116 A presentation of fuel-plate surface temperature-time histories at various longitudinal positions along a fuel plate and the pressure-time history. The symbol θ on the temperature-time histories indicates the boiling temperature with the corresponding temperature rise shown in parentheses adjacent to one of the traces.

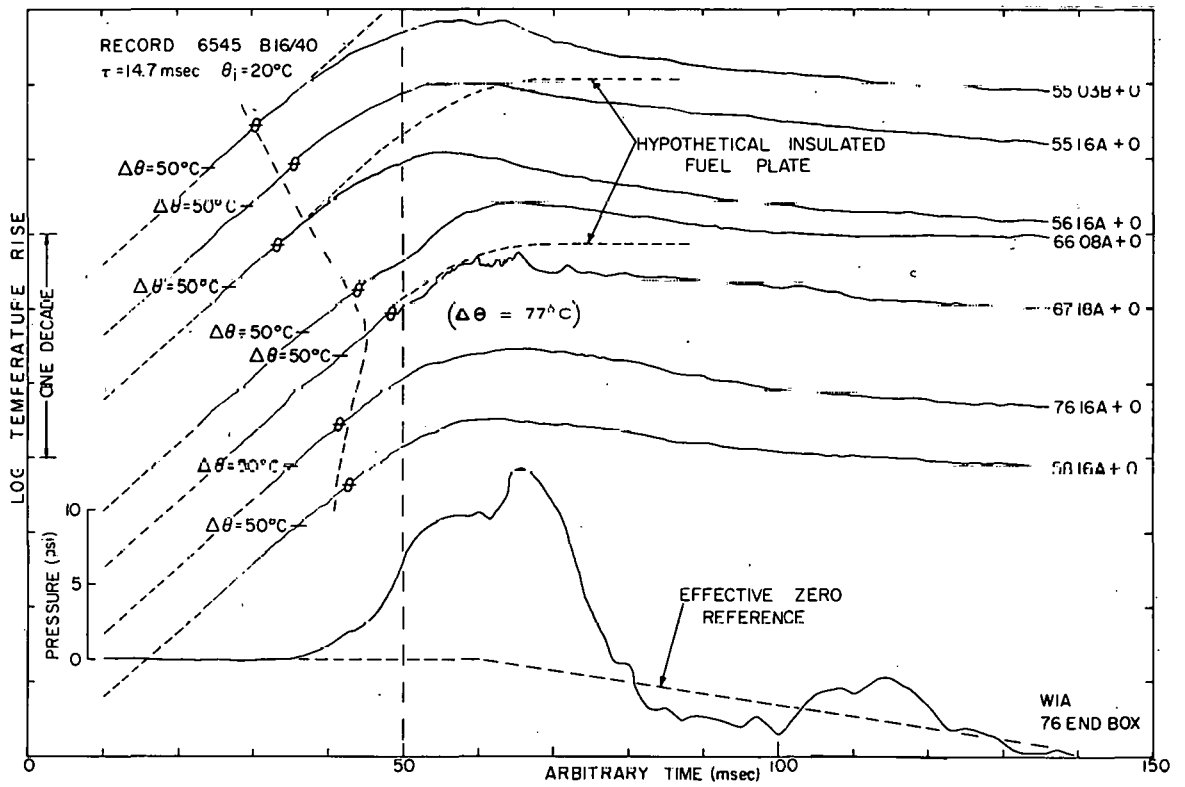

Fig. 117 A presentation of fuel-plate surface temperature-time histories at various radial positions and the pressure-time history. The symbol θ on the temperature-time histories indicates the boiling temperature with the corresponding temperature rise shown in parentheses adjacent to one of the traces.

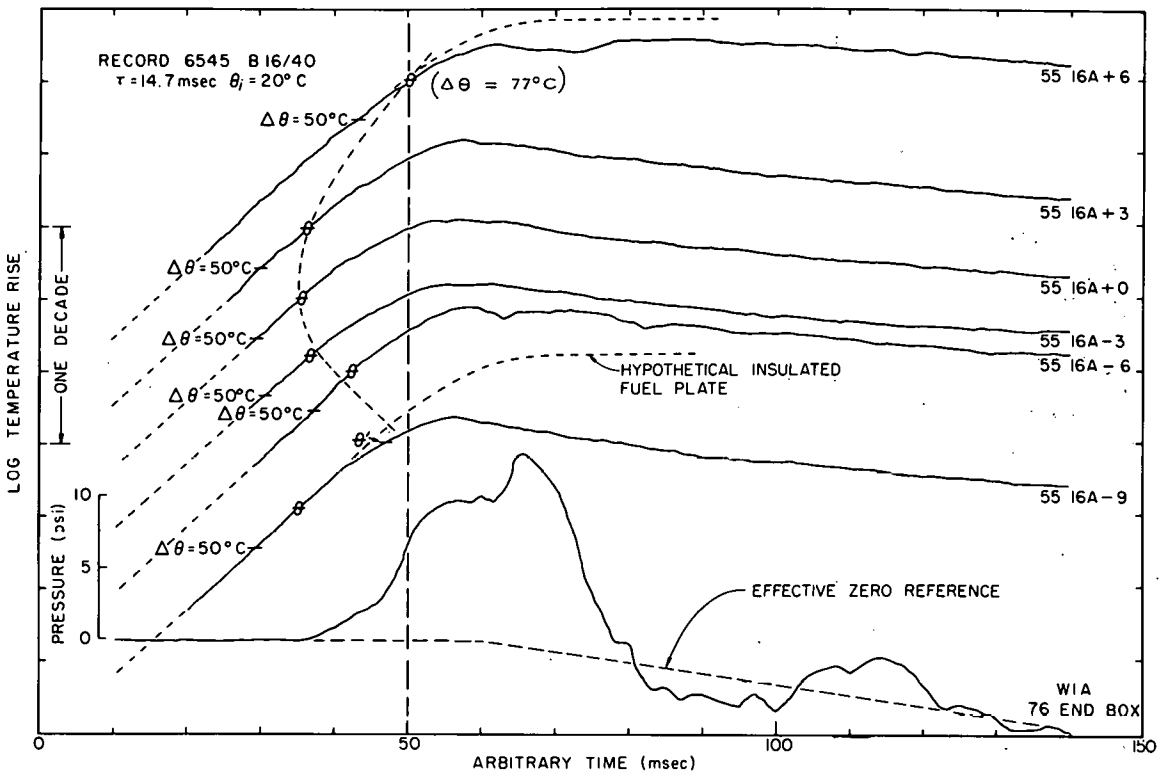

Fig. 118 A presentation of fuel-plate surface temperature-time histories at various longitudinal positions along a fuel plate and the pressure-time history. The symbol θ on the temperature-time histories indicates the boiling temperature with the corresponding temperature rise shown in parentheses adjacent to one of the traces.

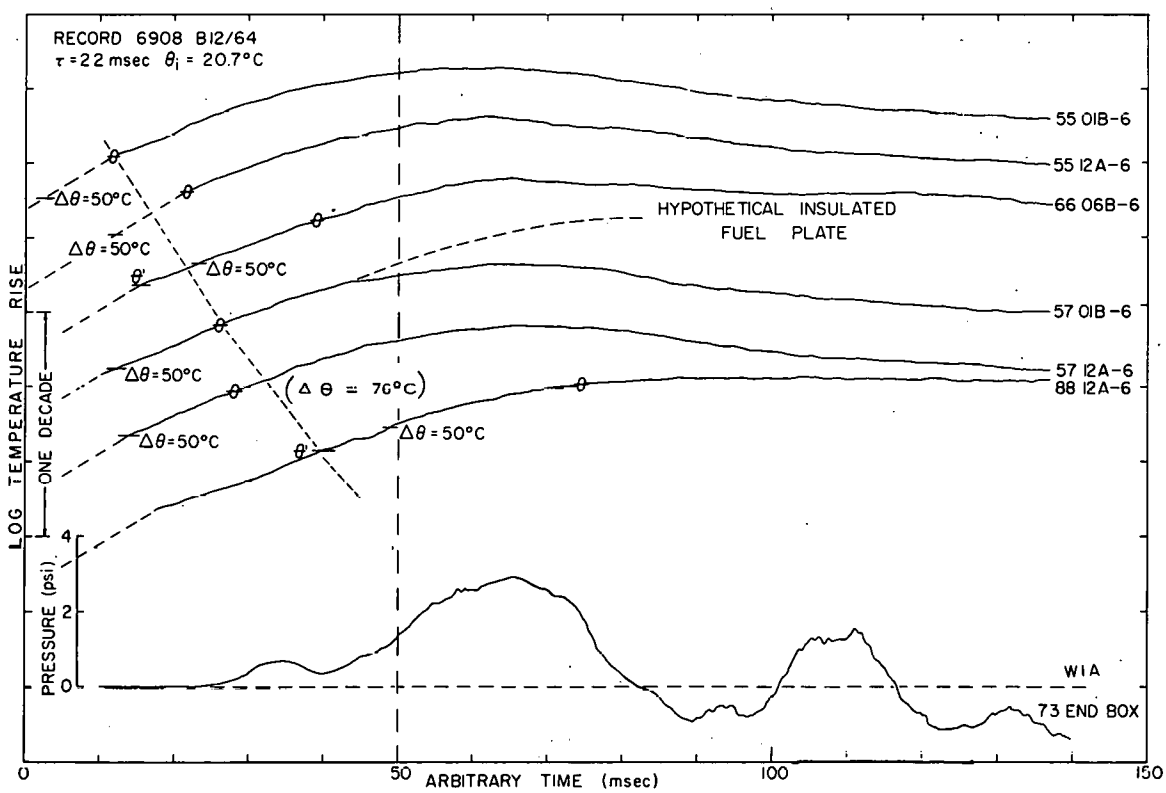

Fig. 119 A presentation of fuel-plate surface temperature-time histories at various radial positions and the pressure-time history. The symbol θ on the temperature-time histories indicates the boiling temperature with the corresponding temperature rise shown in parentheses adjacent to one of the traces.

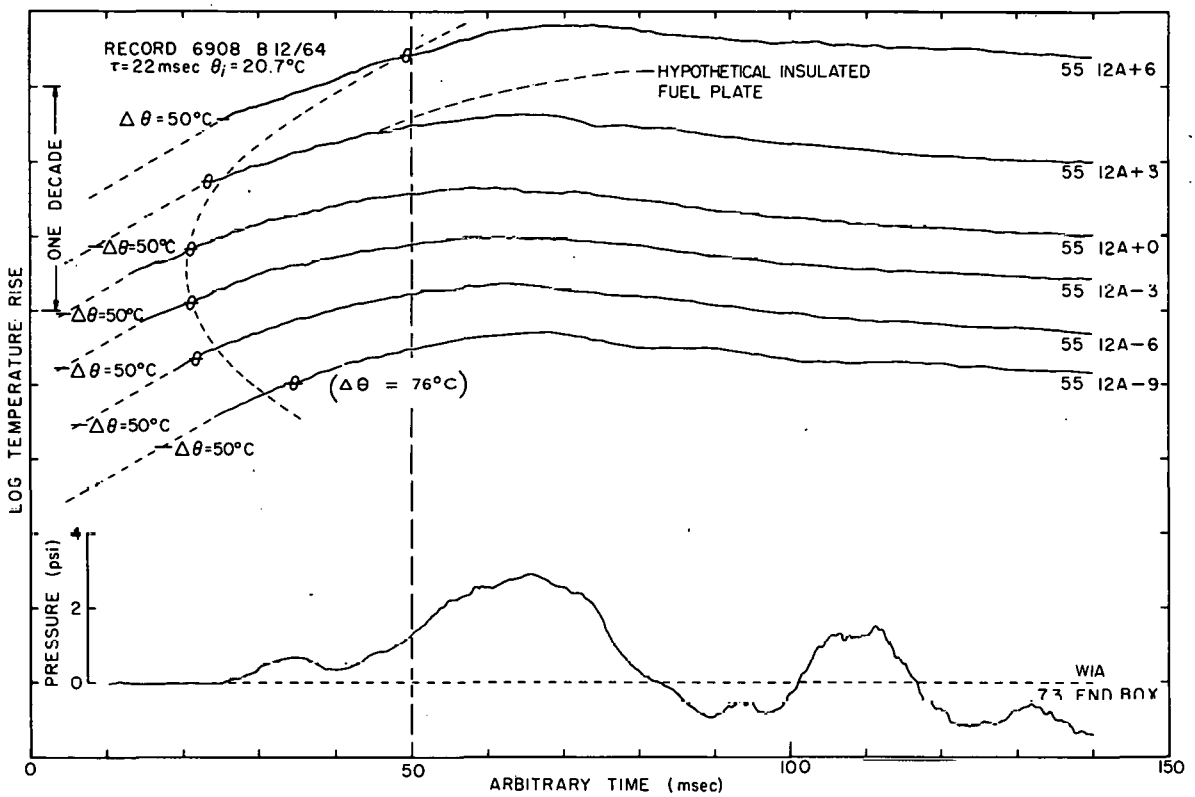

Fig. 120 A presentation of fuel-plate surface temperature-time histories at various longitudinal positions along a fuel plate and the pressure-time history. The symbol θ on the temperature-time histories indicates the boiling temperature with the corresponding temperature rise shown in parentheses adjacent to one of the traces.

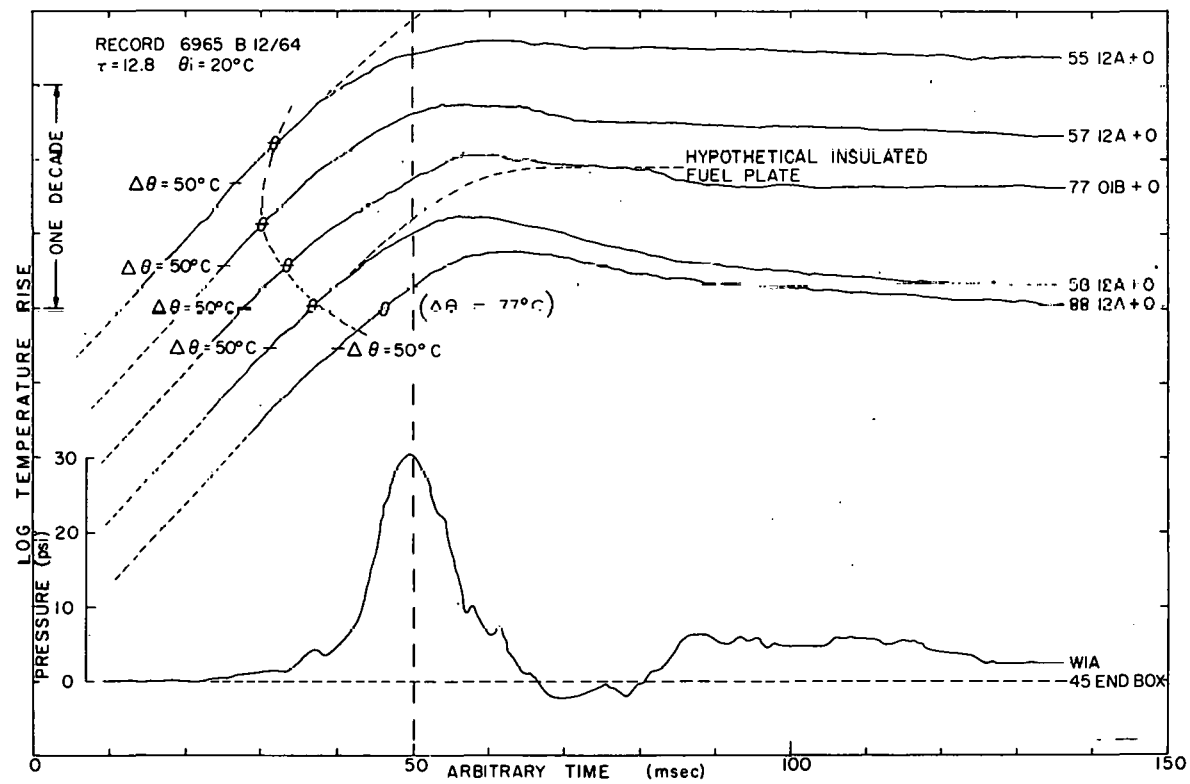

Fig. 121 A presentation of fuel-plate surface temperature-time histories at various radial positions and the pressure-time history. The symbol θ on the temperature-time histories indicates the boiling temperature with the corresponding temperature rise shown in parentheses adjacent to one of the traces.

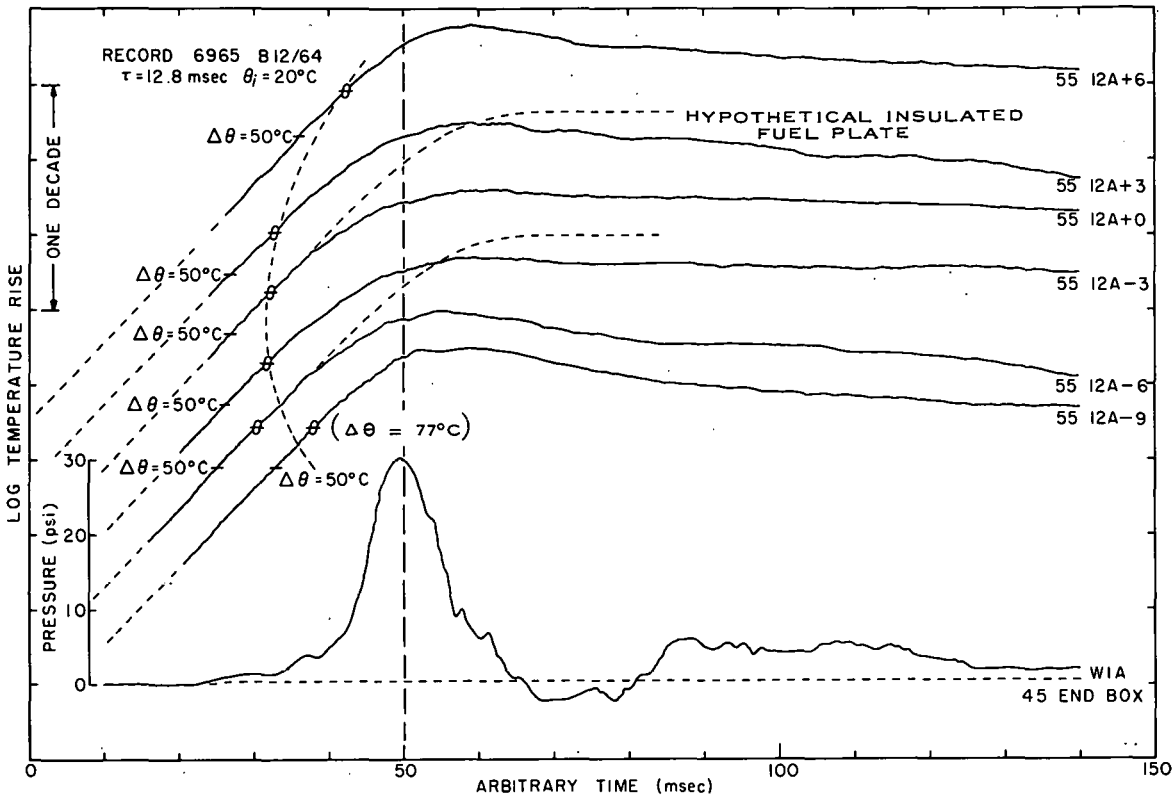

Fig. 122 A presentation of fuel-plate surface temperature-time histories at various longitudinal positions along a fuel plate and the pressure-time history. The symbol θ on the temperature-time histories indicates the boiling temperature with the corresponding temperature rise shown in parentheses adjacent to one of the traces.

thermocouples (ie, failure to record a calibration change). In these instances the symbol θ′ is included by the appropriate trace at the point where a proposed change in calibration would establish the boiling temperature. The boiling point indicated by the as-recorded data is denoted by the symbol θ as before. Examples are shown in Figures 111, 115, 118, and 119.

(3) Effects of Miscellaneous Variables Upon Pressure Generation. Pressure-time histories with reactor period as parameter are compared in Figures 123, 124, and 125. In general, the pressure magnitudes are highest for the B 24/32 core which also has a much broader pressure peak. The pressure pulse for the B 12/64 core is more sharply peaked and occurs much nearer the time of peak power. These effects result primarily from the differences in void coefficients previously noted (Table A-3). Similar data with initial temperature as parameter are presented in Figures 126, 127, and 128. A general broadening of the pulse may be observed at higher initial temperature, especially in the data for the B 24/32 and B 16/40 cores. There seems to be little evidence of any marked variation in pressure level with initial temperature for these long period transients ($\tau \approx 20$ msec).

The pressure-time histories obtained with the three cores are more readily compared in the data of Figures 129 through 133 where data from all three cores have been plotted in the same figure [a]. The contrast between

[a] Note that the data of Figure 130 are for intermediate period tests ($\tau \approx 15$ msec). All other data are for longer period tests ($\tau \approx 20$ msec).

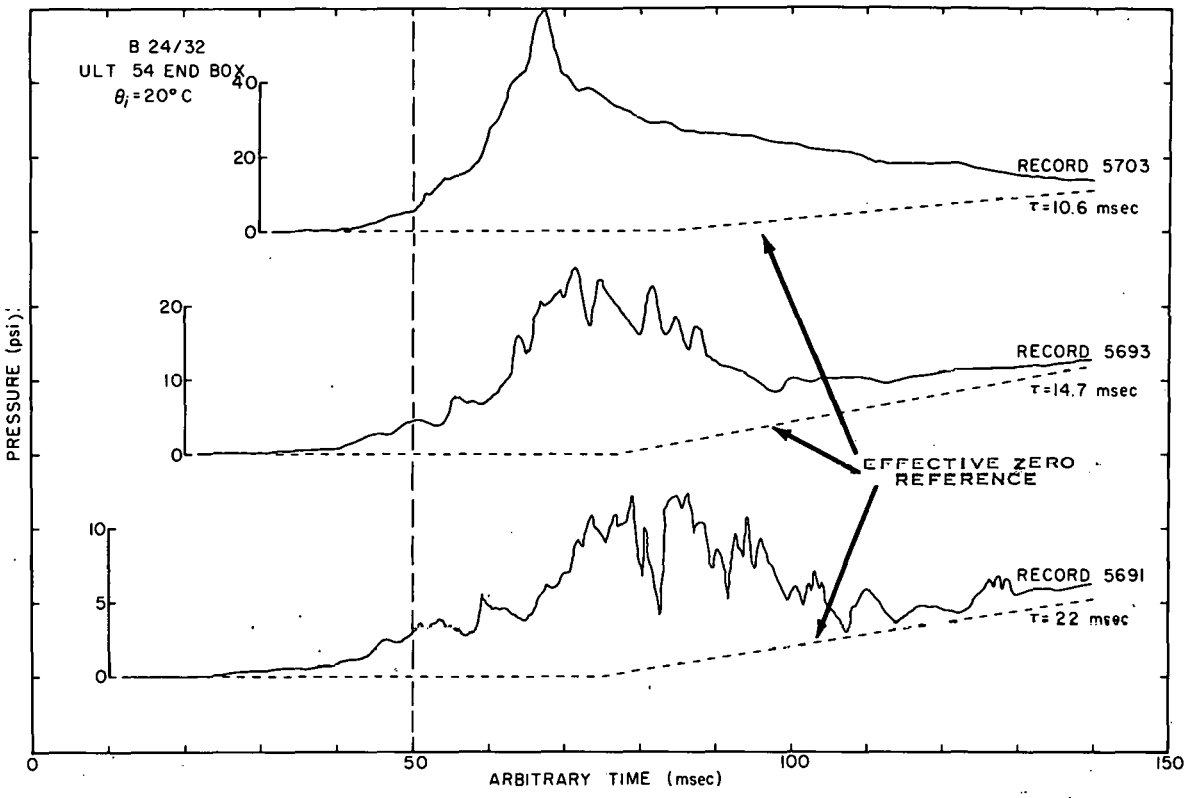

Fig. 123 Representative B 24/32 Core pressure-time histories for ambient temperature reactor transients at various reactor periods.

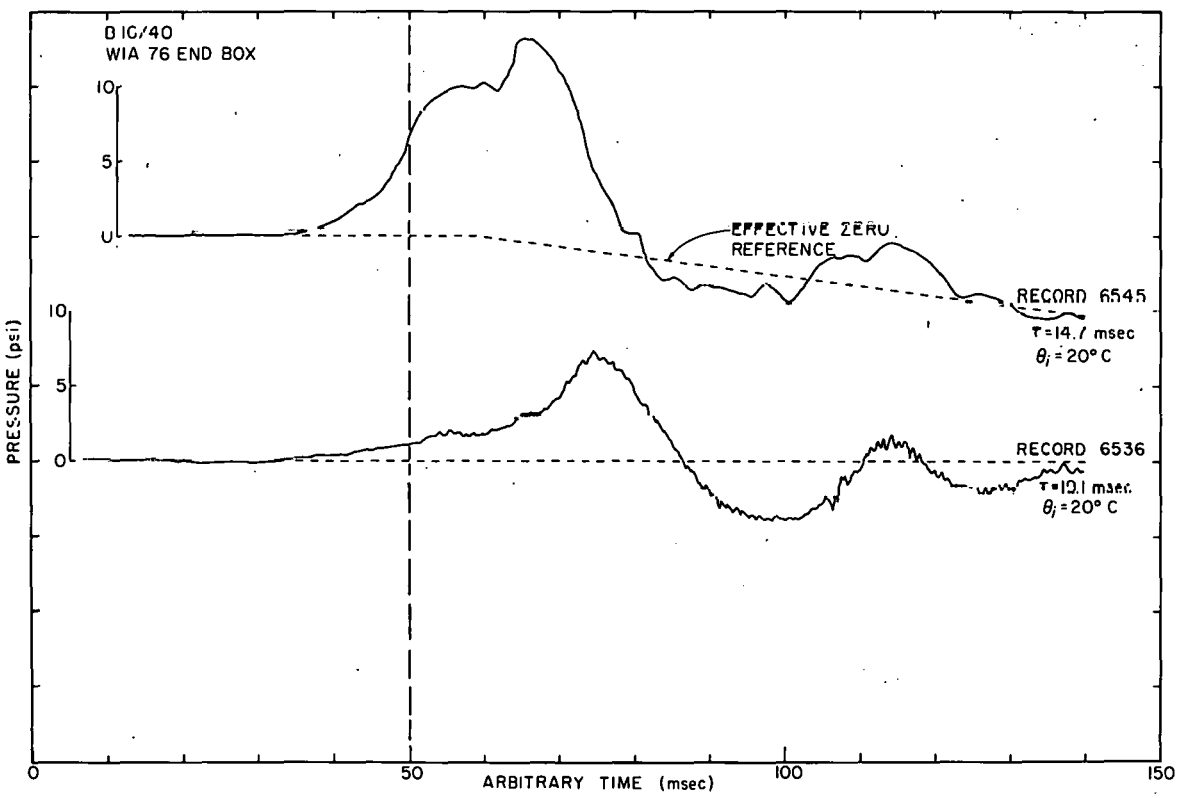

Fig. 124 Representative B 16/40 Core pressure-time histories for ambient temperature reactor transients at various reactor periods.

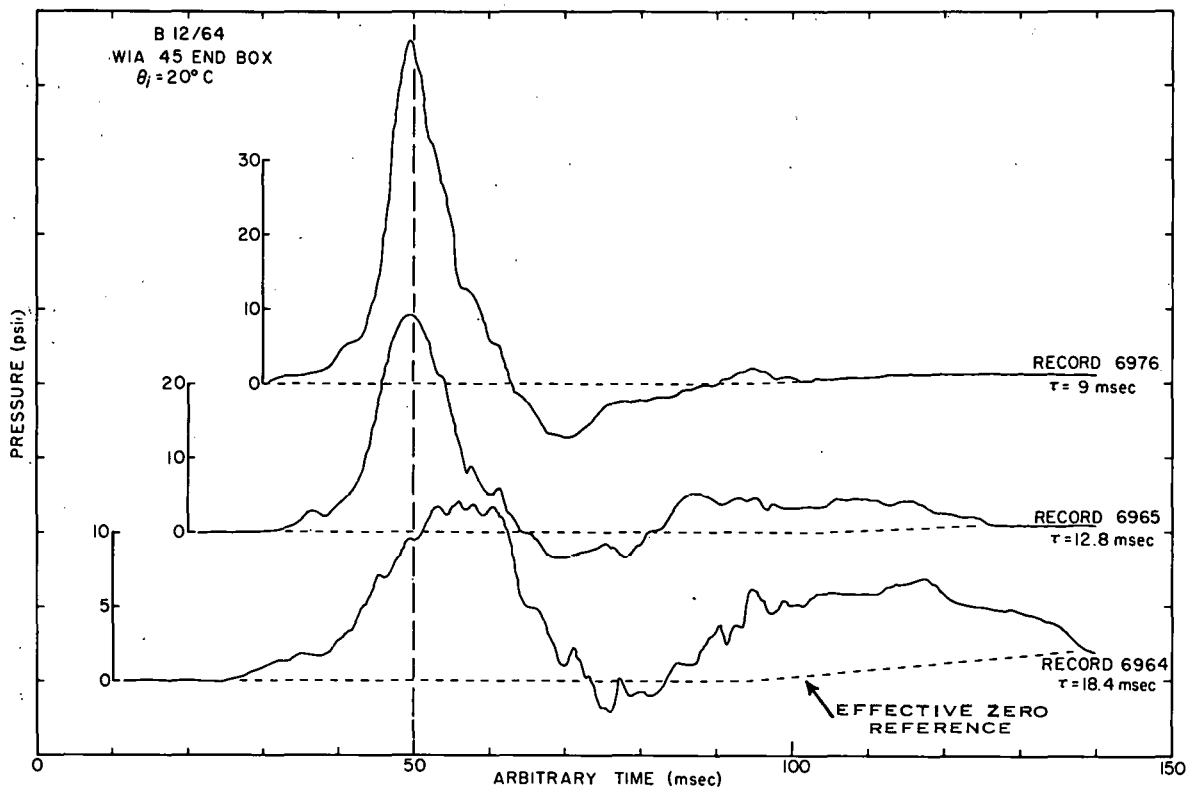

Fig. 125 Representative B 12/64 Core pressure-time histories for ambient temperature reactor transients at various reactor periods.

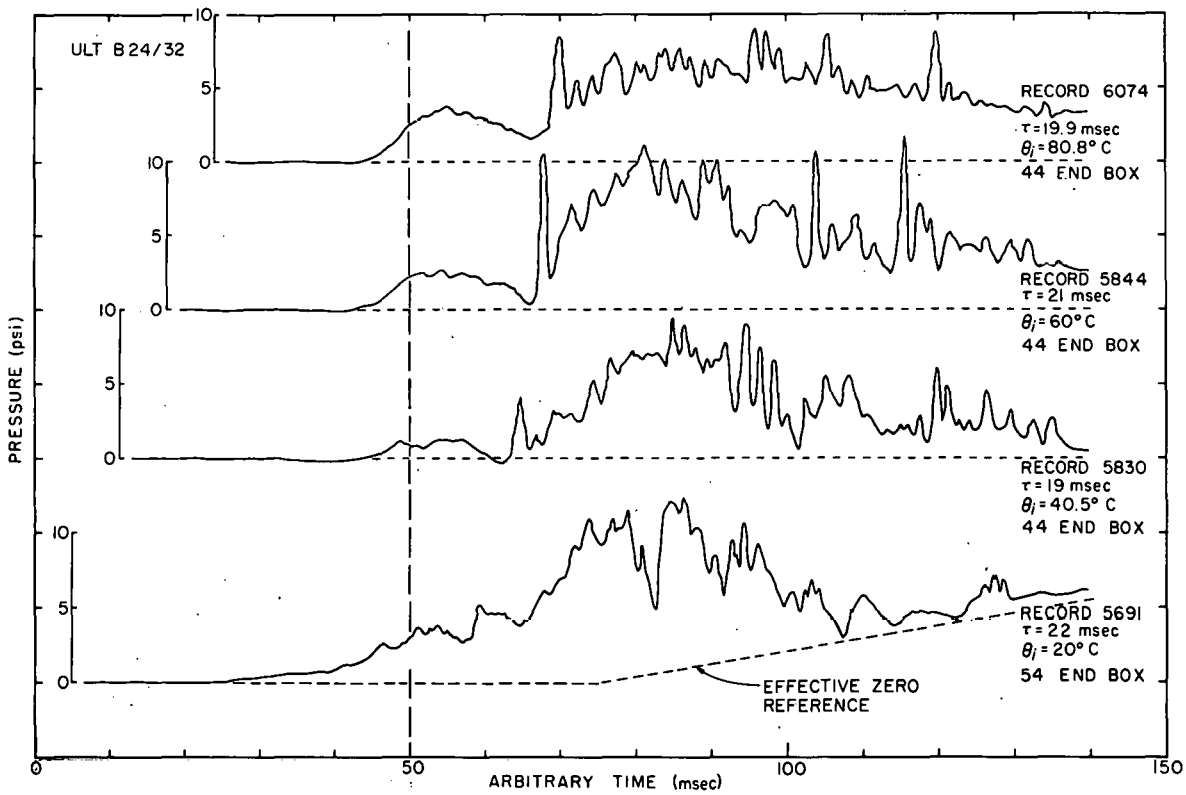

Fig. 126 Representative B 24/32 Core pressure-time histories for various initial temperatures.

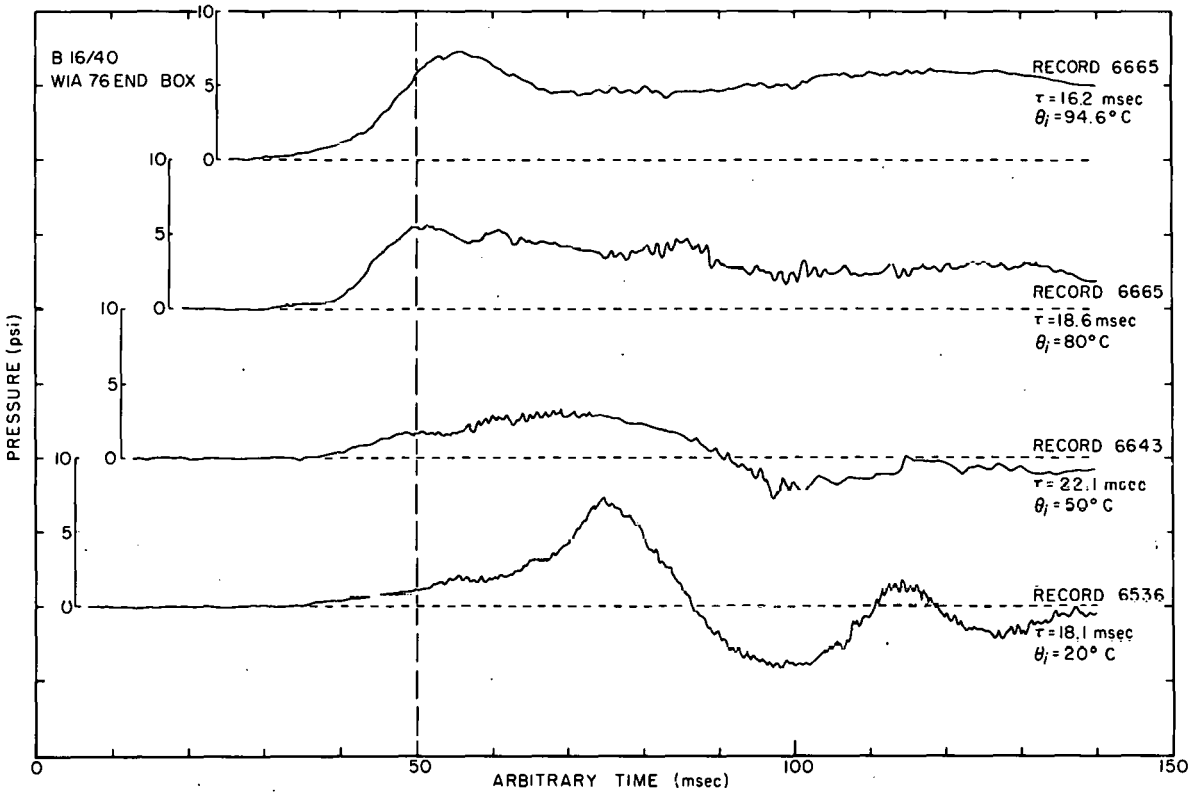

Fig. 127 Representative B 16/40 Core pressure-time histories for various initial temperatures.

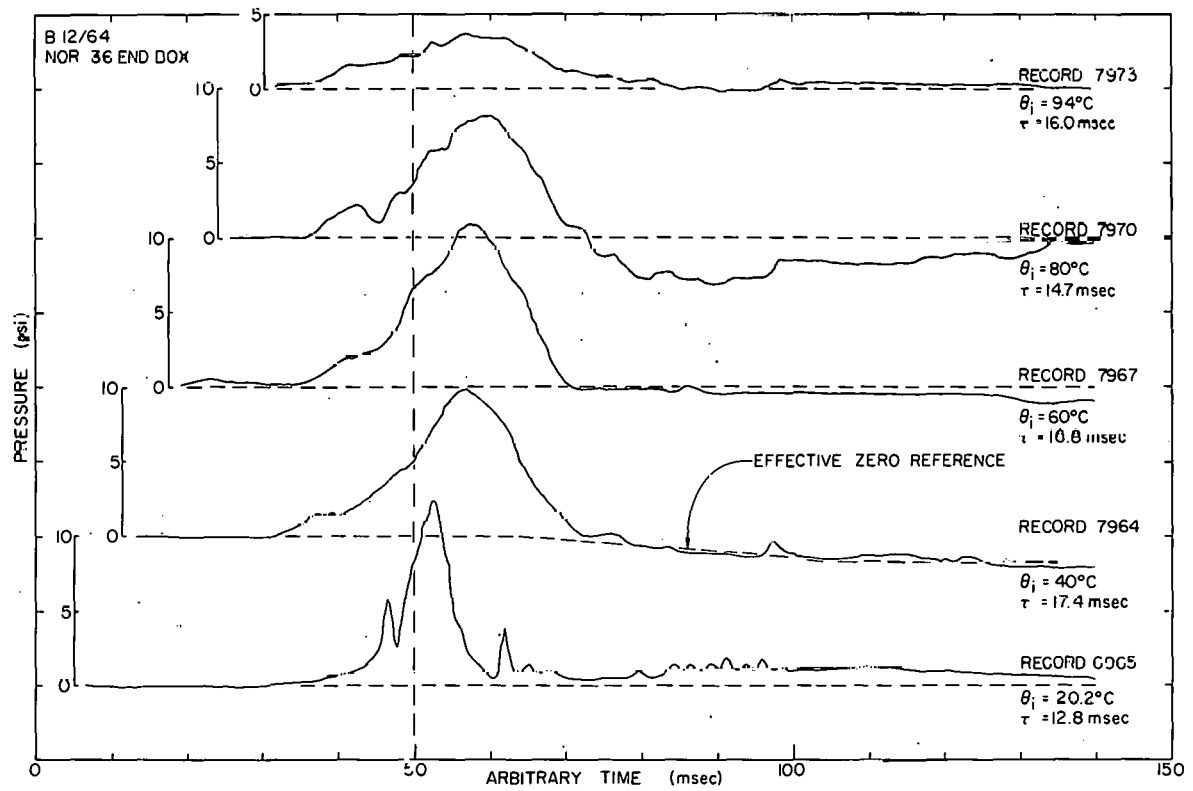

Fig. 128 Representative B 12/64 Core pressure-time histories for various initial temperatures.

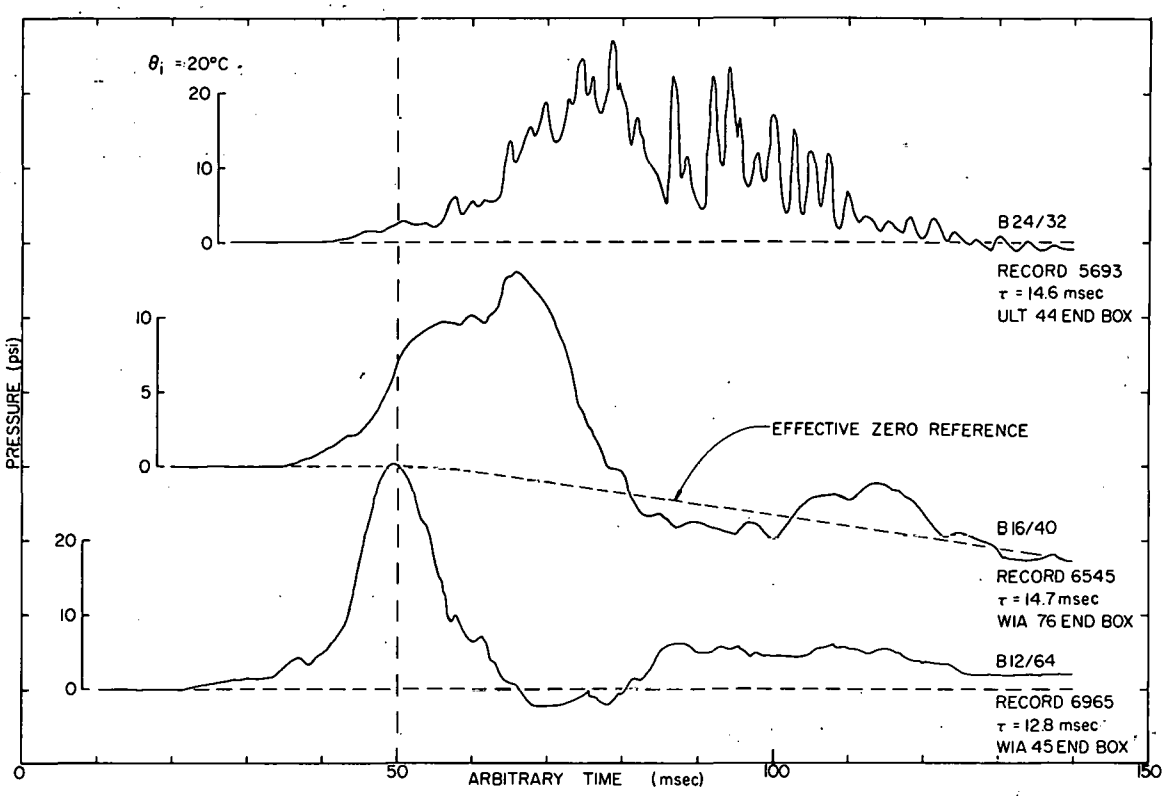

Fig. 129 Representative pressure-time histories for the three B-Cores at ambient initial temperature.

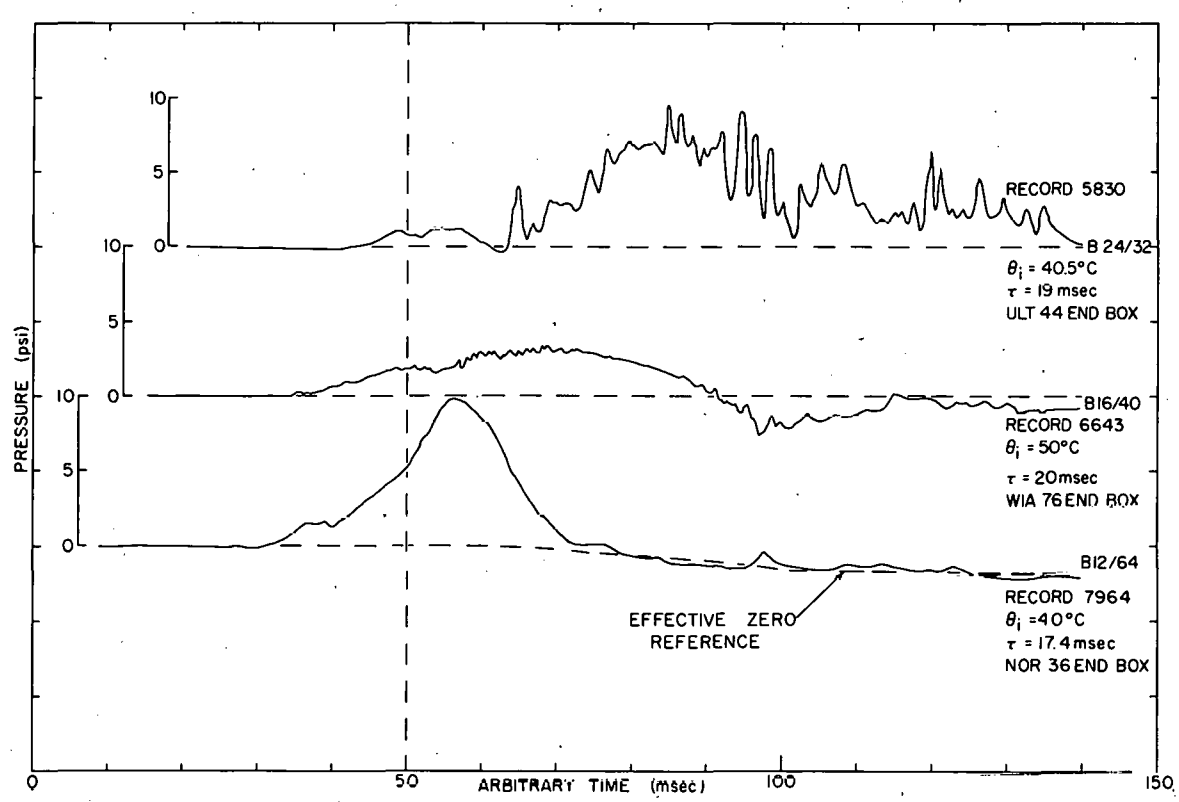

Fig. 130 Representative pressure-time histories for the three B-Cores at a nominal 40°C initial temperature.

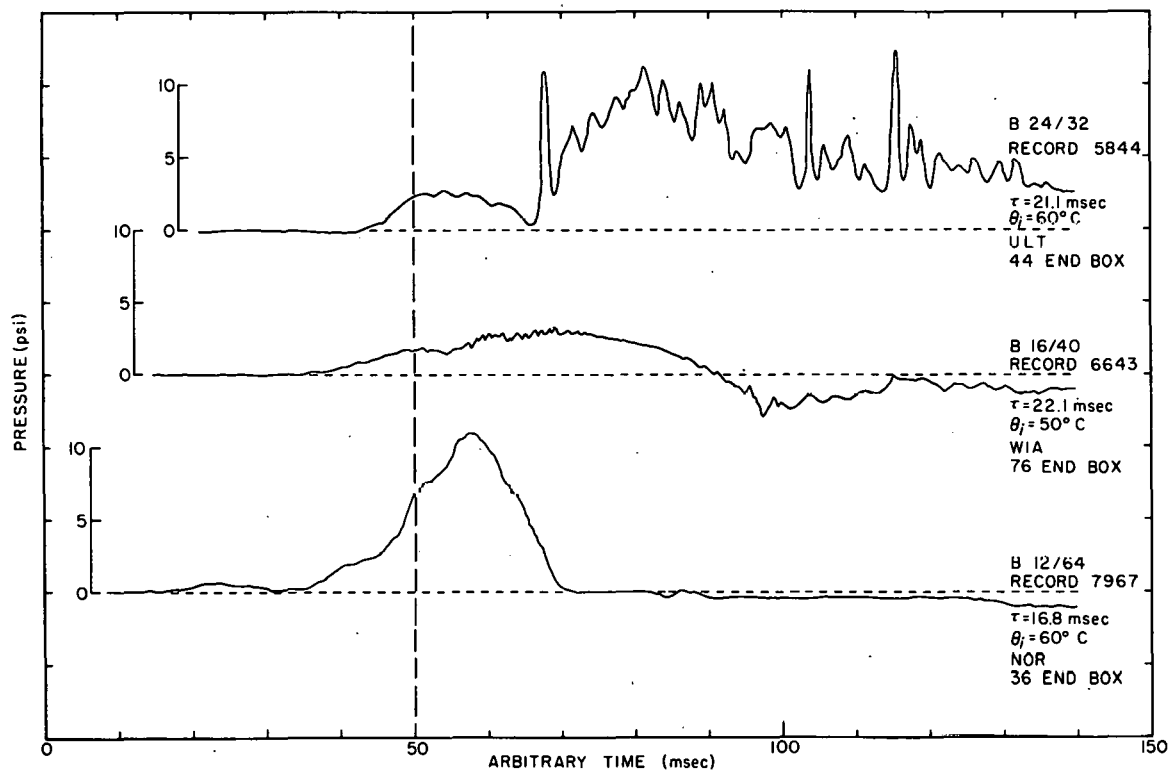

Fig. 131 Representative pressure-time histories for the three B-Cores at a nominal 60°C initial temperature.

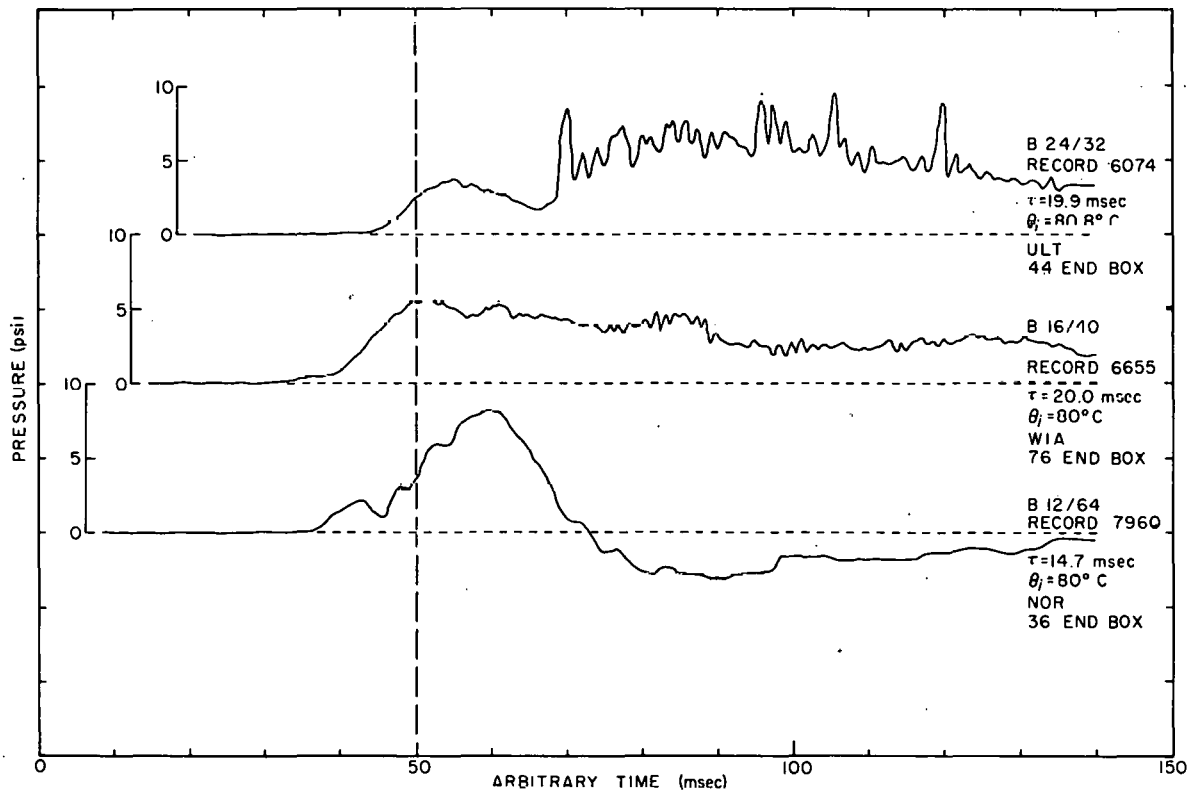

Fig. 132 Representative pressure-time histories for the three B-Cores at a nominal 80°C initial temperature.

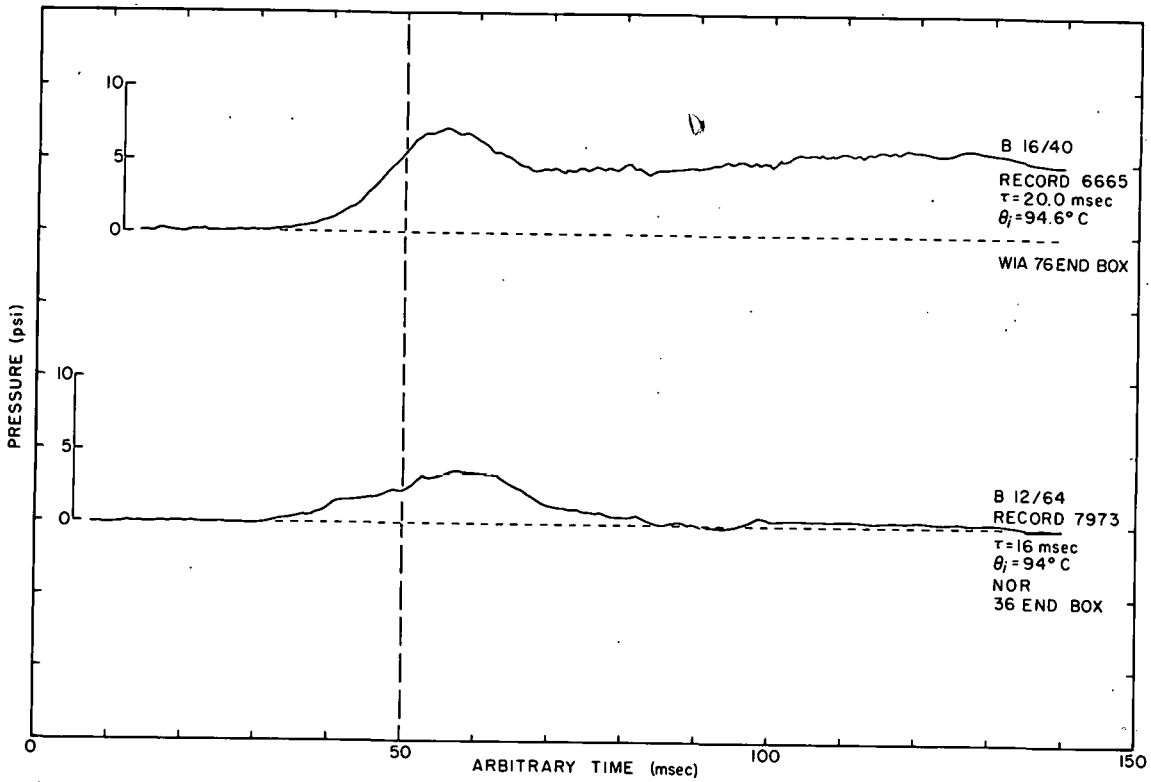

Fig. 133 Representative pressure-time histories for the three B-Cores at a nominal 94°C initial temperature.

the much sharper B 12/64 pulse and those of the other cores is especially evident at low initial temperature (θ_i < 80°C). At higher initial temperatures ($\theta_i \geq$ 80°C) the pulse broadens appreciably, but still lacks the long tail characteristic of the pulses for the other cores.

2.23 Cross Plots. Peak pressure and pressure at peak power are summarized in Table A-4. These data also are plotted for each core in Figures 134, 135, and 136. Lines of specific slope have been drawn through the data primarily as a convenience in reference. The data indicate that the slope is rather insensitive to the geometry of the core as may be observed in the summary of B-Core data shown in Figure 137. Pressure levels obtained with the B-Core are materially greater than those obtained with other Spert I cores. This is partly a consequence of the large core size (ie, large pressure source). For example, the B-Cores have approximately 700 fuel plates compared to 476 for the A-Core and 342 for the P-Core. However, the differences in pressure magnitude are also undoubtedly influenced by other core parameters such as the void and temperature coefficients of reactivity.

TABLE A-4

SUMMARY OF B-CORE PRESSURE DATA

Record Number	Initial Temperature (°C)	Reactor Period (msec)	PXD Type	PXD Location	Pressure at Peak Power (psi)	Peak Pressure (psi)
			B-24/32 CORE			
5517	24.65	20.4	U 1530	54 end box	1.9	6.1
			U 689	44 end box	0.9	2.7
5636	21.5	22.7	U 1530	54 end box	2.0	5.9
			U 689	44 end box	5.1	---
5691	20.0	22.0	U 1530	54 end box	2.3	9.8
5693	20.0	14.6	U 1530	54 end box	4.2	22.5
			U 689	44 end box	2.5	22.0
5701	20.0	12.1	U 1530	54 end box	4.7	42.5
			U 689	44 end box	3.5	---
5703	20.0	10.6	U 1530	54 end box	4.5	59.0
			U 689	44 end box	5.5	87.0
5830	40.0	19.0	U 1530	54 end box	3.0	12.0
			U 689	44 end box	1.0	7.5
5844	60.0	21.1	U 1530	54 end box	3.4	13.5
			U 689	44 end box	2.5	10.2
5846	60.0	10.6	U 1530	54 end box	10.0	---
			U 689	44 end box	7.3	48.5
6074	81.0	19.9	U 1530	54 end box	4.3	7.3
			U 689	44 end box	2.5	6.1
			B-16/40 CORE			
6533	20.0	27.5	U 1530	54 end box	---	---
			N 4080	36 end box	---	1.5
6545	20.0	14.7	U 1529	54 end box	11.3	26.0
			N 4081	33 end box	2.0	10.3
			N 4080	36 end box	1.1	12.5
			W 32910	45 end box	5.9	19.8
6643	50.0	22.1	U 1529	54 end box	1.5	11.2
			U 690	44 end box	---	---
6655	80.0	18.6	U 1529	54 end box	9.0	17.3
			W 32910	45 end box	5.5	11.5
6665	94.6	16.2	U 1529	54 end box	8.4	13.5
			W 32910	45 end box	7.5	---
			B-12/64 CORE			
6908	20.6	24.6	N 4080	36 end box	1.2	3.1
			W 32909	73 end box	1.2	2.5
6964	20.0	18.4	N 4080	36 end box	1.7	3.5
			W 32906	44 end box	16.0	18.5
			W 32909	73 end box	7.0	8.5
			W 32910	45 end box	7.1	13.6

TABLE A-4 (cont'd)

Record Number	Temperature (°C)	Reactor Period (msec)	PXD Type	PXD Location	Pressure at Peak Power (psi)	Peak Pressure (psi)
6965	20.0	12.8	W 32906	44 end box	31.0	39.2
			W 32909	73 end box	14.4	20.8
			W 32910	45 end box	28.8	29.3
6976	20.0	9.0	W 32909	73 end box	25.8	32.8
			W 32910	45 end box	45.5	46.2
7940	20.25	15.6	N 4081	36 end box	3.1	3.9
			W 32907	Below 66	15.5	19.1
7942	19.9	16.1	N 4081	36 end box	9.5	12.2
			W 32907	Below 66	13.3	15.8
7945	20.1	16.15	N 4081	36 end box	9.5	12.7
			W 32907	Below 66	15.3	---
7949	20.5	14.6	N 4081	36 end box	11.4	15.2
			W 32907	Below 66	18.6	21.0
7960	20.0	25.0	N 4080	36 end box	2.3	6.5
7964	40.0	17.4	N 4080	36 end box	5.0	9.7
7967	60.0	16.8	N 4080	36 end box	7.9	11.6
			W 32907	Below 66	0.6	1.0
7970	80.0	14.7	N 4080	36 end box	3.4	8.1
			W 32907	Below 66	16.2	26.5
7973	94.0	16.0	N 4080	36 end box	2.8	3.9
			W 32907	Below 66	11.8	14.0
7991	95.0	9.5	N 4080	36 end box	24.0	37.0
			W 32907	Below 66	45.0	59.5

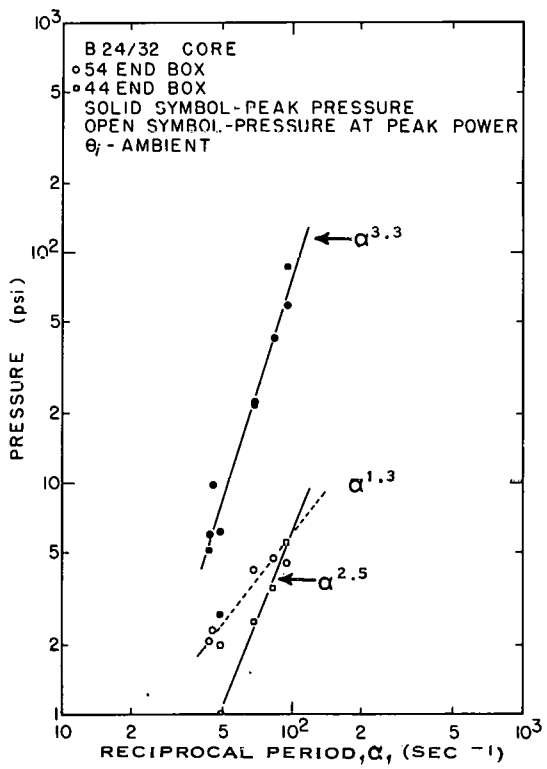

Fig. 134 Peak transient pressure and transient pressure at time of peak power in various lower end boxes of B 24/32 fuel assemblies as a function of reciprocal reactor period.

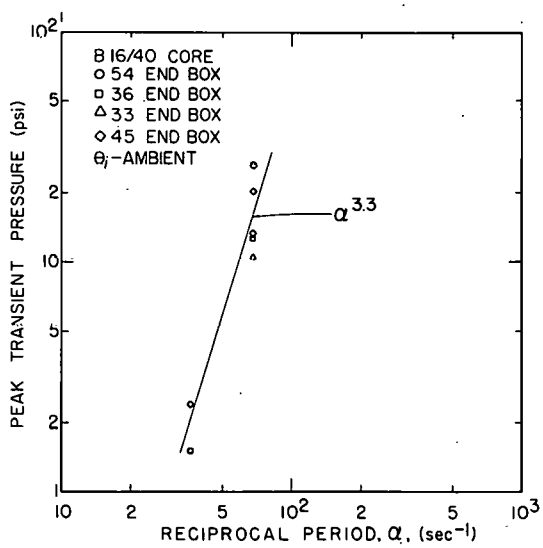

Fig. 135 Peak transient pressure in various lower end boxes of B 16/40 fuel assemblies as a function of reciprocal reactor period.

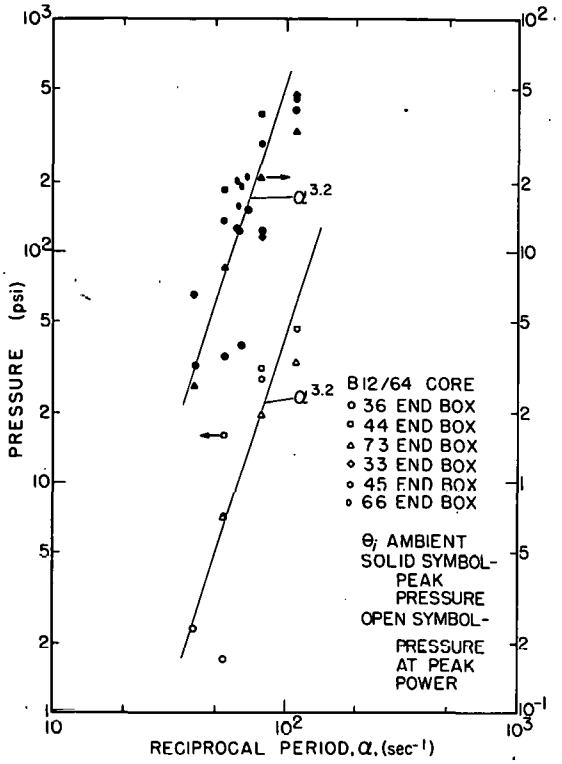

Fig. 136 Peak transient pressure and transient pressure at time of peak power in various lower end boxes of B 12/64 fuel assemblies as a function of reciprocal reactor period.

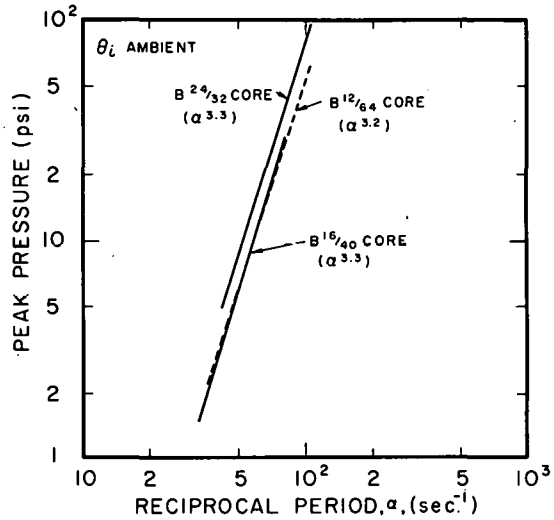

Fig. 137 Peak transient pressure as measured in the lower end boxes of fuel assemblies in the three B-Cores as a function of reciprocal reactor period.

3. BSR-II CORE EXPERIMENTS

3.1 Core Description [27]

The BSR-II Core was a compact stainless steel core composed of 25 assemblies in a five by five array and was quite similar to the P-Core. The fuel plates contained 14.5 gm U-235 as a cermet of 25 wt% U-235 [a] in stainless steel. The meat section was 14 mils thick and was clad in 8 mils of stainless steel. Finished assemblies contained 20 fuel plates (290 gm U-235) and were 2.93 in. square and 15.75 in. long. Four assemblies loaded to 1/4 this U-235 content were placed in the corner core positions; two modified assemblies (32 and 34) containing 261 gms U-235 were located adjacent to the transient rod. The transient rod fuel assembly contained two poison blades with fueled followers. The operational core configuration is shown in Figure 138. All fuel plates were oriented the same direction (east to west) except for the three central assemblies 23, 33, and 43 (Figure 138).

Parameters pertinent to evaluation of the BSR-II data are summarized in Table A-5.

3.2 Data Presentation

3.21 General Considerations. Only a limited number of step transients of the type normally obtained in Spert tests were conducted using this core. Since fuel element deformation was observed for reactor periods of about 15 msec, no data for shorter period transients were obtained.

3.22 Analog Plots. (1) Time-History Correlations for Power, Energy, Temperature, Flow, and Pressure. Time histories of pressure, power, energy, and temperature may be compared in Figures 139 and 140 for 29.8-and 14.5-msec reactor periods. The data are similar to those for other cores reported, especially the P-Core. An expansion contribution to pressure is evident in the data of Figure 139. Pressure levels are modest as for the P-Core. Although

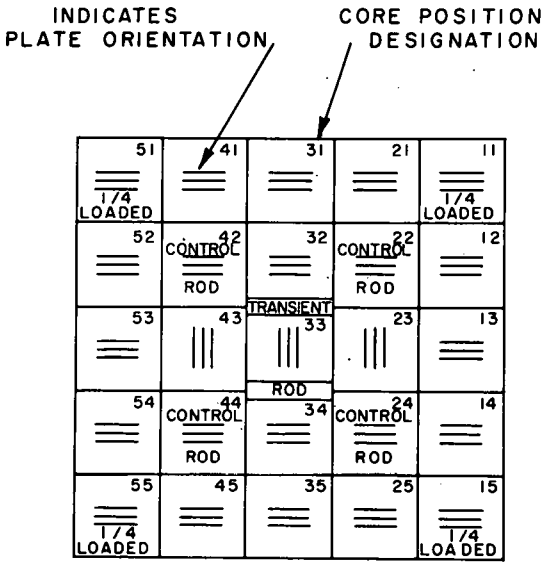

Fig. 138 Layout of Spert I reactor grid showing arrangement of fuel assemblies and fuel-plate orientation for the operational BSR II-Core.

there was considerable variation in water head between these transients (37 in. and 131 in.), the large difference in reactor period precludes any quantitative comparison of the effects of increased head. However, the pressure response for the transient conducted with the higher water head displays a more prominent primary peak of considerably longer duration, indicating the increased delay in arrival of the reflection from the free surface.

TABLE A-5

PERTINENT BSR-II CONSTANTS[28, 29]

Item	Magnitude or Type
Clad material	Stainless Steel
Critical mass	5.778 kg U-235
Total U-235 loaded	6.068 kg U-235
H/U ratio	86
M/W ratio	0.29
Available excess reactivity	2.3 $
Temperature defect 20° - 95°	1.2 $
Temperature coefficient 20°C	n.a † $/°C
Temperature coefficient 95°C	n.a $/°C
Average void coefficient, C_v	8×10^{-4} $/cm^3
Reduced prompt neutron lifetime $\ell^*/\bar{\beta}$	3×10^{-3} sec
Channel width	120 mils

† Data not available at time of publication

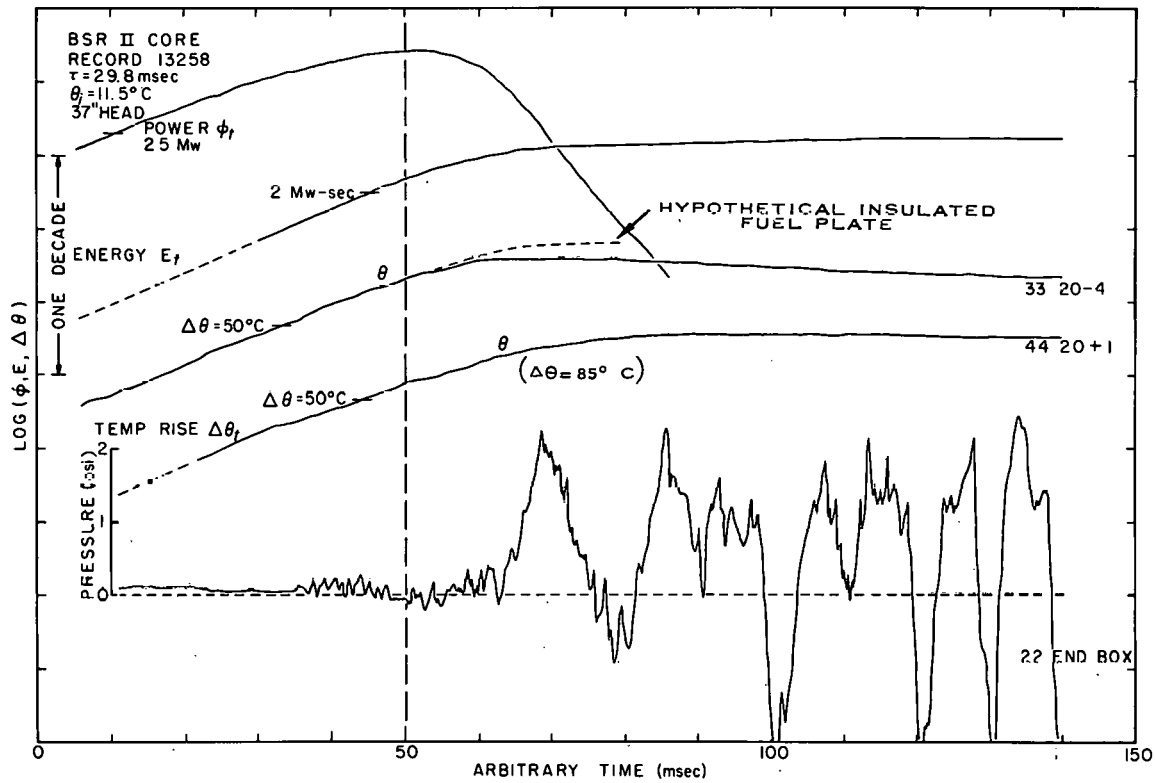

Fig. 139 A presentation of time histories for power, energy, fuel-plate surface temperature, pressure, and flow. The symbol θ on the temperature-time histories indicates the boiling temperature with the corresponding temperature rise shown in parentheses adjacent to one of the traces.

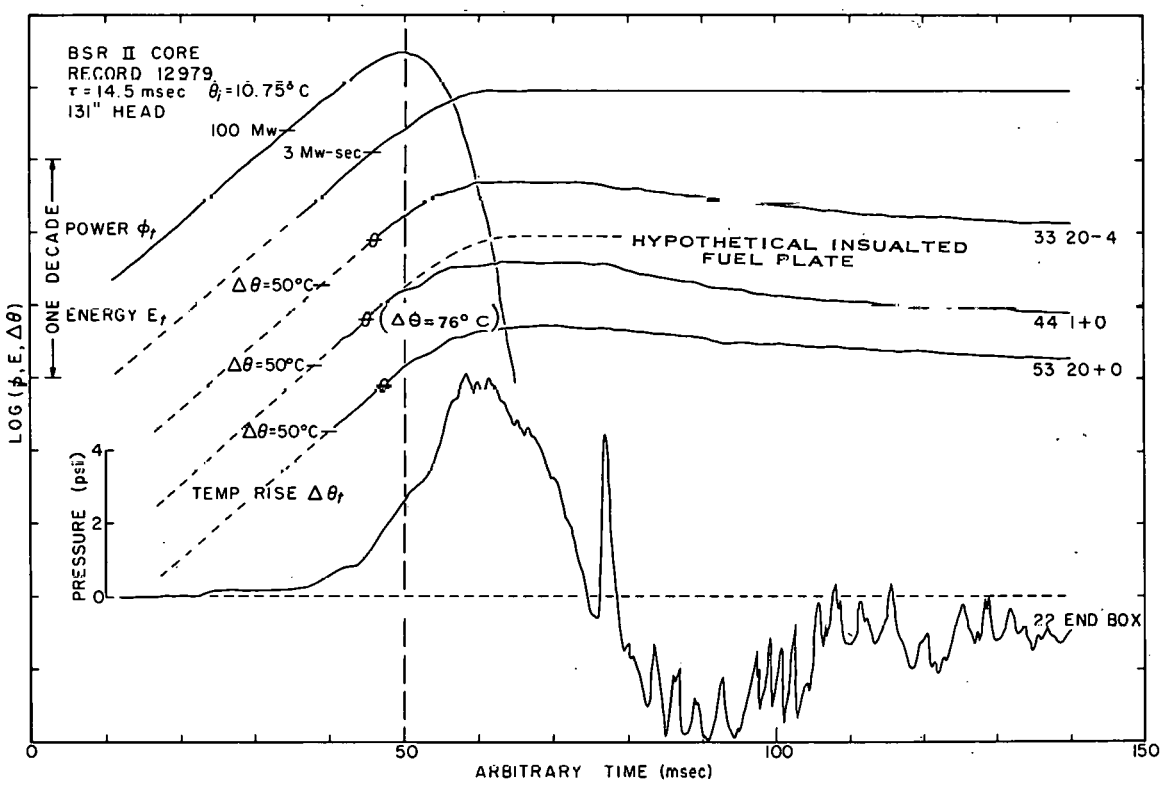

Fig. 140 A presentation of time histories for power, energy, fuel-plate surface temperature, pressure, and flow. The symbol θ on the temperature-time histories indicates the boiling temperature with the corresponding temperature rise shown in parentheses adjacent to one of the traces.

4. COMPARISON OF DATA FOR VARIOUS SPERT I CORES

Under this heading a few comparisons of the data obtained for the various cores will be presented and some observations of general trends will be made. The comparisons are not exhaustive, but do illustrate a few of the typical features pertinent to the pressure behavior.

4.1 Fitting of the Pressure-Time History by Specific Functions

Typical data for long and short reactor periods are shown in Figures 141 and 142 where the data have been fitted by functions of the form A sin Bt and Ce^{kt}, respectively. The data are, in general, well approximated by a sine function, thus facilitating acoustical analysis of the data (ie, the initial pressure pulse may be assigned an "effective frequency"). The data also can be fitted by an expression of the form Ce^{kt} over some portion of the leading edge of the pulse. The fit is best for short reactor periods and in most instances a multiple fit is required (ie, different exponents in different time intervals). In all instances the value of the factor k corresponding to the steep rise portion of the curve exceeded the value of the reciprocal reactor period α by about a factor of two to three as indicated in Table A-6.

4.2 Comparison of Typical Time Histories for the Various Cores

4.21 Pressure-Time Histories. Pressure-time histories for the various cores are compared in Figures 143 and 144 for reactor periods of approximately 20 msec and 10 msec, respectively. For convenience in comparison, the data have been normalized in time to the first perceptible rise in pressure. This procedure to some extent compensates for differences in the time delay in

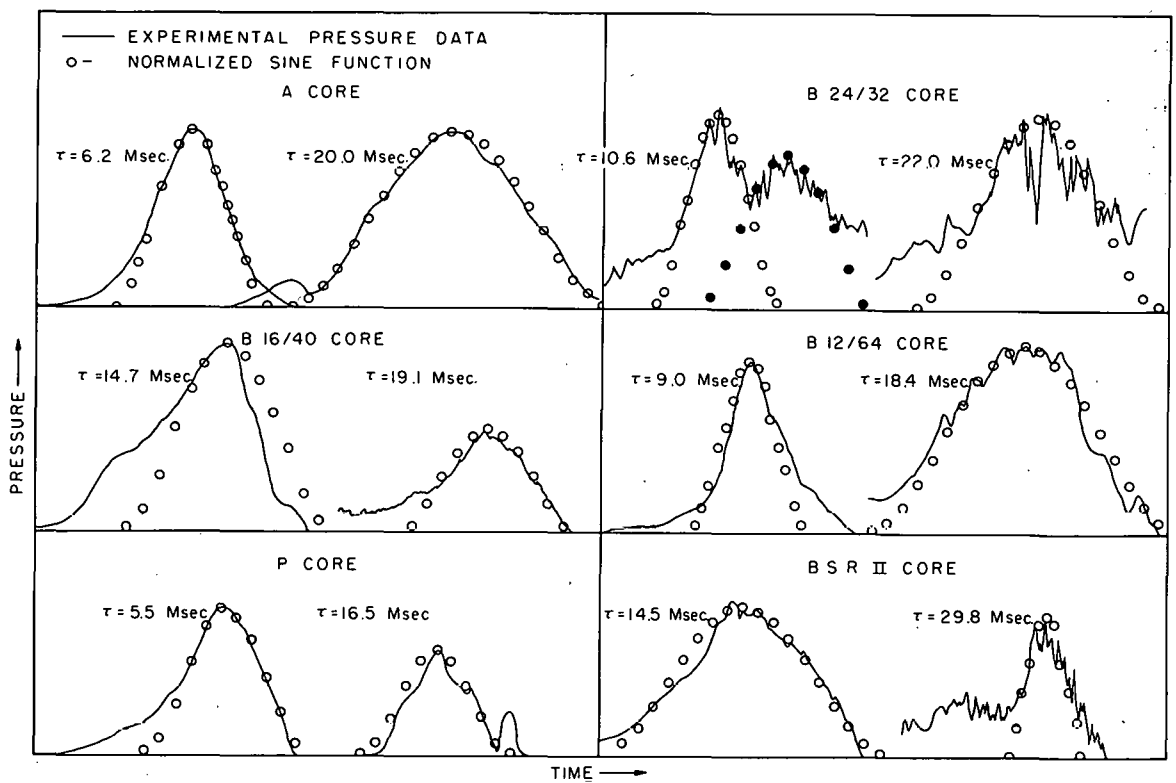

Fig. 141 Display of the degree of fit obtained when sine functions are normalized to the Spert I pressure-time histories.

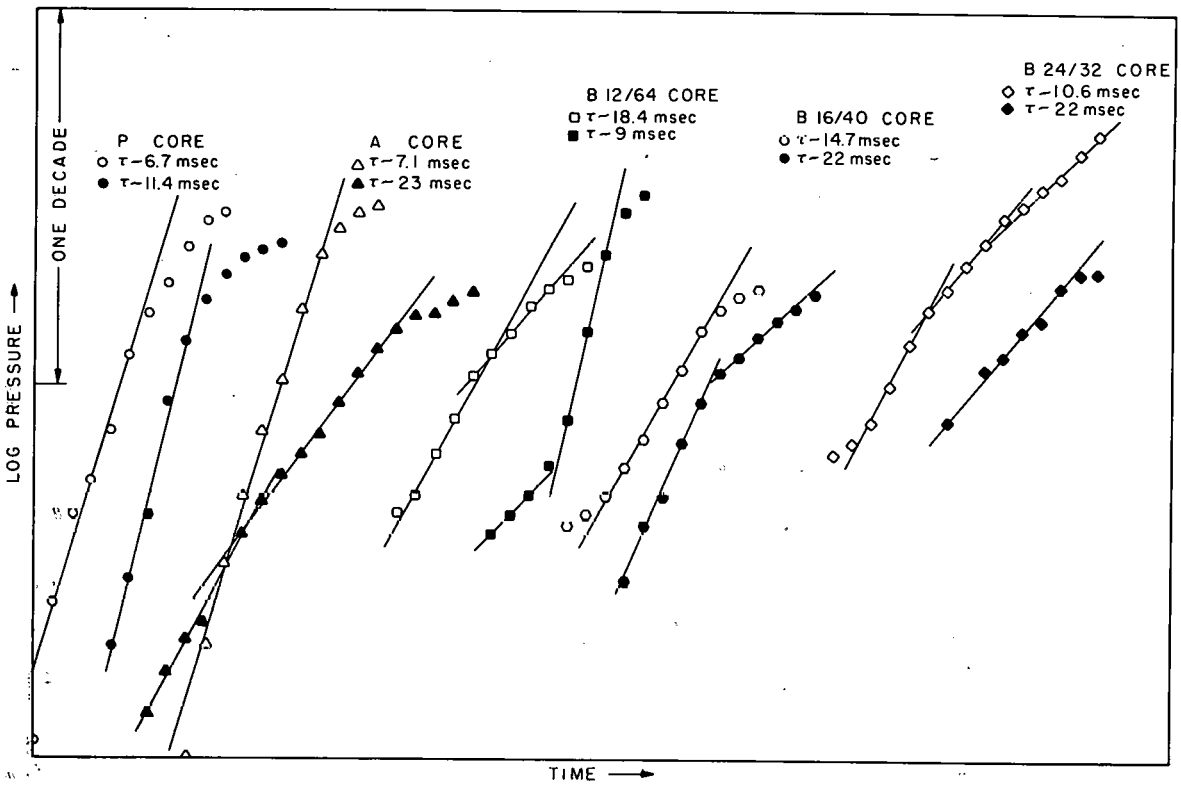

Fig. 142 Display of the degree of fit obtained when exponential functions are normalized to the Spert I pressure-time histories.

establishing effective conduction and boiling heat transfer which may arise from differences in cladding of the fuel. There are remarkable similarities between traces in the early portion of the histories, and striking differences in the traces during the later portions. In the time interval where expansion effects are an appreciable contributor to pressure level, the histories are similar; but, once nucleate boiling develops, each core displays its own unique behavior. The differences in time histories between the high void coefficient B 24/32 core and the low void coefficient B 12/64 core may be observed in Figure 144.

Peak pressure data are summarized in Figure 145. The curves shown are those drawn as a fit to the data in the earlier presentations for the individual cores. Corresponding slopes as a function of reciprocal period α are indicated. These data are further summarized in Table A-7.

TABLE A-6

A COMPARISON OF THE RECIPROCAL PERIOD, α, AND THE SLOPE FACTOR, k, OF EXPONENTIAL FUNCTIONS APPROXIMATING THE STEEP RISE PORTION OF THE PRIMARY PRESSURE PULSE

Spert I Core	Approximate Slope, k	Value of Ratio k/α
P 18/19	380	2.0 - 3.5
A 17/28	370	2.0 - 5.0
B 24/32	160	1.5 - 3.0
B 16/40	150	1.8 - 2.6
B 12/64	240	3.3 - 4.6

4.22 Temperature-Time Histories. Typical temperature-time histories are similarly shown in Figures 146 and 147. All temperature histories have been normalized at the boiling temperature θ and are indicated in the plots by the dotted curves. The appropriate hypothetical insulated-plate behaviors are superimposed on the temperature data to allow a comparison of the effective heat transfer. The vertical displacement

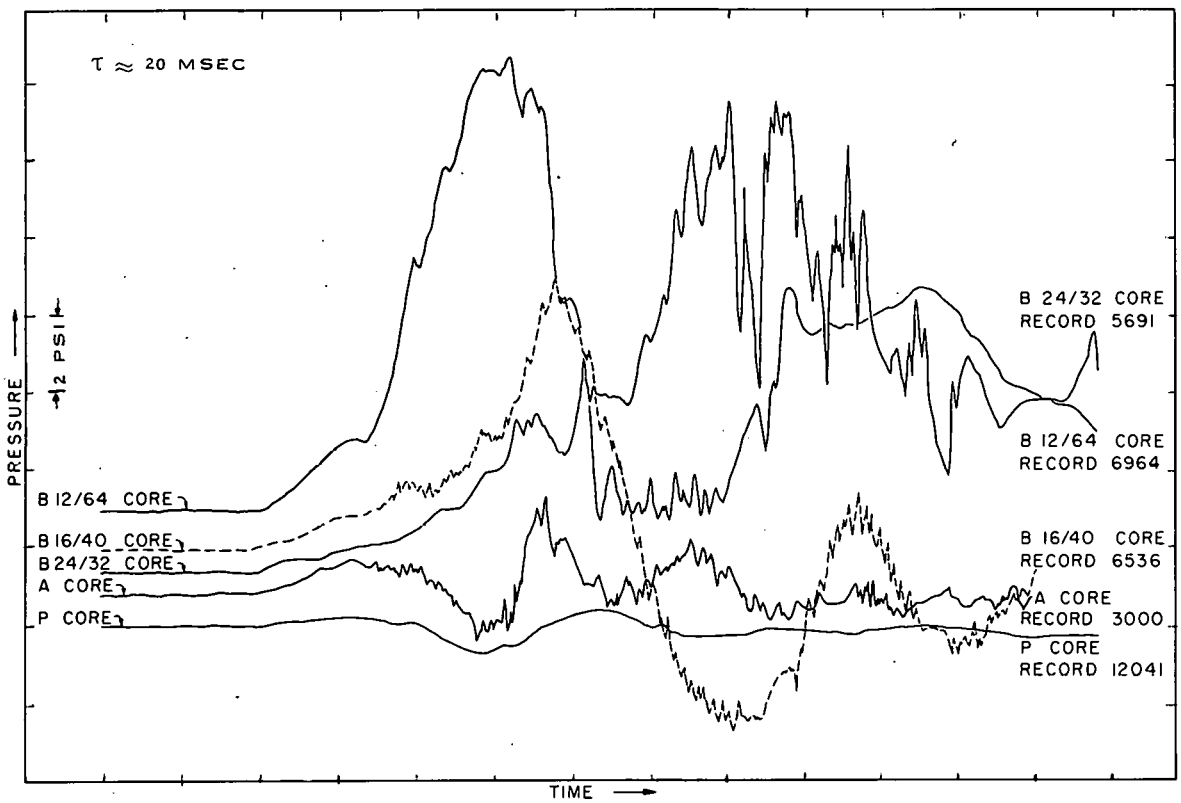

Fig. 143 Representative pressure-time histories for Spert I Cores, time normalized at first perceptible deflection of pressure-time histories.

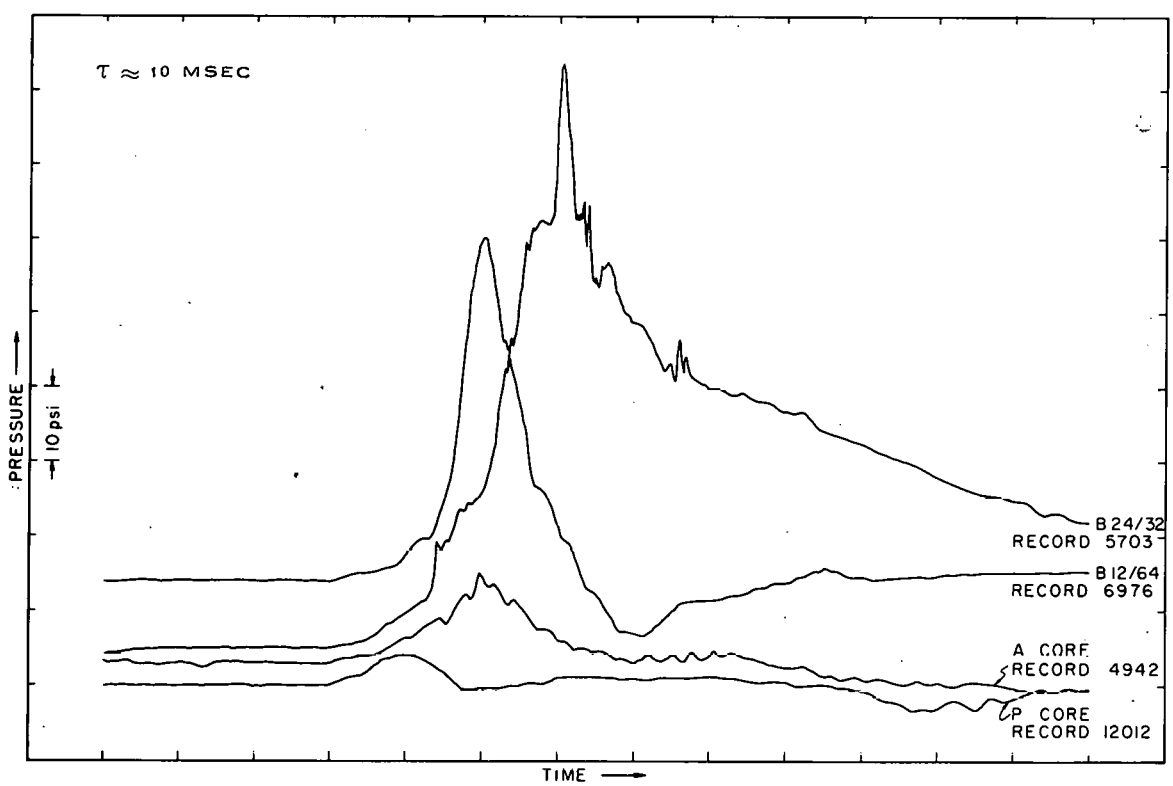

Fig. 144 Representative pressure-time histories for Spert I Cores, time normalized at first perceptible deflection of pressure-time histories.

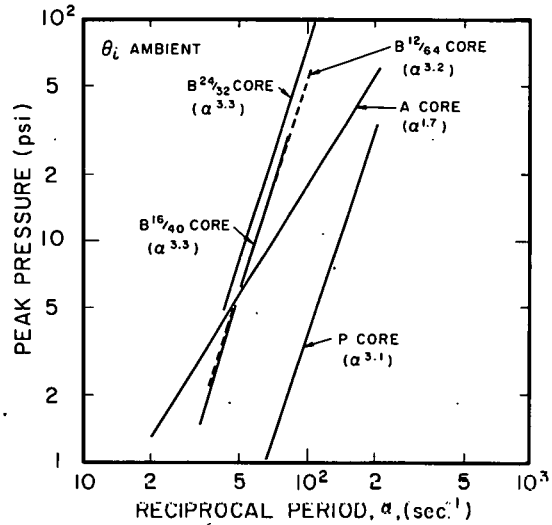

Fig. 145 Peak transient pressure for Spert I cores as a function of reciprocal reactor period.

of the temperature-time history from the insulated-plate behavior is a measure of the energy transfer to the water and should correlate to some extent with the energy associated with the pressure pulse.

4.3 Comparison of Pertinent Core Parameters

Parameters pertinent to a comparison of data for the various cores are summarized in Table A-8.

TABLE A-7

SUMMARY OF DATA OBTAINED FOR PEAK PRESSURE AND PRESSURE AT PEAK POWER DURING SPERT I REACTOR TRANSIENTS

Spert I Core	Reactor Period (msec)	Approximate Pressure Magnitude	
		Pressure at Time of Peak Power (psi)	Peak Pressure (psi)
P 18/19	15	0.5	1
	10	1.5	4
	5	5.5	32
A 17/28	20	0.5	6
	10	8	18
	5	20	55
B 24/32	20	2.5	8
	15	3.5	20
	10	.6.0	75
B 16/40	20	2	5
	15	6	12
B 12/64	20	5	8
	15	15	20
	10	35	40

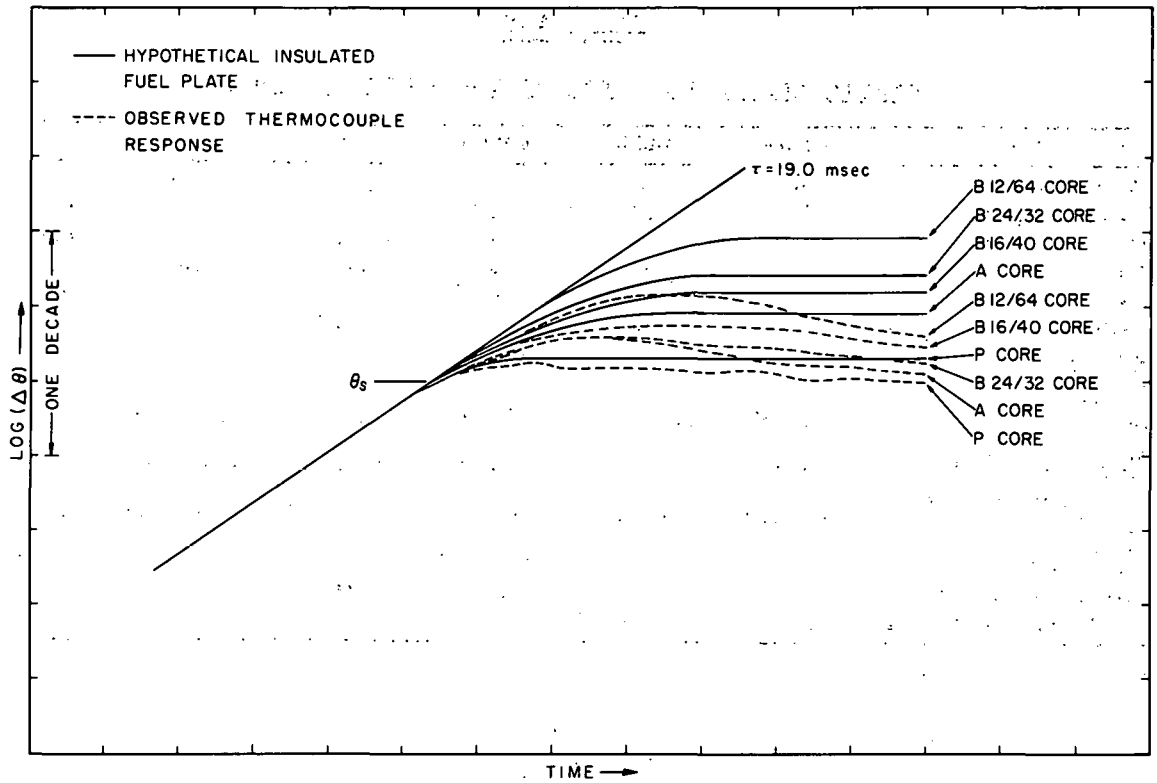

Fig. 146 Representative temperature-time histories and hypothetical insulated-plate behaviors for the Spert I cores.

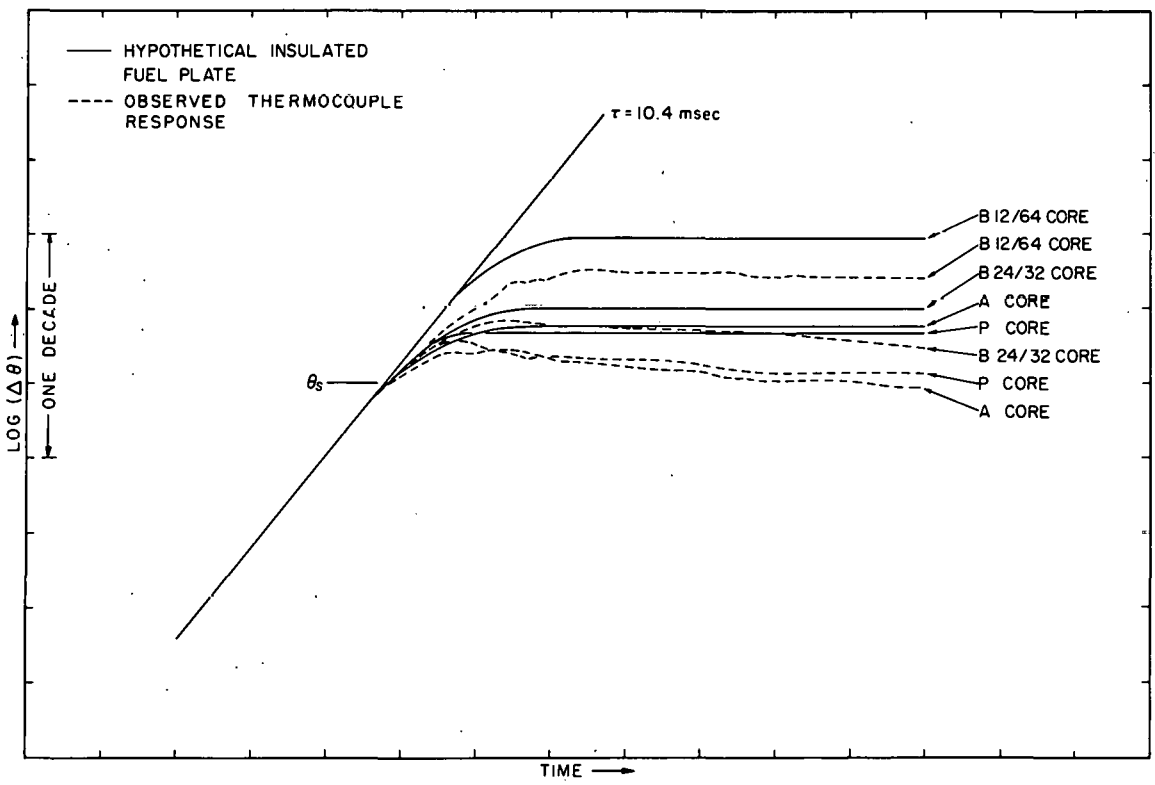

Fig. 147 Representative temperature-time histories and hypothetical insulated-plate behaviors for the Spert I cores.

TABLE A-8

STATIC CHARACTERISTICS OF THE SPERT I CORES

Core	B 12/64	B 16/40	A 17/28	B 24/32	P 18/19	BSR-II
Clad Material	Al	Al	Al	Al	SS	SS
Critical Mass, Kg U-235	4.3	3.6	3.9	4.3	7.6	5.778
Total U-235 Loaded, Kg	5.4	4.5	4.7	5.4	9.3	6.068
H/U Ratio	760	540	320	270	120	86
M/W Ratio	0.46	0.63	0.79	1.14	0.3	0.3
Available Excess Reactivity, $	4.3	5.6	5.2	6.6	4.9	2.3
Temperature Defect, 20° - 95° C, $	1.44	1.67	1.47	1.73	1.48	1.2
Isothermal Temperature Coefficient, 20° C, $/°C	-1.8×10^{-2}	-1.7×10^{-2}	-0.67×10^{-2}	-1.1×10^{-2}	-0.25×10^{-2}	n.a †
Isothermal Temperature Coefficient 95°C, $/°C	-2.0×10^{-2}	-3.4×10^{-2}	-2.7×10^{-2}	-3.4×10^{-2}	-3.4×10^{-2}	n.a
Average Void Coefficient, C_v, $/cm^3	-0.93×10^{-4}	-2.9×10^{-4}	-4.6×10^{-4}	-7.3×10^{-4}	-9.9×10^{-4}	-8×10^{-4}
Reduced Prompt Neutron Lifetime $\ell^*/\bar{\beta}$ (sec)	11×10^{-3}	10×10^{-3}	7×10^{-3}	7×10^{-3}	2×10^{-3}	3×10^{-3}
Channel Width (mils)	190	65/190	116	65	133	120

† Data not available at time of publication.

APPENDIX B – FACTORS AFFECTING RELIABILITY OF THE DATA

1. GENERAL REPRODUCIBILITY

Since the reliability of the power and temperature instrumentation has been discussed elsewhere [29], the present treatment will be restricted to the pressure data. Overall reproducibility of peak pressure level is about ± 30%, the data obtained during later tests being somewhat more consistent than that for earlier tests. Data for pressure at peak power show reproducibility of the order of ± 50% as a consequence of the very low pressure levels (or trace deflections) involved. Although there are isolated data points which differ from the mean value by factors of two or three, in most such instances, there is good reason to suspect problems in calibration (eg, failure to record a calibration change). For example, data for an entire test sequence frequently differ from those of a second test sequence by a fixed factor, as in the A-Core data presentation (Appendix A-1) for boiling initial temperature. This test sequence was the first obtained at Spert using pressure instrumentation, and reflects the calibration problem noted. Subsequent tests display greatly improved reproducibility.

Various factors limit the precision attainable. They may be divided roughly into two categories: those incident to measuring, and those incident to processing of the data.

1.1 Limitations Incident to Measuring

Initial calibration of the transducers was repeatable to within ± 3%. However, neutron activation of the sensors limited accessibility for recalibration so that the effective calibration accuracy during a test sequence was probably about ± 10%. The electronics associated with the conditioning and recording equipment were accurate to about ± 3%. Ability to determine the reactor period for each transient was about ± 5%. Environmental sensitivities such as spurious response due to temperature, radiation, gas entrapment, and acceleration also affected the data to an indeterminate extent. However, empirical corrections for these components should keep the uncertainties involved to less than ± 10% for most data points. Precision of positioning of the detectors was much less important, since at the low acoustic frequencies represented the acoustic wave lengths were long and the corresponding spatial pressure gradients were small. Uncertainties of this origin were of the order of ± 1%.

1.2 Limitations Incident to Data Processing

Pressure magnitudes were obtained in two ways, by direct measurement of the deflections of the oscillographic traces, and by reading from analog reproductions of these traces.

For measurements made directly from the oscillographic recordings, ability to read a data point was about ± 1.5% of full scale. However, to assure coverage of the unexpected, the transducer ranges were purposely set high and most of the measured peak pressure levels corresponded to less than 1/3 of full scale. The resultant uncertainties in pressure magnitude were thus about ± 5%. Pressure level at time of peak power may be uncertain by as much as ± 25% by reason of the very small deflections involved.

For data obtained with the curve follower [5], ability to follow the trace with the pointer also affects data reliability. This uncertainty was about ± 3% of full-scale deflection or about ± 10% of the peak pressure observed. Calibration and setup of the curve follower may have introduced uncertainties up to ± 3%.

1.3 Summary

The uncertainties involved in calibration and operation of the pressure recording system are well within the empirical reproducibility of the data. Environmental changes in the system are known to occur during operation (eg, changes in gas content of water). Such changes definitely contribute to a lack of reproducibility of test results. However, the nature of the effects is so complex that it it is difficult to affix a magnitude to the resulting uncertainty. The existence of this problem area is recognized and will be further investigated in subsequent testing.

PHILLIPS
PETROLEUM
COMPANY

ATOMIC ENERGY DIVISION